Summer 5-4-2019

Induction and metastasis of cancer stem cells in pancreatic cancer

Rama Krishna Nimmakayala
University of Nebraska Medical Center

INDUCTION AND METASTASIS OF CANCER STEM CELLS IN PANCREATIC CANCER

By

RAMA KRISHNA NIMMAKAYALA

A DISSERTATION

Presented to the Faculty of
the University of Nebraska Graduate College
in Partial Fulfillment of Requirements
for the Degree of Doctor of Philosophy

Biochemistry and Molecular Biology

Graduate Program

Under the Supervision of Dr. Moorthy P. Ponnusamy

University of Nebraska Medical Center

Omaha, Nebraska

April 2019

Supervisory Committee:

Surinder K. Batra, Ph.D.

Kaustubh Datta, Ph.D.

Michael A. (Tony) Hollingsworth, Ph.D.

Michel Ouellette, Ph.D.

INDUCTION AND METASTASIS OF CANCER STEM CELLS IN PANCREATIC CANCER

Rama Krishna Nimmakayala

University of Nebraska Medical Center, 2019

Advisor: Moorthy P. Ponnusamy, Ph.D.

Pancreatic cancer is one of the most deadly of all types of cancer with an overall 5-year survival rate of less than 9%. Cancer cells in the pancreatic tumor are heterogeneous, and it is poorly understood which population is most responsible for the cancer initiation, progression, and metastasis. Recent studies provide evidence for the existence of highly tumorigenic and metastatic cells within a heterogeneous tumor known as the cancer stem cells. Studies also provided ample evidence for the existence of distinct types of cancer stem cell populations in a heterogeneous tumor with type-specific genotypic, phenotypic and functional characteristics. However, it is not clear how cancer stem cells are induced, and how these cells are involved in the metastasis process. Several external factors such as cigarette smoking and alcohol consumption have been shown to induce cancer stem cells in lung and breast cancers. Cigarette smoking is also associated with 30% of pancreatic cancer cases. The association of smoking with cancer stemness is also well appreciated in lung cancer and other cancers. Based on these studies, we aimed to investigate whether and how cigarette smoke induces cancer stem cells in pancreatic cancer in the first part of my dissertation.

In this dissertation, the first study of my work was to understand the mechanistic role of cigarette smoke on the induction of pancreatic cancer stem cells. For which we exposed $Kras^{G12D}$ and $Kras^{G12D}$; $Pdx1^{Cre}$ mouse models to cigarette smoke for 20 weeks; and treated pancreatic normal and cancer cell lines with cigarette smoke extract for 80 days. Our results indicated that chronic exposure to cigarette smoke induces stemness in pancreatic normal and cancer cells. We demonstrated that cigarette smoke and its ingredients, NNN and NNK induce stemness by upregulating PAF1, a major stemness regulating factor through CHRNA7/ERK/AP1 signaling axis. Loss of PAF1 reduced the cigarette smoke-induced stemness suggesting that PAF1 regulates smoking-mediated induction of pancreatic stemness/cancer stemness. We also proved that upon PAF1 induction, it interacts with PHF5A, a PAF1 complex stabilizing protein and

stemness factor to form PAF1-PHF5A complex, which is required for the activation of stemness genes. Overall, this first part of the study showed the mechanism of how stemness or cancer stemness is induced in response to cigarette smoking, one of the significant risk factor of pancreatic cancer.

Our second goal primarily explores the metastatic function of cancer stem cells in pancreatic cancer. Previous studies have shown the existence of distinct cancer stem cell populations in a heterogeneous tumor. For instance, breast tumors consist of two distinct CSC populations such as ALDH+ and CD44+CD24-. The study also demonstrated that ALDH+ cells rely on oxidative phosphorylation for their energy needs, whereas CD44+CD24- population rely on glycolysis. Recent studies also proposed the propensity of a specific cancer cell with specific metabolic profile metastasizes to a specific organ. For instance, the liver has a high glycolytic environment, and a metastatic cell required to be highly glycolytic to overcome the glycolytic barrier in the liver. Based on these studies, we have hypothesized that distinct types of cancer stemness populations with type-specific stemness and metabolic profiles metastasize to a specific organ. Investigation of this hypothesis led to the identification of two distinct cancer stem cells populations in pancreatic cancer: ALDH+ or CD133+ population and drug-resistant (MDR1+ or ABCG2+) population. We also demonstrated that these distinct types of cancer stemness populations showed type specific metabolic profile: ALDH+ or CD133+ population were identified as oxidative, whereas drug-resistant population showed a Warburg effect. Altogether, our data provided evidence for the existence of distinct types of cancer stemness populations with type-specific stemness and metabolic profiles. Currently, we are in the process of investigating the organ-specific metastasis of these distinct cancer stem cell populations using an orthotopic nude mice model.

Overall, our findings demonstrate a precise mechanism of cancer stem cell induction. Besides, our investigation suggests the existence of distinct cancer stemness populations with specific metabolic, stemness and metastatic profiles. In conclusion, our work provides a solid foundation for the understanding of cancer stem cells in pancreatic cancer thereby opening new avenues for further research in developing cancer stem cell-targeted therapy for pancreatic cancer.

Table of Contents

LIST OF FIGURES

CHAPTER 1

CHAPTER 4

Supplementary Figure 2. Riboflavin treatment increases AF+ cells.

Supplementary Figure 3. (A) Sphere formation by AF+ and AF- population. (B) *In vivo* tumorigenicity assay.

Supplementary Figure 4. (A) Immunoblot analysis of stemness marker (BMI1) expression in HPNE and Capan1 cells exposed to CSE (1%) for 80 days. (B) Exposure to commercial CSE (C-CSE) (purchased from Murthy Pharmaceuticals) for 80 days increases stemness or cancer stemness markers.

Supplementary Figure 5. Chronic CSE exposure elevates stem cell marker protein expressions and induces aldehyde dehydrogenase (ALDH) activity.

Supplementary Figure 6. Chronic cigarette smoke (CS) exposure induces SOX9 in the pancreas of ten-week-old control and $Kras^{G12D}$ Pdx-Cre mice.

Supplementary Figure 7. Cigarette smoking activates FOSL1 and stem cell genes.

Supplementary Figure 8. Predicted binding sites of phospho-FOSL1 (or AP1) on PAF1 gene promoter. 5' upstream region of PAF1 gene nucleotide sequence was shown.

Supplementary Figure 9. FOSL1 binds to its consensus binding site (BS) 3 ($^{-836}$TCACTCAGT^{-827}) or BS 9 ($^{-2162}$TGACTGACTGAC^{-2157}) on PAF1 gene promoter.

Supplementary Figure 10. Co-relation of CS induced phospho-FOSL1 (p-FOSL1) expression with cancer stemness marker, CD44 *in vivo*.

Supplementary Figure 11. (A) Immunoblotting analysis of CS associated receptors, TLR4 and CHRNA1. **(B)** Immunoblotting assay showing that inhibition of CHRNA7 receptor with Macamylamine (MAA) reduces the protein levels of phospho-FOSL1 (p-FOSL1), FOSL1 and PAF1 in chronic CSE exposed HPNE and Capan1 cells.

Supplementary Figure 12. (A) Confocal images showing the expression of PAF1 and PHF5A in chronic CSE treated HPNE and Capan1 cells.

CHAPTER 5

Figure 1. Distinct sub-types of CSC populations with sub-type specific stem cell features in pancreatic cancer.

Figure 2. Distinct sub-types of CSC populations show sub-type specific metabolic profiles.

Figure 3. Spontaneous liver and lung tropic metastatic cell lines show organ specific stem cell features.

Figure 4. Spontaneous liver and lung tropic metastatic cell lines show organ specific metabolic features.

CHAPTER 6

LIST OF TABLES

CHAPTER 1

CHAPTER 4

CHAPTER 5

ABBREVIATIONS

CSC	Cancer stem cells
AML	Acute myeloid leukemia
SCID	Severe combined immune deficient mice
ESC	Embryonic stem cells
5-FU	5-fluorouracil
ASC	Adult stem cells
MSC	Mesenchymal stem cells
HIF	Hypoxia inducible factor
EMT	Epithelial to mesenchymal transition
MET	Mesenchymal to epithelial transition
CML	Chronic myeloid leukemia
ALL	Acute lymphoid leukemia
ALDH	Aldehyde dehydrogenase
EpCAM	Epithelial cell adhesion molecule
PAF1	RNA Polymerase II Associated Factor 1
PHF5A	PHD finger protein 5A
TME	Tumor microenvironment
PMN	Pre-metastatic niche
PDAC	Pancreatic ductal adenocarcinoma

SP	Side population
CHRNA7	Cholinergic receptor nicotinic alpha 7 subunit
HPNE	Human pancreatic nestin positive epithelial cells
KC	$Kras^{G12D}$; Pdx-1 Cre
CSE	Cigarette smoke extract
C-CSE	Commercial cigarette smoke extract
FTC	Federal trade commission
TPM	Total particulate matter
DMSO	Dimethyl sulfoxide
LC-MS/MS	Liquid chromatography tandem mass spectrometry
MRM	Multiple reaction monitoring
NNK	4-(methylnitrosamino)-1-(3-pyridyl)-1-butanone
NNN	N-Nitrosonornicotine
OCR	Oxygen consumption rate
ECAR	Extracellular acidification rate
MDR	Multidrug resistance
AF	Autofluorescence
ChIP	Chromatin immunoprecipitation
FOSL1	Fos like 1

ACKNOWLEDGMENTS

This journey of pancreatic cancer stem cells would not have been possible without the constant motivation from my mentor, Dr. Moorthy P. Ponnusamy. He has been the best mentor and extremely supportive throughout these four and a half years. I have learned a lot from him both personally and professionally. I am also thankful to him for always being readily available for discussing work despite keeping a busy schedule. I thank him for showing great faith in me and allowing me to think independently.

I sincerely thank my graduate committee members namely Dr. Surinder K. Batra, Dr. Michael Hollingsworth, Dr. Kaustubh Datta and Dr. Michel Ouellette for their constructive critiques and useful suggestions over the years. Further, I would like to specially thank Dr. Surinder K. Batra for his continuous and constructive support. I would also like to acknowledge our collaborators, Dr. DJ Murry and Dr. Yashpal Singh Chhonker (University of Nebraska Medical Center) for helping us with mass spectrometry studies. I would also like to thank Dr. Satyanarayana Rachagani for helping me with animal work.

I express my sincere thanks to past and present lab members: Dr. Parathasarathy Seshacharyulu, Dr. Imayavaramban Lakshmanan, Dr. Raghupathy Vengoji, Dr. Abhijit Aithal, Dr. Muzaffar Macha, Dr. Sushil Kumar, Dr. Sukhwinder Kaur, Dr. Wasim Nasser, Dr. Siddharth Mahapatra, Dr. Javed Siddiqui, Dr. Sakthivel Muniyan, Dr. Ramesh Pothuraju, Dr. Wade Junker, Dr. Shailendra K. Gautham, Dr. Prakash Kshiragar, Dr. Srikanth Barkeer, Dr. Chihiro Hayashi, Dr. Rakesh Bhatia, Dr. Sanjib, Dr. Arokiapriyanka Vaz, Dr. Suhasini Joshi, Dr. Priya Pai, Dr. Shiv Ram Krishn, Dr. Eric Cruz, Dr. Andrew Cannon, Dr. Rahat Jahan, Dr. Kasturi Banerjee, Saswati Karmakar, Garima Kaushik, Pranita Atri, Koelina Ganguly, Christopher Thompson, Dr. Suprit Gupta, Catherine Orzechowski, Dr. Ranjana, Dr. Naveen Kumar, Krishnan Ramakrishnan, Dr. Ashu Shah, Sanchita Rauth, Sunandini Sharma, Rohitesh Gupta, Dr. Palanisamy Nallasamy, Leon Frank, Dr. Saravana Kumar Marimuthu, Dr. Gopalakrishnan Natarajan, Sanjana Eyunni, Brigham Killips and Kavita Mallya. In particular, I thank Dr. Parathasarathy Seshacharyulu, Dr. Imayavaramban Lakshmanan, Dr. Raghupathy Vengoji, Sanchita Rauth, Saswati Karmakar and Dr. Palanisamy Nallasamy for helping me in some of my experiments.

Most importantly, I thank Kavita Mallya and Brigham J Killips for their technical support. I also thank the BMB staff members; Karen Hankins, Amy Dodson, Jeanette Gardner, Coleen Johnson and April Busch. I also thank Dr. Anand Kumar Arachimani, Ph.D., the founder of Autostem

laboratories, Chennai, India and Dr. Lakshmanan Venkatachalapathy, MBBS. MS., FRCS, for their moral support.

No words can thank my parents; my father, Shri Burayya Nimmakayala and my mother, Late Shrimati Satyanarayanamma Nimmakayala for always prioritizing my education and for being a great motivational support. I thank my brothers, Surya Pallapa Srirama Prasad Nimmakayala and Veera Venkata Subbarao Nimmakayala, my sisters-in-law, Satyavani Nimmakayala and Hemalatha Nimmakayala, my wife, Ramya Nimmakayala for the emotional support they gave me, to carry out my thesis with great ease. Also, I thank my father-in-law, Ammiraju Chilukuri, my mother-in-law, Chakramma Chilukuri and brother-in-law, Swamy Chilukuri for the emotional support they gave me throughout this journey.

Finally, I would like to thank God Almighty for giving me the knowledge and strength to undertake this research work efficiently.

Dedicated

to

My Mother

CHAPTER 1

Introduction

The material covered in this chapter is the subject of 1 published review article.

1. Nimmakayala RK, Batra SK and Ponnusamy MP. Unraveling the journey of cancer stem cells from origin to metastasis. Biochim Biophys Acta. 2019; 1871(1):50-63.

Unraveling the journey of cancer stem cells from origin to metastasis

Rama Krishna Nimmakayala[a], Surinder K. Batra[a,b*] , Moorthy P. Ponnusamy[a,b*]

[a]Department of Biochemistry and Molecular Biology, University of Nebraska Medical Center, Omaha, NE 68198-5870, USA

[b]Eppley Institute for Research in Cancer and Allied Diseases, Fred & Pamela Buffett Cancer Center, University of Nebraska Medical Center, Omaha, NE 68198-5870, USA

Funding: This work was supported, in parts, by the following grants from the National Institutes of Health (P01CA217798, R01CA183459, R01CA210637, UO1CA200466, UO1 CA185148, UO1 CA210240, and P50 CA127297), and the Nebraska Department of Health and Human ServicesLB595.

***Corresponding Authors:** Moorthy P. Ponnusamy, Ph.D. (mpalanim@unmc.edu) and Surinder K. Batra (sbatra@unmc.edu)

Synopsis

Cancer biology research over recent decades has given ample evidence for the existence of self-renewing and drug-resistant populations within heterogeneous tumors, widely recognized as cancer stem cells (CSCs). However, a lack of clear understanding of the origin, existence, maintenance, and metastatic roles of CSCs limit efforts towards the development of CSC-targeted therapy. In this review, we describe novel avenues of current CSC biology. In addition to cell fusion and horizontal gene transfer, CSCs are originated by mutations in somatic or differentiated cancer cells, resulting in de-differentiation and reprogramming. Recent studies also provided evidence for the existence of distinct or heterogeneous CSC populations within a single heterogeneous tumor. Our analysis of the literature also opens the doors for a novel hypothesis that CSC populations with specific phenotypes, metabolic profiles, and clonogenic potential metastasize to specific organs.

1. Introduction

Why does a tumor relapse after its initial remission? The quest for an answer to this question led in 1959 to the derivation of the term “tumor stem cells” [1]. Tumors comprise a heterogeneous cell population, with 0.1% to 0.8% of these tumor cells being cancer stem cells (CSCs) [2]. Research on CSCs was launched for the first time in 1994 when Lapidot and colleagues observed in primary human acute myeloid leukemia (AML) that a small subpopulation of cells, $CD34^{+}CD38^{-}$, initiate tumor in severe combined immune deficient mice (SCID) [3]. In the light of this evidence, following studies from 1994 to date investigated for the presence of CSCs or tumor-initiating cells in various cancers and observed that a small population of drug-resistant, tumor-initiating, and stemness-activated CSCs are present in almost all cancer types. Lineage tracing experiments by three independent groups in 2012 further fueled recognition of the existence of CSCs [[4], [5], [6]].

1.1. The relevance of CSCs in cancer initiation

CSCs differentiate into self-renewing cells and differentiated cells that make up the entire bulk of the tumor [7]. According to the CSC hypothesis, “stem cells,” by residing at the top of the cellular hierarchy in each tumor, can self-renew and give rise to heterogeneous cell populations within the tumor. Studies focusing on CSCs demonstrated that implantation of even a small number of CSCs could form tumors suggesting the significance of CSCs in cancer initiation [8].

This was further confirmed in a study by Driessens *et al.*, wherein using genetic lineage tracing experiments it was demonstrated that a fraction of tumor cells and long term persisting stem-like cells have an increased proliferative potential and produce progeny that occupied a significant part of the tumor in squamous skin cancer [5]. Another study also demonstrates that Lgr5+ stem cells in intestinal adenomas produce the cells of entire adenoma by maintaining Lgr5+ stem cell population [6]. These studies suggest that CSCs are the primary culprits for the initiation and progression of cancers.

Four aspects of CSC biology have been investigated in the literature, including origin, manifold existence, maintenance, and metastasis of CSCs (OMMM of CSCs) (Fig. 1). Current evidence suggests that cell fusion, horizontal gene transfer, and mutations drive cellular transformation and reprogramming into CSCs. Besides, metabolic shifts from glycolytic to oxidative phosphorylation, or vice versa, also induce cancer stemness [9].

A challenge in understanding CSC biology is the lack of consensus about the markers of CSCs. Different studies propose varying markers for CSCs in different cancers. Emerging evidence suggests that tumors consist of heterogeneous CSC subtype populations, and each subtype of CSCs display a unique phenotype and unique clonogenic and metastatic potential. Our understanding of how these heterogeneous CSC subtype populations are maintained and contribute to the cancer biogenesis and aggressiveness after their generation also remains limited.

Studies suggest that CSCs within tumors have the potential to migrate to specific organs [10,11]. Exosomes, small extracellular vesicles released by cells, carry cellular components to distant organs, thereby increasing cellular communications [12]. Recent studies have shown that the exosomes released by cancer cells within a primary tumor journey to distant organs and form a pre-metastatic niche [12,13]. However, it is not known which cell type in a heterogeneous primary tumor releases the exosomes with the capacity to form a pre-metastatic niche in distant organs. In this review, we discussed the concept of CSCs from its origin to metastasis and described the perspective about the role of CSCs in organ trophic metastasis.

2. General features of cancer stem cells

The CSC hypothesis emerged a decade ago; however, it is still unclear what makes these CSCs unique compared to normal cells, other non-cancerous stem cells, or cancer cells. Most cell signaling pathways and cell surface and intracellular markers are similar in a normal cell, stem cell, CSC, and cancer cells. For instance, bone marrow-derived mesenchymal stem cells express high levels of the CD90 cell surface marker [14]. However, the same marker has also been proposed as a CSC marker in primary high-grade gliomas and other cancers [15]. Similarly, CD44, an well-known CSC marker, is also highly expressed in normal endometrial cells and regulates the function of normal endometrium [16]. Here, we explore the features that could potentially derive CSCs.

2.1. Recapitulation of embryonic signature in CSCs

The most prominent and specific feature which can be observed in CSCs is the recapitulation of embryonic pluripotent networks and the overexpression of embryonic genes [17]. During development, TGF-β, FGFR/MAPK or Akt, Wnt, Notch, and sonic hedgehog pathways maintain self-renewal and pluripotency of embryonic stem cells (ESCs). These pathways ultimately

activate three major transcription factors: Oct3/4, SOX2, and Nanog. These factors activate ESC-specific genes and maintain the stem cell state of ESCs by inhibiting differentiation genes. During embryo development and organ specification, pluripotent genes are inhibited, and differentiation genes are activated. Thus, in adult tissues, the expression levels of Oct3/4, SOX2, Nanog, and other ESC maintenance genes is very low [18, 19]. However, during the initiation and progression of cancers, these ESC genes and networks are activated. The aberrant expression of ESC genes and activation of stemness networks leads to the enrichment of CSCs, which initiate or aggravate tumor.

2.2. Mutations distinguish CSCs from non-CSCs

CSCs also differ from other non-CSC populations in that CSCs show mutations leading to the aberrant regulation of majority of the stemness and proliferation pathways. Even though the same signaling pathways are seen in CSCs and non-CSCs, their enhanced and aberrant activation distinguishes CSCs from non-CSCs. For instance, aberrant activation of the Wnt pathway has been shown to induce CSCs [20,21].

2.3. CSCs are quiescent

CSCs also have another striking specific property; i.e., CSC quiescence. CSCs are a low-cycling quiescent cell population residing within the tumor. These low-cycling CSCs are responsible for the tumor aggressiveness and metastasis [22,23]. Resistance to chemotherapeutic drugs is another specific property of CSCs, and this resistance is usually conferred by ABCG2 and other drug resistance receptors [24].

3. Origin of cancer stem cells

3.1. Cell fusion and stem cells

CSCs originate through cell fusions (Fig. 2), wherein cells acquire extra properties through a process in which two cells fuse to form hybrids with a higher degree of aneuploidy [25]. The fusion of 5-fluorouracil- (5-FU) resistant cancer cells with methotrexate-resistant cancer cells produces aneuploidy hybrid cells, resistant not only to 5-FU and methotrexate but also to melphalan. Also, Rizvi and colleagues showed that the fusion of bone marrow-derived stem cells with intestinal tumor epithelial cells do not produce a resistant CSC population, nor do the new hybrid cells induce cancer [26]. However, polyploid giant cancer cells (PGCCs), which are aroused because

of cell fusion have been shown to display drug resistance and tumorigenic properties [27,28]. Overall, poor evidence from literature for the fusion-mediated CSC origin limits this model.

3.2. Horizontal gene transfer

Another mechanism that could potentially contribute to the origin of CSCs is horizontal gene transfer [29], which is usually an adaptation mechanism found in bacteria and fungi that use this mechanism to acquire resistance to antibiotics [30]. Horizontal transfer is a mechanism whereby DNA from donor cells is delivered into recipient cells, followed by insertion of donor DNA sequences into the host genome and expression of the inserted gene sequence. The expression of inserted gene sequence in the host helps the host cell to acquire resistance to antibiotics. In eukaryotic cells, the horizontal transfer occurs between an apoptotic cell (donor) and a recipient cell through endocytosis or phagocytosis. Apoptosis and consequent DNA fragmentation in a somatic cell are the results of mutations. The fragmented DNA is endocytosed by another somatic cell [31] or tumor cell [29], leading to the formation of cells with a more aggressive phenotype. This suggests that horizontal gene transfer might play an important role in the generation of resistant CSCs by the transfer of mutated genetic material from apoptotic bodies derived from therapy-sensitive cancer cells to somatic or other therapy-resistant cancer cells. However, a lack of experimental evidence has limited the reliability of this phenomenon.

3.3. Mutations lead to the formation of CSCs

Various conditions, such as radiation treatment, tissue injury, and exposure to toxins (from smoking and the like) induce mutations in certain genes, including p53 (tumor suppressor) and Kras [32]. Fujimori et al. have demonstrated that extracellular stress induces cancerous genes in differentiating embryonic stem cells (ESCs), producing CSC populations [33]. The harmful external signals can also deregulate or enhance certain signaling pathways in normal adult stem cells (ASCs) and can lead to the transformation of these ASCs into CSCs. For instance, arsenic has been shown to induce the transformation of normal prostate epithelial stem cells into CSCs [34]. Also, mutations in symmetrically dividing normal ASCs transform an ASC into a CSC. Furthermore, ASCs undergo continuous division for a long time, and this increases the chances of accumulating mutations that lead to the transformation of a normal ASC into CSC. On the other hand, mutations in oncogenes and tumor suppressor genes of mesenchymal stem cells (MSCs) induce the transformation of MSCs into CSCs, leading to the initiation and progression of sarcomas [35]. Conditional inactivation of p53, NF1, and Pten tumor suppressors in neural

stem/progenitor cells converted these cells into CSCs and initiated brain tumors [36]. A genome-wide mutation pattern analysis in ASCs in the human small intestine, colon, and liver tissues showed that mutations accumulate steadily in these tissues at a rate of 40 mutations per year. The mutation spectra of genes associated with carcinogenesis are also like the mutation spectra of tissue-specific ASCs, suggesting that mutations in ASCs can induce carcinogenesis [37].

3.4. De-differentiation of non-CSCs into CSCs

Another phenomenon responsible for the origin of CSCs is cellular de-differentiation. A differentiated cancer cell can de-differentiate into a CSC in response to various factors, including wounding, stress, and hypoxia, leading to cancer initiation and progression. A recent study showed that glioma cells could de-differentiate into glioma stem-like cells (GSCs) in response to stress and hypoxia-induced HIF1α signaling. Also, angiocrine factors such as nitric oxide (NO) have been shown to drive de-differentiation of glioma cells into GSCs [[38], [39], [40]]. Wounding also induces $Gata6^{+}$ epidermal stem cells into stem-like cells, suggesting that wounding can also de-differentiate a differentiated cell into a stem cell [41]. Ionizing radiation also converted cancer cells into a stem-like phenotype, with increased metastasis [42]. By undergoing EMT, pancreatic ductal cells have been shown to acquire CSC phenotype through de-differentiation [43]. These studies collectively suggest de-differentiation as an important phenomenon involved in the generation of CSCs in various cancers.

3.5. Metabolic reprogramming of CSCs

Metabolic adaptation is central in cancer cells, especially regarding glycolysis. In glycolysis, glucose is broken down through a series of steps into pyruvate, producing two molecules of ATP per one molecule of glucose. In the presence of enough oxygen levels, pyruvate enters oxidative phosphorylation and produces 36 ATP molecules per one glucose molecule. Thus, oxidative phosphorylation is more efficient than glycolysis in generating ATP molecules. However, cancer cells, as hypothesized by Warburg, show increased glycolysis to produce ATP, even in the presence of oxygen, and it converts pyruvate into lactate to create a condition of fermentative metabolism that is highly conducive to the activity of cancer cells. If sufficient levels of glucose are available, aerobic glycolysis can generate more energy more rapidly than can oxidative phosphorylation [44].

Otto Heinrich Warburg, a German physiologist, theorized that one of the most important causes of cancer is variation in metabolism. According to his theory, cancer cells generate energy through the anaerobic breakdown of glucose even in the presence of oxygen. Hence, these cells are mostly glycolytic. According to this theory, then, cancer is a disease of mitochondrial dysfunction. However, healthy cells produce energy through oxidative phosphorylation, in which the product of glycolysis, pyruvate, is oxidized in the mitochondria, and thus these healthy cells are mostly oxyolytic. Very few studies so far have explored the metabolic profiles of CSCs. Several studies suggest that CSCs are mostly glycolytic, while others speculate that these cells are oxyolytic [45,46]. Recently, Folmes and colleagues documented reprogramming of somatic cells into pluripotent cells and demonstrated that a shift from oxidative phosphorylation to glycolysis in differentiated somatic cells is required for reprogramming of these cells into pluripotent stem cells [47]. Based on this study, it is possible that a non-CSC population is reprogrammed into CSCs during the development of cancer. In support of this, hypoxia has been shown to increase breast CSCs regulated by hypoxia-inducible factor 1 alpha (HIF1α) [9].

To conclude this part of the review, there are two major unknown challenges associated with the elucidation of the origin of CSCs. The preceding discussions conclude that de-differentiation is one of the driving factors for CSC generation, and in this regard, it seems possible that CSCs show plasticity. CSCs typically differentiate and form heterogeneous populations. At the same time, a differentiated non-CSC population, in response to certain conditions including toxic exposure and mutations, may de-differentiate into CSCs and lead to further tumor progression. However, further evidence is necessary to shed light on the complex phenomenon of CSC plasticity, given that tumors contain a heterogeneous population with different phenotypes and genotypes. Another challenge in the study of CSCs is the identification of differentiated non-CSC populations that undergo transformation and de-differentiation.

The stem cells in a tissue are known to divide and self-renew for long periods, and studies have suggested that these stem cells are more susceptible to mutations. However, no study has been documented in the literature demonstrating the accumulation of mutations in these long-lived dividing stem cell populations. The suggestion that a metabolic shift can reprogram somatic cell into pluripotent stem cells also requires further investigation and in-depth study as such a shift might relate to cancer.

Since CSCs were first identified, their origin has been a pronounced mystery. Toxic exposure, mutations, metabolic shift, cellular plasticity, and de-differentiation have been suggested as

contributing factors for the origin of CSC. Finding a link between all these factors and investigating whether these events occur sequentially are challenges.

4. Manifold existence of cancer stem cells and its impact on cancer biogenesis and aggressiveness

So far, a description of the existence of CSCs is controversial, as different studies have shown different CSC markers (Table 1). The lack of a universal CSC marker makes it difficult to characterize CSCs in various kinds of cancer, and much of the evidence suggests that CSCs are heterogeneous. According to this, tumors consist of distinct CSC populations with specific phenotypes and clonogenic potentials. In this part of the review, we will describe the CSC heterogeneity or specific clonogenic populations of CSCs in various cancers and their impact on cancer biogenesis and aggressiveness.

4.1. Cancer stem cell heterogeneity in liquid tumors: establishment of original CSC paradigm

The concept of CSCs was first recognized and analyzed in most detail in liquid tumors such as acute myeloid leukemia (AML), chronic myeloid leukemia (CML) and acute lymphoid leukemia (ALL). Bonnet et al., have identified $CD34^{+}CD38^{-}$leukemic stem cells in AML for the first time and demonstrated that this particular subset of leukemic stem cell population shows self-renewal, proliferative and differentiation potential and induce leukemic transformation in NOD/SCID mice [48]. Later, Cox et al., have shown that cells with $CD34^{+}CD19^{-}CD10^{-}$ phenotype are long term proliferative cells with tumorigenic potential [49]. Later studies in leukemia showed distinct CSC populations including CD34-$Lin^{+}CD38^{+}$, $CD45RA^{+}$, $CD34^{+}CD38^{-}CD71^{-}$HLA-DR^{-}, $CD34^{+}CD38^{-}$ $CD123^{+}$, T cell immunoglobulin mucin 3 ($TIM3^{+}$) and $CXCR4^{+}$ [50,51,52,53,54]. However, CSCs in solid tumors display a completely distinct set of markers as described below.

4.2. Cancer stem cell heterogeneity in solid tumors

$CD133^{+}$ and $ABCG2^{+}$ population from surgical biopsy samples of melanoma patients showed an increased tumor initiating property in vivo [55]. In NOD/SCID mice, $ALDH^{+}$ melanoma cells showed increased tumorigenicity as compared to $ALDH^{-}$ population suggesting the existence of $ALDH^{+}$ CSCs in melanoma [56]. Circulating melanoma cells showed Nestin expression suggesting this protein as a potential marker for melanoma

metastatic stem cells [57]. Transplantation of $CD271^+$ melanoma cells into engrafted human skin produced melanoma tumors, while $CD271^-$ population did not, suggesting the $CD271^+$ population as a distinct melanoma stem cell population [58]. Fang et al., showed a small proportion of $CD20^+$ population as melanoma stemness population [59].

Furthermore, bladder tumor consists of distinct heterogeneous CSC populations. For example, $CD44^+BCMab1^+$ population was identified as CSC population in bladder cancer, and they have also shown that this CSC population has an increased GALNT1 expression and Hh signaling leading to increased tumorigenesis [60]. Also, the $CD133^+$ population also showed tumorigenic and stemness potential in bladder cancer [61]. In addition to $CD44^+$ and $CD133^+$ CSCs, glioma tumors consist of distinct other CSC subtype populations expressing MUSASHI1, NESTIN, CD15, L1CAM, and A2B5 [[62], [63], [64], [65]].

A recent emerging study demonstrated that the breast CSCs exist as two distinct populations such as epithelial-to-mesenchymal (EMT) CSCs and mesenchymal-to-epithelial (MET) CSCs [66]. Evidence from this study showed that EMT CSCs ($Vimentin^+$ and $EpCAM^-$) are quiescent; however, MET CSCs ($Vimentin^-$ and $EpCAM^+$) are proliferative [66]. Another study demonstrated that single $CD49f^+CD24^-CD44^+$ cell-derived clones show aggressive phenotype and activation of OCT4/SOX2/lincRNA-RoR signaling suggesting that this subset of the population is also a stemness population in breast tumors [67].

In contrast, a different set of CSC populations were identified in gastric cancer. Li et al., have shown that invasive intestinal-type gastric cancer is originated from Lgr5+ stem cells. Also, Lgr5+CD54+ cells showed elevated expression of pluripotent and EMT markers in gastric cancer [68]. Apart from these, ALDH+ and CD133+ populations were identified as CSCs in gastric cancer [69]. A similar subset of CSC populations was also identified in colorectal tumors. A different subset of CXCR4+Lgr5+ expressing population showed significant tumorigenic activity in colorectal cancer [70]. Also, CD133+ CSCs showed increased tumorigenicity, and a subset of CD133+CXCR4+ CSCs showed increased metastatic potential along with poor survival in colorectal tumors [71]. DCLK1 has been showed to be associated with increased tumorigenesis, and knockdown of DCLK1 reduced tumor cell pluripotency and pro-survival signaling in colorectal cancer, suggesting the existence of a distinct DCLK1+ subset of CSCs in colorectal tumors [72].

In addition to CD44+, ALDH+ and CD133+ CSC populations, ovarian and head-and-neck tumors consist of distinct CSC subtype populations. CD117+ CSCs in ovarian cancer is

associated with poor survival and increased tumorigenesis. [73]. In contrast, head and neck tumors harbor $CD98^+$, $CD200^+$ and $GRP78^+$ CSC population [74]. Among these, CD200+ CSCs showed increased stemness features and resistance to chemo and radiation treatments [75]. Similarly, liver tumors consist of $CD133^+$, $ALDH^+$ and $CD44^+$ cancer stemness populations [76,77]. Also, $CD90^+$CD44+ subset of liver cancer cells showed elevated tumorigenicity and metastasis in immunodeficient mice [78]. CSCs in lung tumor is also highly heterogeneous, and for example, CD44+, ALDH+, and EpCAM+ maintain stemness and tumorigenic potential in lung adenocarcinoma [79]. In addition, lung tumor also consists of highly tumorigenic CD166+$CD44^+$ CSC population [80].

Pancreatic tumor harbors several distinct stemness populations such as $CD44^+$, $CD133^+$, $ALDH1^+$, $ABCG2^+$ (SP), $EpCAM^+$, $autofluorescence^+$ (AF) and $CXCR4^+$ CSC populations [81]. Hermann et al., have shown that CD133+ population is highly tumorigenic and a CD133+CXCR4+ subset of the population is highly metastatic in pancreatic cancer [11]. Recently, an emerging study demonstrated that intracellular autofluorescence (AF) was used as a CSC marker in pancreatic cancer [82]. Riboflavin-loaded intracellular vesicles expressing ABCG2 shows autofluorescence and maintains stemness potential in pancreatic CSCs [82]. ABCG2 receptors on cell surface confer chemo-resistance to cells, and cells with a higher number of these receptors are considered stem cells or side population (SP). Hence, ABCG2 is also used as a CSC marker in various cancers [83,84]. The autofluorescence assay and SP assay are mainly based on ABCG2 expression. However, the autofluorescence population did not overlap with SP cells, further confirming and supporting the non-uniqueness of stemness markers in CSCs.

$CD44^+$ and $CD133^+$ cells have been proposed to be CSCs of medullary thyroid carcinoma [85], endometrial cancers [86] and rectal cancer [87]. Also, choroidal and ciliary body melanoma CSCs express CD117 and CD15 markers [88]. Overall, these studies suggest that tumors of various organs consist of distinct CSC populations with different stemness phenotypes.

4.3. Evidence for the existence of distinct CSC population based on nuclear transcription factors

Studies have demonstrated that specific embryonic genes, including Oct3/4, SOX2, Nanog, KLF4, and PAF1/PD2 are recapitulated during cancer initiation and progression. Most recently, SOX2 was identified as a CSC prognostic marker in pediatric sarcomas and prostate cancer [89,90]. Polycomb group proteins (e.g., EZH2, BMI1) are significant drivers of stem cells,

and a group of researchers from the University of Queensland has proposed BMI1 and EZH2 as prostate and oral CSC markers, respectively [89,91]. We have identified the novel role of PAF1/PD2 in the maintenance of ovarian and pancreatic CSCs, demonstrating that PAF1/PD2 interacts with Oct3/4 or PHF5A and maintains the stem cell features of ovarian/pancreatic CSCs [92, 93, 94]. It is also known that VEGF promotes stemness and has been shown as a breast CSC marker [95].

4.4. Metabolic profiles of CSCs

A previous study demonstrated that self-renewing normal pluripotent stem cells (PSCs) are glycolytic and that during differentiation, these PSCs switch their metabolic profile from glycolytic to oxidative phosphorylation [96]. According to this study, even CSCs should be glycolytic, since self-renewal is one of the characteristic properties of normal stem cells and CSCs. Ciavardelli et al. have demonstrated that $CD44^+$ $CD24^-$breast CSCs are glycolytic and that the inhibition of glycolysis reduced proliferation of this CSC population [45]. Also, radio and drug-resistant populations in nasopharyngeal carcinoma relied on glycolysis for their energy needs. However, upon differentiation, this CSCs shifted their metabolic profile from glycolytic to oxidative phosphorylation [97]. In contrast, reduced glycolysis and increased mitochondrial oxidative phosphorylation are characteristic features of CSCs. Song and colleagues demonstrated that colon CSCs utilize mitochondrial oxidative phosphorylation for their energy needs [98]. Similarly, glioma and leukemic stem cells have been reported to be oxyolytic [99].

Based on the above studies, there is wide metabolic variability in CSCs. Recent research suggests the existence of distinct CSC populations, and it may be possible that a specific CSC population subtype shows a unique metabolic profile. Gammon and colleagues showed that there exist two different types of CSC populations in breast tumors, EMT CSC, which is a $CD44^+$CD24- and quiescent population, and MET CSCs, which comprise $ALDH^+$ and cycling population [50]. The group studied the metabolic profiles of these two CSC subtypes and suggested that EMT CSCs are glycolytic, whereas MET CSCs are oxyolytic [100].

4.5. Plasticity of cancer stem cells

Based on the discussion above, CSCs in a tumor is heterogeneous. In addition to this complexity, CSC plasticity is another process, in which there is a transformation between non-stem cells to stem cells or vice versa contribute to the development of heterogeneity within a tumor. One of the

significant processes of CSC plasticity is EMT. As described above, studies in breast cancer showed two distinct CSC populations such as EMT CSCs and MET CSCs, which maintain the plasticity [66]. In pancreatic cancer, metformin treatment induced the transition of oxidative CSCs into drug-resistant glycolytic CSCs, further confirming the plasticity of CSCs [8].

In addition to these studies, other reports also demonstrated the transformation of non-CSC into CSCs. For example, JARID1B, a histone demethylase has been shown to regulate tumorigenicity, and however, cells negative for JARID1B also acquired self-renewal suggesting the plasticity of melanoma CSCs [101]. ZEB1, an EMT transcription factor induces the plasticity of CSCs by converting non-CSCs into CSCs in breast cancer [102]. The combined induction of pluripotent transcription factors POU3F2+SOX2+SALL2+OLIG2 reprograms glioblastoma cells into glioma CSCs [103]. Moreover, silencing of PTEN, a tumor suppressor gene induced stemness features in mammary epithelial cells resulting in the development of pre-malignant lesions [104].

To sum up this section, the current major challenge in CSC biology is the lack of a specific CSC marker that can be used to characterize virtually any kind of CSC from any cancer. Self-renewal and cellular quiescence can be exploited to characterize CSCs; however, these properties are common in both normal stem cells and CSCs. To overcome these challenges, the scientific community proposed various biomarkers for CSCs, but great disagreement remains within the scientific community regarding CSC biomarkers. Different studies have proposed different markers, but these markers are not unique to a particular cancer type. Studies have also proposed different markers for CSCs from different cancers. These studies conclude that there is no unique marker for CSCs in different cancers. On the other hand, this discussion can open doors to a novel hypothesis that tumors consist of heterogeneous and distinct CSC populations, and that each CSC subtype shows a unique metabolic profile and clonogenic potential that results in the derivation of heterogenic populations within tumors. Isolation of CSCs from various cancers using various established markers and investigating the common property or marker expression in all these CSC population types may further reveal a single, unique property in CSCs. Such investigation can also address whether different types of CSCs exist, and, if so, describe the function of each type of CSC within tumors.

5. Maintenance of “Cancer stemness.”

Controlled signaling networks in normal stem cells maintain tissue homeostasis; however, loss of control in these networks and consequent abnormalities result in elevated self-renewal, increased survival and increased proliferation that lead to CSC generation and enhanced CSC maintenance. Stem cell niche, various signaling molecules, and transcription factors maintain stemness homeostasis in normal stem cells. Similarly, CSC niche, mutations and various abnormal extrinsic and intrinsic signals de-regulate the pathways leading to the emergence and maintenance of CSCs. In this section of the review, we will discuss the role of tumor microenvironment (TME), specific stemness signaling molecules and transcription factors in CSC maintenance in detail (Fig. 3).

5.1. Role of tumor microenvironment in the maintenance of CSCs

The interactions between CSCs and its “niche” a specific tumor microenvironment (TME) of CSCs maintain “stemness.” Stromal cells, mesenchymal stem cells, hypoxic regions, inflammatory cells, extracellular matrix (ECM) and angiogenesis are the significant components of this specific microenvironment that induce and maintain stem cell features in CSCs. The effect of inflammatory stroma on the dedifferentiation and generation of CSCs was shown recently by Schwitalla et al. in which they showed that increased activation of NF-kB, a transcription factor in the inflammatory TME elevates Wnt signaling and induces dedifferentiation of non-stem cell population into CSC population in intestinal tumors [105]. Another evidence for TME mediated maintenance of CSCs showed that Notch signaling prevents CSCs from differentiation by inhibiting the differentiation signals coming from TME [106]. Besides, mesenchymal stem cells support CSC by secreting a variety of cytokines such as CXCL12 and interleukins that induce stemness through NF-kB pathway [107]. In TME, CSCs escape from NK cell-mediated cytotoxic effects, and for instance, CD133+ CSCs express low levels of MHC-class 1 molecules leading to poor recognition by NK cells in glioblastoma [108]. TME hypoxia also promotes tumor progression and therapy resistance by preferentially maintaining CSCs in breast cancer [109]. Human renal CSCs release macrovesicles (containing miRNAs and mRNAs for VEGF) and induce angiogenesis [110]. These studies collectively suggest that TME is functionally essential for the maintenance of CSCs.

5.2. Wnt molecules in the maintenance of self-renewal of cancer stem cells

Wnt proteins are involved in a signaling mechanism that maintains the ability of self-renewal in stem cells. The Wnt ligands bind to different receptors and result in the activation of either canonical or non-canonical signaling pathways that control various cellular functions such as self-renewal, proliferation, survival, and differentiation. In the canonical Wnt signaling pathway, the Wnt ligand binds to the Frizzled receptor (Fzd) and low-density lipoprotein receptor-related protein 5/6 co-receptors (LRP5/6), leading to the formation of the Fzd/LRP5/6 complex. As a result, Axin and disheveled (Dvl) are recruited to the plasma membrane, leading to the disruption of the *β*-catenin degradation complex. Free and active forms of *β*-catenin in the cytoplasm then translocate to the nucleus. In the nucleus, these molecules form complexes with T-cell factor (TCF)/lymphoid enhancer factor (LEF) and lead to the transcriptional activation of Wnt target genes [111]. Various non-canonical Wnt molecules such as Wnt4, Wnt5a, Wnt9b, Wnt10a, and Wnt10b are involved in the fine-tuning of the canonical Wnt signaling mechanism [112]. These non-canonical Wnt molecules bind to the Fzd receptor and Ror1/2 co-receptor, thereby activating non-canonical signaling pathways such as the Wnt/Calcium ($Ca2^{+}$) and Wnt/planar cell polarity (PCP) pathways.

Previous studies have shown that Wnt signaling regulates the maintenance of healthy intestinal stem cells. The regenerative capacity of intestinal stem cells is reduced with the decline in canonical Wnt signaling, suggesting that Wnt signaling plays a vital role in the improvement of aging of these cells [113]. Intestinal stem cell markers such as CD44 and Lgr5 are also the direct target genes of the Wnt pathway [114]. It was also shown that $Lgr5^{+}$ cells are multipotent intestinal stem cells, rapidly cycling and long-lived, with high regenerative capacity [114]. Reduced expression of DKK1, an antagonist of the Wnt pathway, increased the stemness of intestinal stem cells, suggesting the importance of this signaling in intestinal stem cells [115]. Previous studies have shown that Wnt signaling maintains the self-renewal of mammary stem cells, and inhibition of Wnt signaling reduced the stemness of mammary stem cells [116]. Protein C receptor, a Wnt target gene, has been shown to maintain mammary stem cells [117]. Another Wnt target gene, Sox9 has been shown to maintain the stemness state of mammary stem cells [118]. Lgr4, a leucine-rich repeat G-protein coupled receptor, is involved in stemness maintenance of intestinal and epidermal stem cells. Lgr4 activates Sox2 through Wnt signaling to maintain stemness in mammary stem cells [119]. In contrast to the stemness maintenance role of Lgr4, a recent study has shown that Lgr4 upregulation also induces the differentiation of prostate stem

cells [120]. These studies suggest that Wnt signaling has distinct roles in different organs and the importance of Wnt signaling in the maintenance of normal mammary stem cells.

Mutations in Wnt signaling molecules are the primary drivers of intestinal cancers, including colorectal cancer. A loss of function mutation in APC, a tumor suppressor, and a Wnt signaling controller, leads to the deregulation of the Wnt pathway and the emergence of colorectal CSCs, and consequently to the initiation and progression of colorectal cancer [121]. Mutations in the GSK3β phosphorylation site in β-catenin leads to aberrant Wnt signaling and development of colorectal cancer [122]. Wnt signaling has also been shown to be involved in the maintenance of colon CSCs [123]. Inhibition of Wnt signaling reduces the stemness of breast CSCs and suppresses breast cancer metastasis [124], while the activation of Wnt/β-catenin signaling increased mammosphere formation ability and enriched breast CSCs [125].

5.3. Hedgehog (Hh) in cancer stem cell maintenance

In addition to Wnt, Hh proteins maintain the self-renewal property of stem cells. The Hh signaling pathway begins with the binding of three ligands: Indian hedgehog or desert hedgehog or sonic hedgehog to Patched1 (PTCH1) or Patched2(PTCH2) receptors. After this binding, the receptor-mediated inhibitory effect on Smoothened (SMO), a G-protein coupled signaling protein, is removed, leading to the activation of a signaling cascade that facilitates the nuclear translocation of GLI family transcription factors (a glioma-associated oncogene homolog transcription factors). Once GLI transcription factors enter the nucleus, they bind to DNA and regulate various genes such as Fox, Myc, and Cyclin D [126].

Hh signaling regulates significant cellular and molecular events during embryo development and maintains adult tissue homeostasis. It has been shown that Hh signaling regulates the differentiation of ESCs. The signaling is highly activated during the differentiation of ESCs and effects the lineage determination of ESCs [127]. During embryonic chick lung development, the expression patterns of various Hh signaling proteins such as PTCH1 and GLI was also observed [128]. These studies collectively suggest the importance of Hh signaling during embryonic organogenesis and for the regulation of ESC.

On the other hand, Hh signaling also regulates the stemness of various CSCs. Studies have suggested that multiple myeloma (MM) stem cells, for example, are CD138 negative and that the inhibition of Hh signaling in these cells reduces their clonal ability, suggesting its importance in

maintaining MM stem cells [129]. Cyclopamine-mediated inhibition of Hh signaling in GBM neurospheres reduced other stemness markers, such as Nanog, Sox2, and Nestin [130]. The Shh target gene, BMI1, is highly upregulated in $CD44^+$ $CD24^-$ breast CSCs and maintains the regulation of self-renewal of breast CSCs [131]. Inhibition of SMO using its antagonist, GDC-0449, and consequent inhibition of Hh signaling, led to apoptosis of pancreatic tumorspheres [132]. These studies implicate Hh signaling in the regulation of stemness in CSCs.

5.4. Notch signaling and self-renewal maintenance

The Notch signaling pathway also governs the self-renewal of stem cells and the development and homeostasis of various tissues. Notch signaling is initiated when two cells, one signal releasing and the other signal receiving, are in contact with each other. The signal-releasing cell produces a ligand, which binds to the receptor on the signal receiving cells and thereby cleaves and translocates the intracellular part of the Notch receptor into the nucleus. Once this enters the nucleus, it acts as a transcriptional co-activator. The binding of the Notch transcriptional co-activators to target gene promoter regions leads to the activation of its target genes, including Myc, p21, and Hes1 [133].

The stemness property of adult normal stem cells in various adult tissues is maintained by Notch signaling. $Lgr5^+$ cells in intestinal tissues are intestinal stem cells, and this $Lgr5^+$ population is responsible for the homeostasis of intestinal tissue. Recent studies have shown that the inhibition of Notch signaling reduces the $Lgr5^+$ intestinal stem cell population [134]. Notch signaling also mainly regulates the maintenance of neural stem cells. Inhibition of Rbpj, a Notch receptor-effector molecule, in the adult brain led to the differentiation of neural stem cells into neurons, suggesting that the signaling is crucial for the maintenance of neural stem cells [135].

As in normal stem cells, Notch signaling also plays a crucial role in the regulation of stemness or self-renewal in CSCs, and abnormal activation of the pathway leads to increased self-renewal of CSCs. For instance, Notch signaling controls pancreatic CSCs in pancreatic ductal adenocarcinoma (PDAC), and silencing of Hes1, a Notch pathway target gene, reduced the percentage of pancreatic CSCs [38]. Hes1 upregulation also increases the number of $CD133^+$ cells, side populations, and the ability to form tumorspheres in colon cancer. The stemness of renal cell carcinoma CSC has also been shown to be regulated through the Notch pathway. Blockade of Notch receptors using Numb, an endogenous inhibitor of Notch receptors in $CD133^+CD24^+$ renal cell carcinoma CSC, led to a reduction in self-renewal and drug

resistance in these CSCs [136]. Treatment with gamma-secretase inhibitor IX (GSI), a Notch inhibitor, inhibited proliferation and induced apoptosis in $CD44^{+}$gastric CSCs [137]. These studies collectively suggest the importance of Notch signaling in the maintenance of stemness in CSCs.

5.5. ABC transporters in the maintenance of drug resistance in CSCs

Drug resistance in CSCs is caused by multiple factors including ABC transporter-mediated drug efflux, immune escape due to loss of MHC class 1 molecule, extracellular acidic pH, ALDH enzyme-mediated cellular detoxification system and increased DNA repair ability. Among these, the ABC transporters mediated drug efflux mechanism is highly activated and unique in CSCs. Previous studies have shown that aberrant regulation of ATP binding cassette (ABC) transporters leads to drug resistance of CSCs [138]. Three major ABC transporters, ABCB1 (MDR1), ABCC1, and ABCG2, have been demonstrated for the drug resistance in CSCs. Multiple signaling mechanisms have been shown to regulate the expression of ABC transporters. MDR1, a multidrug-resistant gene, is responsible for the drug resistance of CSCs, and the MDR1 gene is directly regulated by the MYC oncoprotein [139]. Also, the expression of ABCG2 is regulated by an increase in JNK1 signaling [140]. HIF2α and PPARγ/PTEN/PI3K/Akt have been shown to regulate the ABCG2 gene in breast cancer [141,142]. Increased expression of the estrogen receptor β (ERβ) induces cancer by regulating ABCG2 [143]. NRF2, a redox-sensing transcription factor, regulates ABCG2 in lung CSCs [144]. The YAP pathway (Hippo pathway) is a highway for drug resistance in tumors [145]. On the other hand, Notch1 signaling has been shown to regulate the ABCC1 transporter, leading to increased drug resistance in prostate CSCs [146]. In summary, ABCB1, ABCC1, and ABCG2 drug efflux transporters are the major players in the drug resistance of CSCs. Developing therapeutic strategies to target these transporters may be a better strategy to eliminate CSCs from tumor bulk.

5.6. Anti-apoptotic proteins and its importance in CSCs

Anti-apoptotic pathways are primarily responsible for drug resistance in CSCs. Identification of various targets specifically involved in anti-apoptosis of CSCs is crucial for developing CSC-targeted therapies. Most studies have repeatedly shown that up-regulation of various anti-apoptotic proteins, such as Bcl-2, Mcl-1, c-FLIP, and survivin, and the down-regulation of pro-apoptotic proteins such as Bid, lead to increased drug resistance in CSCs. Bcl-2, an anti-apoptotic protein, is required for the survival of leukemia stem cells [147]. Glioma stem cells also showed increased expression of Bcl-2, along with another anti-apoptotic protein, Mcl-1 [148,149]. Another

significant anti-apoptotic protein, c-FLIP, exerts its function by activating major signaling molecules, such as Akt and ERK. c-FLIP is overexpressed in breast CSCs and leads to their increased survival [150]. Survivin, another anti-apoptotic protein, is up-regulated in breast CSCs and to lead to therapeutic resistance of breast CSCs [151]. Targeting Bid, a proapoptotic protein, in ovarian CSC reduced the stemness of these cells, suggesting that Bid is responsible for the elevated stemness in ovarian CSCs [152]. Targeting these pro-apoptotic and anti-apoptotic proteins in CSCs may increase the sensitivity of CSCs to drug-mediated cell death.

5.7. NF-ƘB in CSC maintenance

One of the many characteristic features of CSCs is epithelial to mesenchymal transition [50]. Recent studies have suggested that EMT is not only responsible for metastasis, but also for drug resistance the TWIST-mediated NF-ƘB pathway regulates EMT in papillary thyroid carcinoma [153]. Besides, SDF-1 activates NF-ƘB, leading to the induction of EMT in breast CSCs [154]. The multidrug-resistant gene, MDR1, is regulated by CD133 and the DNA dependent protein kinase (DNA-PK) via the PI3K- or Akt-NF-κB network [155]. Osteopontin, an oncoprotein, induces hepatocellular CSCs through an integrin- NF-κB-HIF-1α pathway [156]. Activation of TLR3 was also shown to induce the co-activation of β-catenin and NF-ƘB, leading to the promotion of breast CSCs [156]. In addition to various signaling molecules, miRNAs also induce CSCs by activating the NF-κB pathway; for instance, Let7a induces mammosphere formation by activating the Ras/NF-κB pathway [157].

Given these results, targeting ABC transporters, pro, and anti-apoptotic molecules and NF-κB together may be proved to be an effective therapeutic strategy to eradicate CSC populations from tumor bulk.

5.8. HIF1-mediated metabolic alteration in CSCs

Hypoxia-inducible factor 1 (HIF1) is a transcription factor that mediates metabolic configuration under hypoxic conditions. HIF1 consists of two subunits, HIF1α (controlled by oxygen) and HIF1β (expressed constitutively) [158]. HIF1α, under normoxic conditions, is also degraded by oxygen-dependent prolyl-hydroxylases (PHD1–3). Hypoxic conditions or inhibition of PHD enzymes increases the stabilization and nuclear translocation of HIF1α, where it activates its target metabolic genes such as glucose transporters (GLUT1) and pyruvate dehydrogenase kinases (PDK1-3) and results in the switch from mitochondrial oxidative phosphorylation to glycolysis.

Increased expression of GLUT1 elevates glucose uptake by cells, and the augmentation of PDK1-3 expression inhibits oxidative phosphorylation by inhibiting pyruvate dehydrogenase (PDH). Furthermore, HIF1α activates pyruvate kinase (PKM2) gene transcription, and this is facilitated by its interaction with the PKM2 gene. PKM2 catalyzes the final step of glycolysis by dephosphorylating phosphoenolpyruvate to pyruvate. Thus, HIF1α plays an important role in increasing glycolysis and decreasing oxidative phosphorylation [158].

A recent study demonstrated that reprogramming of a somatic cell into a pluripotent stem cell requires a metabolic shift from oxidative phosphorylation into glycolysis [158]. In detail, the transfection of dermal fibroblasts with pluripotent factors such as OCT4, SOX2, KLF4, and c-MYC increases expression of HIF1α, which in turn activates its target genes, including PDK1, PDK3, and PKM2. The activation of PDK1 and PDK3 inhibits PDH, leading to a shift from oxidative phosphorylation to glycolysis. These results suggest that a metabolic shift from mitochondrial respiration to glycolysis is mandatory during the reprogramming of somatic cells into stem cells.

In terms of CSCs, HIF1α expression is elevated in prostate CSCs, suggesting that an HIF1α signaling-mediated glycolytic shift may be required for maintenance of CSCs [159]. Also, HIF1α has been shown to increase β-catenin transcription and to result in the activation of Wnt signaling in leukemia stem cells [160]. Iida et al. showed that HIF1α activates Oct3/4 and Sox2 expression and induces CD133 expression under hypoxic conditions [161]. Despite this evidence, it is not known whether the activation of HIF1α can completely reprogram a cancer cell or a differentiated cell into a CSC through a HIF1α-mediated glycolytic shift.

5.9. Myc and Nanog maintain metabolic alteration in CSCs

The oncoproteins of the Myc family (MYC, MYCN, and MYCL) control cell proliferation in various cancers. Apart from this, these oncoproteins have been shown to play a crucial role in metabolic reprogramming under cancerous conditions. MYC activates various metabolic genes, including GLUT1, ENO1, HK1, LDHA, and PKM2, and thus regulate the uptake of glucose, glycolysis, and lactic acid production. MYC has a further significant role in the regulation of metabolic pathways in stem cells. The MYC oncoproteins (MYC and MYCN) present in neuronal progenitor cells activate HK2 and LDHA, leading to their increased reliance on glycolysis for energy production. However, during differentiation of these neuronal progenitor cells into neurons, a shift from glycolysis to oxidative phosphorylation was observed that led to a reduction in MYC and MYCN proteins as well as in the glycolytic enzymes [162].

Pancreatic CSCs are oxyolytic as the inhibition of MYC contributes to the suppression of mitochondrial respiration in these CSCs [8,163]. Moreover, treatment with metformin, an inhibitor of mitochondrial respiration, induced apoptosis in pancreatic CSCs. However, a tiny subset of pancreatic CSCs developed resistance to metformin and displayed intermediate metabolic phenotype. Metformin-induced Myc overexpression also led to a shift from oxidative phosphorylation into glycolysis in these metformin-resistant CSCs.

Nanog is a transcription factor required for the maintenance of pluripotency in stem cells. It binds to the promoter of the genes involved in oxidative phosphorylation, and its overexpression reduces the expression of mitochondrial respiration genes but increases mitochondrial fatty acid oxidation in liver CSCs. The upregulation of genes involved in mitochondrial respiration interestingly reduces self-renewal of liver CSCs [164]. Nanog thus maintains cancer stemness of liver cancer cells by inhibiting mitochondrial oxidative phosphorylation and by inducing fatty acid oxidation.

6. Cancer stemness in metastasis

6.1. “Seed” and “Soil” theory of metastasis

Although there are novel targeted therapies and advanced surgical techniques available to reduce or remove primary tumors, cancer remains one of the leading causes of mortality worldwide with the primary cause of cancer-related deaths being the progressive development of metastasis. Organ-specific metastasis has been a mystery to researchers for over a century. In 1889, Stephen Paget proposed the “seed” and “soil” theory, in which tumor cells (seed) from the primary site travel to a distant organ (soil), which in turn is a favorable environment to support the colonization and growth of the tumor cell. A specific organ, according to this theory, can provide a suitable environment for the growth of a specific tumor cell, resulting in the organ-specific metastasis of given tumor cells [165] (Fig. 4). In support of this notion, it has also been shown that tumor cells create an environment in targeted distant organs that are suitable for the growth of future metastatic cells [166].

6.2. Impact of cancer stem cell heterogeneity on the establishment of organotropic metastasis

Previous studies have shown that CSCs can not only initiate and aggravate cancer but that they are also involved in metastasis. However, the role of CSCs in this organ-specific metastasis and

the formation of a pre-metastatic niche is poorly understood in the literature. Most studies suggest that metastatic cells show a CSC phenotype. In pancreatic cancer, the $CD133^+$ cell population is highly metastatic. CXCR4 expressing CSCs showed an increased tumorigenic property and elevated metastatic potential. In colon cancer, $CD26^+$CSCs are known to have metastatic potential. $ALDH^+$ and $CD44^+$CD24- breast CSCs also show high metastatic potential [167]. However, it is not completely understood in the literature whether heterogeneous CSC subtype populations with a specific phenotype and clonogenic potential can metastasize to a specific organ. Gao et al. have shown that CD110-positive CSCs show liver organotropism, whereas CDCP1 promotes lung tropism in colorectal cancer. $CD110^+$ and $CDCP1^+$ metastatic CSCs in colorectal cancer determine organ-specific metastasis [168]. Besides, CXCR4 positive breast CSCs have been shown to metastasize to the lymph node and lung. Among CD44+CD24- breast CSC populations, a subset of CD44v (variant forms of CD44) populations showed enhanced lung metastasis potential [169]. Studies also suggested that distinct CSC populations display differential metabolic profiles. For instance, breast tumors consist of EMT CSCs and MET CSCs, with EMT CSCs being glycolytic but MET CSCs oxyolytic [100]. In pancreatic cancer, Reichert et al. have shown that EMT-MET plasticity is involved in regulating organotropic metastasis. The authors in this study believe that epithelial plasticity, which is regulated by P120CTN is an important factor for the establishment of cancer cell colonization in liver or lung [100,170]. Investigating whether a specific CSC subtype with a specific metabolic phenotype can metastasize to a specific organ remains a challenge (Fig. 4).

6.3. Exosomes in cancer stem cell-mediated metastasis

Of interest, recent studies also showed that exosomes released by certain primary tumor cells travel to a specific target organ and mediate the formation of PMN. The exosomes released by primary tumor cells carry integrins α6β4 and $\alpha_v\beta5$ to the lung and liver, respectively. The resident cells of liver and lung then receive these integrin-containing exosomes, resulting in the activation of Src phosphorylation and pro-inflammatory S100 gene expression in these target organs, and leading to the formation of PMN [171]. It is unclear whether exosomes released by a specific CSC with a specific phenotype can reach and form a pre-metastatic niche in a specific distant organ. Cancer cells and CSCs communicate continuously with each other by sharing their protein and nucleic acid contents through exosomes [172]. It has been shown that the exosomes derived from a stem cell can fuse with a non-stem cell and convert this non-stem cell into a stem cell. In this process, the stem cell-derived exosome carries stem cell signature proteins, nucleic acids, and other regulatory RNAs, and that they share these contents with the non-stem cell,

transforming from a non-stem cell into a stem cell [173]. Based on this finding, it is possible to suggest that the exosomes derived from CSCs with a specific phenotype can reach a specific organ and can form a pre-metastatic niche in the target organ (Fig. 4).

7. Concluding remarks

The CSCs are self-renewing, drug-resistant cells within the tumor bulk. Understanding their origin, existence, and maintenance and their role in metastasis is crucial to develop an efficient CSC-targeted therapy. Apart from cell fusion and horizontal gene transfer, mutations have been shown to contribute to the origin of CSCs. External factors, such as hypoxia and toxic exposure, induce mutations in differentiated cells and lead to the de-differentiation and reprogramming of these cells into CSCs. It is also possible that a metabolic shift can reprogram somatic or differentiated cancer cells into CSCs. Most studies suggest the existence of distinct CSC population in tumors. The Wnt, Hh, and Notch signaling molecules, along with metabolic regulators such as HIF1α, maintain CSC populations within heterogeneous tumors. Recent evidence fuels the concept that a specific CSC subtype with subtype-specific clonogenic potential and metabolic profiles metastasizes to specific organs.

Figure legends

Figure. 1. The overall journey of CSCs from origin to metastasis. a) Origin of CSCs. Mutations in adult stem cells (ASCs) or differentiated somatic cells can lead to CSC origin. Dedifferentiation of somatic differentiated cell in response to various external toxic exposures can give rise to CSC phenotype. Other factors, such as metabolic reprogramming, cell fusion, and horizontal gene transfer can also induce CSCs. b) Multiple CSC populations reside within tumors. CSCs with detoxification systems such as ABCG2-mediated drug efflux mechanism and ALDH-mediated aldehyde toxic substance detoxification systems exist in various tumors. CSCs expressing cell surface markers such as CD44, CD24, and EpCAM together are also significant constituents within various heterogeneous tumors, such as pancreatic tumors. Other CSC, which express CD133 and CXCR4, also reside within the same tumor. Intestinal tumors consist of Lgr5-expressing CSCs. c) 'Stemness' maintenance mechanisms. The stemness in CSCs is largely maintained by specific stemness molecules such as Wnt/β-catenin, Notch and hedgehog, along with other factors such as YAP, HIF1α, NF-kB, PPARγ, and antiapoptotic. d) Role of CSCs in metastasis. The "seed" and "soil" theory, as proposed by Stephen Paget, states that primary site tumor cells (seed) travel to a distant organ (soil), and colonize and initiate the growth of the tumor. Based on this theory, it is possible that CSCs from the primary site will travel to distant organs to initiate metastatic tumors. Another possible view suggests that exosomes released by CSCs in the primary site travel to target sites and form the pre-metastatic niche (PMN) that supports upcoming CSCs or cancer cells. Another view also suggests that distinct CSC population subtypes with subtype-specific metabolic profiles travel to different organs (organ-specific metastasis).

Figure 1

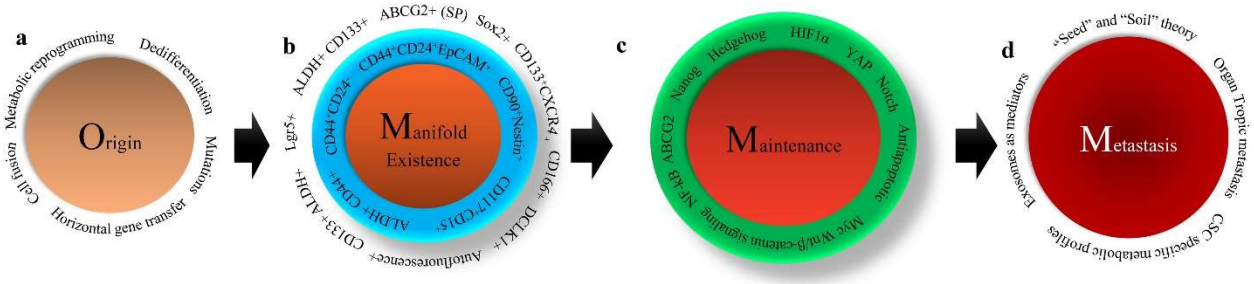
a
Origin
Metabolic reprogramming
Dedifferentiation
Mutations
Horizontal gene transfer
Cell fusion
b
Manifold Existence
ABCG2+ (SP)
Sox2+
CD133+CXCR4+
CD166+
DCLK1+
Autofluorescence+
CD133+ALDH+
ALDH+ CD44+
CD117+CD15+
Lgr5+
CD44+ CD24-
ALDH+ CD133+
CD44+CD24+EpCAM+
CD90+Nestin+
c
Maintenance
Hedgehog
HIF1α
YAP
Notch
Antiapoptotic
Mye Wnt/β-catenin signaling
NF-kB
ABCG2
Nanog
d
Metastasis
"Seed" and "Soil" theory
Organ Tropic metastasis
CSC specific metabolic profiles
Exosomes as mediators

Figure. 2. Different modes of CSC origin. a) 'Cell fusion' is a process whereby two cells (one stem cell and another cancer cell) fuse together to form CSCs. b) In horizontal gene transfer, mutant and fragmented DNA (from a mutant somatic cell that is undergoing apoptosis) is taken up by another somatic or cancer cell, leading to the emergence of CSCs. c) Continuous symmetric divisions in adult stem cells (ASC) lead to mutation in these cells and give rise to CSCs. d) A metabolic shift in somatic or differentiated cells could reprogram these cells into CSCs. e) Ionizing radiation, wounding, or exposure to toxic chemicals can de-differentiate somatic cells into CSCs.

Figure 2

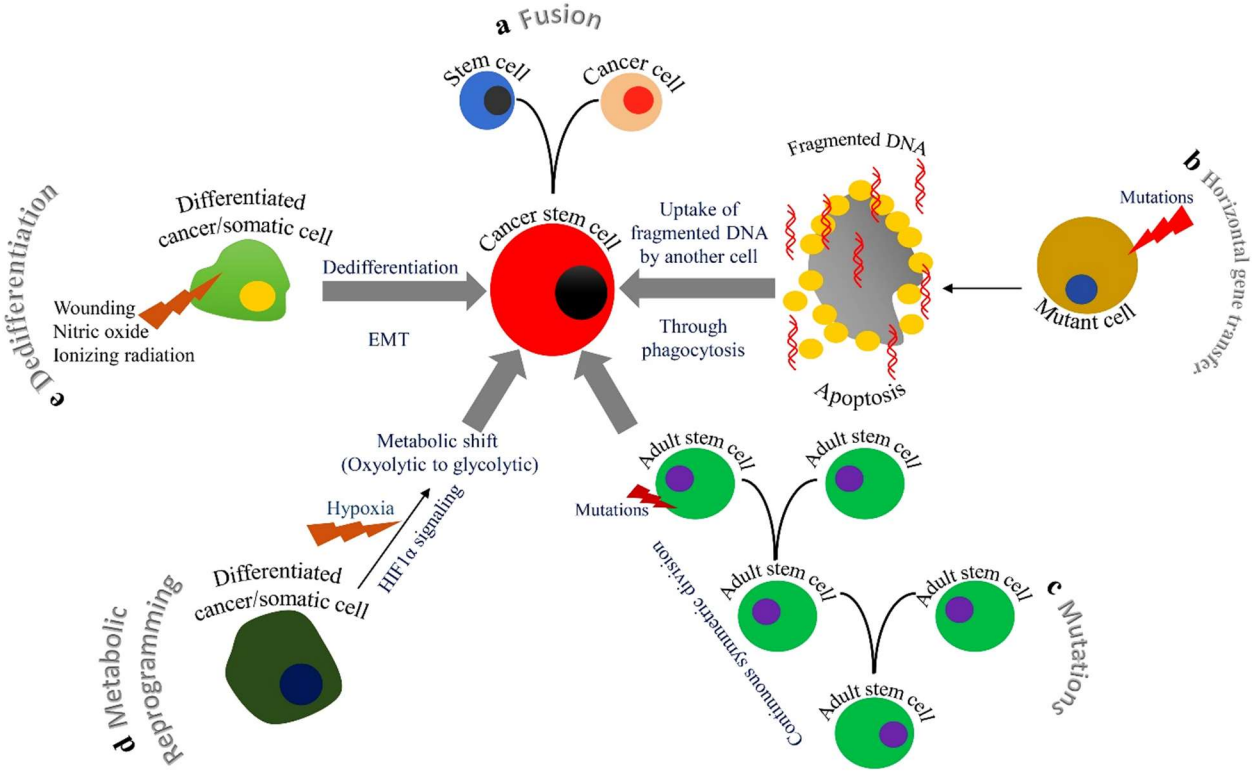
a Fusion
Stem cell
Cancer cell
Fragmented DNA
b Horizontal gene transfer
Mutations
Mutant cell
Uptake of fragmented DNA by another cell
Through phagocytosis
Apoptosis
e Dedifferentiation
Differentiated cancer/somatic cell
Wounding
Nitric oxide
Ionizing radiation
Dedifferentiation
EMT
Cancer stem cell
Metabolic shift (Oxyolytic to glycolytic)
Hypoxia
HIF1α signaling
Differentiated cancer/somatic cell
d Metabolic Reprogramming
Adult stem cell
Mutations
Adult stem cell
Adult stem cell
Continuous symmetric division
Adult stem cell
Adult stem cell
Adult stem cell
c Mutations

Figure. 3. 'Stemness' maintenance pathways in CSCs. a) Canonical Wnt/β-catenin pathway starts with the binding of Wnt ligand to Frizzled receptor (Fzd) and low-density lipoprotein receptor-related protein 5/6 co-receptors (LRP5/6). This results in the recruitment of Axin and disheveled (Dvl) to the plasma membrane and leads to protection of *β*-catenin from degradation. Free *β*-catenin in the cytoplasm then translocates to the nucleus and complexes with TCF/LEF to regulate Wnt target stem cell genes. b) Hh signaling pathway is initiated by binding of hedgehog class of ligands to Patched1 (PTCH1) or Patched2 (PTCH2) receptors. The receptor-ligand binding removes Patched receptor-mediated inhibition of a G-protein coupled protein, Smoothened (Smo), leading to the nuclear translocation of Gli family transcription factors (a glioma-associated oncogene homolog transcription factors). c) Notch signaling is initiated when a notch ligand of a cell binds to the notch receptor of an adjacent cell. This results in the release of the intracellular part of the notch, which translocates into the nucleus and acts as a transcriptional co-activator. When the Notch transcriptional co-activators bind to target gene promoter regions, this leads to the activation of its target CSC genes. d) Phosphorylation of the cytoplasmic portion of CD133 leads to the phosphorylation of AKT. Activated AKT activates the NF-kB pathway, resulting in activation of stemness genes. e) ATP-dependent mechanism of drug efflux by ABC transporters. f) HIF1α and cMyc increase glycolysis (or Warburg effect) and inhibit oxidative phosphorylation in CSCs for rapid energy production. HIF1α activates pyruvate dehydrogenase kinases (PDK1-3), which inhibit pyruvate dehydrogenase (PDH), and thus inhibits oxidative phosphorylation. c-Myc and HIF1α also activate lactate dehydrogenase A (LDHA) to favor the Warburg effect (aerobic glycolysis). C-Myc also activates the GLUT-1 receptor, hexokinase, and phosphofructokinase (PFK) that favor glycolysis.

Figure 3

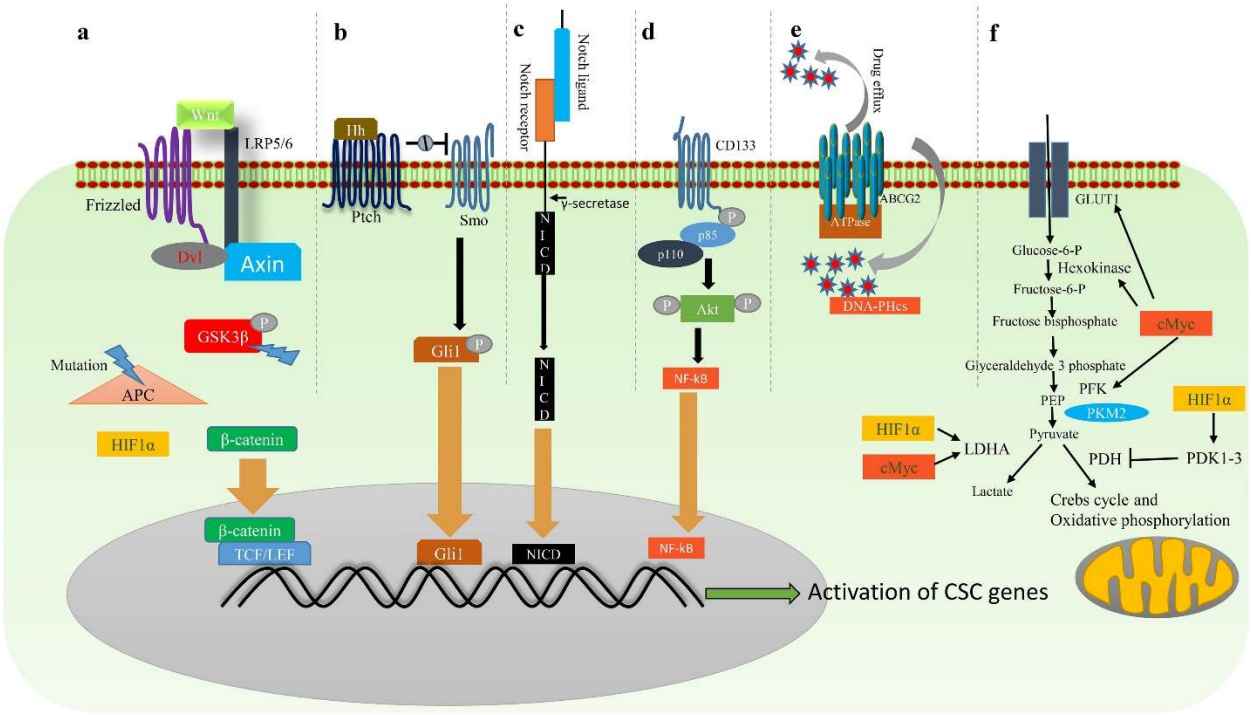
a
b
c
d
e
f
Wnt
LRP5/6
Frizzled
Dvl
Axin
GSK3β
P
Mutation
APC
HIF1α
β-catenin
β-catenin
TCF/LEF
Hh
Ptch
Smo
Gli1
P
Gli1
Notch ligand
Notch receptor
γ-secretase
N
I
C
D
NICD
NICD
CD133
p85
p110
P
Akt
P
NF-kB
NF-kB
Drug efflux
ABCG2
ATPase
DNA-PHcs
GLUT1
Glucose-6-P
Hexokinase
Fructose-6-P
Fructose bisphosphate
cMyc
Glyceraldehyde 3 phosphate
PFK
PEP
PKM2
Pyruvate
HIF1α
cMyc
LDHA
Lactate
PDH
PDK1-3
HIF1α
Crebs cycle and
Oxidative phosphorylation
Activation of CSC genes

Figure. 4. Hypothetical model is showing organ-specific metastasis of CSCs. Distinct CSC populations with differential metabolic profiles (either glycolytic, oxyolytic or intermediate) reside in heterogeneous tumors. The exosomes released by a specific CSC subtype population in the primary tumor site may travel to a specific distant organ to form a pre-metastatic niche (PMN), required for survival of upcoming metastatic CSC.

Figure 4

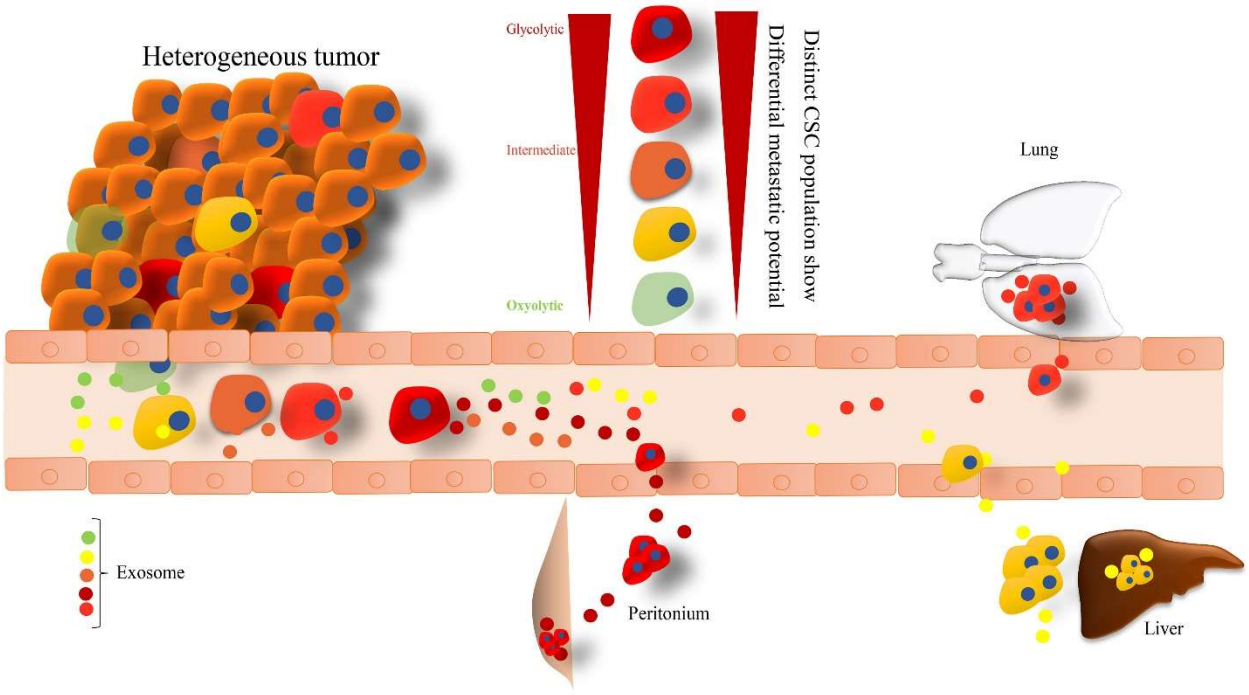
Heterogeneous tumor
Glycolytic
Intermediate
Oxyolytic
Distinct CSC population show
Differential metastatic potential
Lung
Exosome
Peritonium
Liver

TABLE 1

	Tumor Type	Type of Cancer stem cell existed
1	Melanoma	$CD133^+$, $ABCG2^+$, $CD271^+$, $ABCB5^+$, $ALDH1^+$, $CD20^+$, $PD1^+$ and $CXCR6^+$
2	Bladder cancer	$CD44^+$, $CD67LR^+$, EMA^+, $ALDH1A1^+$ and $BCMab1^+$.
3	Breast cancer	$CD44^+CD24^-$, $ALDH^+$, $CD44^+ALDH^+$ and $CD49f^+CD24^+$
5	Leukemia	$CD34^+CD38^-$; $CD34\text{-}Lin^+CD38^+$; $CD45RA^+$; $CD34^+CD38^-CD71^-HLA\text{-}DR^-$;$CD123^+$; $TIM3^+$; $CXCR4^+$
6	Gastric cancer	$Lgr5^+$, $CD26^+$, $CD44^+$, $ALDH1^+$, $CD133^+$
7	Colorectal cancer	CD133+, CD133+CXCR4+, CD44+, CD166+, ALDH+, CD29+, Lgr5+ and CD44+CD24+EpCAM+
8	Ovarian cancer	CD44+, CD24+, CD117+ and CD133+
9	Head and Neck cancers	CD44+, CD133+, ALDH+, CD98+, CD200+, GRP78+, ALDH+CD44+ and Bmi1+
10	Liver cancer	CD133+, ALDH+, CD44+, CD90+, CD13+, OV6+, EpCAM+, ABCG2+ (side population), DLK1+, K19+ and c-Kit+
11	Lung cancer	$CD44^+$, $CD87^+$, $CD90^+$, $CD117^+$, $CD133^+$, $CD166^+$, $ALDH^+$, $BMI1^+$, $EpCAM^+$ and Side population.
12	Pancreatic cancer	$CD44^+$, $CD133^+$, $ALDH1^+$, Side population, $CD44^+CD24^+EpCAM^+$, $autofluorescence^+$ and $CD133^+CXCR4^+$

REFERENCES

[1] S. Makino, The role of tumor stem-cells in regrowth of the tumor following drastic applications, Acta - Unio Internationalis Contra Cancrum, 15(Suppl 1) (1959) 196-198.

[2] C.V. Konrad, R. Murali, B.A. Varghese, R. Nair, The role of cancer stem cells in tumor heterogeneity and resistance to therapy, Canadian journal of physiology and pharmacology, 95 (2017) 1-15.

[3] T. Lapidot, C. Sirard, J. Vormoor, A cell initiating human acute myeloid leukemia after transplantation into SCID mice, Nature, 367 (1994).

[4] J. Chen, Y. Li, T.S. Yu, R.M. McKay, D.K. Burns, S.G. Kernie, L.F. Parada, A restricted cell population propagates glioblastoma growth following chemotherapy, Nature, 488 (2012) 522-526.

[5] G. Driessens, B. Beck, A. Caauwe, B.D. Simons, C. Blanpain, Defining the mode of tumor growth by clonal analysis, Nature, 488 (2012) 527-530.

[6] A.G. Schepers, H.J. Snippert, D.E. Stange, M. van den Born, J.H. van Es, M. van de Wetering, H. Clevers, Lineage Tracing Reveals Lgr5+ Stem Cell Activity in Mouse Intestinal Adenomas, Science (New York, N.Y.), 337 (2012) 730-735.

[7] P.R. Prasetyanti, J.P. Medema, Intra-tumor heterogeneity from a cancer stem cell perspective, Molecular cancer, 16 (2017) 41.

[8] P. Sancho, E. Burgos-Ramos, A. Tavera, T. Bou Kheir, P. Jagust, M. Schoenhals, D. Barneda, K. Sellers, R. Campos-Olivas, O. Graña, Catarina R. Viera, M. Yuneva, B. Sainz, C. Heeschen, MYC/PGC-1α Balance Determines the Metabolic Phenotype and Plasticity of Pancreatic Cancer Stem Cells, Cell Metabolism, 22 (2015) 590-605.

[9] S.J. Conley, E. Gheordunescu, P. Kakarala, B. Newman, H. Korkaya, A.N. Heath, S.G. Clouthier, M.S. Wicha, Antiangiogenic agents increase breast cancer stem cells via the generation of tumor hypoxia, Proceedings of the National Academy of Sciences of the United States of America, 109 (2012) 2784-2789.

[10] M. Cioffi, C. D'Alterio, R. Camerlingo, V. Tirino, C. Consales, A. Riccio, C. Ierano, S.C. Cecere, N.S. Losito, S. Greggi, S. Pignata, G. Pirozzi, S. Scala, Identification of a distinct population of CD133(+)CXCR4(+) cancer stem cells in ovarian cancer, Sci Rep, 5 (2015).

[11] P.C. Hermann, S.L. Huber, T. Herrler, A. Aicher, J.W. Ellwart, M. Guba, C.J. Bruns, C. Heeschen, Distinct populations of cancer stem cells determine tumor growth and metastatic activity in human pancreatic cancer, Cell Stem Cell, 1 (2007) 313-323.

[12] B. Costa-Silva, N.M. Aiello, A.J. Ocean, S. Singh, H. Zhang, Basant K. Thakur, A. Becker, A. Hoshino, M.T. Mark, H. Molina, J. Xiang, T. Zhang, T.-M. Theilen, G. García-Santos, C. Williams, Y. Ararso, Y. Huang, G. Rodrigues, T.-L. Shen, K.J. Labori, I.M.B. Lothe, E.H. Kure, J. Hernandez, A. Doussot, S.H. Ebbesen, Paul M. Grandgenett, Michael A. Hollingsworth, M. Jain, K. Mallya, S.K. Batra, William R. Jarnagin, Robert E. Schwartz, I. Matei, H. Peinado, B.Z. Stanger, J. Bromberg, D. Lyden, Pancreatic cancer exosomes initiate pre-metastatic niche formation in the liver, Nature Cell Biology, 17 (2015) 816.

[13] Z. Yu, S. Zhao, L. Ren, L. Wang, Z. Chen, R.M. Hoffman, J. Zhou, Pancreatic cancer-derived exosomes promote tumor metastasis and liver pre-metastatic niche formation, Oncotarget, 8 (2017) 63461-63483.

[14] F. Mercati, L. Pascucci, P. Ceccarelli, C. Dall'Aglio, V. Pedini, A.M. Gargiulo, Expression of mesenchymal stem cell marker CD90 on dermal sheath cells of the anagen hair follicle in canine species, European journal of histochemistry: EJH, 53 (2009) 159-166.

[15] J. He, Y. Liu, T. Zhu, J. Zhu, F. Dimeco, A.L. Vescovi, J.A. Heth, K.M. Muraszko, X. Fan, D.M. Lubman, CD90 is identified as a candidate marker for cancer stem cells in primary high-grade gliomas using tissue microarrays, Molecular & cellular proteomics: MCP, 11 (2012) M111.010744.

[16] N. Fujita, N. Yaegashi, Y. Ide, S. Sato, M. Nakamura, I. Ishiwata, A. Yajima, Expression of CD44 in normal human versus tumor endometrial tissues: possible implication of reduced expression of CD44 in lymph-vascular space involvement of cancer cells, Cancer Res, 54 (1994) 3922-3928.

[17] I. Ben-Porath, M.W. Thomson, V.J. Carey, R. Ge, G.W. Bell, A. Regev, R.A. Weinberg, An embryonic stem cell-like gene expression signature in poorly differentiated aggressive human tumors, Nat Genet, 40 (2008) 499-507.

[18] T. Dvash, Y. Mayshar, H. Darr, M. McElhaney, D. Barker, O. Yanuka, K.J. Kotkow, L.L. Rubin, N. Benvenisty, R. Eiges, Temporal gene expression during differentiation of human embryonic stem cells and embryoid bodies, Human Reproduction, 19 (2004) 2875-2883.

[19] K. Okita, S. Yamanaka, Intracellular signaling pathways regulating pluripotency of embryonic stem cells, Current stem cell research & therapy, 1 (2006) 103-111.

[20] B.-S. Moon, W.-J. Jeong, J. Park, T.I. Kim, D.S. Min, K.-Y. Choi, Role of oncogenic K-Ras in cancer stem cell activation by aberrant Wnt/β-catenin signaling, Journal of the National Cancer Institute, 106 (2014) djt373.

[21] C. Karamboulas, L. Ailles, Developmental signaling pathways in cancer stem cells of solid tumors, Biochim Biophys Acta, 1830 (2013) 2481-2495.

[22] Y.X. Jiang, S.W. Yang, P.A. Li, X. Luo, Z.Y. Li, Y.X. Hao, P.W. Yu, The promotion of the transformation of quiescent gastric cancer stem cells by IL-17 and the underlying mechanisms, Oncogene, 36 (2016) 1256.

[23] H. Kojima, T. Okumura, T. Yamaguchi, T. Miwa, Y. Shimada, T. Nagata, Enhanced cancer stem cell properties of a mitotically quiescent subpopulation of p75NTR-positive cells in esophageal squamous cell carcinoma, Int J Oncol, 51 (2017) 49-62.

[24] M.D. Samant, C.M. Jackson, C.L. Felix, A.J. Jones, D.W. Goodrich, B.A. Foster, W.J. Huss, Multi-Drug Resistance ABC Transporter Inhibition Enhances Murine Ventral Prostate Stem/Progenitor Cell Differentiation, Stem Cells Dev, 24 (2015) 1236-1251.

[25] T. Dittmar, C. Nagler, S. Schwitalla, G. Reith, B. Niggemann, K.S. Zänker, Recurrence cancer stem cells – Made by cell fusion?, Medical Hypotheses, 73 (2009) 542-547.

[26] A.Z. Rizvi, J.R. Swain, P.S. Davies, A.S. Bailey, A.D. Decker, H. Willenbring, M. Grompe, W.H. Fleming, M.H. Wong, Bone marrow-derived cells fuse with normal and transformed intestinal stem cells, Proceedings of the National Academy of Sciences, 103 (2006) 6321-6325.

[27] J.J. Spies, S.M.C. van Wyk, Cell fusion: A possible mechanism for the origin of polyploidy, South African Journal of Botany, 61 (1995) 60-65.

[28] S. Zhang, I. Mercado-Uribe, Z. Xing, B. Sun, J. Kuang, J. Liu, Generation of Cancer Stem-like Cells through Formation of Polyploid Giant Cancer Cells, Oncogene, 33 (2014) 10.1038/onc.2013.1096.

[29] R. Bjerkvig, B.B. Tysnes, K.S. Aboody, J. Najbauer, A.J.A. Terzis, The origin of the cancer stem cell: current controversies and new insights, Nature reviews. Cancer, 5 (2005) 899-904.

[30] K.L. Palmer, V.N. Kos, M.S. Gilmore, Horizontal Gene Transfer and the Genomics of Enterococcal Antibiotic Resistance, Current opinion in microbiology, 13 (2010) 632-639.

[31] L. Holmgren, A. Szeles, E. Rajnavölgyi, J. Folkman, G. Klein, I. Ernberg, K.I. Falk, Horizontal Transfer of DNA by the Uptake of Apoptotic Bodies, Blood, 93 (1999) 3956-3963.

[32] R. Gealy, L. Zhang, J.M. Siegfried, J.D. Luketich, P. Keohavong, Comparison of mutations in the p53 and K-ras genes in lung carcinomas from smoking and nonsmoking women, Cancer epidemiology, biomarkers & prevention : a publication of the American Association for Cancer Research, cosponsored by the American Society of Preventive Oncology, 8 (1999) 297-302.

[33] H. Fujimori, M. Shikanai, H. Teraoka, M. Masutani, K. Yoshioka, Induction of cancerous stem cells during embryonic stem cell differentiation, J Biol Chem, 287 (2012) 36777-36791.

[34] E.J. Tokar, B.A. Diwan, M.P. Waalkes, Arsenic exposure transforms human epithelial stem/progenitor cells into a cancer stem-like phenotype, Environmental health perspectives, 118 (2010) 108-115.

[35] R. Rodriguez, R. Rubio, P. Menendez, Modeling sarcomagenesis using multipotent mesenchymal stem cells, Cell research, 22 (2012) 62-77.

[36] S. Alcantara Llaguno, J. Chen, C.H. Kwon, E.L. Jackson, Y. Li, D.K. Burns, A. Alvarez-Buylla, L.F. Parada, Malignant astrocytomas originate from neural stem/progenitor cells in a somatic tumor suppressor mouse model, Cancer cell, 15 (2009) 45-56.

[37] F. Blokzijl, J. de Ligt, M. Jager, V. Sasselli, S. Roerink, N. Sasaki, M. Huch, S. Boymans, E. Kuijk, P. Prins, I.J. Nijman, I. Martincorena, M. Mokry, C.L. Wiegerinck, S. Middendorp, T. Sato,

G. Schwank, E.E.S. Nieuwenhuis, M.M.A. Verstegen, L.J.W. van der Laan, J. de Jonge, J.N.M. Ijzermans, R.G. Vries, M. van de Wetering, M.R. Stratton, H. Clevers, E. Cuppen, R. van Boxtel, Tissue-specific mutation accumulation in human adult stem cells during life, Nature, 538 (2016) 260-264.

[38] E.V. Abel, E.J. Kim, J. Wu, M. Hynes, F. Bednar, E. Proctor, L. Wang, M.L. Dziubinski, D.M. Simeone, The Notch Pathway Is Important in Maintaining the Cancer Stem Cell Population in Pancreatic Cancer, PLOS ONE, 9 (2014) e91983.

[39] G. Lee, B. Auffinger, D. Guo, T. Hasan, M. Deheeger, A.L. Tobias, J.Y. Kim, F. Atashi, L. Zhang, M.S. Lesniak, C.D. James, A.U. Ahmed, Dedifferentiation of Glioma Cells to Glioma Stem-like Cells By Therapeutic Stress-induced HIF Signaling in the Recurrent GBM Model, Molecular cancer therapeutics, 15 (2016) 3064-3076.

[40] P. Wang, C. Lan, S. Xiong, X. Zhao, Y. Shan, R. Hu, W. Wan, S. Yu, B. Liao, G. Li, J. Wang, D. Zou, B. Chen, H. Feng, N. Wu, HIF1α regulates single differentiated glioma cell dedifferentiation to stem-like cell phenotypes with high tumorigenic potential under hypoxia, Oncotarget, 8 (2017) 28074-28092.

[41] G. Donati, E. Rognoni, T. Hiratsuka, K. Liakath-Ali, E. Hoste, G. Kar, M. Kayikci, R. Russell, K. Kretzschmar, K.W. Mulder, S.A. Teichmann, F.M. Watt, Wounding induces dedifferentiation of epidermal Gata6+ cells and acquisition of stem cell properties, Nat Cell Biol, 19 (2017) 603-613.

[42] S.Y. Lee, E.K. Jeong, M.K. Ju, H.M. Jeon, M.Y. Kim, C.H. Kim, H.G. Park, S.I. Han, H.S. Kang, Induction of metastasis, cancer stem cell phenotype, and oncogenic metabolism in cancer cells by ionizing radiation, Molecular cancer, 16 (2017).

[43] K. Miura, K. Kimura, R. Amano, S. Yamazoe, G. Ohira, K. Nishio, N. Kametani, K. Hirakawa, M. Ohira, Analysis of the origin of anaplastic pancreatic cancer and the mechanism of its dedifferentiation, Journal of Hepato-Biliary-Pancreatic Sciences, 24 (2017) 176-184.

[44] M.V. Liberti, J.W. Locasale, The Warburg Effect: How Does it Benefit Cancer Cells?, Trends in Biochemical Sciences, 41 211-218.

[45] D. Ciavardelli, C. Rossi, D. Barcaroli, S. Volpe, A. Consalvo, M. Zucchelli, A. De Cola, E. Scavo, R. Carollo, D. D'Agostino, F. Forli, S. D'Aguanno, M. Todaro, G. Stassi, C. Di Ilio, V. De

Laurenzi, A. Urbani, Breast cancer stem cells rely on fermentative glycolysis and are sensitive to 2-deoxyglucose treatment, Cell Death Dis, 5 (2014) e1336.

[46] A. Pasto, C. Bellio, G. Pilotto, V. Ciminale, M. Silic-Benussi, G. Guzzo, A. Rasola, C. Frasson, G. Nardo, E. Zulato, M.O. Nicoletto, M. Manicone, S. Indraccolo, A. Amadori, Cancer stem cells from epithelial ovarian cancer patients privilege oxidative phosphorylation and resist glucose deprivation, Oncotarget, 5 (2014) 4305-4319.

[47] Clifford D.L. Folmes, Timothy J. Nelson, A. Martinez-Fernandez, D.K. Arrell, Jelena Z. Lindor, Petras P. Dzeja, Y. Ikeda, C. Perez-Terzic, A. Terzic, Somatic Oxidative Bioenergetics Transitions into Pluripotency-Dependent Glycolysis to Facilitate Nuclear Reprogramming, Cell Metabolism, 14 264-271.

[48] D. Bonnet, J.E. Dick, Human acute myeloid leukemia is organized as a hierarchy that originates from a primitive hematopoietic cell, Nat Med, 3 (1997) 730-737.

[49] C.V. Cox, R.S. Evely, A. Oakhill, D.H. Pamphilon, N.J. Goulden, A. Blair, Characterization of acute lymphoblastic leukemia progenitor cells, Blood, 104 (2004) 2919-2925.

[50] S. Tavor, I. Petit, S. Porozov, A. Avigdor, A. Dar, L. Leider-Trejo, N. Shemtov, V. Deutsch, E. Naparstek, A. Nagler, T. Lapidot, CXCR4 regulates migration and development of human acute myelogenous leukemia stem cells in transplanted NOD/SCID mice, Cancer Res, 64 (2004) 2817-2824.

[51] Y. Kikushige, T. Miyamoto, Identification of TIM-3 as a Leukemic Stem Cell Surface Molecule in Primary Acute Myeloid Leukemia, Oncology, 89 Suppl 1 (2015) 28-32.

[52] A. Al-Mawali, D. Gillis, I. Lewis, Immunoprofiling of leukemic stem cells CD34+/CD38-/CD123+ delineate FLT3/ITD-positive clones, J Hematol Oncol, 9 (2016) 61.

[53] B. Kersten, M. Valkering, R. Wouters, R. van Amerongen, D. Hanekamp, Z. Kwidama, P. Valk, G. Ossenkoppele, W. Zeijlemaker, G. Kaspers, J. Cloos, G.J. Schuurhuis, CD45RA, a specific marker for leukemia stem cell subpopulations in acute myeloid leukemia, Br J Haematol, 173 (2016) 219-235.

[54] Q. Sun, C.C. So, S.F. Yip, T.S. Wan, S.K. Ma, L.C. Chan, Functional alterations of Lin-CD34+CD38+ cells in chronic myelomonocytic leukemia and on progression to acute leukemia, Leuk Res, 32 (2008) 1374-1381.

[55] E. Monzani, F. Facchetti, E. Galmozzi, E. Corsini, A. Benetti, C. Cavazzin, A. Gritti, A. Piccinini, D. Porro, M. Santinami, G. Invernici, E. Parati, G. Alessandri, C.A. La Porta, Melanoma contains CD133 and ABCG2 positive cells with enhanced tumourigenic potential, Eur J Cancer, 43 (2007) 935-946.

[56] Y. Luo, K. Dallaglio, Y. Chen, W.A. Robinson, S.E. Robinson, M.D. McCarter, J. Wang, R. Gonzalez, D.C. Thompson, D.A. Norris, D.R. Roop, V. Vasiliou, M. Fujita, ALDH1A isozymes are markers of human melanoma stem cells and potential therapeutic targets, Stem Cells, 30 (2012) 2100-2113.

[57] A. Fusi, U. Reichelt, A. Busse, S. Ochsenreither, A. Rietz, M. Maisel, U. Keilholz, Expression of the stem cell markers nestin and CD133 on circulating melanoma cells, J Invest Dermatol, 131 (2011) 487-494.

[58] A.D. Boiko, O.V. Razorenova, M. van de Rijn, S.M. Swetter, D.L. Johnson, D.P. Ly, Human melanoma-initiating cells express neural crest nerve growth factor receptor CD271, Nature, 466 (2010).

[59] D. Fang, T.K. Nguyen, K. Leishear, R. Finko, A.N. Kulp, S. Hotz, P.A. Van Belle, X. Xu, D.E. Elder, M. Herlyn, A tumorigenic subpopulation with stem cell properties in melanomas, Cancer Res, 65 (2005) 9328-9337.

[60] C. Li, Y. Du, Z. Yang, L. He, Y. Wang, L. Hao, M. Ding, R. Yan, J. Wang, Z. Fan, GALNT1-Mediated Glycosylation and Activation of Sonic Hedgehog Signaling Maintains the Self-Renewal and Tumor-Initiating Capacity of Bladder Cancer Stem Cells, Cancer Res, 76 (2016) 1273-1283.

[61] P. Huang, M. Watanabe, H. Kaku, H. Ueki, H. Noguchi, M. Sugimoto, T. Hirata, H. Yamada, K. Takei, S. Zheng, K. Xu, Y. Nasu, Y. Fujii, C. Liu, H. Kumon, Cancer stem cell-like characteristics of a CD133(+) subpopulation in the J82 human bladder cancer cell line, Molecular and clinical oncology, 1 (2013) 180-184.

[62] H.A. Kenny, C.Y. Chiang, E.A. White, E.M. Schryver, M. Habis, I.L. Romero, A. Ladanyi, C.V. Penicka, J. George, K. Matlin, A. Montag, K. Wroblewski, S.D. Yamada, A.P. Mazar, D. Bowtell, E. Lengyel, Mesothelial cells promote early ovarian cancer metastasis through fibronectin secretion, J Clin Invest, 124 (2014).

[63] J.D. Lathia, S.C. Mack, E.E. Mulkearns-Hubert, C.L.L. Valentim, J.N. Rich, Cancer stem cells in glioblastoma, Genes & Development, 29 (2015) 1203-1217.

[64] J. Muto, T. Imai, D. Ogawa, Y. Nishimoto, Y. Okada, Y. Mabuchi, T. Kawase, A. Iwanami, P.S. Mischel, H. Saya, K. Yoshida, Y. Matsuzaki, H. Okano, RNA-Binding Protein Musashi1 Modulates Glioma Cell Growth through the Post-Transcriptional Regulation of Notch and PI3 Kinase/Akt Signaling Pathways, PLOS ONE, 7 (2012) e33431.

[65] T.A. Read, M.P. Fogarty, S.L. Markant, R.E. McLendon, Z. Wei, D.W. Ellison, P.G. Febbo, R.J. Wechsler-Reya, Identification of CD15 as a marker for tumor-propagating cells in a mouse model of medulloblastoma, Cancer cell, 15 (2009) 135-147.

[66] S. Liu, Y. Cong, D. Wang, Y. Sun, L. Deng, Y. Liu, R. Martin-Trevino, L. Shang, S.P. McDermott, M.D. Landis, S. Hong, A. Adams, R. D'Angelo, C. Ginestier, E. Charafe-Jauffret, S.G. Clouthier, D. Birnbaum, S.T. Wong, M. Zhan, J.C. Chang, M.S. Wicha, Breast cancer stem cells transition between epithelial and mesenchymal states reflective of their normal counterparts, Stem cell reports, 2 (2014) 78-91.

[67] N. Duru, R. Gernapudi, P.K. Lo, Y. Yao, B. Wolfson, Y. Zhang, Q. Zhou, Characterization of the CD49f+/CD44+/CD24- single-cell derived stem cell population in basal-like DCIS cells, Oncotarget, 7 (2016) 47511-47525.

[68] B. Wang, Q. Chen, Y. Cao, X. Ma, C. Yin, Y. Jia, A. Zang, W. Fan, LGR5 Is a Gastric Cancer Stem Cell Marker Associated with Stemness and the EMT Signature Genes NANOG, NANOGP8, PRRX1, TWIST1, and BMI1, PLoS One, 11 (2016) e0168904.

[69] D. Brungs, M. Aghmesheh, K.L. Vine, T.M. Becker, M.G. Carolan, M. Ranson, Gastric cancer stem cells: evidence, potential markers, and clinical implications, Journal of Gastroenterology, 51 (2016) 313-326.

[70] W. Wu, J. Cao, Z. Ji, J. Wang, T. Jiang, H. Ding, Co-expression of Lgr5 and CXCR4 characterizes cancer stem-like cells of colorectal cancer, Oncotarget, 7 (2016) 81144-81155.

[71] S.S. Zhang, Z.P. Han, Y.Y. Jing, S.F. Tao, T.J. Li, H. Wang, Y. Wang, R. Li, Y. Yang, X. Zhao, X.D. Xu, E.D. Yu, Y.C. Rui, H.J. Liu, L. Zhang, L.X. Wei, CD133(+)CXCR4(+) colon cancer cells exhibit metastatic potential and predict poor prognosis of patients, BMC medicine, 10 (2012) 85.

[72] P. Chandrakesan, J. Yao, D. Qu, R. May, N. Weygant, Y. Ge, N. Ali, S.M. Sureban, M. Gude, K. Vega, E. Bannerman-Menson, L. Xia, M. Bronze, G. An, C.W. Houchen, Dclk1, a tumor stem cell marker, regulates pro-survival signaling and self-renewal of intestinal tumor cells, Mol Cancer, 16 (2017) 30.

[73] I. Conic, Z. Stanojevic, L. Jankovic Velickovic, S. Stojnev, A. Ristic Petrovic, M. Krstic, M. Stanojevic, D. Bogdanovic, V. Stefanovic, Epithelial ovarian cancer with CD117 phenotype is highly aggressive and resistant to chemotherapy, The journal of obstetrics and gynecology research, 41 (2015) 1630-1637.

[74] F. Bhaijee, D.J. Pepper, K.T. Pitman, D. Bell, Cancer stem cells in head and neck squamous cell carcinoma: A review of current knowledge and future applications, Head & Neck, 34 (2012) 894-899.

[75] Y.S. Jung, P.D. Vermeer, D.W. Vermeer, S.J. Lee, A.R. Goh, H.J. Ahn, J.H. Lee, CD200: association with cancer stem cell features and response to chemoradiation in head and neck squamous cell carcinoma, Head Neck, 37 (2015) 327-335.

[76] S. Ma, K.W. Chan, T.K. Lee, K.H. Tang, J.Y. Wo, B.J. Zheng, X.Y. Guan, Aldehyde dehydrogenase discriminates the CD133 liver cancer stem cell populations, Mol Cancer Res, 6 (2008) 1146-1153.

[77] M.S. Rozeik, O.A. Hammam, A.I. Ali, M. Magdy, H. Khalil, A. Anas, A.A. Abo El Hassan, A.A. Rahim, A.I. El-Shabasy, Evaluation of CD44 and CD133 as markers of liver cancer stem cells in Egyptian patients with HCV-induced chronic liver diseases versus hepatocellular carcinoma, Electronic physician, 9 (2017) 4708-4717.

[78] Z.F. Yang, D.W. Ho, M.N. Ng, C.K. Lau, W.C. Yu, P. Ngai, P.W. Chu, C.T. Lam, R.T. Poon, S.T. Fan, Significance of CD90+ cancer stem cells in human liver cancer, Cancer Cell, 13 (2008) 153-166.

[79] K. Okudela, T. Woo, H. Mitsui, M. Tajiri, M. Masuda, K. Ohashi, Expression of the potential cancer stem cell markers, CD133, CD44, ALDH1, and beta-catenin, in primary lung adenocarcinoma--their prognostic significance, Pathology international, 62 (2012) 792-801.

[80] N. Zakaria, N.M. Yusoff, Z. Zakaria, M.N. Lim, P.J. Baharuddin, K.S. Fakiruddin, B. Yahaya, Human non-small cell lung cancer expresses putative cancer stem cell markers and exhibits the transcriptomic profile of multipotent cells, BMC Cancer, 15 (2015) 84.

[81] A.P. Vaz, M.P. Ponnusamy, P. Seshacharyulu, S.K. Batra, A concise review on the current understanding of pancreatic cancer stem cells, Journal of cancer stem cell research, 2 (2014) e1004.

[82] I. Miranda-Lorenzo, J. Dorado, E. Lonardo, S. Alcala, A.G. Serrano, J. Clausell-Tormos, M. Cioffi, D. Megias, S. Zagorac, A. Balic, M. Hidalgo, M. Erkan, J. Kleeff, A. Scarpa, B. Sainz Jr, C. Heeschen, Intracellular autofluorescence: a biomarker for epithelial cancer stem cells, Nat Meth, 11 (2014) 1161-1169.

[83] N. Kim, H.K. Choung, M.J. Lee, S.I. Khwarg, J.E. Kim, Cancer Stem Cell Markers in Eyelid Sebaceous Gland Carcinoma: High Expression of ALDH1, CD133, and ABCG2 Correlates With Poor Prognosis, Investigative ophthalmology & visual science, 56 (2015) 1813-1819.

[84] S. Yanamoto, S. Yamada, H. Takahashi, T. Naruse, Y. Matsushita, H. Ikeda, T. Shiraishi, S. Seki, S. Fujita, T. Ikeda, I. Asahina, M. Umeda, Expression of the cancer stem cell markers CD44v6 and ABCG2 in tongue cancer: effect of neoadjuvant chemotherapy on local recurrence, Int J Oncol, 44 (2014) 1153-1162.

[85] Y. Bi, Y. Meng, H. Wu, Q. Cui, Y. Luo, X. Xue, Expression of the potential cancer stem cell markers CD133 and CD44 in medullary thyroid carcinoma: A ten-year follow-up and prognostic analysis, Journal of surgical oncology, 113 (2016) 144-151.

[86] S.S. Elbasateeny, A.A. Salem, W.A. Abdelsalam, R.A. Salem, Immunohistochemical expression of cancer stem cell related markers CD44 and CD133 in endometrial cancer, Pathology, research and practice, 212 (2016) 10-16.

[87] T. Nagata, C. Sakakura, S. Komiyama, A. Miyashita, M. Nishio, Y. Murayama, S. Komatsu, A. Shiozaki, Y. Kuriu, H. Ikoma, M. Nakanishi, D. Ichikawa, H. Fujiwara, K. Okamoto, T. Ochiai, Y. Kokuba, T. Sonoyama, E. Otsuji, Expression of cancer stem cell markers CD133 and CD44 in locoregional recurrence of rectal cancer, Anticancer Res, 31 (2011) 495-500.

[88] A. Lukenda, S. Dotlic, N. Vukojevic, B. Saric, S. Vranic, K. Zarkovic, Expression and prognostic value of putative cancer stem cell markers CD117 and CD15 in choroidal and ciliary body melanoma, J Clin Pathol, 69 (2016) 234-239.

[89] A. Matsika, B. Srinivasan, C. Day, S.A. Mader, D.M. Kiernan, A. Broomfield, J. Fu, J.D. Hooper, J.G. Kench, H. Samaratunga, Cancer stem cell markers in prostate cancer: an immunohistochemical study of ALDH1, SOX2 and EZH2, Pathology, 47 (2015) 622-628.

[90] J. Skoda, A. Nunukova, T. Loja, I. Zambo, J. Neradil, P. Mudry, K. Zitterbart, M. Hermanova, A. Hampl, J. Sterba, R. Veselska, Cancer stem cell markers in pediatric sarcomas: Sox2 is associated with tumorigenicity in immunodeficient mice, Tumour Biol, 37 (2016) 9535-9548.

[91] J.Q. Feng, Z.Y. Xu, L.J. Shi, L. Wu, W. Liu, Z.T. Zhou, Expression of cancer stem cell markers ALDH1 and Bmi1 in oral erythroplakia and the risk of oral cancer, Journal of oral pathology & medicine : official publication of the International Association of Oral Pathologists and the American Academy of Oral Pathology, 42 (2013) 148-153.

[92] S. Karmakar, P. Seshacharyulu, I. Lakshmanan, A.P. Vaz, S. Chugh, Y.M. Sheinin, S. Mahapatra, S.K. Batra, M.P. Ponnusamy, hPaf1/PD2 interacts with OCT3/4 to promote self-renewal of ovarian cancer stem cells, Oncotarget, 8 (2017) 14806-14820.

[93] A.P. Vaz, M.P. Ponnusamy, S. Rachagani, P. Dey, A.K. Ganti, S.K. Batra, Novel role of pancreatic differentiation 2 in facilitating self-renewal and drug resistance of pancreatic cancer stem cells, British journal of cancer, 111 (2014) 486-496.

[94] R.K. Nimmakayala, P. Seshacharyulu, I. Lakshmanan, S. Rachagani, S. Chugh, S. Karmakar, S. Rauth, R. Vengoji, P. Atri, G.A. Talmon, S.M. Lele, L.M. Smith, I. Thapa, D. Bastola,

M.M. Ouellette, S.K. Batra, M.P. Ponnusamy, Cigarette Smoke Induces Stem Cell Features of Pancreatic Cancer Cells via PAF1, Gastroenterology, 155 (2018) 892-908.e896.

[95] Z. Wang, Q. Shi, Z. Wang, Y. Gu, Y. Shen, M. Sun, M. Deng, H. Zhang, J. Fang, S. Zhang, F. Xie, Clinicopathologic correlation of cancer stem cell markers CD44, CD24, VEGF and HIF-1alpha in ductal carcinoma in situ and invasive ductal carcinoma of breast: an immunohistochemistry-based pilot study, Pathology, research and practice, 207 (2011) 505-513.

[96] J. Zhang, E. Nuebel, G.Q. Daley, C.M. Koehler, M.A. Teitell, Metabolic Regulation in Pluripotent Stem Cells during Reprogramming and Self-Renewal, Cell stem cell, 11 (2012) 589-595.

[97] Y.A. Shen, Metabolic reprogramming orchestrates cancer stem cell properties in, 14 (2015) 86-98.

[98] I.-S. Song, Y.J. Jeong, J. Han, Mitochondrial metabolism in cancer stem cells: a therapeutic target for colon cancer, BMB Reports, 48 (2015) 539-540.

[99] E. Vlashi, C. Lagadec, L. Vergnes, T. Matsutani, K. Masui, M. Poulou, R. Popescu, L. Della Donna, P. Evers, C. Dekmezian, K. Reue, H. Christofk, P.S. Mischel, F. Pajonk, Metabolic state of glioma stem cells and nontumorigenic cells, Proceedings of the National Academy of Sciences, 108 (2011) 16062-16067.

[100] L. Gammon, A. Biddle, H.K. Heywood, A.C. Johannessen, I.C. Mackenzie, Sub-Sets of Cancer Stem Cells Differ Intrinsically in Their Patterns of Oxygen Metabolism, PLOS ONE, 8 (2013) e62493.

[101] A. Roesch, M. Fukunaga-Kalabis, E.C. Schmidt, S.E. Zabierowski, P.A. Brafford, A. Vultur, D. Basu, P. Gimotty, T. Vogt, M. Herlyn, A temporarily distinct subpopulation of slow-cycling melanoma cells is required for continuous tumor growth, Cell, 141 (2010) 583-594.

[102] C.L. Chaffer, I. Brueckmann, C. Scheel, A.J. Kaestli, P.A. Wiggins, L.O. Rodrigues, M. Brooks, F. Reinhardt, Y. Su, K. Polyak, L.M. Arendt, C. Kuperwasser, B. Bierie, R.A. Weinberg, Normal and neoplastic nonstem cells can spontaneously convert to a stem-like state, Proc Natl Acad Sci U S A, 108 (2011) 7950-7955.

[103] M.L. Suva, N. Riggi, B.E. Bernstein, Epigenetic reprogramming in cancer, Science, 339 (2013) 1567-1570.

[104] H. Korkaya, A. Paulson, E. Charafe-Jauffret, C. Ginestier, M. Brown, J. Dutcher, S.G. Clouthier, M.S. Wicha, Regulation of mammary stem/progenitor cells by PTEN/Akt/beta-catenin signaling, PLoS Biol, 7 (2009) e1000121.

[105] S. Schwitalla, A.A. Fingerle, P. Cammareri, T. Nebelsiek, S.I. Goktuna, P.K. Ziegler, O. Canli, J. Heijmans, D.J. Huels, G. Moreaux, R.A. Rupec, M. Gerhard, R. Schmid, N. Barker, H. Clevers, R. Lang, J. Neumann, T. Kirchner, M.M. Taketo, G.R. van den Brink, O.J. Sansom, M.C. Arkan, F.R. Greten, Intestinal tumorigenesis initiated by dedifferentiation and acquisition of stem-cell-like properties, Cell, 152 (2013) 25-38.

[106] L.A. Milner, A. Bigas, Notch as a mediator of cell fate determination in hematopoiesis: evidence and speculation, Blood, 93 (1999) 2431-2448.

[107] X.B. Wu, Y. Liu, G.H. Wang, X. Xu, Y. Cai, H.Y. Wang, Y.Q. Li, H.F. Meng, F. Dai, J.D. Jin, Mesenchymal stem cells promote colorectal cancer progression through AMPK/mTOR-mediated NF-kappaB activation, Sci Rep, 6 (2016) 21420.

[108] R. Castriconi, A. Daga, A. Dondero, G. Zona, P.L. Poliani, A. Melotti, F. Griffero, D. Marubbi, R. Spaziante, F. Bellora, L. Moretta, A. Moretta, G. Corte, C. Bottino, NK cells recognize and kill human glioblastoma cells with stem cell-like properties, J Immunol, 182 (2009) 3530-3539.

[109] H. Kim, Q. Lin, P.M. Glazer, Z. Yun, The hypoxic tumor microenvironment in vivo selects the cancer stem cell fate of breast cancer cells, Breast Cancer Res, 20 (2018) 16.

[110] C. Grange, M. Tapparo, F. Collino, L. Vitillo, C. Damasco, M.C. Deregibus, C. Tetta, B. Bussolati, G. Camussi, Microvesicles released from human renal cancer stem cells stimulate angiogenesis and formation of lung premetastatic niche, Cancer Res, 71 (2011) 5346-5356.

[111] S.-G. Pohl, N. Brook, M. Agostino, F. Arfuso, A.P. Kumar, A. Dharmarajan, Wnt signaling in triple-negative breast cancer, Oncogenesis, 6 (2017) e310.

[112] J. Fan, Q. Wei, J. Liao, Y. Zou, D. Song, D. Xiong, C. Ma, X. Hu, X. Qu, L. Chen, L. Li, Y. Yu, X. Yu, Z. Zhang, C. Zhao, Z. Zeng, R. Zhang, S. Yan, T. Wu, X. Wu, Y. Shu, J. Lei, Y. Li, W.

Zhang, R.C. Haydon, H.H. Luu, A. Huang, T.C. He, H. Tang, Noncanonical Wnt signaling plays an important role in modulating canonical Wnt-regulated stemness, proliferation and terminal differentiation of hepatic progenitors, Oncotarget, 8 (2017) 27105-27119.

[113] K. Nalapareddy, K.J. Nattamai, R.S. Kumar, R. Karns, K.A. Wikenheiser-Brokamp, L.L. Sampson, M.M. Mahe, N. Sundaram, M.-B. Yacyshyn, B. Yacyshyn, M.A. Helmrath, Y. Zheng, H. Geiger, Canonical Wnt Signaling Ameliorates Aging of Intestinal Stem Cells, Cell Reports, 18 (2017) 2608-2621.

[114] W. de Lau, W.C. Peng, P. Gros, H. Clevers, The R-spondin/Lgr5/Rnf43 module: regulator of Wnt signal strength, Genes & Development, 28 (2014) 305-316.

[115] S. Koch, P. Nava, C. Addis, W. Kim, T.L. Denning, L. Li, C.A. Parkos, A. Nusrat, The Wnt Antagonist Dkk1 Regulates Intestinal Epithelial Homeostasis and Wound Repair, Gastroenterology, 141 (2011) 259-268.e258.

[116] Q.C. Yu, E.M. Verheyen, Y.A. Zeng, Mammary Development and Breast Cancer: A Wnt Perspective, Cancers, 8 (2016).

[117] D. Wang, C. Cai, X. Dong, Q.C. Yu, X.-O. Zhang, L. Yang, Y.A. Zeng, Identification of multipotent mammary stem cells by protein C receptor expression, Nature, 517 (2015) 81-84.

[118] W. Guo, Z. Keckesova, J.L. Donaher, T. Shibue, V. Tischler, F. Reinhardt, S. Itzkovitz, A. Noske, U. Zürrer-Härdi, G. Bell, W.L. Tam, S.A. Mani, A. van Oudenaarden, R.A. Weinberg, Slug and Sox9 Cooperatively Determine the Mammary Stem Cell State, Cell, 148 (2012) 1015-1028.

[119] Y. Wang, J. Dong, D. Li, L. Lai, S. Siwko, Y. Li, M. Liu, Lgr4 regulates mammary gland development and stem cell activity through the pluripotency transcription factor Sox2, Stem cells (Dayton, Ohio), 31 (2013) 1921-1931.

[120] W. Luo, M. Rodriguez, J.M. Valdez, X. Zhu, K. Tan, D. Li, S. Siwko, L. Xin, M. Liu, Lgr4 is a key regulator of prostate development and prostate stem cell differentiation, Stem cells (Dayton, Ohio), 31 (2013) 2492-2505.

[121] N. Tanaka, T. Mashima, A. Mizutani, A. Sato, A. Aoyama, B. Gong, H. Yoshida, Y. Muramatsu, K. Nakata, M. Matsuura, R. Katayama, S. Nagayama, N. Fujita, Y. Sugimoto, H.

Seimiya, APC mutations as a potential biomarker for sensitivity to tankyrase inhibitors in colorectal cancer, Molecular cancer therapeutics, (2017).

[122] P. Kaler, L. Augenlicht, L. Klampfer, Activating Mutations in β-Catenin in Colon Cancer Cells Alter Their Interaction with Macrophages; the Role of Snail, PLOS ONE, 7 (2012) e45462.

[123] S. Basu, G. Haase, A. Ben-Ze'ev, Wnt signaling in cancer stem cells and colon cancer metastasis [version 1; referees: 3 approved], 2016.

[124] G.-B. Jang, J.-Y. Kim, S.-D. Cho, K.-S. Park, J.-Y. Jung, H.-Y. Lee, I.-S. Hong, J.-S. Nam, Blockade of Wnt/β-catenin signaling suppresses breast cancer metastasis by inhibiting CSC-like phenotype, Scientific Reports, 5 (2015) 12465.

[125] C.O. Tse, S. Kim, J. Park, Activation of Wnt signaling pathway by AF1q enriches stem-like population and enhance mammosphere formation of breast cells, Biochemical and Biophysical Research Communications, 484 (2017) 884-889.

[126] A. Hanna, L.A. Shevde, Hedgehog signaling: modulation of cancer properies and tumor mircroenvironment, Molecular Cancer, 15 (2016) 24.

[127] S.M. Wu, A.B.H. Choo, M.G.S. Yap, K.K.-K. Chan, Role of Sonic hedgehog signaling and the expression of its components in human embryonic stem cells, Stem Cell Research, 4 (2010) 38-49.

[128] R.S. Moura, C. Silva-Gonçalves, P. Vaz-Cunha, J. Correia-Pinto, Expression analysis of Shh signaling members in early stages of chick lung development, Histochemistry and Cell Biology, 146 (2016) 457-466.

[129] C.D. Peacock, Q. Wang, G.S. Gesell, I.M. Corcoran-Schwartz, E. Jones, J. Kim, W.L. Devereux, J.T. Rhodes, C.A. Huff, P.A. Beachy, D.N. Watkins, W. Matsui, Hedgehog signaling maintains a tumor stem cell compartment in multiple myeloma, Proceedings of the National Academy of Sciences of the United States of America, 104 (2007) 4048-4053.

[130] V. Clement, P. Sanchez, N. de Tribolet, I. Radovanovic, A.R. Altaba, HEDGEHOG-GLI1 signaling regulates human glioma growth, cancer stem cell self-renewal and tumorigenicity, Current biology : CB, 17 (2007) 165-172.

[131] S. Liu, G. Dontu, I.D. Mantle, S. Patel, N. Ahn, K.W. Jackson, P. Suri, M.S. Wicha, Hedgehog Signaling and Bmi-1 Regulate Self-renewal of Normal and Malignant Human Mammary Stem Cells, Cancer research, 66 (2006) 6063-6071.

[132] B.N. Singh, J. Fu, R.K. Srivastava, S. Shankar, Hedgehog Signaling Antagonist GDC-0449 (Vismodegib) Inhibits Pancreatic Cancer Stem Cell Characteristics: Molecular Mechanisms, PLoS One, 6 (2011).

[133] C.S. Nowell, F. Radtke, Notch as a tumour suppressor, Nature reviews. Cancer, 17 (2017) 145-159.

[134] T. Srinivasan, E.B. Than, P. Bu, K.-L. Tung, K.-Y. Chen, L. Augenlicht, S.M. Lipkin, X. Shen, Notch signalling regulates asymmetric division and inter-conversion between lgr5 and bmi1 expressing intestinal stem cells, Scientific Reports, 6 (2016) 26069.

[135] I. Imayoshi, M. Sakamoto, M. Yamaguchi, K. Mori, R. Kageyama, Essential Roles of Notch Signaling in Maintenance of Neural Stem Cells in Developing and Adult Brains, The Journal of Neuroscience, 30 (2010) 3489-3498.

[136] W. Xiao, Z. Gao, Y. Duan, W. Yuan, Y. Ke, Notch signaling plays a crucial role in cancer stem-like cells maintaining stemness and mediating chemotaxis in renal cell carcinoma, Journal of Experimental & Clinical Cancer Research, 36 (2017) 41.

[137] S. Barat, X. Chen, K. Cuong Bui, P. Bozko, J. Götze, M. Christgen, T. Krech, N.P. Malek, R.R. Plentz, Gamma-Secretase Inhibitor IX (GSI) Impairs Concomitant Activation of Notch and Wnt-Beta-Catenin Pathways in CD44+ Gastric Cancer Stem Cells, STEM CELLS Translational Medicine, 6 (2017) 819-829.

[138] P.D.W. Eckford, F.J. Sharom, ABC Efflux Pump-Based Resistance to Chemotherapy Drugs, Chemical Reviews, 109 (2009) 2989-3011.

[139] E.K.H. Chow, L. Fan, X. Chen, J.M. Bishop, Oncogene-specific formation of chemoresistant murine hepatic cancer stem cells, Hepatology, 56 (2012) 1331-1341.

[140] M.M. Zhu, J.L. Tong, Q. Xu, F. Nie, X.T. Xu, S.D. Xiao, Z.H. Ran, Increased JNK1 Signaling Pathway Is Responsible for ABCG2-Mediated Multidrug Resistance in Human Colon Cancer, PLOS ONE, 7 (2012) e41763.

[141] K.K.W. To, B. Tomlinson, Targeting the ABCG2-overexpressing multidrug resistant (MDR) cancer cells by PPARγ agonists, British Journal of Pharmacology, 170 (2013) 1137-1151.

[142] L. Xiang, Z.-H. Liu, Q. Huan, P. Su, G.-J. Du, Y. Wang, P. Gao, G.-Y. Zhou, Hypoxia-inducible factor-2a is associated with ABCG2 expression, histology-grade and Ki67 expression in breast invasive ductal carcinoma, Diagnostic Pathology, 7 (2012) 32.

[143] C.M. Martin, A. Ferdous, T. Gallardo, C. Humphries, H. Sadek, A. Caprioli, J.A. Garcia, L.I. Szweda, M.G. Garry, D.J. Garry, Hypoxia-Inducible Factor-2α Transactivates Abcg2 and Promotes Cytoprotection in Cardiac Side Population Cells, Circ Res, 102 (2008).

[144] A. Singh, H. Wu, P. Zhang, C. Happel, J. Ma, S. Biswal, Expression of ABCG2 (BCRP), a Marker of Stem Cells, is Regulated by Nrf2 in Cancer Cells That Confers Side Population and Chemoresistance Phenotype, Molecular cancer therapeutics, 9 (2010) 2365-2376.

[145] A. Keren-Paz, R. Emmanuel, Y. Samuels, YAP and the drug resistance highway, Nature genetics, 47 (2015) 193-194.

[146] Z. Liu, J. Xu, J. He, Y. Zheng, H. Li, Y. Lu, J. Qian, P. Lin, D.M. Weber, J. Yang, Q. Yi, A critical role of autocrine sonic hedgehog signaling in human CD138+ myeloma cell survival and drug resistance, Blood, 124 (2014).

[147] E.D. Lagadinou, A. Sach, K. Callahan, R.M. Rossi, S.J. Neering, M. Minhajuddin, J.M. Ashton, S. Pei, V. Grose, K.M. O'Dwyer, J.L. Liesveld, P.S. Brookes, M.W. Becker, C.T. Jordan, BCL-2 inhibition targets oxidative phosphorylation and selectively eradicates quiescent human leukemia stem cells, Cell stem cell, 12 (2013) 329-341.

[148] M. Schwickart, X. Huang, J.R. Lill, J. Liu, R. Ferrando, D.M. French, H. Maecker, K. O'Rourke, F. Bazan, J. Eastham-Anderson, P. Yue, D. Dornan, D.C.S. Huang, V.M. Dixit, Deubiquitinase USP9X stabilizes MCL1 and promotes tumour cell survival, Nature, 463 (2010) 103-107.

[149] K.E. Tagscherer, A. Fassl, B. Campos, M. Farhadi, A. Kraemer, B.C. Bock, S. Macher-Goeppinger, B. Radlwimmer, O.D. Wiestler, C. Herold-Mende, W. Roth, Apoptosis-based treatment of glioblastomas with ABT-737, a novel small molecule inhibitor of Bcl-2 family proteins, Oncogene, 27 (2008) 6646-6656.

[150] L. Piggott, N. Omidvar, S.M. Pérez, M. Eberl, R.W. Clarkson, Suppression of apoptosis inhibitor c-FLIP selectively eliminates breast cancer stem cell activity in response to the anti-cancer agent, TRAIL, Breast Cancer Research, 13 (2011) R88.

[151] S. Siddharth, S. Das, A. Nayak, C.N. Kundu, SURVIVIN as a marker for quiescent-breast cancer stem cells—An intermediate, adherent, pre-requisite phase of breast cancer metastasis, Clinical & Experimental Metastasis, 33 (2016) 661-675.

[152] Q. Long, R. Yang, W. Lu, W. Zhu, J. Zhou, C. Zheng, D. Zhou, L. Yu, J. Wu, Adenovirus-mediated truncated Bid overexpression induced by the Cre/LoxP system promotes the cell apoptosis of CD133+ ovarian cancer stem cells, Oncol Rep, 37 (2017) 155-162.

[153] N. Lv, Z. Shan, Y. Gao, H. Guan, C. Fan, H. Wang, W. Teng, Twist1 regulates the epithelial-mesenchymal transition via the NF-kappaB pathway in papillary thyroid carcinoma, Endocrine, 51 (2016) 469-477.

[154] L. Kong, S. Guo, C. Liu, Y. Zhao, C. Feng, Y. Liu, T. Wang, C. Li, Overexpression of SDF-1 activates the NF-kappaB pathway to induce epithelial to mesenchymal transition and cancer stem cell-like phenotypes of breast cancer cells, Int J Oncol, 48 (2016) 1085-1094.

[155] G. Xi, E. Hayes, R. Lewis, S. Ichi, B. Mania-Farnell, K. Shim, T. Takao, E. Allender, C.S. Mayanil, T. Tomita, CD133 and DNA-PK regulate MDR1 via the PI3K- or Akt-NF-kappaB pathway in multidrug-resistant glioblastoma cells in vitro, Oncogene, 35 (2016) 241-250.

[156] L. Cao, X. Fan, W. Jing, Y. Liang, R. Chen, Y. Liu, M. Zhu, R. Jia, H. Wang, X. Zhang, Y. Zhang, X. Zhou, J. Zhao, Y. Guo, Osteopontin promotes a cancer stem cell-like phenotype in hepatocellular carcinoma cells via an integrin-NF-kappaB-HIF-1alpha pathway, Oncotarget, 6 (2015) 6627-6640.

[157] C. Xu, X. Sun, S. Qin, H. Wang, Z. Zheng, S. Xu, G. Luo, P. Liu, J. Liu, N. Du, Y. Zhang, D. Liu, H. Ren, Let-7a regulates mammosphere formation capacity through Ras/NF-kappaB and Ras/MAPK/ERK pathway in breast cancer stem cells, Cell Cycle, 14 (2015) 1686-1697.

[158] A. Prigione, N. Rohwer, S. Hoffmann, B. Mlody, K. Drews, R. Bukowiecki, K. Blümlein, E.E. Wanker, M. Ralser, T. Cramer, J. Adjaye, HIF1α Modulates Cell Fate Reprogramming Through Early Glycolytic Shift and Upregulation of PDK1–3 and PKM2, Stem cells (Dayton, Ohio), 32 (2014) 364-376.

[159] M. Marhold, E. Tomasich, A. El-Gazzar, G. Heller, A. Spittler, R. Horvat, M. Krainer, P. Horak, HIF1α Regulates mTOR Signaling and Viability of Prostate Cancer Stem Cells, Molecular Cancer Research, 13 (2015) 556-564.

[160] V. Giambra, C.E. Jenkins, S.H. Lam, C. Hoofd, M. Belmonte, X. Wang, S. Gusscott, D. Gracias, A.P. Weng, Leukemia stem cells in T-ALL require active Hif1α and Wnt signaling, Blood, 125 (2015) 3917-3927.

[161] H. Iida, M. Suzuki, R. Goitsuka, H. Ueno, Hypoxia induces CD133 expression in human lung cancer cells by up-regulation of OCT3/4 and SOX2, International journal of oncology, 40 (2012) 71-79.

[162] X. Zheng, L. Boyer, M. Jin, J. Mertens, Y. Kim, L. Ma, L. Ma, M. Hamm, F.H. Gage, T. Hunter, Metabolic reprogramming during neuronal differentiation from aerobic glycolysis to neuronal oxidative phosphorylation, eLife, 5 (2016) e13374.

[163] A. Viale, Giulio F. Draetta, Sugar? No Thank You, Just a Deep Breath of Oxygen for Cancer Stem Cells, Cell Metabolism, 22 (2015) 543-545.

[164] C.-L. Chen, D.B. Uthaya Kumar, V. Punj, J. Xu, L. Sher, S.M. Tahara, S. Hess, K. Machida, NANOG metabolically reprograms tumor-initiating stem-like cells through tumorigenic changes in oxidative phosphorylation and fatty acid metabolism, Cell metabolism, 23 (2016) 206-219.

[165] E. Fokas, R. Engenhart-Cabillic, K. Daniilidis, F. Rose, H.-X. An, Metastasis: the seed and soil theory gains identity, Cancer and Metastasis Reviews, 26 (2007) 705-715.

[166] B. Psaila, D. Lyden, The Metastatic Niche: Adapting the Foreign Soil, Nature reviews. Cancer, 9 (2009) 285-293.

[167] K. Sampieri, R. Fodde, Cancer stem cells and metastasis, Seminars in Cancer Biology, 22 (2012) 187-193.

[168] W. Gao, L. Chen, Z. Ma, Z. Du, Z. Zhao, Z. Hu, Q. Li, Isolation and Phenotypic Characterization of Colorectal Cancer Stem Cells With Organ-Specific Metastatic Potential, Gastroenterology, 145 (2013) 636-646.e635.

[169] J. Hu, G. Li, P. Zhang, X. Zhuang, G. Hu, A CD44v(+) subpopulation of breast cancer stem-like cells with enhanced lung metastasis capacity, Cell Death Dis, 8 (2017) e2679.

[170] M. Reichert, B. Bakir, L. Moreira, J.R. Pitarresi, K. Feldmann, L. Simon, K. Suzuki, R. Maddipati, A.D. Rhim, A.M. Schlitter, M. Kriegsmann, W. Weichert, M. Wirth, K. Schuck, G. Schneider, D. Saur, A.B. Reynolds, A.J. Klein-Szanto, B. Pehlivanoglu, B. Memis, N.V. Adsay, A.K. Rustgi, Regulation of Epithelial Plasticity Determines Metastatic Organotropism in Pancreatic Cancer, Developmental Cell, 45 (2018) 696-711.e698.

[171] A. Hoshino, B. Costa-Silva, T.L. Shen, G. Rodrigues, A. Hashimoto, M.T. Mark, H. Molina, S. Kohsaka, A. Di Giannatale, S. Ceder, S. Singh, C. Williams, N. Soplop, K. Uryu, L. Pharmer, T. King, L. Bojmar, A.E. Davies, Y. Ararso, T. Zhang, H. Zhang, J. Hernandez, J.M. Weiss, V.D. Dumont-Cole, K. Kramer, L.H. Wexler, A. Narendran, G.K. Schwartz, J.H. Healey, P. Sandstrom, K.J. Labori, E.H. Kure, P.M. Grandgenett, M.A. Hollingsworth, M. de Sousa, S. Kaur, M. Jain, K. Mallya, S.K. Batra, W.R. Jarnagin, M.S. Brady, O. Fodstad, V. Muller, K. Pantel, A.J. Minn, M.J. Bissell, B.A. Garcia, Y. Kang, V.K. Rajasekhar, C.M. Ghajar, I. Matei, H. Peinado, J. Bromberg, D. Lyden, Tumour exosome integrins determine organotropic metastasis, Nature, 527 (2015) 329-335.

[172] T. Lopatina, C. Gai, M.C. Deregibus, S. Kholia, G. Camussi, Cross Talk between Cancer and Mesenchymal Stem Cells through Extracellular Vesicles Carrying Nucleic Acids, Frontiers in Oncology, 6 (2016).

[173] F. Fatima, M. Nawaz, Stem cell-derived exosomes: roles in stromal remodeling, tumor progression, and cancer immunotherapy, Chinese Journal of Cancer, 34 (2015).

CHAPTER 2

Dissertation General Hypothesis and Objectives

1. Background and rationale

Pancreatic ductal adenocarcinoma (PDAC) remains the most aggressive and deadliest primary cancer with a five-year survival rate of 9 percent (Cancer Facts & Figures 2018, American Cancer Society). Recent evidence suggests the presence of cancer stem cell (CSC) populations within a heterogeneous pancreatic tumor and provides clues for their association with the aggressiveness of PDAC [1, 2]. However, how this CSCs are induced and involved in the metastasis process are poorly understood.

Of several risk factors, cigarette smoking is one of the most important and established risk factors for pancreatic cancer. Hoarding experimental and epidemiological evidence has established a direct correlation between cigarette smoking and the risk of pancreatic cancer (PC) [3]. Recent studies provide ample evidence to the cigarette smoke-mediated induction of pancreatic CSCs. An et al. have revealed the critical role of condensed smoke lysate in increasing the size of the side population (SP or CSCs) in lung and head & neck cancers [4]. Another study has shown that chronic smoke injury in non-small-cell lung cancer is associated with increased K14-positive tumor-initiating cells that lead to poor prognosis [5].

Further, in breast cancer, it has been shown that nicotine increases CSCs via alpha CHRNA7 and the PKC-Notch dependent pathways [6]. Cigarette smoke treatment of breast cancer cells also resulted in their epithelial-to-mesenchymal (EMT) transition and augmented metastatic ability. This was associated with the increased emergence of stem cell-like cells [7]. Apart from these malignancies, Hermann et al. have shown that nicotine can promote the initiation and progression of Kras-induced PC via Gata6-dependent de-differentiation of acinar cells in mice [8]. In our editorial commentary for this proposal, we have provided our view of the role of nicotine in pancreatic stem cell activation and acinar de-differentiation [9]. Taken together, all these studies support the concept of smoke-induced CSC activation. Despite these pieces of evidence, it is still unclear whether and how CSCs are induced in response to cigarette smoking. The first part of this thesis is primarily focused on deciphering the mechanistic role of the cigarette smoke on the induction of pancreatic CSC populations.

Further, studies have also reported that CSCs are the major culprits in the metastatic activity of pancreatic cancer [1]. Majority of recent pieces of evidence suggest the existence of distinct sub-types of pancreatic CSCs with sub-type specific stemness features. Previous studies have shown the existence of distinct CSC populations in a heterogeneous tumor. For instance, breast tumors

consist of two distinct CSC populations such as ALDH+ and CD44+CD24-. The study also demonstrated that ALDH+ cells rely on oxidative phosphorylation for their energy needs, whereas CD44+CD24- population rely on glycolysis [10]. Recent studies also proposed the propensity of a specific cancer cell with specific metabolic profile metastasizes to a specific organ [11]. For instance, the liver has a high glycolytic environment, and a metastatic cell required to be highly glycolytic to overcome the glycolytic barrier in the liver. Similarly, the lung has an oxidative environment, and an upcoming metastatic cell has to be oxyolytic to survive in the lung environment [11]. My second goal of this dissertation primarily explores the metastatic function of CSCs in pancreatic cancer.

2. Hypothesis

Based on the previous studies, we hypothesized that CSCs are induced by cigarette smoking and that these CSCs are involved in the organ-specific metastasis process in pancreatic cancer.

3. Objectives

Aim 1: To investigate the mechanistic role of cigarette smoke on the induction of CSCs in pancreatic cancer.

Aim 2: To investigate the metabolic and stem cell features of distinct sub-types of pancreatic CSC populations.

Aim 3: To delineate whether these distinct sub-types of CSC populations with sub-type specific metabolic and stem cell features metastasize to specific organs.

4. References

[1] P.C. Hermann, S.L. Huber, T. Herrler, A. Aicher, J.W. Ellwart, M. Guba, C.J. Bruns, C. Heeschen, Distinct populations of cancer stem cells determine tumor growth and metastatic activity in human pancreatic cancer, Cell Stem Cell, 1 (2007) 313-323.

[2] C. Li, C.J. Lee, D.M. Simeone, Identification of human pancreatic cancer stem cells, Methods in molecular biology (Clifton, N.J.), 568 (2009) 161-173.

[3] N. Momi, M.P. Ponnusamy, S. Kaur, S. Rachagani, S.S. Kunigal, S. Chellappan, M.M. Ouellette, S.K. Batra, Nicotine/cigarette smoke promotes metastasis of pancreatic cancer through alpha7nAChR-mediated MUC4 upregulation, Oncogene, 32 (2013) 1384-1395.

[4] Y. An, A. Kiang, J.P. Lopez, S.Z. Kuo, M.A. Yu, E.L. Abhold, J.S. Chen, J. Wang-Rodriguez, W.M. Ongkeko, Cigarette Smoke Promotes Drug Resistance and Expansion of Cancer Stem Cell-Like Side Population, PLOS ONE, 7 (2012) e47919.

[5] A.T. Ooi, V. Mah, D.W. Nickerson, J.L. Gilbert, V.L. Ha, A.E. Hegab, S. Horvath, M. Alavi, E.L. Maresh, D. Chia, A.C. Gower, M.E. Lenburg, A. Spira, L.M. Solis, I.I. Wistuba, T.C. Walser, W.D. Wallace, S.M. Dubinett, L. Goodglick, B.N. Gomperts, Presence of a putative tumor-initiating progenitor cell population predicts poor prognosis in smokers with non-small cell lung cancer, Cancer research, 70 (2010) 6639-6648.

[6] N. Hirata, Y. Sekino, Y. Kanda, Nicotine increases cancer stem cell population in MCF-7 cells, Biochem Biophys Res Commun, 403 (2010) 138-143.

[7] F. Di Cello, V.L. Flowers, H. Li, B. Vecchio-Pagan, B. Gordon, K. Harbom, J. Shin, R. Beaty, W. Wang, C. Brayton, S.B. Baylin, C.A. Zahnow, Cigarette smoke induces epithelial to mesenchymal transition and increases the metastatic ability of breast cancer cells, Mol Cancer, 12 (2013) 90.

[8] P.C. Hermann, P. Sancho, M. Canamero, P. Martinelli, F. Madriles, P. Michl, T. Gress, R. de Pascual, L. Gandia, C. Guerra, M. Barbacid, M. Wagner, C.R. Vieira, A. Aicher, F.X. Real, B. Sainz, Jr., C. Heeschen, Nicotine promotes initiation and progression of KRAS-induced pancreatic cancer via Gata6-dependent dedifferentiation of acinar cells in mice, Gastroenterology, 147 (2014) 1119-1133.e1114.

[9] M.P. Ponnusamy, S.K. Batra, Insights into the role of nicotine in pancreatic stem cell activation and acinar dedifferentiation, Gastroenterology, 147 (2014) 962-965.

[10] M. Luo, L. Shang, M.D. Brooks, E. Jiagge, Y. Zhu, J.M. Buschhaus, S. Conley, M.A. Fath, A. Davis, E. Gheordunescu, Y. Wang, R. Harouaka, A. Lozier, D. Triner, S. McDermott, S.D. Merajver, G.D. Luker, D.R. Spitz, M.S. Wicha, Targeting Breast Cancer Stem Cell State Equilibrium through Modulation of Redox Signaling, Cell metabolism, 28 (2018) 69-86.e66.

[11] T. Schild, V. Low, J. Blenis, A.P. Gomes, Unique Metabolic Adaptations Dictate Distal Organ-Specific Metastatic Colonization, Cancer cell, 33 (2018) 347-354.

CHAPTER 3

Materials and Methods

Some of the material covered in this chapter was taken from one published research article:

Nimmakayala RK, Seshacharyulu P, Lakshmanan I, Rachagani S, Chugh S, Karmakar S, Rauth S, Vengoji R, Atri P, Talmon GA, Lele SM, Smith LM, Thapa I, Bastola D, Ouellette MM, Batra SK, Ponnusamy MP, Cigarette Smoke Induces Stem Cell Features of Pancreatic Cancer Cells via PAF1, **Gastroenterology 2018;** 155 (3): 892-908.e6.

1. Cell lines and cell culture

An immortalized human pancreatic nestin-positive epithelial (hTERT-HPNE) cell line was obtained as a generous gift from Dr. Ouellette at the University of Nebraska Medical Center. It was cultured in Dulbecco's modified Eagle's medium (low glucose) with 25% M3 Base Media (Incell, San Antonio, TX), supplemented with 5% (vol/vol) fetal bovine serum, 10 ng/mL epidermal growth factor, and antibiotics (100 units/mL penicillin and 100 µg/mL streptomycin). The Capan1 and Miapaca-2 cell lines were cultured in Dulbecco's modified Eagle's medium (4.5 mg/mL glucose), supplemented with 10% fetal bovine serum and antibiotics (100 units/mL penicillin and 100 µg/mL streptomycin). Cells were incubated in a humidified incubator at 37°C supplied with 5% CO_2.

Cells were cultured in stem cell medium: DMEM/F12 (Invitrogen, Grand Island, NY) medium supplemented with 1% B27 supplement, epidermal growth factor (20 ng/mL), basic fibroblast growth factor (10 ng/mL). In some experiments, cells (2000/well) were plated in 96-well low-attachment culture plates in 200 µL of the medium. The number of spheres (Φ >100 µm) for each well was evaluated after 10 days of culture. Images were captured using Carl Zeiss Confocal Fluorescent Microscope (Oberkochen, Germany) using a 488-nm laser.

For the secondary and tertiary sphere-forming assays, primary spheres or secondary spheres were centrifuged and dissociated using enzymatic (trypsin EDTA) and mechanical methods (pipette). Then, 2000 cells were seeded in stem cell medium in ultra-low-attachment 96-well plates. The total number of spheres (Φ >100 µm) for each well was counted after 10 days of culture.

Miapaca-2 cells were grown under sphere culture conditions in DMEM/F12 medium supplemented with 1 % B27 supplement, epidermal growth factor (20 ng/mL), basic fibroblast growth factor (bFGF) (10 ng/mL) in the presence and absence of Gemcitabine (3µM) to derive drug sensitive and drug resistant CSC populations, respectively. The Miapaca-2 cells cultured under adherent culture conditions using 10% DMEM were utilized as differentiated control cells.

L3.6pL, a spontaneous liver metastatic pancreatic cancer cell line was obtained as a generous gift from Dr. Ouellette at the University of Nebraska Medical Center. S2-VP10, a spontaneous lung metastatic pancreatic cancer cell line was obtained as a kind gift from Dr. Ashok K. Saluja at Miller School of Medicine, University of Miami.

2. Animal studies

Animal experiments were carried out in compliance with the regulations of the University of Nebraska Medical Center Institutional Animal Care and Use Committee. Ten-week-old LSL-$Kras^{G12D}$(Control) and $Kras^{G12D}$;Pdx-1 Cre animals were used for cigarette (University of Kentucky Reference Cigarette, 3R4F) smoke exposure, and the process of smoke exposure was performed for 20 weeks, 3 hours twice a day, using the Teague TE-10C system (Davis, CA) by delivering smoke at a rate of 150 mg total suspended particles/m^3 [22] (Figure 3*A*). CS exposure was started when $Kras^{G12D}$; Pdx-1Cre animals begin to form low-grade pancreatic intraepithelial neoplasia lesions. Sham animals, exposed to filtered air for the same number of hours and days, were used as controls.

3. Preparation of cigarette smoke extract

Two 3R4F research cigarettes (University of Kentucky) were used to generate cigarette smoke extract (CSE). The detailed procedure for the preparation of CSE was adapted from previous studies [1, 2]. Briefly, 2 cigarettes were bubbled through 20 mL serum-free Dulbecco's modified Eagle's medium (DMEM) (by drawing the smoke into the medium using a vacuum) and this solution was considered 100% CSE. CSE after preparation was filtered through a 0.2-μm filter (Millipore, Bedford, MA), and stored at −80°C immediately after preparation to prevent degradation of cigarette components. Commercially available CSE (C-CSE) (Murthy Pharmaceuticals, Lexington KY) was used in some experiments to compare the effect CSE prepared in our laboratory with standard C-CSE. According to the manufacturer protocol, C-CSE was prepared by burning 3R4F standard research cigarettes (University of Kentucky) using the Federal Trade Commission (FTC) smoke machine. The total particulate matter (TPM) retained on filters was extracted with dimethyl sulfoxide (DMSO) by soaking and sonication. The extracted TPM was packaged as 40 mg/mL solution, which is equal to 3.6 cigarettes/mL.

4. Liquid chromatography-tandem mass spectrometry analysis of nicotine in CSE

Liquid Chromatography-Tandem Mass Spectrometry (LC-MS/MS) analysis of nicotine in 100% CSE was performed using the multiple reaction monitoring (MRM) method as shown previously [3]. For calibration standards, nicotine stock (1 mg/mL) solution was diluted to 50, 100, 200, 400, and 800 ng/mL in 100% MS grade methanol. For CSE sample preparation, 2 3R4F research cigarettes (University of Kentucky) were bubbled through 20 mL of LC-MS grade water (Fisher

Chemical, Waltham, MA), and the resulting solution was filtered and considered 100%; 100 µL of 100% CSE was subjected to speed vacuum evaporation, and the dried sample was dissolved in 100 µL of 100% LC-MS grade methanol for LC-MS/MS analysis. A 50 ng/mL amount of nicotine D4 (Sigma, St. Louis, MO) was added in all samples as an internal standard (IS) control.

Nexera UHPLC (Shimadzu, Kyoto, Japan) with Acquity UPLC BEH Shield RP18 1.7 µm, 2.1 × 150-mm column (part #186003376; Waters, Milford, MA) was used for chromatographic separation. Mobile phase A is 5 mM ammonium bicarbonate buffer (pH not adjusted), and Mobile phase B is composed of acetonitrile: methanol (3:1, vol/vol). The temperature of the autosampler was 40°C and the sample injection volume was 5 µL. Flow rate was set to 0.4 mL/min. The chromatographic gradient program is described in Supplementary Table 1. Total run time of the program is 3 minutes and retention times for nicotine and nicotine D4 (IS) are 2.27 minutes and 2.29 minutes, respectively.

LC-MS/MS was performed using the MRM method, using AB Sciex QTRAP 6500 mass spectrometer (AB SCIEX, Framingham, MA) operated in positive mode. Published MRM values of nicotine (m/z 163.2/132.1 and 163.2/117.1) and nicotine D4 (m/z 167.3/121.4 and 167.3/136), including other published parameters,3, 4 were used for analysis. Electrospray ionization parameters are as follows: electrospray voltage of 5500 V, a temperature of 550°C, curtain gas of 35 psi, gas 1 of 50 psi, and gas 2 of 50 psi. Analyst1.6 software (AB Sciex) was used to acquire data and peaks were integrated using Multiquant (AB Sciex). Peak areas were normalized with IS peak areas. A calibration curve was generated and nicotine concentration in 100% CSE was calculated using GraphPad Prism software (GraphPad, La Jolla, CA). The overall nicotine concentration in 100% CSE was 33.073 ± 0.698 µg/mL ($P < .001$).

5. Analysis of cellular energy metabolism

Liquid Chromatography-Tandem Mass Spectrometry Analysis of metabolites in energy metabolism: Mass spectrometric metabolomics analyses were performed in collaboration with Dr. Daryl J. Murry at the Clinical Pharmacology Laboratory, Department of Pharmacy Practice, College of Pharmacy, University of Nebraska Medical Center. Cells were seeded in 10 cm culture dishes and two hours before the collection of metabolites the culture medium was replaced with fresh medium. After trypsinization, single cells were counted. Five million cells were used to extract metabolites. Metabolites were extracted (An aliquot of the cell solution was counted using Trypan blue staining and a Bio-Rad TC20 automated cell counter. Cells were spun down, washed

with PBS, and then the cell pellet was stored at −20 ºC. To each cell pellet, 0.3mL of 2-propanol: 100 mM NH4HCO3, pH7.4 (1:1v/v), was added, cells were then sonicated, and 300 µL of the resulting cell homogenate was used for further preparation. A 10 µL spiking of the IS was added to the samples, which were then vortexed. Subsequently, 1.0 mL of methanol was added for deproteinization, and then mixture was cooled (-80 ºC) for 10 min. The samples were then centrifuged for 10 min at 14,000×g at 4 ºC. After centrifugation, supernatants were transferred to glass tubes and dried under a stream of nitrogen at 40◦C. The residues were then dissolvedin100 µL acetonitrile: water 1:1, v/v) and 3 µL of this solution was injected into the LC–MS/ MS system. Metabolites analysis was conducted using a Shimadzu Nexera ultra high-performance liquid chromatography (UPLC) system (Columbia, MD, USA) equipped with two pumps (LC-30 AD), a column oven (CTO-30AS) and an auto-sampler (SIL-30AC). Peak resolution and separation for all samples were achieved by using a Mastro C18 (2.0 mm I.D. × 150 mm L., 3 µm) equipped with a C18 guard column. The mobile phase consisted of a 15 mM Acetate, 10 mM Tributylamine-Water (mobile phase A) and methanol (mobile phase B) at a total flow rate of 0.25 mL/min. The chromatographic separation was achieved using a25 min gradient elution. Mass spectrometric detection was performed on an LC-MS/MS 8060 system (Shimadzu Scientific, Inc., Columbia, MD, USA), equipped with a dual ionization source (DUIS) operated in the negative electrospray ionization and multiple reaction monitoring mode in order to achieve unit resolution. Parameters for multiple reaction monitoring (MRM) detection in the negative mode were as follows: Nebulizer gas: 2.0L/min; heating gas: 10L/min; drying gas: 10L/min; interface temperature: 350ºC; desolvation line temperature: 250ºC; heat block temperature: 400ºC. Mass transitions were monitored at 10 ms dwell times and unit mass resolutions and individual parameters. Lab Solutions LCMS Ver.5.80 (Shimadzu Scientific, Inc. Columbia, MD, USA) was used for data collection and quantitation.

Glucose uptake, lactate release and glutamine uptake assays: 10,000 cells were seeded per well in 96 well white clear flat bottom tissue culture plate (Corning, ME, USA). Glucose uptake, lactate release, and glutamine uptake assays were performed using Glucose uptake-GloTM assay, Lactate-GloTM assay and Glutamine/Glutamate-GloTM assay kits (all kits from Promega, Madison, USA) by following the manufacturer's protocol. Luminescence readings were taken using Synergy Neo2 multimode reader (BioTek, VT, USA).

XF96 extracellular flux analysis: Analysis of extracellular acidification rate (ECAR) and oxygen consumption rate (OCR) were performed using an XF96 extracellular flux analyzer (Seahorse Biosciences, North Billerica, MA) as shown previously (Wu et al., 2014). Thirty thousand single

cells were seeded per well in 96-well cell culture plates (Seahorse Biosciences, North Billerica, MA). Manufacturer's protocols were used to measure ECAR and OCR.

6. Cell treatments

CSE treatment was performed as shown previously [2]. Cells were left untreated or were treated with CSE (10 µL/mL or 1%) for 48 hours per passage. We continued this process for 40 passages (17 weeks or 120 days) so that cells were exposed to CSE for 80 days (Figure 1*A*). Similarly, cells were exposed to cigarette smoke components, nicotine (Sigma; 2 µM) or 4-(methylnitrosamino)-1-(3-pyridyl)-1-butanone (NNK) (Sigma; 2 µM) or N-Nitrosonornicotine (NNN) (Sigma; 2 µM) for 80 days. In some experiments, PD98059 (Sigma; 25 µM; 24 hours), an inhibitor of ERK1/2, and Macamylamine (Sigma; 200 µM; 24 hours), specific inhibitor and antagonist of CHRNA7 were added in 40th passage cultures, followed by 48-hour stimulation with CSE. In experiments using C-CSE, cells were treated with 20 µg/mL C-CSE or an equal volume of DMSO vehicle for 80 days by following the same treatment process used for CSE treatment (Figure 1*A*).

7. Flow cytometry

Autofluorescence Assay: Cells with stem cell or cancer stem cell features were analyzed and isolated using flow cytometry-based autofluorescence (AF) assay as shown previously [5]. In some experiments, riboflavin (30 µM) was added to cells and incubated for 1 hour at 37°C followed by AF analysis using BD LSR II Green flow cytometer (BD Biosciences, San Jose, CA). DAPI (4′,6-diamidino-2-phenylindole; 1 µg/mL) was used for live cell staining. AF cells were excited using a 488-nm blue laser and filters, 530/30 and 585/42 1 550LP Blue Det A-A. AF+ and AF− cells were sorted using BD FACS Aria (BD Biosciences) using 488 blue laser and similar filters (Blue E-A and Blue F-A). Gating strategy for AF+ and AF− population is shown in Supplementary Figure 2A. Data were analyzed using FACS DIVA software (BD Biosciences).

Aldefluor Assay: The activity of aldehyde dehydrogenase was detected using an ALDEFLUOR assay kit (StemCell Technologies, Vancouver, BC, Canada) according to manufacturer instructions. Stained cells were analyzed using LSR II Green (BD Biosciences) with the green fluorescence channel (515–545 nm), and data analyzed using FACS DIVA software program (BD Biosciences).

Side population assay: Side population analysis was performed with flow cytometry using Hoechst 33342 (AnaSpec Inc., Fremont, CA, USA) (5µg/ml) Verapamil (Sigma) control, an inhibitor of ABC transporters, was used for SP identification at 50 µM final concentration.

Analysis of stem cell surface markers: One million cells in 100µL buffer (PBS supplemented with 2% fetus bovine serum) were stained with ABCB1 PerCP efluor 710 and CD133 PerCP efluor 710 antibodies (Miltenyi Biotec, Germany) at concentrations suggested by the manufacturer for 20 min on ice. Cells were washed twice in the buffer and analyzed by LSR II Green flow cytometer (BD Biosciences). Respective isotype antibodies conjugated with the same fluorophore were used as controls.

Mitotracker staining: One million cells in 1mL of 10% DMEM medium were incubated for 20 min at 37^0C with 1nM Mitotracker^{TM} Deep Red FM (Life Technologies, Carlsbad, CA) followed by flow cytometry analysis using LSR II Green (BD Biosciences).

8. Western blotting

Cell lysis was performed in RIPA buffer (50 mM Tris-HCl, 150 mM NaCl, 1% NP-40, 0.5% sodium deoxycholate, 0.1% sodium dodecyl sulphate [SDS]) containing protease inhibitors (1 mM phenyl-methyl sulphonyl fluoride, 1 µg/mL aprotinin, 1 µg/mL leupeptin). Cell lysates were centrifuged at 15000g for 30 minutes to remove debris, and proteins quantified using Bio-Rad DC Protein Assay kit (Bio-Rad Laboratories, Hercules, CA). Total protein (40 µg/well) was fractionated by 10% or 15% SDS–polyacrylamide gel electrophoresis (PAGE). Fractionated proteins were electrophoretically transferred onto polyvinylidene difluoride membranes. Following transfer, membranes were washed in PBST (phosphate-buffered saline [PBS] and 0.1% Tween 20) followed by 1 hour blocking in 5% nonfat dry milk in PBST. Blots were incubated overnight at 4°C with primary antibodies with respective dilutions (diluted in 2% bovine serum albumin in PBS) (Supplementary Table 2). Glyceraldehyde 3-phosphate dehydrogenase and β-actin were used as loading controls for protein normalization. The membranes were then washed in PBST (3 × 10 minutes), probed with the appropriate secondary antibodies (Supplementary Table 2), incubated for an hour at room temperature, then washed with PBST (3 × 10 minutes). Signals were detected with the ECL chemiluminescence kit (Thermo Scientific, Rockford, IL).

9. Immunoprecipitation

Protein lysates were prepared (900 µg in 750 µL) and incubated overnight with PAF1 (4 µg), PHF5A (4 µg), and control immunoglobulin (Ig)-G antibodies (4 µg) (Supplementary Table 3). We next added the lysate-antibody mix with protein A/G Sepharose beads (Sigma-Aldrich Corp., St Louis, MO), followed by incubation on a rotating platform overnight at 4°C. After incubation, we washed the lysate-antibody-bead mix 4 times with lysis buffer. We then resolved immunoprecipitates and total cell lysates electrophoretically on SDS-PAGE (15%), followed by transferring resolved proteins onto the polyvinyldifluoride membrane. After blocking membranes with 5% nonfat dry milk in PBST for at least 1 hour, we added anti-PHF5A primary antibody (Supplementary Table 3). Next, we washed immunoblots 5 times (5 × 10 minutes) with PBST, followed by incubation for 2 hours with respective secondary antibodies (Supplementary Table 2). After washing with PBST 5 times, we performed the reaction with enhanced chemiluminescence ECL reagent (Thermo Scientific), and exposed the immunoblots to X-ray film to detect signals.

10. Immunohistochemistry

Pancreatic tissues were fixed, embedded in paraffin and sectioned. Immunohistochemistry (IHC) was performed as described previously [6]. Briefly, glass slides containing tissue sections were baked for 2 hours at 60°C. Tissue sections were deparaffinized using xylene and rehydrated in decreasing concentrations of ethanol. The activity of endogenous peroxidase was blocked by incubating tissue sections in Bloxall blocking solution (Vector Laboratories, Inc, Burlingame, CA) for 10 minutes at room temperature. After peroxidase blocking, antigen retrieval was performed by boiling tissue sections in 0.5% citrate buffer for 15 minutes. Next, tissue sections were blocked in 2.5% normal horse serum for 1 hour at room temperature. After blocking, sections were incubated with primary antibodies overnight at 4°C. Primary antibodies and respective dilutions used for IHC are listed in Supplementary Table 3. After overnight incubation with primary antibody, tissue sections were washed in PBS and incubated for 1 hour with horseradish peroxidase-conjugated secondary antibodies. After washing in PBS, sections were developed for colorimetric detection using the 3,3′diaminobenzidine kit (Vector Laboratories, Inc). Then, hematoxylin counterstaining was performed followed by dehydration with increasing concentrations of ethanol. After dehydration, tissue sections were dried and mounted with Permount (Cat. No. 17986-05; Fisher Scientific, Hatfield, PA).

Slides containing human pancreatic tissue sections (of the benign pancreas, PDAC without smoking history, and PDAC with smoking history) (n = 15) were the kind gifts from Dr. Talmon A. Geoffrey (pathologist, University of Nebraska Medical Center [UNMC]). Smoking status and tumor grade details of these human tissue sections are listed in Supplementary Table 8. IHC for PAF1 was performed on these human tissue sections as described previously. For FOSL1 IHC staining on these human tissues sections, double stain IHC kit (M&R on human tissue; Abcam, Cambridge, MA) was used and performed IHC by following the manufacturer's instructions. IHC-stained mice and human tissue sections were scored by Dr. Subodh M. Lele (Pathologist, UNMC), and **intensity** of FOSL1, PAF1, PHF5A, and SOX9 expression was graded on a scale of 0 to 3 (0, no staining; 1+, weakly positive; 2+, moderately positive; 3+, strongly positive). **The percentage** of FOSL1, PAF1, PHF5A, and SOX9 positive staining in PDAC ducts (Nuclear) was scored in a range of (0–100% or 0–1). A histoscore was calculated by multiplying intensity (0–3) and positivity (0–1), ranging between 0 and 3. Graph Pad Prism software was used to calculate *P* values and to design graphs.

Human PDAC tissues of primary, liver metastasis and lung metastasis were obtained from the Rapid Autopsy Program of the University of Nebraska Medical Center. IHC for MDR1, ALDH1A1, LDH-A, and ATP5B was performed and scored as described above by Dr. Dipak Kumar Prajapati.

11. Immunofluorescence

Immunofluorescence analysis on tissue sections was performed as shown previously [6]. Briefly, slides containing tissue sections were baked for 2 hours at 60°C. Then tissue sections were deparaffinized using xylene, rehydrated with decreasing concentrations of ethanol, and permeabilized by incubating in methanol for 30 minutes. After antigen retrieval and blocking in 5% normal goat serum, sections were incubated with primary antibody overnight at 4°C. After washing in PBS, tissue sections were incubated with fluorophore-conjugated secondary antibody for 1 hour at room temperature. Primary and secondary antibodies used for immunofluorescence and respective antibody dilutions are listed in Supplementary Table 3. Slides were washed in PBS and mounted with Vectashield containing DAPI. Fluorescent images were captured using Carl Zeiss imager.

12. Nile red staining

For AF on tissues, Nile red was used to visualize/track lipid content (lipid droplets) and to distinguish riboflavin-derived AF from lipid (Lipofuscin)-derived AF. After deparaffinization and rehydration, tissue sections were incubated with Bloxall blocking solution (Vector Laboratories, Inc) for 10 minutes at room temperature to block peroxidase and phosphatase activities, which are the sources of background AF. After washing in PBS, tissue sections were then incubated with Nile red (Invitrogen) at dilutions of 1:10,000 for 30 minutes at 37°C. Tissue sections were washed in PBS and mounted with Vectashield containing DAPI. AF was captured using Carl Zeiss imager.

For AF on cells, we seeded cells on coverslips, fixed with 100% ice-cold methanol for 5 minutes at −20°C, followed by washing with PBST 3 times (3 × 5 minutes) and PBS (1 × 5 minutes). After blocking in 5% normal goat serum for 1 hour at room temperature, cells were incubated with the anti-ABCG2 antibody (1:200) overnight. Next, we washed with PBS (3 × 5 minutes) followed by incubation with anti-mouse Alexa Fluor-568 secondary antibody. After washing, we mounted coverslips in DAPI medium (DAPI fluoromount-G; Southern Biotech, Birmingham, AL). AF was captured using Carl Zeiss Confocal Microscope using 488-nm blue laser.

For immunofluorescence on spheres, 10-day-old spheres were transferred from low-attachment plate to chamber slide and were allowed to attach by incubating at 37°C and 5% Co_2 for 12 hours. Immunofluorescence staining was performed for Oct3/4 on attached spheres using normal immunofluorescence procedure as described previously for cells. Oct3/4 staining and AF (green) were captured using Carl Zeiss Confocal Microscope.

13. Whole transcriptome analysis

Whole transcriptome analysis (RNA sequencing) was performed on chronic CSE-exposed and control cells at the Functional Genomics Core Facility at the City of Hope National Medical Center (Duarte, CA). The RNA quality was checked with an Agilent Bioanalyzer (Agilent Technologies, Inc, Santa Clara, CA) and all RNA integrity numbers were 10. Library preparation was achieved using Illumina (San Diego, CA) TruSeq RNA Sample Preparation Kit according to manufacturer protocol. Fifteen cycles of polymerase chain reaction (PCR) amplification were performed for each library, followed by an examination of size distribution using an Agilent Bioanalyzer (Agilent Technologies, Inc) and a DNA 1000 chip. Each sample used 1 of 12 unique indices (Illumina). All

libraries displayed a band between 200 and 500 bp with a peak at approximately 260 bp. The Qubit 2.0 Fluorometer (Life Technologies, Inc, Carlsbad, CA) was used to quantitate the libraries. Loading was performed at a concentration of 8.6 pM. Sequencing was done on Illumina HiScanSQ or HiSeq 2000 Sequencing Systems.

14. Quantitative real-time PCR

Total RNA was isolated and complementary DNA was synthesized. Primer sequences were designed using Primer Quest and Oligo Analyzer (Integrated DNA Technologies, Inc, Coralville, IA) tools. The specificity of each primer set to its target gene was confirmed using Primer BLAST. The list of primers used in the study are given in Supplementary Table 4. Real-time PCR was performed on the Roche 480 Real-Time PCR System (Indianapolis, IN). Reactions were performed in triplicate and template controls were run for each assay under the same conditions as described previously.[7]

15. Small interfering RNA and CRISPR/Cas9-based knockdown/knockout of PAF1

Twenty-four hours before small interfering RNA (siRNA) transfection, chronic CSE-treated HPNE and Capan1 cells were seeded at a density of 0.5×10^6 cells per well in a 6-well plate. Commercially available siRNA against human FOSL1 and PAF1 and control siRNA were purchased from OriGene (Rockville, MD). Lipofectamine-2000 transfection reagent (Invitrogen) was used to transfect siRNA, carefully following manufacturer recommendations. Down-regulation of proteins of interest was monitored after 48 hours of siRNA transfection by Western blot analysis. Knockout of PAF1 in Capan1 cells was also performed, as shown previously, using CRISPR/Cas9 system.[8]

16. Chromatin immunoprecipitation assay

Chromatin immunoprecipitation (ChIP) assay was performed by washing cells twice with PBS followed by crosslinking in PBS containing 1.5 mM EGS (Ethylene Glycol-bis, Succinimidysuccinate). After 15 minutes of incubation at room temperature with agitation, cells were fixed by adding 0.4% formaldehyde directly to the PBS-EGS followed by incubation for 15 minutes. Next, to arrest the cross-linking, cells were added with 125 mM glycine solution and incubated for 10 minutes at room temperature with agitation. After washing with PBS, cells were scraped in 1 mL of cold PBS and were pelleted by centrifugation at 1200g for 10 minutes at 4°C. After centrifugation, pellets were suspended in cell lysis buffer and kept on ice for 15 minutes.

Cells were pelleted at 1200g for 10 minutes, and nuclei lysed by resuspending in SDS lysis buffer followed by incubation on ice for 10 minutes. After sonication and centrifugation, supernatants were collected and incubated with phospho-FOSL1 antibody (4 µg) and control IgG antibody (4 µg) and incubated at 4°C overnight. Next, 30 µL of protein A and protein G agarose beads (Santa Cruz, Dallas, TX) were added and incubated for 6 hours, followed by bead collection and washing in low-salt buffer, high-salt buffer, lice buffer, and TE buffer, followed by reverse crosslinking in NaCl. After the last wash, ChIP DNA was purified using the ChIP DNA Clean & Concentrator kit (The Epigenetics, Irvine, CA). The eluted DNA was used for PCR reaction. The binding of phospho-FOSL1 to the region −2170 to +514 of the PAF1 gene was analyzed by PCR. PCR primers used for ChIP are listed in Supplementary Table 5. After PCR, products were run on 2% agarose gel; DNA bands were excised from the gel and purified the DNA using QIAquick gel extraction kit (Qiagen, Valencia, CA) followed by sequencing using forward primers. Chromatograms of ChIP DNA sequence quality was verified using Finch TV software program (Geospiza, Inc, Seattle, WA).

17. In vivo tumorigenicity assay

AF^+ and AF^- cells were sorted using fluorescence-activated cell sorter from chronic CSE-exposed HPNE and Capan1 cells. Cells (40,000) were suspended in 500 µL PBS and mixed with Matrigel (Fisher Scientific) (1:1 ratio). Cells (4000) in 100 µL were injected subcutaneously into the right (AF^+) and left (AF^-) flanks of 5-week-old athymic nude mice. Four mice were used per group and the appearance of tumors was checked by palpitation 2 times a week. Animals were sacrificed soon after tumor nodule reached 0.8 cm in diameter.

18. Quantification and statistical analysis

Sigma Plot and Graph Pad Prism were used for statistical analysis. Data are presented as the mean ± SD and mean ± SEM. Significance was determined using simple Student t-test. The details of the statistics of each experiment can be found in the figure legends.

19. Data and software availability

Data resources

The accession number for RNA sequencing data of smoke-treated HPNE and Capan1 cells is GSE101726. Original FCS files of flow cytometry experiments are available

at http://flowrepository.org and the repository IDs of all these flow cytometry experiments are FR-FCM-ZYJ3, FR-FCM-ZYJ4, FR-FCM-ZYJ5, FR-FCM-ZYJ6, FR-FCM-ZYJ7, FR-FCM-ZYJ8, and FR-FCM-ZYJ9.

References

1. N. Momi, M.P. Ponnusamy, S. Kaur, *et al.* Nicotine/cigarette smoke promotes metastasis of pancreatic cancer through alpha7nAChR-mediated MUC4 upregulation. Oncogene, 32 (2013), pp. 1384-1395.
2. Y. Liu, F. Luo, Y. Xu, *et al.* Epithelial-mesenchymal transition and cancer stem cells, mediated by a long non-coding RNA, HOTAIR, are involved in cell malignant transformation induced by cigarette smoke extract. Toxicol Appl Pharmacol, 282 (2015), pp. 9-19.
3. M.A. Kaisar, R.R. Kallem, R.K. Sajja, *et al.* A convenient UHPLC-MS/MS method for routine monitoring of plasma and brain levels of nicotine and cotinine as a tool to validate newly developed preclinical smoking model in mouse. BMC Neurosci, 18 (2017), p. 71.
4. R. Earla, A. Ande, C. McArthur, *et al.* Enhanced nicotine metabolism in HIV-1–positive smokers compared with HIV-negative smokers: simultaneous determination of nicotine and its four metabolites in their plasma using a simple and sensitive electrospray ionization liquid chromatography–tandem mass spectrometry technique. Drug Metab Dispos, 42 (2014), pp. 282-293
5. Miranda-Lorenzo, J. Dorado, E. Lonardo, *et al.* Intracellular autofluorescence: a biomarker for epithelial cancer stem cells. Nat Methods, 11 (2014), pp. 1161-1169.
6. S. Kumar, M.P. Torres, S. Kaur, *et al.* Smoking accelerates pancreatic cancer progression by promoting differentiation of MDSCs and inducing HB-EGF expression in macrophages. Oncogene, 34 (2015), pp. 2052-2060.
7. M.P. Ponnusamy, S. Deb, P. Dey, *et al.* RNA polymerase II associated factor 1/PD2 maintains self-renewal by its interaction with Oct3/4 in mouse embryonic stem cells. Stem Cells, 27 (2009), pp. 3001-3011.
8. S. Karmakar, P. Seshacharyulu, I. Lakshmanan, *et al.* hPaf1/PD2 interacts with OCT3/4 to promote self-renewal of ovarian cancer stem cells. Oncotarget (2017), pp. 14806-14820.

CHAPTER 4

Induction of pancreatic cancer stem cells by risk factor: cigarette smoking

The material covered in this chapter is the subject of one published research article:

Nimmakayala RK, Seshacharyulu P, Lakshmanan I, Rachagani S, Chugh S, Karmakar S, Rauth S, Vengoji R, Atri P, Talmon GA, Lele SM, Smith LM, Thapa I, Bastola D, Ouellette MM, Batra SK, Ponnusamy MP, Cigarette Smoke Induces Stem Cell Features of Pancreatic Cancer Cells via PAF1, **Gastroenterology 2018;** 155 (3): 892-908.e6.

Cigarette Smoke Induces Stem Cell Features of Pancreatic Cancer Cells via PAF1.

Nimmakayala RK[1], Seshacharyulu P[1], Lakshmanan I[1], Rachagani S[1], Chugh S[1], Karmakar S[1], Rauth S[1], Vengoji R[1], Atri P[1], Talmon GA[2], Lele SM[2], Smith LM[3], Thapa I[4], Bastola D[4], Ouellette MM[5], Batra SK[6], Ponnusamy MP[7].

Author information

[1]Department of Biochemistry and Molecular Biology, College of Medicine, University of Nebraska Medical Center, Omaha, Nebraska.

[2]Department of Pathology and Microbiology, College of Medicine, University of Nebraska Medical Center, Omaha, Nebraska.

[3]Department of Biostatistics, College of Public Health, University of Nebraska Medical Center, Omaha, Nebraska.

[4]School of Interdisciplinary Informatics, University of Nebraska at Omaha, Omaha, Nebraska.

[5]Department of Internal Medicine, College of Medicine, University of Nebraska Medical Center, Omaha, Nebraska.

[6]Department of Biochemistry and Molecular Biology, College of Medicine, University of Nebraska Medical Center, Omaha, Nebraska; Eppley Institute for Research in Cancer and Allied Diseases, Fred & Pamela Buffett Cancer Center, University of Nebraska Medical Center, Omaha, Nebraska. Electronic address: sbatra@unmc.edu.

[7]Department of Biochemistry and Molecular Biology, College of Medicine, University of Nebraska Medical Center, Omaha, Nebraska; Eppley Institute for Research in Cancer and Allied Diseases, Fred & Pamela Buffett Cancer Center, University of Nebraska Medical Center, Omaha, Nebraska. Electronic address: mpalanim@unmc.edu.

***Correspondence**: Moorthy P. Ponnusamy and Surinder K. Batra, Department of Biochemistry and Molecular Biology, University of Nebraska Medical Center, Omaha, Nebraska, 68198-5870, U.S.A.

Phone: 402-559-1170, Fax: 402-559-6650, Email: mpalanim@unmc.edu (M.P.P) and sbatra@unmc.edu (S.K.B).

Synopsis

Cigarette smoking is a major risk factor for pancreatic cancer. Aggressive pancreatic tumors contain cancer cells with stem cell features. We investigated whether cigarette smoke induces stem cell features in pancreatic cancer cells. $Kras^{G12D}$; Pdx1-Cre mice were exposed to cigarette smoke or clean air (controls) for up to 20 weeks; pancreata were collected and analyzed by histology, quantitative reverse transcription polymerase chain reaction, and confocal immunofluorescence microscopy. HPNE and Capan1 cells were exposed to cigarette smoke extract (CSE), nicotine and nicotine-derived carcinogens (NNN or NNK), or clean air (controls) for 80 days and evaluated for stem cell markers and features using flow cytometry-based autofluorescence, sphere formation, and immunoblot assays. Proteins were knocked down in cells with small interfering RNAs. We performed RNA sequencing analyses of CSE-exposed cells. We used chromatin immunoprecipitation assays to confirm the binding of FOS-like 1, AP-1 transcription factor subunit (FOSL1) to RNA polymerase II-associated factor (PAF1) promoter. We obtained pancreatic ductal adenocarcinoma (PDAC) and matched non-tumor tissues (n = 15) and performed immunohistochemical analyses. Chronic exposure of HPNE and Capan1 cells to CSE caused them to increase markers of stem cells, including autofluorescence and sphere formation, compared with control cells. These cells increased expression of ABCG2, SOX9, and PAF1, via cholinergic receptor nicotinic alpha 7 subunit (CHRNA7) signaling to mitogen-activated protein kinase 1 and FOSL1. CSE-exposed pancreatic cells with knockdown of PAF1 did not show stem cell features. Exposure of cells to NNN and NNK led to increased expression of CHRNA7, FOSL1, and PAF1 along with stem cell features. Pancreata from $Kras^{G12D}$; Pdx1-Cre mice exposed to cigarette smoke had increased levels of PAF1 mRNA and protein, compared with control mice, as well as increased expression of SOX9. Levels of PAF1 and FOSL1 were increased in PDAC tissues, especially those from smokers, compared with non-tumor pancreatic tissue. CSE exposure increased expression of PHD-finger protein 5A, a pluripotent transcription factor and its interaction with PAF1. Exposure to cigarette smoke activates stem cell features of pancreatic cells, via CHRNA7 signaling and FOSL1 activation of PAF1 expression. Levels of PAF1 are increased in pancreatic tumors of humans and mice with chronic cigarette smoke exposure.

Background and rationale

Pancreatic cancer (PC) is recognized as one of the deadliest diseases [1]. Of various established risk factors, cigarette smoking causes 30% of all cases of PC [1], and therefore there is an urgent need to develop novel therapeutic strategies to specifically treat patients with PC who have a history of smoking. Currently, efforts for the development of such strategies are limited because there is no mechanistic understanding of how cigarette smoking is involved in PC initiation and progression.

A previous study from our laboratory showed that cigarette smoke and its major addictive component, nicotine, induces progression and metastasis of PC through cholinergic receptor nicotinic alpha 7 subunit (CHRNA7)-mediated MUC4up-regulation [2]. Cigarette smoke contains more than 4000 chemical components, and among them, nicotine and nicotine-derived carcinogens, 4-(methyltyramine)-1-(3-pyridyl)-1-butanone (NNK), N-Nitrosonornicotine (NNN), are associated with carcinogenesis [3,4,5]. Recent studies provide evidence for the association of cigarette smoke and its ingredients with the enrichment of cancer stemness population in various cancers [6,7]. In mice, nicotine promotes initiation and progression of Kras-induced PC via Gata6-dependent de-differentiation of acinar cells [8]. In our editorial commentary, we have proposed a role for nicotine in pancreatic stemness induction and acinar cell de-differentiation [9]. Despite these studies, it still remains uncertain whether and how cigarette smoke induces stem cell features in pancreatic cells or PC cells.

Recent studies have shown that FOS-like 1, AP-1 transcription factor subunit (FOSL1) is significantly overexpressed in PC [10]. Loss of FOSL1 reduces stemness properties in hepatocellular carcinoma [11]. FOSL1 belongs to the Fos gene family, which consists of 4 members: FOS, FOSB, FOSL1 (or FRA1), and FOSL2. FOS family members dimerize with JUN family proteins, such as c-Jun, JunB, and JunD, forming a dimeric transcription factor called Activator Protein-1 (AP-1) transcription factor. FOSL1 transcription factor levels are increased in response to a variety of stimuli, including smoking [12]. However, to our knowledge, the role of FOSL1 in smoking-induced activation of pancreatic stemness has not been investigated before.

PAF1, human RNA polymerase II-associated factor also known as pancreatic differentiation protein 2 (PD2) is a subunit of the PAF1 complex, which is composed of PAF1, Ctr9, Cdc73, Rtf1, Ski8, and Leo1, and regulates multiple processes, including transcription initiation and elongation

[13,14,15,16]. We and others have demonstrated that PAF1 plays an important role in the maintenance of embryonic stem cell (ESC) signature in a complex independent manner. The PAF1 maintains pluripotency and self-renewal of mouse ESCs [17, 18]. PHD-finger protein 5A (PHF5A) has recently been shown to regulate the self-renewal of ESCs. The endogenous PAF1, by interacting with PHF5A activates more than 600 pluripotent genes in ESCs by regulating RNA polymerase II elongation in pluripotent loci [19]. We also showed that PAF1 maintains cancer stemness population and induces tumorigenesis and metastasis in PC [20, 21]. Overall, these studies suggest that PAF1 is a major ESC maintenance factor, and its levels are increased in PC. To our knowledge, the role of PAF1 in cigarette smoke-induced PC is unknown.

In the present study, we sought to determine whether chronic exposure to cigarette smoke and its ingredients, nicotine, NNN, and NNK, could enrich pancreatic stemness. We investigated the mechanism involved in the smoking-induced promotion of pancreatic stemness and cancer stemness population, using in vitro and in vivo models. We observed that chronic exposure to cigarette smoke increases PAF1, a major ESC signature protein through CHRNA7/extracellular signal-regulated kinase (ERK)/FOSL1/cJun (AP1) signaling pathway. We concluded that chronic cigarette smoke exposure promotes pancreatic stemness and that NNN and NNK are the major contributing factors for the smoking-induced stemness induction.

Results

A. Chronic exposure to cigarette smoking increases stemness in normal pancreatic duct cells and PC cells

To study the effect of cigarette smoking on pancreatic stemness, we prepared CSE using a standard protocol in our laboratory [2, 23]. Because nicotine is a major cancer-causing agent in cigarette smoke, we first sought to determine the levels of nicotine in CSE. Using liquid chromatography-tandem mass spectrometry analysis, we determined the concentration of nicotine in CSE to be 33.073 ± 0.698μg/mL (Supplementary Figure 1*A*, *B*, and *C*).

To determine whether cigarette smoke induces stemness signature in pancreatic duct epithelial cells and PC cells, we exposed HPNE and Capan1 cells to CSE (1%) for up to 80 days (Figure 1*A*). Lorenzo et al. [24] recently developed a novel autofluorescence-based technique to identify cancer stemness population. The source of AF is riboflavin-loaded intracellular vesicles: the riboflavin enters vesicles through ABCG2 transporters using an ATP-dependent process.

Because the technique is mainly based on riboflavin, we sought to investigate whether the addition of riboflavin increases AF. Flow cytometry analysis of AF showed that the addition of riboflavin (30 μM) increased the AF-positive (AF^+) population to 0.4% and 1.0% in HPNE and Capan1 cells, respectively (Supplementary Figure 2*A*). We were also interested to observe riboflavin-loaded intracellular vesicles with membranous ABCG2 expression using confocal microscopy (Supplementary Figure 2*B*). Confocal microscopy also revealed that CSE significantly increases AF^+content in HPNE and Capan1 cells (Figure 1*B*). AF analysis using flow cytometry on days 20, 40, and 80 of CSE treatment showed a time-dependent increase in the percentage of AF^+ cells as compared with respective time point controls (Figure 1*C*).

To confirm whether AF^+ cells are indeed a stemness population, we sorted AF^+ and non-autofluorescent (AF^-) cells using fluorescence activated cell sorting. As expected, AF^+ cells show elevated expressions of major stemness signature genes, such as Sox2, PAF1, Oct3/4, and ABCG2 (Figure 1*D*). Further, flow cytometry analysis showed more $ABCG2^+$ and $CD44^{High}$ population in AF^+ cells as compared with AF^-cells (Figure 1*E*).

Previous studies have shown that the ability to form spheres in vitro is one of the standard ways to assess the self-renewal potential of normal and cancer cells [25, 26]. To determine the self-renewal property of AF^+ and AF^- populations, we performed the sphere assay and observed that AF^+ cells showed an increased number of spheres as compared with AF^- cells. Besides, AF^+ cells showed the capacity to form secondary and tertiary spheres (Supplementary Figure 3*A*). Next, to determine in vivo tumorigenicity of AF^+ and AF^- cells, 4000 cells were injected subcutaneously into the left and right flanks of athymic nude mice. AF^+ cells sorted from CSE-exposed Capan1 cells started forming tumor nodules 2 weeks after implantation. After 27 days, mice were euthanized and tumors were excised. Compared with AF^-cells, AF^+ cells sorted from CSE-induced Capan1 cells showed increased tumor weight (Supplementary Figure 3*B*). However, the AF^+ population sorted from CSE-induced HPNE cells could not form tumors even after 4 months (Supplementary Figure 3*C*).

B. Smoking induces stemness signature in pancreatic ductal epithelial cells and cancer cells

To determine the ability of sphere formation by the CSE-induced whole cell population, we performed sphere assay on CSE-exposed HPNE and Capan1 cells on days 20, 40, and 80 of CSE exposure. Compared with respective time point controls, CSE-exposed cells showed an

increase in the number and size of spheres (Figure 2*A*). In agreement with this observation, Liu and colleagues [23] reported that chronic treatment with CSE increases the number of spheres in normal human bronchial epithelial cells. To determine whether cells within the spheres show AF and stemness marker expression, we performed immunofluorescence assay for Oct3/4 and AF. Cells within spheres formed by CSE-induced HPNE and Capan1 cells showed co-localization of AF and Oct3/4 expression (Figure 2*B*).

To further investigate the impact of CSE on pancreatic stemness, we analyzed protein expression levels of major stemness signature proteins, SOX2, Oct3/4, KLF4, BMI1, Nanog, β-catenin and PAF1, the pancreatic progenitor cell marker, SOX9, and the cancer stemness markers, aldehyde dehydrogenase 1 (ALDH1) and CD44. In HPNE and Capan1 cells, CSE markedly induced the expression of stemness signature and cancer stemness markers (Figure 2*C*); however, BMI1 did not show any variation (Supplementary Figure 4*A*). Of interest, CSE induced a more than 3-fold increase in the protein expression levels of PAF1, a master regulator of stemness [19] suggesting its importance in smoking-mediated stemness enrichment (Figure 2*C*). To investigate whether commercial CSE (C-CSE) also shows a similar effect on stemness marker expressions, HPNE, and Capan1 cells were exposed to 20 μg/mL C-CSE for 80 days. Increased expression of PAF1 and SOX9 was observed in C-CSE–exposed cells as compared with vehicle- (dimethyl sulfoxide) treated control cells (Supplementary Figure 4*B*).

Next, we also observed increased expression of ABCG2, SOX9, PAF1, β-catenin, CD44, and CD24 in CSE-exposed cells, as revealed by immunofluorescence staining (Figure 2*D* and Supplementary Figure 5*A*). CSE also significantly up-regulated PAF1 and SOX9 messenger RNA (mRNA) levels (Figure 2*E*). Aldefluor assay [27] showed that CSE induces ALDH activity up to 2% in HPNE cells, but up to 50% in Capan1 cells (Supplementary Figure 5*B*). These data suggest that cigarette smoke induces a stemness signature, specifically PAF1, in human pancreatic ductal epithelial cells and in PC cells.

C. Cigarette smoking induces PAF1 in $Kras^{G12D}$; Pdx-1 Cre mouse

The findings described previously suggest that cigarette smoke significantly up-regulates PAF1 in vitro. Previously, we and others showed the importance of PAF1 in the maintenance of stemness in ESCs and PC stemness populations [17, 18, and 19] and this triggered us to further explore its role in cigarette smoke–enriched stemness in vivo. We observed significantly elevated expression of PAF1 in the pancreas of 20 weeks cigarette smoke-exposed control and $Kras^{G12D}$;

Pdx-1Cre mice[22] (Figure 3*B*and *C*). Of note, PAF1 mRNA levels are also significantly higher in cigarette smoke-exposed mouse groups (Figure 3*D*). We also observed an increased expression of SOX9 (Supplementary Figure 6*A*) and elevated coexpression of PAF1 with CD44 (Figure 3*E*) and SOX9 (Supplementary Figure 6*B*) in cigarette smoke-exposed mice. Also, cigarette smoke-exposed pancreas tissues showed an increased AF content as compared with controls (Figure 3*F*). In addition to riboflavin, another source of AF is lipid content or lipofuscin [28]. Therefore, we analyzed colocalization of AF and Nile red (lipid content marker) staining in the pancreas of cigarette smoke-exposed mice. Results indicated that AF does not emanate from lipid content or lipofuscin, and this provides evidence for the purity of riboflavin-derived AF.

Furthermore, AF is colocalized with PAF1 and ABCG2 (Figure 3*G*). Colocalization of PAF1 expression with AF in CSE-exposed HPNE cells is also shown in Supplementary Figure 6*B*. These in vivo data clearly correlated with in vitro findings, suggesting that smoking induces PAF1 and stemness markers in vivo.

D. Cigarette smoke induces the enrichment of stemness through PAF1

Next, we investigated whether up-regulation of the stemness signature in response to cigarette smoke exposure is regulated through PAF1. To elucidate this hypothesis, we performed CRISPR/Cas9-based knockout (KO) and small interfering RNA–based knockdown (KD) of PAF1 in Capan1 and HPNE cells, respectively (Figure 4*A*). We were interested in finding that loss of PAF1 reduced protein expression of SOX9 and β-catenin (Figure 4*A*). Further, silencing of PAF1 reduced the percentage of cigarette smoke-induced AF cells (Figure 4*B* and *C*) and the ABCG2+ population (Figure 4*D*–*F*) as compared with scramble control. These results suggest that smoking induces pancreatic stemness through PAF1.

E. Smoking-Induced PAF1 is regulated through FOSL1 transcription factor

To unveil the mechanism involved in the smoking-mediated induction of pancreatic stemness, whole transcriptome analysis was performed using RNA sequencing (Gene Expression Omnibus database accession number: GSE101726) in CSE-treated HPNE and Capan1 cells (Supplementary Figure 7*A* and *B*). We found that four stemness-associated genes, including LIF (maintains stemness in ESC), ALDH1A3 (cellular detoxifying enzyme and cancer stemness marker), ABCC4, ABCG2 (associated with drug resistance), and FOSL1 are commonly overexpressed in CSE-exposed HPNE and Capan1 cells. We further validated the precision of

our RNA sequencing data by performing quantitative reverse transcriptase polymerase chain reaction on these stemness genes (Supplementary Figure 7*C*).

We focused on FOSL1, given that it showed up-regulation in both HPNE and Capan1 cells, due to its involvement in a variety of cellular events mediated by smoking (Supplementary Figure 4*A*; Supplementary Tables 6 and 7) and to its association with stemness [11]. We thus performed PAF1 gene promoter analysis for potential transcription factor binding sites of FOSL1, using TRANSFAC software (geneXplain GmbH, Wolfenbüttel, Germany), and observed 10 FOSL1 binding sites (Supplementary Figure 8). Further, we silenced FOSL1 and observed down-regulation of cigarette smoking-induced PAF1 in both HPNE and Capan1 cells (Figure 5*A*). However, FOSL1 knockdown did not show any effect on untreated HPNE and Capan1 cells, suggesting that FOSL1-mediated PAF1 up-regulation is specific to cigarette smoking (Figure 5*A*). To determine whether cigarette smoke-induced FOSL1 binds to PAF1 promoter, we performed chromatin immunoprecipitation (ChIP) assay. ChIP results indicated that FOSL1 specifically binds to 3 binding sites (BS9: $^{-2162}$TGACTGACTGAC^{-2150}; BS1: $^{-67}$TGAGCAT^{-61}; BS3: $^{-836}$TCACTCAGT^{-828}) among ten predicted binding sites (Figure 5*B* and Supplementary Figure 8). This observation was further confirmed by sequencing of ChIP polymerase chain reaction products for these specific sites (Supplementary Figure 9*A* and *B*). These results indicate that cigarette smoke-induced FOSL1 is involved in the up-regulation of PAF1.

We also observed the overexpression of FOSL1 (Figure 5*C*) and its colocalization with PAF1 (Figure 5*C*) and CD44 (Supplementary Figure 10) in the pancreas of smoke-exposed control and Kras^{G12D}; Pdx-Cre mice. Taken together, accumulating data suggest that smoking-induced FOSL1 regulates the PAF1 gene.

F. PAF1 and FOSL1 co-overexpressed in human pancreatic ductal adenocarcinoma

To study the relevance of PAF1 and FOSL1 to the human PDAC, we analyzed the expression of FOSL1 and PAF1 in PDAC tissues with smoking history. PAF1 and FOSL1 showed significantly increased expression in PDAC tissues as compared with normal pancreas (Figure 5*D*). Of interest, increased expression of PAF1 and FOSL1 was observed in smoker PDAC tissues as compared with nonsmoker PDAC (Figure 5*D*). FOSL1 and PAF1 also showed increased colocalization in PDAC tissues of smokers compared with nonsmokers (Figure 5*D*).

G. Smoking induces PAF1 through nACHRα7/ERK/FOSL1-cJUN (AP1) signaling pathway

The observations presented previously indicate that FOSL1 regulates PAF1 under smoking treatment. We next investigated the mechanism involved in this process. The up-regulation of phospho-FOSL1 (Ser 265) was confirmed in HPNE and Capan1 cells following chronic exposure to CSE and C-CSE (Figure 5*E* and Supplementary Figure 4*B*). We further examined whether CSE would also activate FOSL1 interacting partner (phospho c-Jun, AP-1 family member). We found that the expression of phospho c-Jun (Ser 73) is significantly elevated in response to CSE treatment, demonstrating that chronic exposure to cigarette smoke induces up-regulation of the AP1 (FOSL1-c-Jun) transcription factor (Figure 5*E*). Next, we aimed to study the upstream regulators that mediate cigarette smoke-induced AP1 activation by examining Erk1/2, known upstream regulators of AP1 [29, 30]. CSE exposure increased the protein levels of phospho Erk1/2 (Thr202/Tyr204) (Figure 5*E*). The inhibition of phosphoErk1/2 abolished cigarette smoke-induced phospho--FOSL1, phospho-cJUN, and PAF1 in CSE-exposed cells (Figure 5*F*). These data suggested that cigarette smoke induces Erk1/2 phosphorylation and that the subsequent phosphorylation of FOSL1 may lead to direct transcriptional activation of PAF1.

Our next goal was to find the upstream receptor that activates the ERK1/2-FOSL1 signaling pathway. We analyzed the activation of smoking-associated receptors, including CHRNA1, CHRNA7, and TLR4 and observed an increased expression only in CHRNA7 in CSE-exposed cells. (Figure 5*E* and Supplementary Figure 11*A*). Furthermore, inhibition and knockdown of CHRNA7 resulted in decreased expression of phospho-ERK, phospho-FOSL1, and PAF1 in these CSE-exposed cells (Figure 5*G* and Supplementary Figure 11*B*). These results indicate that smoking induces PAF1 through the CHRNA7/ERK/FOSL1-cJUN (AP1) signaling pathway.

H. Specific cigarette smoke components, Nicotine, NNK, and NNN induce pancreatic stemness and PAF1

To determine the major cigarette smoke components responsible for pancreatic stemness induction, we treated HPNE and Capan1 cells with cigarette smoke components, nicotine, NNK, and NNN, for 80 days and analyzed for stemness enrichment. Specifically, NNN and NNK treatment significantly enriched the AF population (Figure 6*A*) and significantly increased sphere formation (Figure 6*B*) in HPNE and Capan1 cells. Further, treatment with NNN and NNK

increased the protein expression levels of CHRNA7, p-FOSL1, FOSL1, and PAF1, and this effect is similar to that observed with CSE treatment (Figure 6*C* and *D*). These data suggest that NNK and NNN specifically contribute to cigarette smoke-induced pancreatic stemness through the PAF1 mechanism.

I. Smoking induces interaction between PAF1 and PHF5A, an event required for stemness enrichment

Recent evidence shows that PAF1 interacts with PHF5A and that this complex regulates more than 600 pluripotent genes in ESCs [19]. PHF5A is a PHD-finger protein required for PAF1 complex recruitment, complex stabilization, release of RNA polymerase II proximal promoter pause, serine 2 phosphorylation of RNA polymerase II (Ser-2-P-Pol II) and elongation of pluripotency gene transcription in ESCs [19,31,32,33]. The PAF1-PHF5A complex-mediated activation of pluripotent genes was well studied in ESCs; however, its role in smoking-induced enrichment of stemness in PC has not been investigated. Based on this study, we developed a hypothesis that PAF1 interacts with PHF5A and regulates the smoking-mediated stemness enrichment. Our results showed an increased expression of PHF5A in CSE- and C-CSE-treated cells (Figure 7*A* and Supplementary Figure 4*B*), as well as in the pancreas of cigarette smoke-exposed control and $Kras^{G12D}$; Pdx-Cre mice (Figure 7*B* and *C*). A clear co-localization of PAF1 and PHF5A was also observed by immunofluorescence staining in the pancreas tissues of cigarette smoke-exposed mice and CSE-exposed cells (Figure 7*B* and *D* and Supplementary Figure 12). Also, cigarette smoke increased the interaction between PAF1 and PHF5A compared with untreated controls as evidenced by immunoprecipitation assay (Figure 7*E*). We also observed increased protein expression of Ser-2-P-Pol II and Leo1, a PAF1 complex molecule; however, other PAF1 complex subunits, including CTR9, CDC73, and SKI8, did not show any variation (Figure 7*A*). Taken together, our data suggest that smoking induces PHF5A and increases the interaction between PAF1 and PHF5A, an event required for the activation of stemness genes.

Discussion

Cigarette smoking is a well-established risk factor for PC; however, a mechanistic understanding of PC development in response to cigarette smoking is limited. Accumulating evidence indicates that the stemness signature is induced in various cancers that initiate and aggravates tumors [34, 35]. However, whether and how cigarette smoking induces pancreatic stemness is unknown.

Here, we establish for the first time a novel PAF1-mediated mechanism of cigarette smoke-induced pancreatic stemness.

Despite several studies showing an association between cigarette smoking and stemness induction in various cancers [36, 37], it remains unclear whether exposure to cigarette smoke induces stemness in PC. To explore this critical gap in understanding, we performed chronic exposure to cigarette smoke in pancreatic normal and cancer cells and found that cigarette smoking increases pancreatic stemness. Cigarette smoke exposure increased the pancreas-specific multipotent stemness factor, SOX9, and the stemness markers, ALDH1, and CD44 in pancreatic normal and cancer cells, suggesting that exposure to cigarette smoke induces multipotent stemness fraction and cancer stemness in the pancreas.

Cigarette smoke-exposed pancreatic normal and cancer cells also showed SOX2, Oct3/4, Nanog, and KLF4 expression along with significant overexpression of PAF1, an ESC signature maintenance factor, suggesting that cigarette smoking augments an ESC-like stemness program. We further found that cigarette smoke-induced stemness signatures in normal cells are almost similar to those of PC cells. However, the cigarette smoke-induced stemness population of normal pancreatic duct cells did not show any oncogenic potential. Cigarette smoke-induced stemness population isolated from normal duct cells failed to form subcutaneous tumors, whereas the stemness population of cigarette smoke-induced cancer cells did produce tumors. These data suggest that the observed stemness induction under cigarette smoke stress in normal duct cells is an early step toward cancerous reprogramming. Consistent with this observation, a recent report indicated that airway basal cells of healthy smokers acquire an ESC-like phenotype or signature, itself an early step toward malignant transformation [38].

Our data suggest the possibility that cigarette smoking expands the stemness population in normal tissues, and that this mechanism may be responsible for PC initiation. There are two possibilities for the expansion of stemness population in response to cigarette smoke exposure. First, a cigarette smoke-induced increase in stemness may be due to the promotion of an existing stemness population within normal pancreatic tissues. Second, a benign and differentiated cell may also take on the stemness phenotype on chronic exposure to cigarette smoke. In the first possibility, long-term, continuous, and rapid cell divisions in the stemness population in response to extracellular stress may eventually induce mutations leading to complete malignant transformation [39]. Investigation of this possibility by increasing the length and amount of cigarette smoke exposure would provide clues to PC initiation caused by cigarette smoke.

However, we conclude that cigarette smoking does induce stemness signatures in normal and PC cells.

Previous studies suggested PAF1 as a major stemness signature maintenance factor in ESCs and cancer cells [18, 19, 20, and 40]. Observations presented previously also show that PAF1 is one of the significantly overexpressed stemness factors under the oncogenic stress of cigarette smoke. Based on these, we sought to further explore its mechanistic role in cigarette smoke-induced stemness. As an important piece of evidence that PAF1 maintains stemness, PAF1 loss showed reduced expression levels of stemness markers, SOX9, and β-catenin in normal pancreatic cells and PC cells. Further, we also identified overexpression of PAF1 in 20 weeks cigarette smoke-exposed normal and $Kras^{G12D}$; Pdx-Cre mice. Additional evidence that PAF1 is associated with stemness is found in the fact that cigarette smoke-induced PAF1 expression correlates with the expression of other stemness markers, SOX9 and CD44, in cigarette smoke-exposed normal and $Kras^{G12D}$; Pdx-Cre mice. Of note, the loss of PAF1 decreased cigarette smoke-induced pancreatic stemness, suggesting that PAF1 is a major regulator of cigarette smoke-induced pancreatic stemness.

Furthermore, elevation of FOSL1, a critical transcription factor, was observed in cigarette smoke-exposed cells along with other stemness genes, including LIF, ALDH1, and ABCG2. Consistent with this finding, cigarette smoke was found to activate the AP1 (FOSL1-cJun) signaling pathway to induce epithelial-mesenchymal transition in bladder cancer [30]. The loss of FOSL1 also down-regulated stemness marker expressions and inhibited sphere formation in hepatocellular carcinoma cells, suggesting a role for FOSL1 in the maintenance of stemness [11]. We also demonstrated that cigarette smoke increases the expression of the FOSL1 gene and that it activates the AP1 transcription factor. Given the association between the FOSL1 transcription factor and stemness, we investigated whether the cigarette smoke-induced PAF1 gene is regulated by the FOSL1 transcription factor. We observed 10 FOSL1 binding sites near or on the PAF1 gene promoter, suggesting the potential of FOSL1 (AP1) binding on the PAF1 promoter and FOSL1-mediated regulation of the PAF1 gene. Our data suggest that FOSL1 specifically binds to 3 of 10 predicted binding sites: 2 are at the distal ($^{-2161}$TGACTGACTGAC^{-2150} and $^{-836}$TCACTCAGT^{-828}) and the other at the proximal promoter region ($^{-67}$TGAGCAT^{-61}) of the PAF1 gene. Of interest, cigarette smoke-exposed cells with FOSL1 depletion also displayed reduced expression of PAF1, indicating that cigarette smoke–activated FOSL1 regulates PAF1.

Our data also demonstrated that the pancreas of patients with PDAC shows increased PAF1 and FOSL1 expression as compared with healthy persons. Also, PAF1 and FOSL1 expressions are higher in the pancreas of patients with PDAC who have a smoking history, suggesting a strong correlation of PAF1 and FOSL1 expressions with smoking history in patients with PDAC.

We also proved that cigarette smoke induces PAF1 through a CHRNA7-ERK1/2-FOSL1 signaling pathway. The FOSL1 is a known downstream effector of the ERK pathway [29] and a previous study from our laboratory showed that cigarette smoke and its component, nicotine, induces PC by activating CHRNA7-ERK1/2-MUC4 pathway [2]. Consistent with these findings, CHRNA7 and its downstream effector ERK show up-regulation in response to cigarette smoke treatment. Inhibition of CHRNA7 and ERK reduces expression levels of the downstream signaling molecules, phospho-FOSL1 and PAF1. Thus, our data suggest that one mechanism by which cigarette smoke promotes pancreatic stemness is through the CHRNA7-ERK1/2-FOSL1-PAF1 signaling pathway.

We next sought to investigate the cigarette smoke ingredients most responsible for activation of the CHRNA7-ERK1/2-FOSL1-PAF1 signaling pathway. We demonstrated that cigarette smoke components, specifically NNN and NNK, induce pancreatic stemness, as evidenced by the increased percentage of AF and up-regulation of stemness markers, SOX9 and KLF4. Moreover, these cigarette smoke components induced signaling molecules of the CHRNA7-ERK1/2-FOSL1-PAF1 signaling pathway. Overall, NNK and NNN are the major cigarette smoke components that are responsible for cigarette smoke-mediated stemness enrichment.

We further found that cigarette smoke induces PHF5A, a PAF1 complex recruiting and stabilizing protein, and increases the interaction between PHF5A and PAF1. A recent study showed that PAF1 interacts with PHF5A and that the PAF1-PHF5A complex regulates 686 stemness genes in ESCs [19]. Another study demonstrated that pluripotent genes in differentiated somatic cells are in an inactive state due to the RNA polymerase II proximal promoter pause [31]. Loss of PHF5A in ESCs increased RNA polymerase pausing and reduced Ser-2-P-Pol II levels in the promoter regions of PAF1 target or pluripotent genes, thereby reducing the expression of these genes [19]. These studies indicate that PHF5A and PAF1 are required for the pause release and for maximum levels of Ser-2-P-Pol II at the promoter regions of pluripotent genes. In agreement with this, cigarette smoke increased the levels of Ser-2-P-Pol II in pancreatic normal and cancer cells. Overall, our observations suggest that cigarette smoking increases the PAF1-PHF5A interaction that is required for the activation of stemness genes.

Altogether, our results show that cigarette smoke induces the PAF1 gene through the CHRNA7-ERK-FOSL1 signaling pathway, resulting in the induction of a stemness signature (Figure 7*F*). On induction of PAF1 in response to cigarette smoke, PAF1 interacts with PHF5A and may reprogram a differentiated cell or cancer cell population into stemness or a cancer stemness population by up-regulating stemness genes; however, this suggestion requires further research. However, our study shows for the first time a novel mechanism of cigarette smoke-induced expansion of the pancreatic stemness population. In the future, our findings may contribute to the development of targeted therapy for patients with PC who have a smoking history.

Figure legends

Figure 1. Exposure to cigarette smoke increases pancreatic stemness. (*A*) HPNE and Capan1 cells were exposed to CSE (1%), commercial CSE (C-CSE) (20 μg/mL), or to cigarette smoke components, nicotine (2 μM), NNK (2 μM) and NNN (2 μM), for 80 days (2 days exposure per passage; thus, up to 40 passages). (*B*) Confocal imaging for AF in CSE-treated (CSE-T) cells compared with untreated controls. AF (green) and nuclei were stained using DAPI (blue) (n = 4). Scale bars = 50 μm. (*C*) Left: Flow cytometry analysis of AF content in CSE-exposed cells at different treatment time points. AF cells were excited using a 488-nm blue laser and filters, 530/30 and 585/42 1 550LP Blue Det A-A. Right: Percentage of AF cells at different time points of CSE exposure as compared with respective time point controls. (n = 3). (*D*) Quantitative reverse transcription polymerase chain reaction assays for stemness genes in AF^- and AF^+ population sorted from CSE-exposed cells. Data shown are normalized with β-actin expression (n = 3). (*E*) Left: Flow cytometry analysis for ABCG2+ and $CD44^{High}$ population in AF^- and AF^+ cells. CSE-exposed cells were subjected to immunophenotyping using anti-ABCG2-APC or anti-CD44-APC antibody. AF^+ and AF^- populations were selected and analyzed for ABCG2 or CD44 positivity using flow cytometer. Right: Percentage of $ABCG2^+$ and $CD44^{High}$population in selected AF^- and AF^+ populations of CSE-exposed cells (n = 3). (*B*–*E*) Data represent mean ± SD (*P* values were calculated by Student *t* test.) $*P < .05$, $**P < .01$ $***P < .001$. DAPI, 4′,6-diamidino-2-phenylindole.

Figure 1

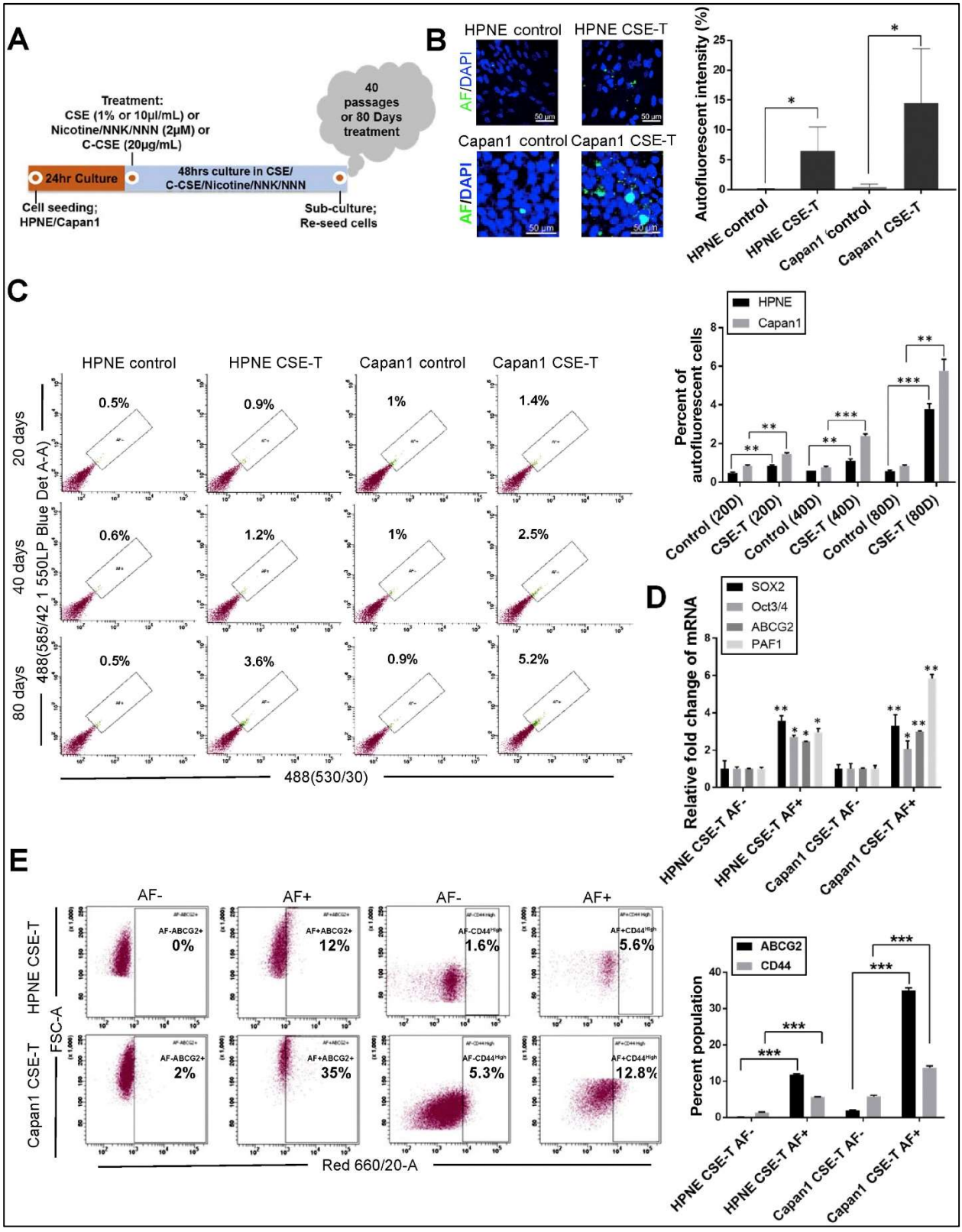
A
Treatment:
CSE (1% or 10µl/mL) or
Nicotine/NNK/NNN (2µM) or
C-CSE (20µg/mL)
40
passages
or 80 Days
treatment
24hr Culture
48hrs culture in CSE/
C-CSE/Nicotine/NNK/NNN
Cell seeding;
HPNE/Capan1
Sub-culture;
Re-seed cells
B
HPNE control
HPNE CSE-T
AF/DAPI
Capan1 control
Capan1 CSE-T
Autofluorescent intensity (%)
HPNE control
HPNE CSE-T
Capan1 control
Capan1 CSE-T
C
HPNE control
HPNE CSE-T
Capan1 control
Capan1 CSE-T
20 days
40 days
80 days
488(585/42 1 550LP Blue Det A-A)
0.5%
0.9%
1%
1.4%
0.6%
1.2%
1%
2.5%
0.5%
3.6%
0.9%
5.2%
488(530/30)
HPNE
Capan1
Percent of autofluorescent cells
Control (20D)
CSE-T (20D)
Control (40D)
CSE-T (40D)
Control (80D)
CSE-T (80D)
D
SOX2
Oct3/4
ABCG2
PAF1
Relative fold change of mRNA
HPNE CSE-T AF-
HPNE CSE-T AF+
Capan1 CSE-T AF-
Capan1 CSE-T AF+
E
AF-
AF+
AF-
AF+
HPNE CSE-T
Capan1 CSE-T
FSC-A
AF-ABCG2+
0%
AF+ABCG2+
12%
AF-CD44High
1.6%
AF+CD44High
5.6%
AF-ABCG2+
2%
AF+ABCG2+
35%
AF-CD44High
5.3%
AF+CD44High
12.8%
Red 660/20-A
ABCG2
CD44
Percent population
HPNE CSE-T AF-
HPNE CSE-T AF+
Capan1 CSE-T AF-
Capan1 CSE-T AF+

Figure 2. Cigarette smoke exposure augments pancreatic stemness in vitro. (*A*) Sphere formation assays performed on CSE-exposed and -unexposed HPNE and Capan1 cells; 2000 cells/well were seeded in 96-well ultra-low attachment plates in stem cell medium. Left: Morphology of 10-day-old spheres. Scale bar = 200 μm. Right: Number of spheres per 2000 cells at different time points of CSE exposure as compared with respective time point controls. Data represent mean ± SD (n = 6). (*P* values were calculated by Student *t* test.) $^{*}P < .05$, $^{***}P < .001$. (*B*) Confocal imaging. Spheres were immunostained for Oct3/4. Confocal images were captured for Oct3/4 (red staining), AF (green staining), and DAPI (blue staining for nuclei). Scale bar = 100 μm. (*C*) Immunoblotting assays for stemness or cancer stemness markers in untreated and CSE-treated HPNE and Capan1 cells. β-actin was used as a loading control. (*D*) Immunofluorescence staining on chronically CSE-exposed and -unexposed cells for stemness markers, ABCG2, SOX9, and PAF1. Nuclei were stained in blue (DAPI) and red staining indicates ABCG2, SOX9, and PAF1 expression. Scale bar = 100 μm. (*E*) Quantitative reverse transcription polymerase chain reaction assay on CSE-exposed and -unexposed HPNE and Capan1 cells for PAF1 and SOX9 genes. Data shown are normalized for β-actin expression. Data represent mean ± SD (n = 3). (*P* values were calculated by Student *t* test.) $^{*}P < .05$, $^{**}P < .01$ $^{***}P < .001$. DAPI, 4′,6-diamidino-2-phenylindole; β-cat, β-catenin.

Figure 2

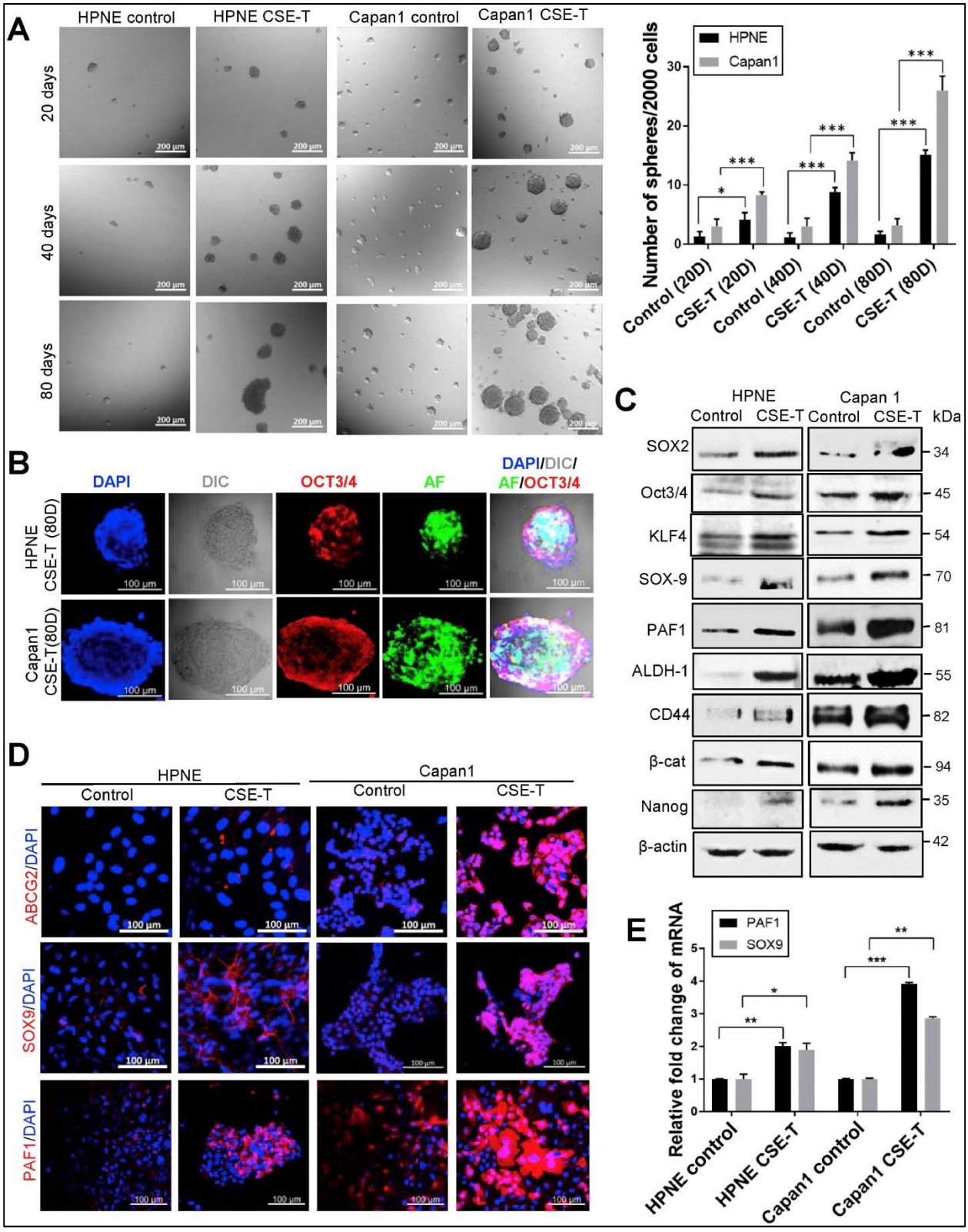
A
HPNE control
HPNE CSE-T
Capan1 control
Capan1 CSE-T
20 days
40 days
80 days
200 μm
Number of spheres/2000 cells
HPNE
Capan1
Control (20D)
CSE-T (20D)
Control (40D)
CSE-T (40D)
Control (80D)
CSE-T (80D)
B
DAPI
DIC
OCT3/4
AF
DAPI/DIC/
AF/OCT3/4
HPNE CSE-T (80D)
Capan1 CSE-T(80D)
100 μm
C
HPNE
Capan 1
Control
CSE-T
kDa
SOX2
Oct3/4
KLF4
SOX-9
PAF1
ALDH-1
CD44
β-cat
Nanog
β-actin
34
45
54
70
81
55
82
94
35
42
D
HPNE
Capan1
Control
CSE-T
ABCG2/DAPI
SOX9/DAPI
PAF1/DAPI
100 μm
E
PAF1
SOX9
Relative fold change of mRNA
HPNE control
HPNE CSE-T
Capan1 control
Capan1 CSE-T

Figure 3. Cigarette smoke exposure induces PAF1 in vivo. (*A*) Ten-week-old control and $Kras^{G12D}$ Pdx-Cre mice were exposed to cigarette smoke for 20 weeks (3 hours; twice a day) using Teague TE-10C system. Filtered air was used to expose control animals. (*B*) Immunohistochemistry staining of PAF1 protein in pancreatic tissues obtained from cigarette smoke–exposed (CS-T) control and $Kras^{G12D}$ Pdx-Cre mice. Scale bars = 100 μm. (*C*) Histo score (H score) of PAF1 protein expression. Data represent mean ± SD (n = 6). (*P* values were calculated by Student *t* test.) $^{**}P < .01$. (*D*) Quantitative reverse transcription polymerase chain reaction assay on pancreatic tissues obtained from cigarette smoke–exposed control and $Kras^{G12D}$ Pdx-Cre mice for PAF1. Data shown are normalized for β-actin expression. Data represent mean ± SD (n = 3). (*P* values were calculated by Student *t* test.) $^{*}P < .05$, $^{**}P < .01$. (*E*) Immunofluorescence staining for PAF1 (green) and CD44 in cigarette smoke–exposed pancreatic tissues. Scale bar = 50 μm. (*F*) Confocal images of pancreatic tissues obtained from cigarette smoke–exposed mice showing the AF (green) and localization of Nile red (lipid droplet staining). Scale bar = 50 μm. Enlarged boxed image shows the absence of colocalization of AF with Nile red (Lipofuscin). (*G*) Confocal images of pancreatic tissue collected from cigarette smoke–exposed floxed mice showing the colocalization of PAF1 with ABCG2 and AF (green). Arrowheads point to colocalization of PAF1, ABCG2, and AF. Enlarged boxed image shows the colocalization. Scale bar = 50 μm. (*E*–*G*) Nuclei were stained with DAPI, 4′,6-diamidino-2-phenylindole.

Figure 3

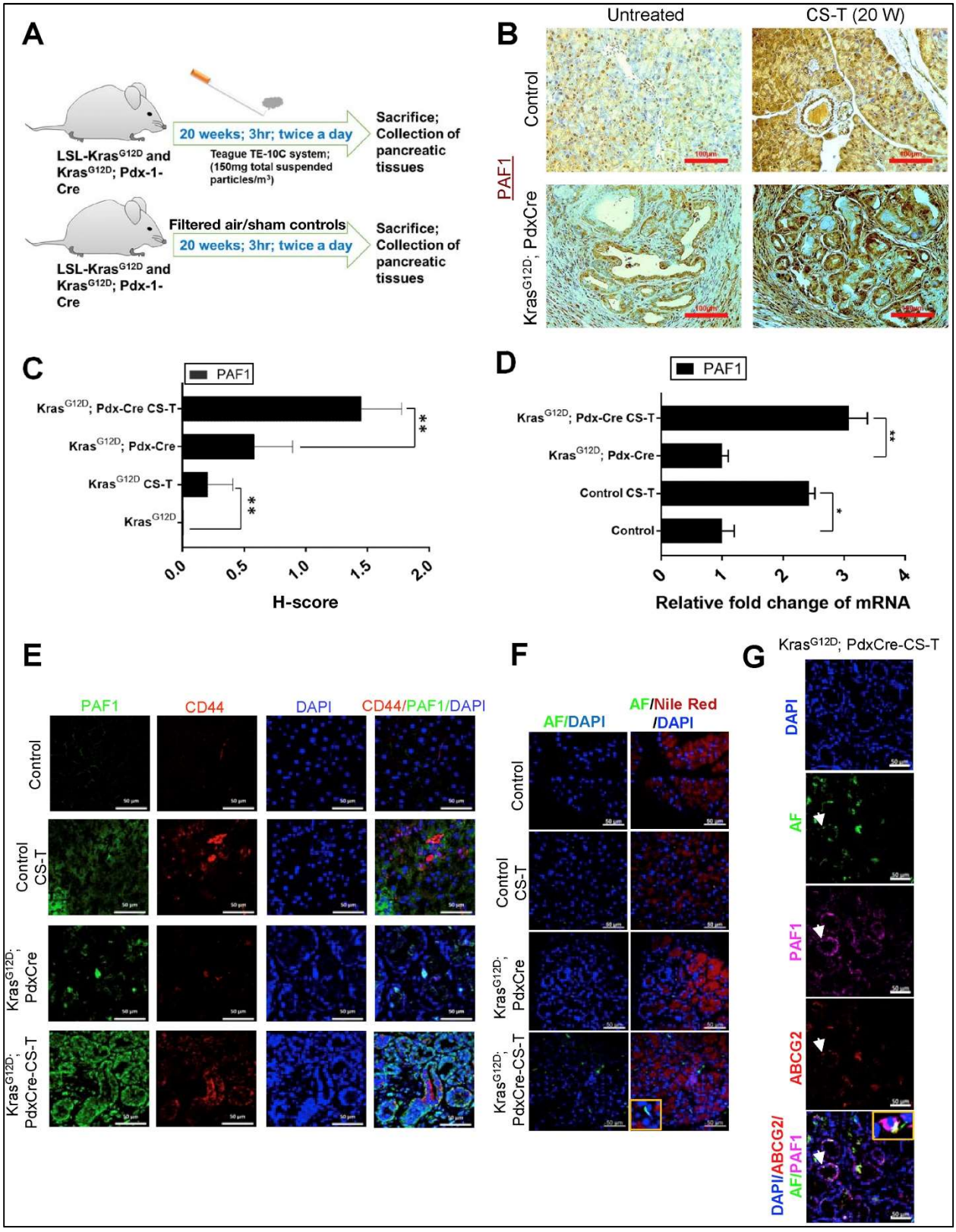
A
LSL-Kras^{G12D} and Kras^{G12D}; Pdx-1-Cre
20 weeks; 3hr; twice a day
Teague TE-10C system; (150mg total suspended particles/m^3)
Sacrifice; Collection of pancreatic tissues
Filtered air/sham controls
20 weeks; 3hr; twice a day
Sacrifice; Collection of pancreatic tissues
B
Untreated
CS-T (20 W)
Control
PAF1
Kras^{G12D}; PdxCre
C
PAF1
Kras^{G12D}; Pdx-Cre CS-T
Kras^{G12D}; Pdx-Cre
Kras^{G12D} CS-T
Kras^{G12D}
H-score
D
PAF1
Kras^{G12D}; Pdx-Cre CS-T
Kras^{G12D}; Pdx-Cre
Control CS-T
Control
Relative fold change of mRNA
E
PAF1
CD44
DAPI
CD44/PAF1/DAPI
Control
Control CS-T
Kras^{G12D}; PdxCre
Kras^{G12D}; PdxCre-CS-T
F
AF/DAPI
AF/Nile Red /DAPI
Control
Control CS-T
Kras^{G12D}; PdxCre
Kras^{G12D}; PdxCre-CS-T
G
Kras^{G12D}; PdxCre-CS-T
DAPI
AF
PAF1
ABCG2
DAPI/ABCG2/ AF/PAF1

Figure 4. Smoking-mediated induction of pancreatic stemness is regulated by PAF1. (*A*) Immunoblotting assay for PAF1, SOX9, and β-catenin in PAF1 KD HPNE and PAF1 CRISPR/Cas9 KO Capan1 cells. (*B*) Flow cytometry analysis of AF cells in CSE-exposed HPNE and Capan1 cells transfected with PAF1 small interfering RNA and control siRNA. (*C*) Percentage of AF cells in scramble control and PAF1 KD CSE-exposed cells. Data represent mean ± SD (n = 3). (*P* values were calculated by Student *t* test.) $^{*}P < .05$, $^{**}P < .01$. (*D* and *E*) Flow cytometry analysis for ABCG2+ population in scramble control and PAF1 KD CSE-exposed HPNE and Capan1 cells. (*F*) Percentage of ABCG2+ population in scramble control and PAF1 KD CSE-exposed cells (n = 3). Data represent mean ± SD (n = 3). (*P* values were calculated by Student *t* test.) $^{**}P < .01$.

Figure 4

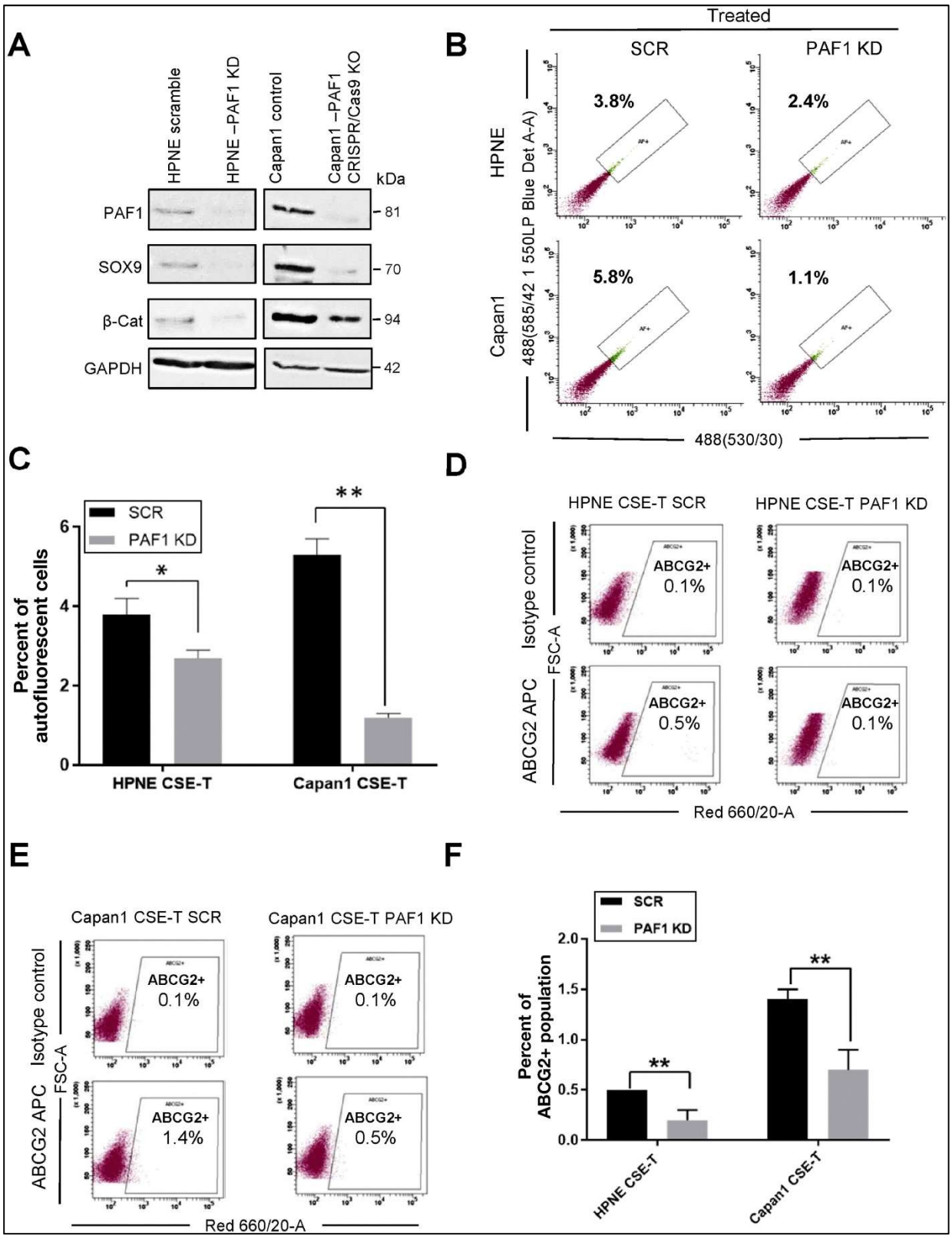
A
HPNE scramble
HPNE –PAF1 KD
Capan1 control
Capan1 –PAF1 CRISPR/Cas9 KO
kDa
PAF1
SOX9
β-Cat
GAPDH
81
70
94
42
B
Treated
SCR
PAF1 KD
HPNE
Capan1
488(585/42 1 550LP Blue Det A-A)
3.8%
2.4%
5.8%
1.1%
488(530/30)
C
SCR
PAF1 KD
Percent of autofluorescent cells
HPNE CSE-T
Capan1 CSE-T
D
HPNE CSE-T SCR
HPNE CSE-T PAF1 KD
Isotype control
ABCG2 APC
FSC-A
ABCG2+ 0.1%
ABCG2+ 0.5%
Red 660/20-A
E
Capan1 CSE-T SCR
Capan1 CSE-T PAF1 KD
ABCG2+ 0.1%
ABCG2+ 1.4%
ABCG2+ 0.5%
F
SCR
PAF1 KD
Percent of ABCG2+ population
HPNE CSE-T
Capan1 CSE-T

Figure 5. Smoking induces PAF1 through the nACHRα7-ERK1/2-FOSL1/cJun (AP1) signaling pathway. (*A*) Small interfering RNA knockdown of FOSL1. Western blot analysis showing FOSL1 knockdown and its effect on PAF1 in CSE-treated and -untreated HPNE and Capan1 cells. Glyceraldehyde 3-phosphate dehydrogenase(GAPDH) was used as loading control. (*B*) ChIP assays were performed using chromatin from CSE-exposed cells and the control immunoglobulin (Ig) G or phospho-FOSL1 antibodies. Phospho-FOSL1 enriched DNA was used in polymerase chain reaction (PCR) assay using primers specific to FOSL1 or AP1 binding sites (see Supplementary Figure 8) on the promoter region of PAF1 gene. Chip DNA PCR product was resolved on 2% agarose gel, and the DNA bands for BS1–9 are shown. (*C*) Left: Representative images of immunohistochemistry for FOSL1 in pancreatic tissues obtained from cigarette smoke–exposed control and $Kras^{G12D}$ Pdx-Cre mice. Scale bar = 100 μm. Middle: Immunofluorescence staining for PAF1 (stained in red) and p-FOSL1 (stained in green) in cigarette smoke–exposed control and $Kras^{G12D}$ Pdx-Cre tissues (nuclei were stained with DAPI). Scale bar = 50 μm. Right: Bar chart represents the H score of FOSL1 staining. Data represent mean ± SD (n = 6). (*P* values were calculated by Student *t* test.) $^{*}P < .05$, $^{**}P < .01$. (*D*) Left: Immunohistochemical staining for FOSL1 and PAF1 in human PDAC tissues (with and without smoking history) and in normal pancreas. Scale bar = 100 μm. Right: Confocal images showing the coexpression of FOSL1 (stained in red) and PAF1 (stained in green) in these tissues. Scale bar = 100 μm. Nuclei were stained in blue using DAPI. Bar charts below show quantification of FOSL1 and PAF1 staining in normal pancreas (n = 15), PDAC without (n = 15) and with (n = 15) smoking history. Data represent mean ± SD. (*P* values were calculated by Student *t* test.) $^{***}P < .001$. (*E*) Immunoblotting assays for CHRNA7, p-ERK1/2, ERK1/2, p-FOSL1, FOSL1, p-cJun and cJun signaling molecules in CSE-treated cells as compared with untreated controls. (*F*) Immunoblotting assays for p-ERK1/2, ERK1/2, p-FOSL1, FOSL1, PAF1 in CSE-exposed HPNE and Capan1 cells with or without ERK1/2 inhibition using PD98059. (*G*) Small interfering RNA knockdown of nACHRα7 in CSE-treated cells. Western blot analysis showing the effect of nACHRα7 knockdown on p-FOSL1 and PAF1. (*E*–*G*) β-actin was used as loading control. DAPI, 4′,6-diamidino-2-phenylindole.

Figure 5

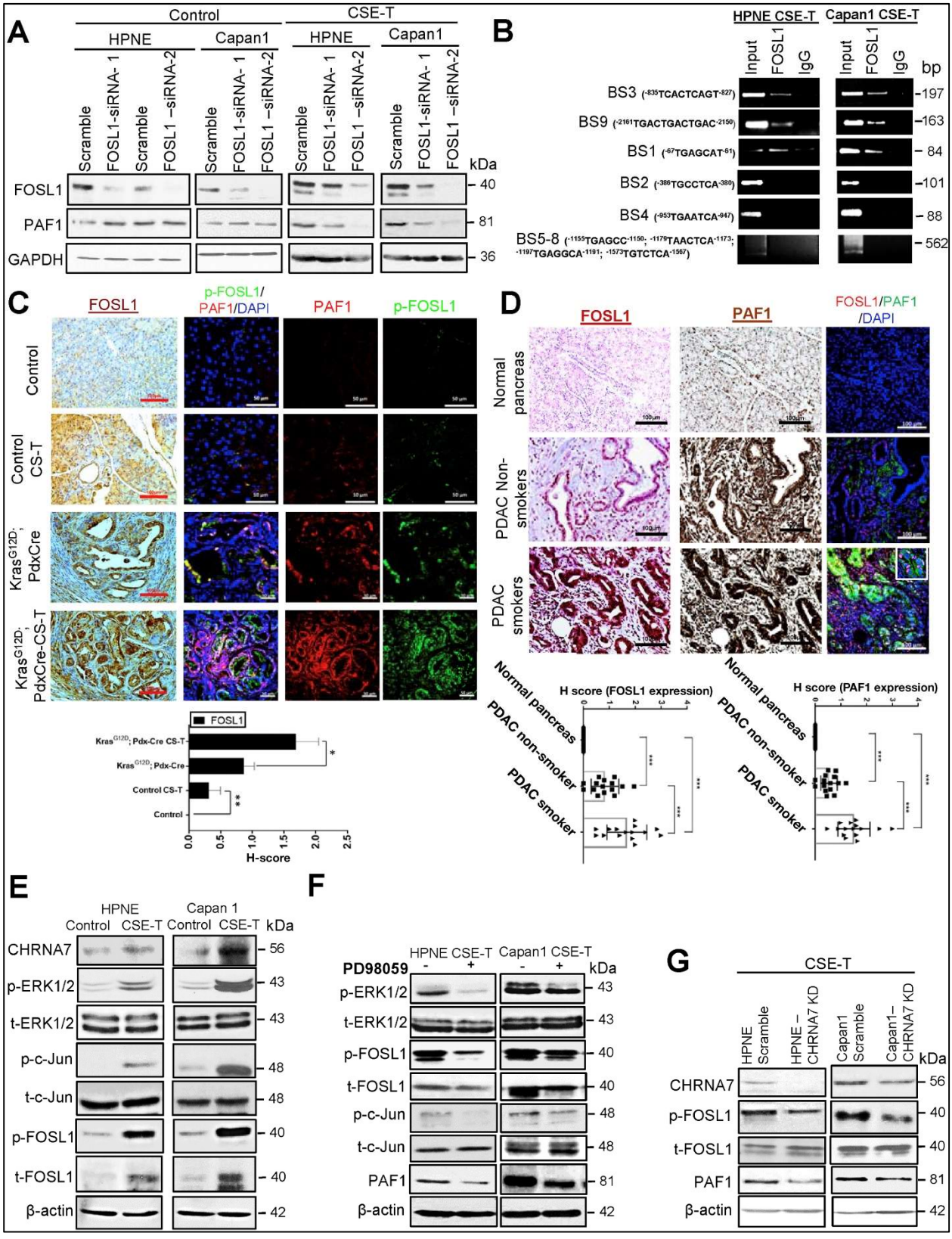
A
Control
CSE-T
HPNE
Capan1
Scramble
FOSL1-siRNA- 1
FOSL1 –siRNA-2
kDa
FOSL1
PAF1
GAPDH
40
81
36
B
HPNE CSE-T
Capan1 CSE-T
Input
FOSL1
IgG
bp
BS3 (-835TCACTCAGT-827)
BS9 (-2161TGACTGACTGAC-2150)
BS1 (-67TGAGCAT-61)
BS2 (-386TGCCTCA-380)
BS4 (-953TGAATCA-947)
BS5-8 (-1155TGAGCC-1150; -1179TAACTCA-1173; -1197TGAGGCA-1191; -1573TGTCTCA-1567)
197
163
84
101
88
562
C
FOSL1
p-FOSL1/ PAF1/DAPI
PAF1
p-FOSL1
Control
Control CS-T
KrasG12D; PdxCre
KrasG12D; PdxCre-CS-T
FOSL1
KrasG12D; Pdx-Cre CS-T
KrasG12D; Pdx-Cre
Control CS-T
Control
H-score
D
FOSL1
PAF1
FOSL1/PAF1 /DAPI
Normal pancreas
PDAC Non-smokers
PDAC smokers
H score (FOSL1 expression)
H score (PAF1 expression)
Normal pancreas
PDAC non-smoker
PDAC smoker
E
HPNE
Capan 1
Control
CSE-T
kDa
CHRNA7
p-ERK1/2
t-ERK1/2
p-c-Jun
t-c-Jun
p-FOSL1
t-FOSL1
β-actin
56
43
43
48
48
40
40
42
F
HPNE CSE-T
Capan1 CSE-T
PD98059
kDa
p-ERK1/2
t-ERK1/2
p-FOSL1
t-FOSL1
p-c-Jun
t-c-Jun
PAF1
β-actin
43
43
40
40
48
48
81
42
G
CSE-T
HPNE Scramble
HPNE – CHRNA7 KD
Capan1 Scramble
Capan1– CHRNA7 KD
kDa
CHRNA7
p-FOSL1
t-FOSL1
PAF1
β-actin
56
40
40
81
42

Figure 6. Cigarette smoke components, nicotine, NNN, and NNK are highly responsible for augmentation of pancreatic stemness. HPNE and Capan1 cells were left untreated or treated with nicotine (2 μM), NNK (2 μM), and NNN (2 μM) for 80 days. (*A*) Left: Flow cytometry analysis of AF content. Right: Percentage of AF^+ population in HPNE and Capan1 cells exposed to cigarette smoke components as compared with respective controls. Data represent mean ± SD (n = 3) (*P* values were calculated by Student *t* test.) $^*P < .05$, $^{**}P < .01$. (*B*) Sphere formation assay was performed on HPNE and Capan1 cells exposed to cigarette smoke components; 2000 cells/well were seeded in 96-well ultra-low attachment plates in stem cell medium. Left: Morphology of 10-day-old spheres. Scale bar = 200μm. Right: Number of spheres per 2000 cells in HPNE and Capan1 cells exposed to cigarette smoke components as compared with untreated controls. Data represent mean ± SD (n = 6). (*P* values were calculated by Student *t* test.) $^{***}P < .001$. (*C*, *D*) Immunoblotting assay for CHRNA7, p-FOSL1, PAF1, KLF4, and SOX9. β-actin was used as loading control.

Figure 6

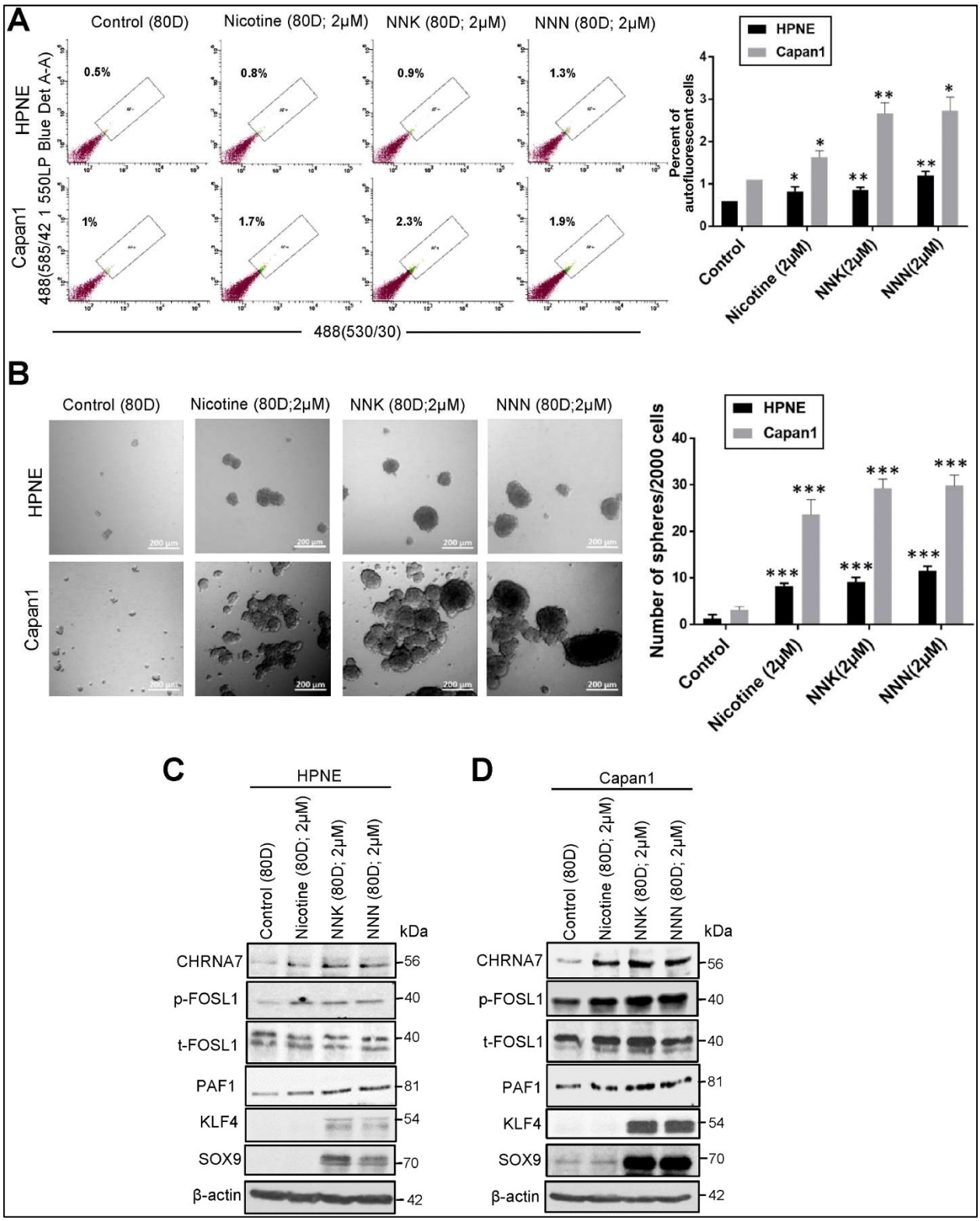
A
Control (80D)
Nicotine (80D; 2μM)
NNK (80D; 2μM)
NNN (80D; 2μM)
HPNE
Capan1
488(585/42 1 550LP Blue Det A-A)
0.5%
0.8%
0.9%
1.3%
1%
1.7%
2.3%
1.9%
488(530/30)
HPNE
Capan1
Percent of autofluorescent cells
Control
Nicotine (2μM)
NNK(2μM)
NNN(2μM)
B
Control (80D)
Nicotine (80D;2μM)
NNK (80D;2μM)
NNN (80D;2μM)
HPNE
Capan1
200 μm
HPNE
Capan1
Number of spheres/2000 cells
Control
Nicotine (2μM)
NNK(2μM)
NNN(2μM)
C
HPNE
Control (80D)
Nicotine (80D; 2μM)
NNK (80D; 2μM)
NNN (80D; 2μM)
kDa
CHRNA7
p-FOSL1
t-FOSL1
PAF1
KLF4
SOX9
β-actin
56
40
40
81
54
70
42
D
Capan1
Control (80D)
Nicotine (80D; 2μM)
NNK (80D; 2μM)
NNN (80D; 2μM)
kDa
CHRNA7
p-FOSL1
t-FOSL1
PAF1
KLF4
SOX9
β-actin
56
40
40
81
54
70
42

Figure 7. Cigarette smoke exposure increases PHF5A and augments interaction between PAF1 and PHF5A. (*A*) HPNE and Capan1 cells were left untreated or treated with CSE (1%) for 80 days. Immunoblot analysis showing the protein expression levels of PAF1 complex (PAF1C) molecules along with serine 2 phosphorylated RNA polymerase II (S2-Phos RNA Pol II) and PHF5A. β-actin was used as loading control. (*B*) Left: Representative images of immunohistochemistry for PHF5A in pancreatic tissues obtained from 20 weeks cigarette smoke–exposed control and $Kras^{G12D}$ Pdx-Cre mice. Scale bar = 100 μm. Right: Immunofluorescence staining for PAF1 (stained in red) and PHF5A (stained in green) in pancreas of cigarette smoke–exposed control and $Kras^{G12D}$Pdx-Cre mice models (nuclei were stained with DAPI). Scale bar = 50 μm. Bar chart below (*C*) represents the H score of PHF5A staining in the pancreas of cigarette smoke–exposed mice. Data represent mean ± SD (n = 6). (*P* values were calculated by Student *t*-test.) $^{*}P < .05$, $^{**}P < .01$. (*D*) Immunofluorescence staining for PAF1 and PHF5A on HPNE and Capan1 cells exposed to CSE. Coexpression of PAF1 with PHF5A is shown. Nuclei were stained with DAPI. (*E*) Immunoblots showing that PAF1 interacts with PHF5A in untreated and CSE-treated HPNE and Capan1 cells. Pull down was performed using PAF1 antibody, and immunoprecipitates were probed with PHF5A antibody. Immunoglobulin (Ig)G control and input, 10% of total lysate, were used as negative and positive controls, respectively. (*F*) Schematic showing overall mechanism involved in the cigarette smoke–mediated induction of pancreatic stemness. Exposure of human pancreatic ductal cells and cancer cells to cigarette smoke and its components induces stemness by increasing PAF1 through CHRNA7-ERK1/2-AP1 (FOSL1-cJUN) signaling pathway. Cigarette smoke–induced PAF1 and PHF5A interacts and forms PAF1-PHF5A complex, required for the activation of stemness genes.

Figure 7

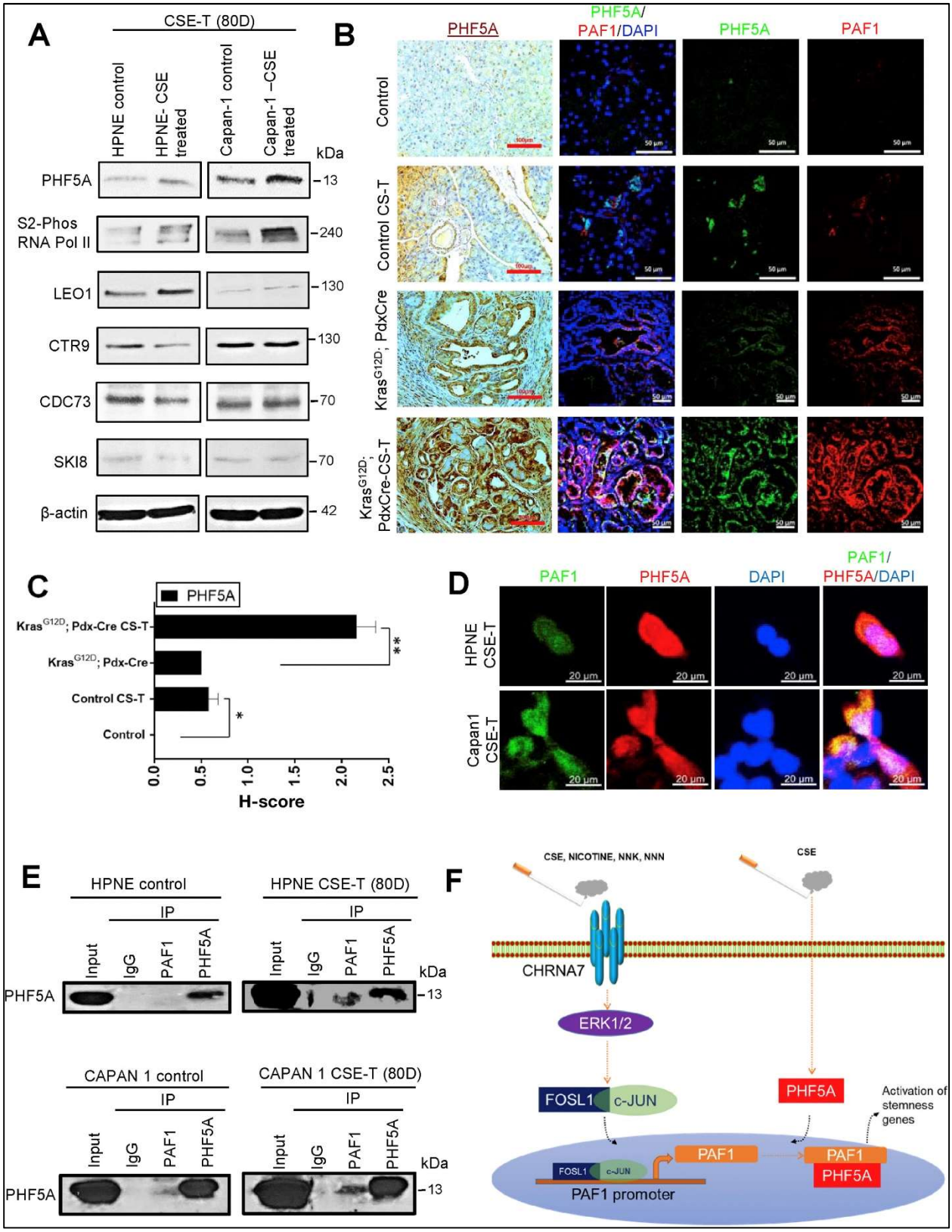
A
CSE-T (80D)
HPNE control
HPNE- CSE treated
Capan-1 control
Capan-1 –CSE treated
kDa
PHF5A
13
S2-Phos RNA Pol II
240
LEO1
130
CTR9
130
CDC73
70
SKI8
70
β-actin
42
B
PHF5A
PHF5A/ PAF1/DAPI
PHF5A
PAF1
Control
Control CS-T
KrasG12D; PdxCre
KrasG12D; PdxCre-CS-T
C
PHF5A
KrasG12D; Pdx-Cre CS-T
KrasG12D; Pdx-Cre
Control CS-T
Control
**
*
0.0
0.5
1.0
1.5
2.0
2.5
H-score
D
PAF1
PHF5A
DAPI
PAF1/ PHF5A/DAPI
HPNE CSE-T
Capan1 CSE-T
20 µm
E
HPNE control
HPNE CSE-T (80D)
IP
Input
IgG
PAF1
PHF5A
kDa
PHF5A
13
CAPAN 1 control
CAPAN 1 CSE-T (80D)
F
CSE, NICOTINE, NNK, NNN
CSE
CHRNA7
ERK1/2
FOSL1
c-JUN
PHF5A
Activation of stemness genes
PAF1
PAF1 promoter

Supplementary figure legends

Supplementary Figure 1. LC-MS/MS analysis of Nicotine in CSE. (**A)** Flow diagram showing steps followed for LC-MS/MS analysis of Nicotine concentration in 100% CSE. **(B)** Calibration curve standards and linear regression lines for analysis of nicotine standard solution that were used for calculating its concentration in 100% CSE. Nicotine concentration in 100% CSE was calculated by data calibration and interpolation analysis. Table below shows mean nicotine (m/z 163.2/132.1) peak areas of nicotine calibration standard samples and unknown 100% CSE test sample and their normalized mean values (Peak area of analyte/IS peak area) (n=3). (p values were calculated by Student's t test). ***$p < 0.001$. **(C)** LC-MS/MS MRM chromatograms of nicotine and IS in samples: blank (100% methanol), blank with IS, 100% CSE and nicotine calibration standards.

Supplementary Figure 1

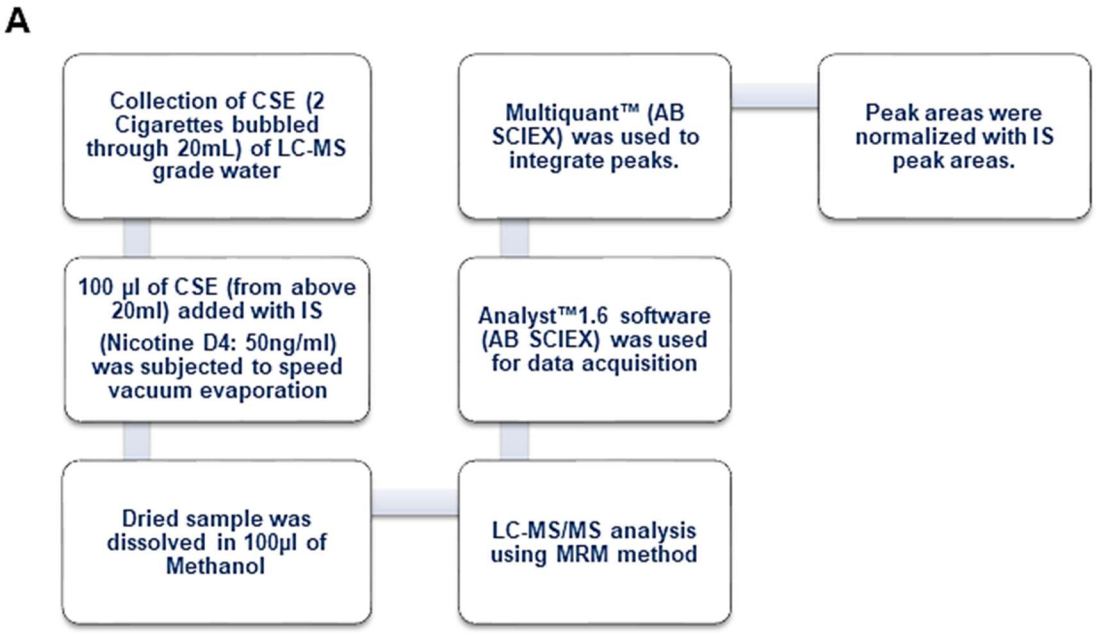

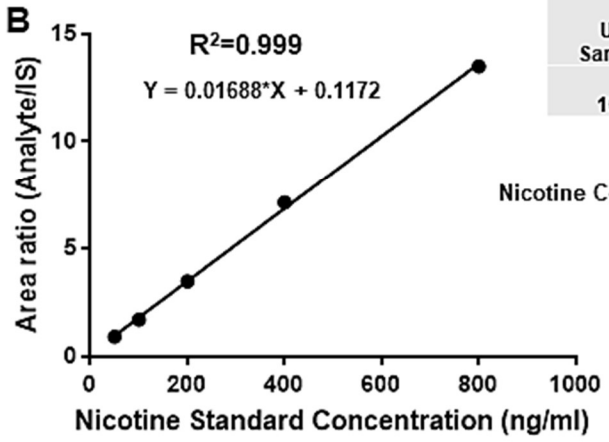

Unknown Sample Name	Concentration (ng/ml) (Interpolated)	Area ratio (Entered)
100% CSE	33073.6852794981	558.269713

Nicotine Concentration in 100% CSE = 33.073 ± 0.698 µg/ml

***p < 0.001

Sample Name	Analyte	Mean (n=3) Analyte Area	Mean (n=3) IS Area	Mean (n=3) Area ratio (Analyte/IS)
Nicotine (S) 50ng/mL+IS	Nicotine1 (163.2 / 132.1)	647296.0904	701529.669	0.92269239
Nicotine (S) 100ng/mL+IS	Nicotine1 (163.2 / 132.1)	1336565.003	785109.148	1.70239387
Nicotine (S) 200ng/mL+IS	Nicotine1 (163.2 / 132.1)	2953984.469	849750.504	3.47629622
Nicotine (S) 400ng/mL+IS	Nicotine1 (163.2 / 132.1)	6231323.234	872369.855	7.14298322
Nicotine (S) 800ng/mL+IS	Nicotine1 (163.2 / 132.1)	12106789.79	896825.032	13.4996118
100% CSE +IS	Nicotine1 (163.2 / 132.1)	274927716.5	492463.965	558.269713

Supplementary Figure 1

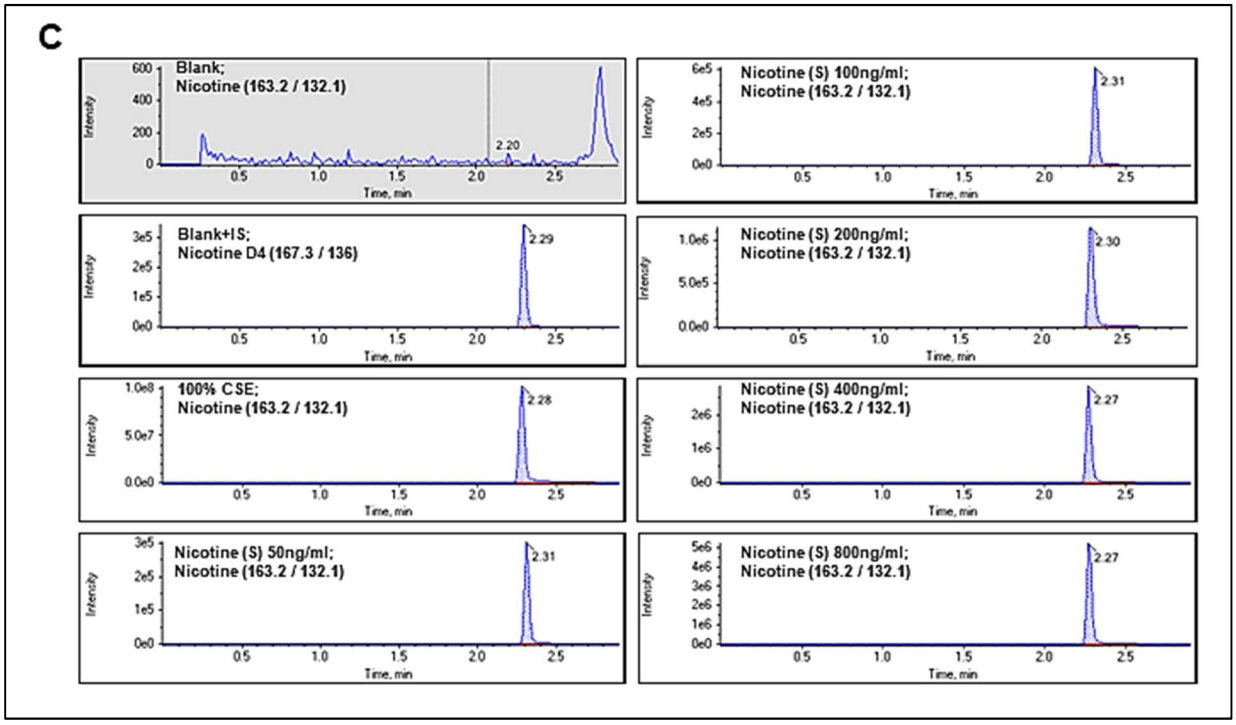

Supplementary Figure 2. Riboflavin treatment increases AF+ cells. (A) Flow cytometry based autofluorescence assay. Flow cytometry plots showing increase in AF+ cells in riboflavin treated HPNE and Capan1 cells. HPNE and Capan1 cells were stained with Riboflavin (30μM) for 1hr at 37^0C followed by analysis using LSR II Green (BD Biosciences). AF cells were captured using 488-nm blue laser and best selected as the intersection with filters Blue 530/30-A and 585/42 1 550LP Blue Det A-A. **(B)** Representative confocal image showing ABCG2 expression (red staining) in membrane of riboflavin (Green staining)-loaded intracellular vesicle. 80 days CSE treated HPNE cells were stained with mouse anti-ABCG2 antibody followed by staining with alexafluor anti-mouse 568. Scale bar, 20μm.

Supplementary Figure 2

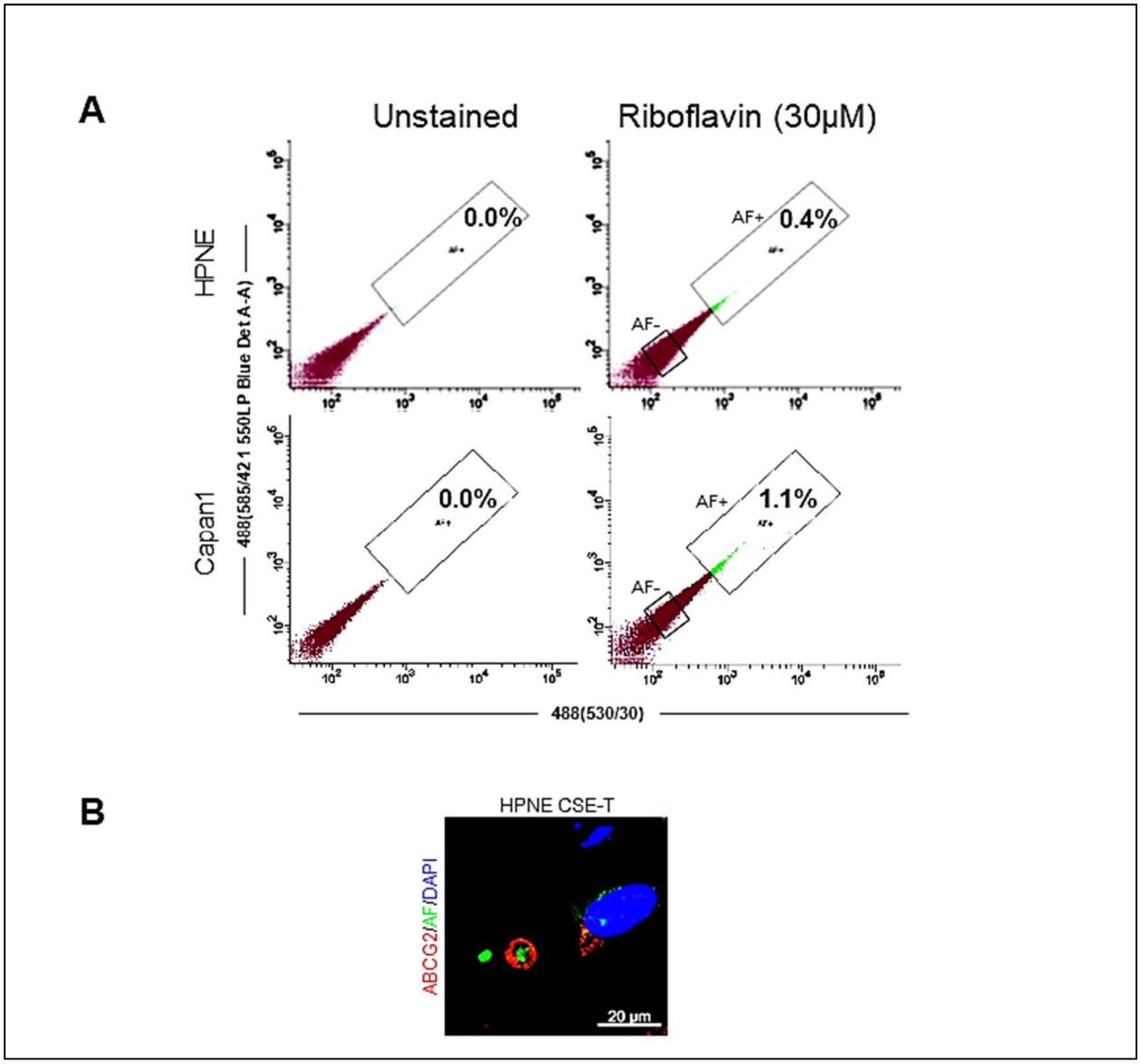

Supplementary Figure 3. (A) Sphere formation by AF+ and AF- population. Left: AF- and AF+ cells were sorted from chronic CSE exposed HPNE and Capan1 cells, and seeded (2000 cells/well) in stem cell medium in ultra-low attachment 96 well plate. Pancospheres (formed by CSE exposed HPNE) and tumor spheres (formed by CSE exposed Capan1 cells) were imaged 10 days post-seeding. Primary or secondary spheres were dissociated using enzymatic (Trypsin EDTA) and mechanical (using pipette) methods followed by re-seeding for secondary or tertiary sphere formation. **Right:** Bar graph showing the number of spheres per total number of cells seeded. Data represent mean ± SD (n=6). (p values were calculated by Student's t test). ***$p < 0.001$. **(B) *In vivo* tumorigenicity assay. Left:** AF+ and AF- cells were sorted using Fluorescence activated cell sorter (FACS) from HPNE and Capan1 cells exposed to CSE, and 4,000 cells in 100µl were injected subcutaneously into the right (AF+) and left (AF-) flanks of athymic nude mice. Animals were sacrificed when tumor nodules reached 0.8 cm diameter. **Right:** Bar graph showing the tumor weights. Data represent mean ± SD (n=4). (p values were calculated by Student's t test). ***$p < 0.001$.

Supplementary Figure 3

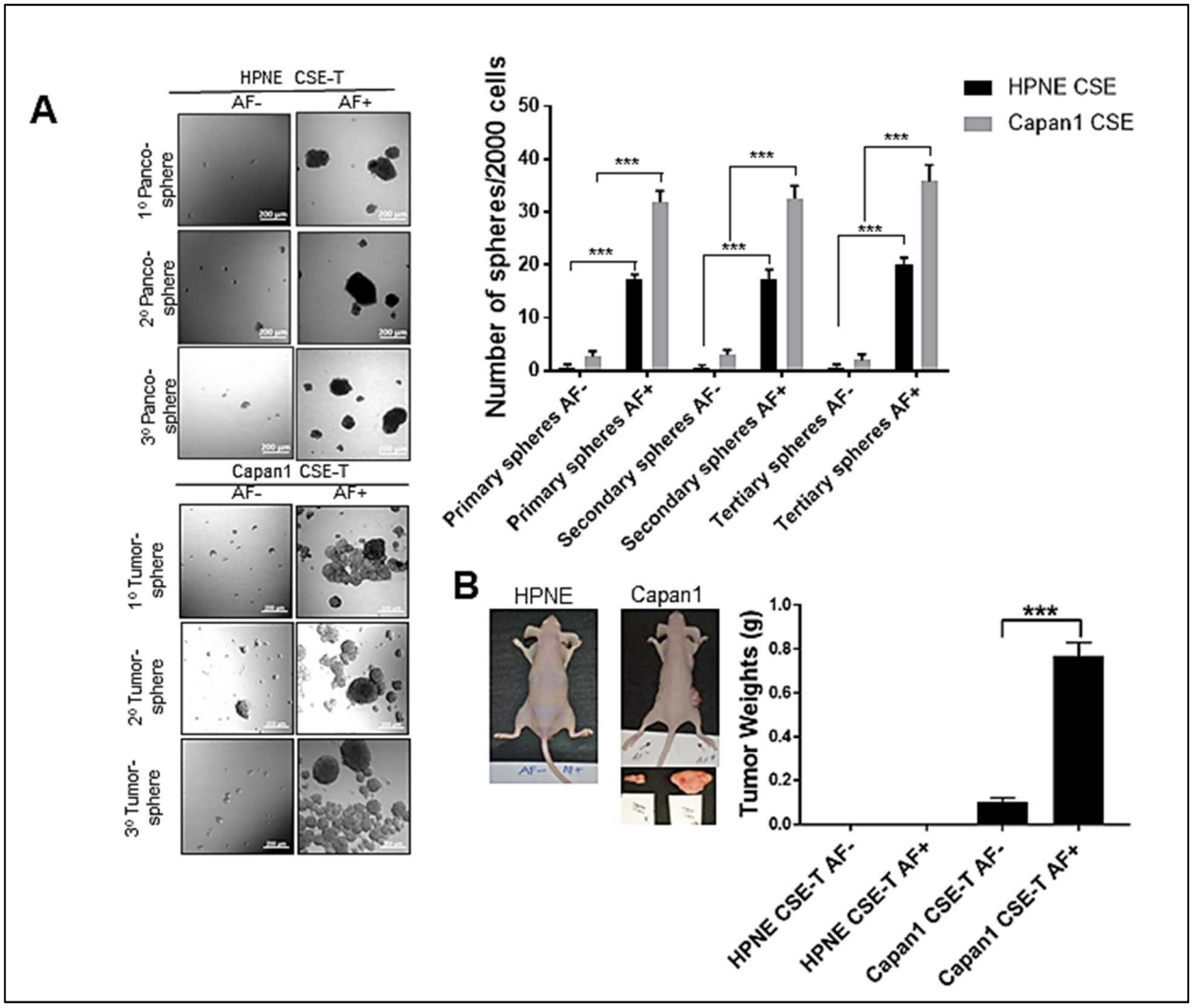

Supplementary Figure 4. (A) Immunoblot analysis of stemness marker (BMI1) expression in HPNE and Capan1 cells exposed to CSE (1%) for 80 days. β-actin was used as a loading control. **(B) Exposure to commercial CSE (C-CSE) (purchased from Murthy Pharmaceuticals) for 80 days increases stemness or cancer stemness markers.** HPNE and Capan1 cells were exposed to 20µg/mL C-CSE or equal volume of DMSO (vehicle) for 80 days as shown in Figure 1A, and analyzed for protein levels of stemness markers, PAF1/PD2 and SOX9 along with p-FOSL1 and total FOSL1 (t-FOSL1) signaling protein. β-actin was used as a loading control.

Supplementary Figure 4

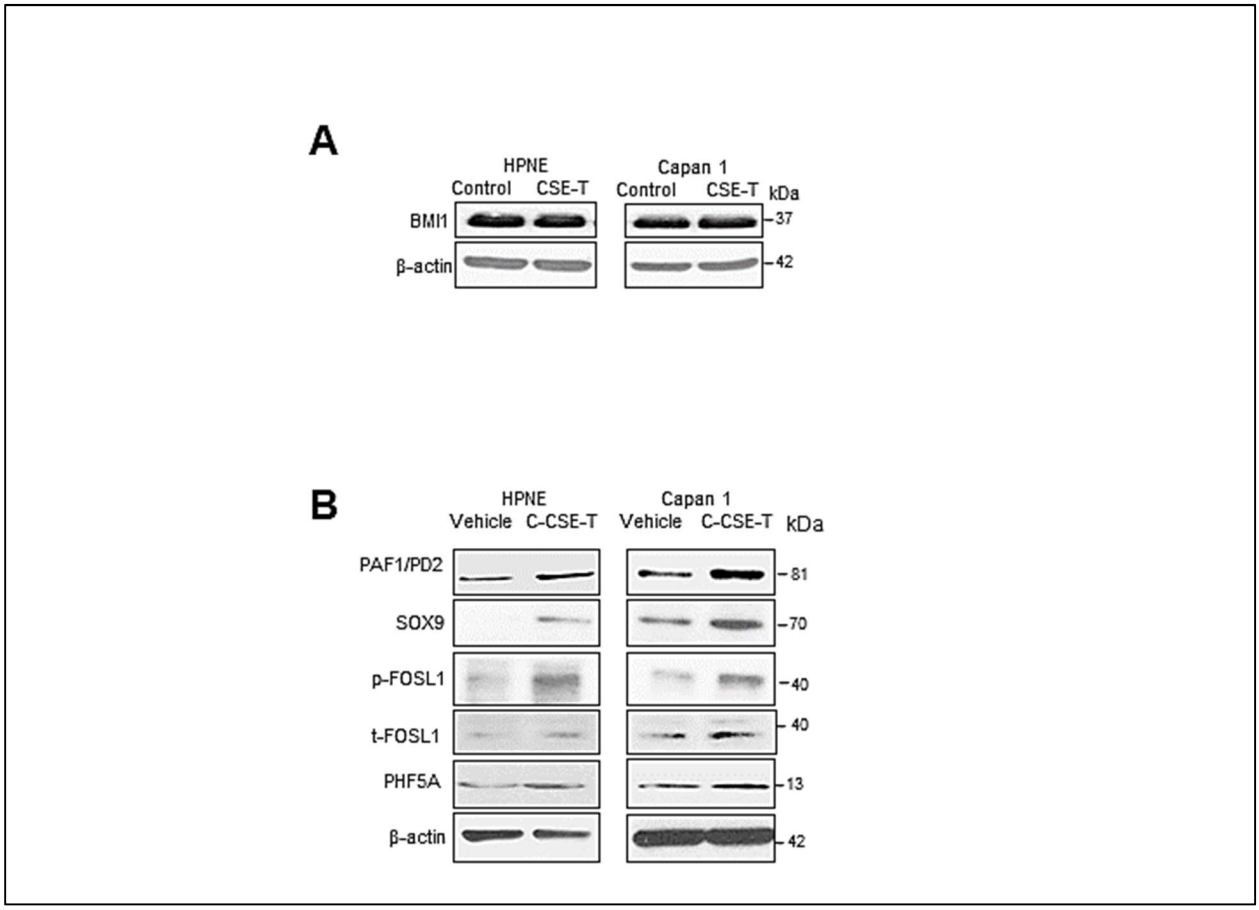

Supplementary Figure 5. Chronic CSE exposure elevates stem cell marker protein expressions and induces aldehyde dehydrogenase (ALDH) activity. (A) Immunofluorescent staining of β-catenin, CD44, ALDH1 and CD24 (red staining). Nuclei were counterstained with DAPI. Scale bar, 100μm. **(B)** Representative flow cytometry plots of ALDEFLUOR assay in 80 days CSE exposed and unexposed HPNE and Capan1 cells. Cells were incubated with ALDEFLUOR substrate in the presence and absence of DEAB. A shift in BAAA (activated ALDEFLUOR reagent) fluorescence in the absence of DEAB defines the ALDEFLUOR-positive population. DEAB, Diethylaminobenzaldehyde. BAAA, BODIPY-aminoacetaldehyde.

Supplementary Figure 5

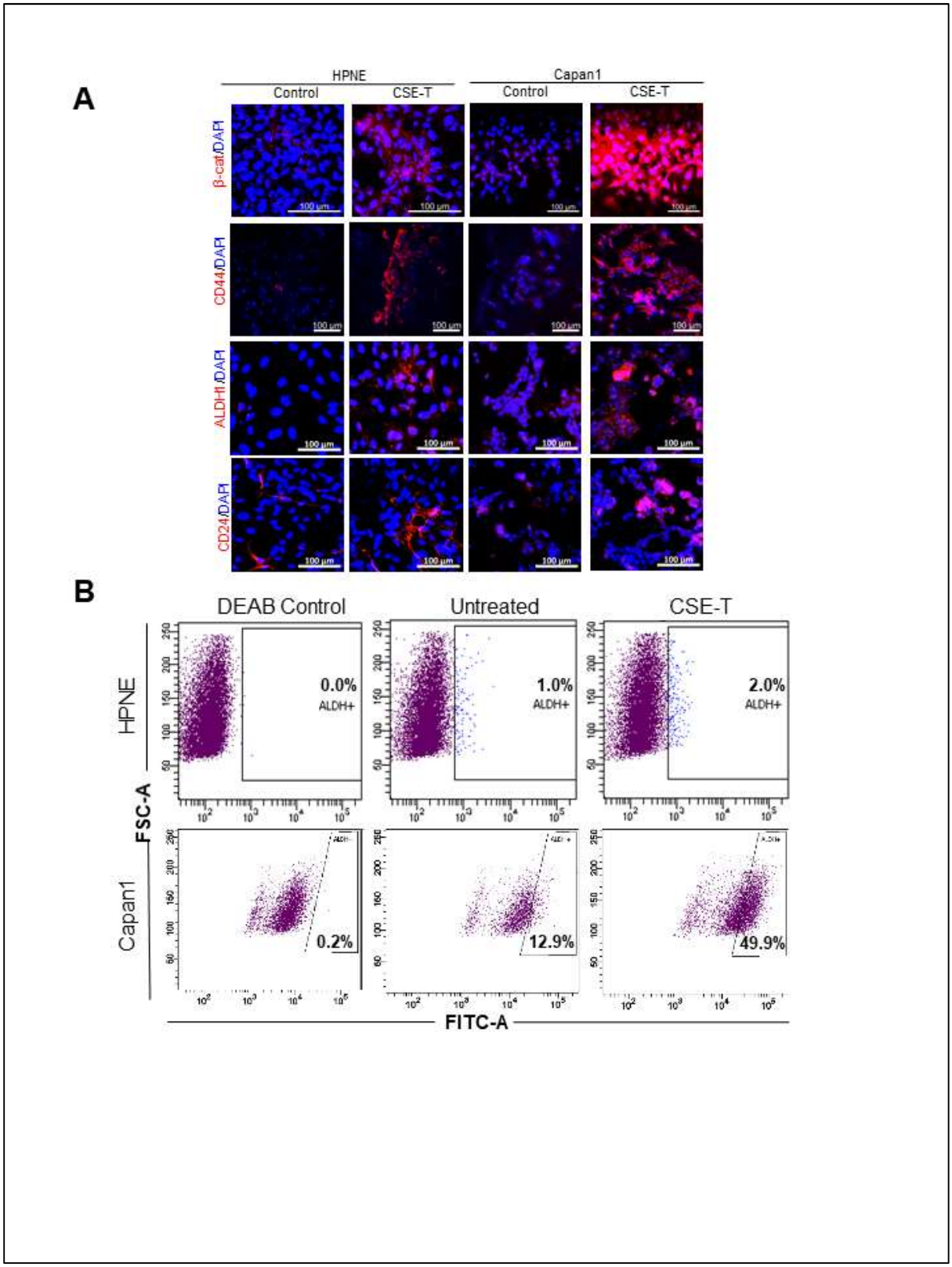

Supplementary Figure 6. Chronic cigarette smoke (CS) exposure induces SOX9 in the pancreas of ten-week-old control and Kras^{G12D} Pdx-Cre mice. (A) Left: Immunohistochemistry staining of SOX9 protein in pancreatic tissues obtained from 20 weeks CS-exposed (CS-T) control and Kras^{G12D} Pdx-Cre mice. Scale bars, 100μm. **Bottom:** Histo score (H-Score) of SOX9 expression. Data represent mean ± SD (n=6). (p values were calculated by Student's t test). $^{*}p < 0.05$. **(B)** Immunofluorescence staining for SOX9 (Green) and PAF1/PD2(Red) in CS-exposed pancreatic tissues. Boxes within the images are an enlarged sections showing co-expression of SOX9 and PAF1/PD2. Scale bar: 50μm. Nuclei were stained with DAPI, 4',6-diamidino-2-phenylindole. **(C)** Immunofluorescence images showing co-localization of PAF1/PD2 expression and AF (autofluorescence) in HPNE cells chronically exposed to CSE. Scale bar, 20μm. Nuclei were stained with DAPI, 4',6-diamidino-2-phenylindole.

Supplementary Figure 6

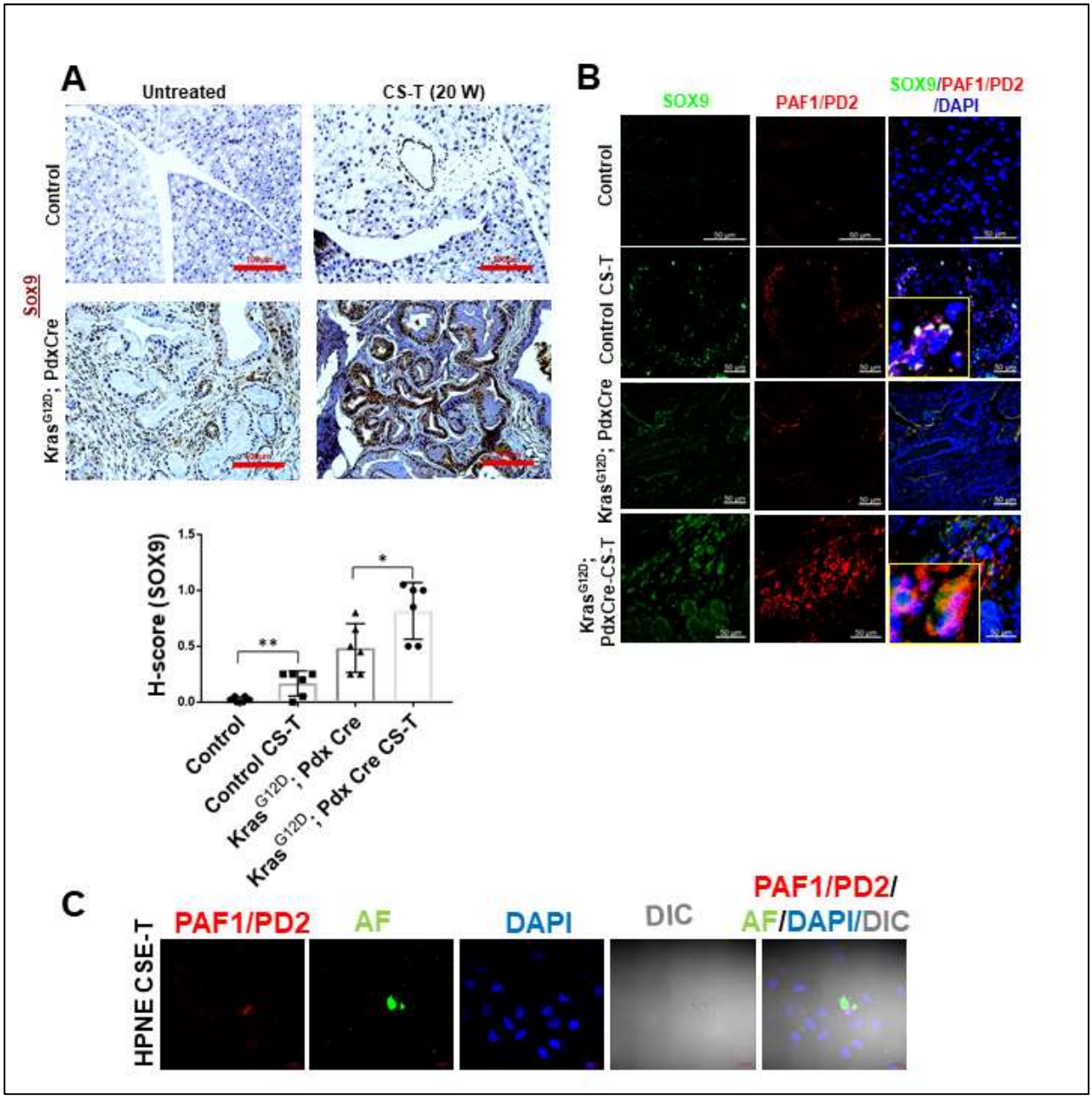

Supplementary Figure 7. Cigarette smoking activates FOSL1 and stem cell genes. (A) Heat map, generated from whole transcriptome analysis (RNA sequencing), showing top 50 up and down regulated genes in chronic (80 days) CSE exposed HPNE cells (RPKM_10245) as compared to HPNE untreated control (RPKM_10244). The log2 RPKM values of differentially expressed genes were used to draw the heat map. The RPKM values smaller than 1 corresponded to scale value of 0 and dark blue. With increasing RPKM values, color progressed through blue to red. FPKM values greater than 425 (scale value of 8) shown as red. **(B)** Heat map showing top 100 up- and down-regulated genes in chronic (80 days) CSE exposed Capan1 cells (RPKM_10249) compared to untreated control (RPKM_10248). The log2 RPKM values of differentially expressed genes were used to draw the heat map. RPKM values smaller than 1 corresponded to the scale value of 0 and dark blue. With increasing RPKM values, color progressed through blue to red. FPKM values greater than 524 (scale value of 8) shown as red. **(C)** Validation of major differentially expressed stem cell genes from RNA sequencing using quantitative reverse transcription polymerase chain reaction assay. Data shown are normalized for β-actin expression. Data represent mean ± SD (n=3). (p values were calculated by Student's t test). $^{*}p < 0.05$, $^{**}p < 0.01$ $^{***}p < 0.001$.

Supplementary Figure 7

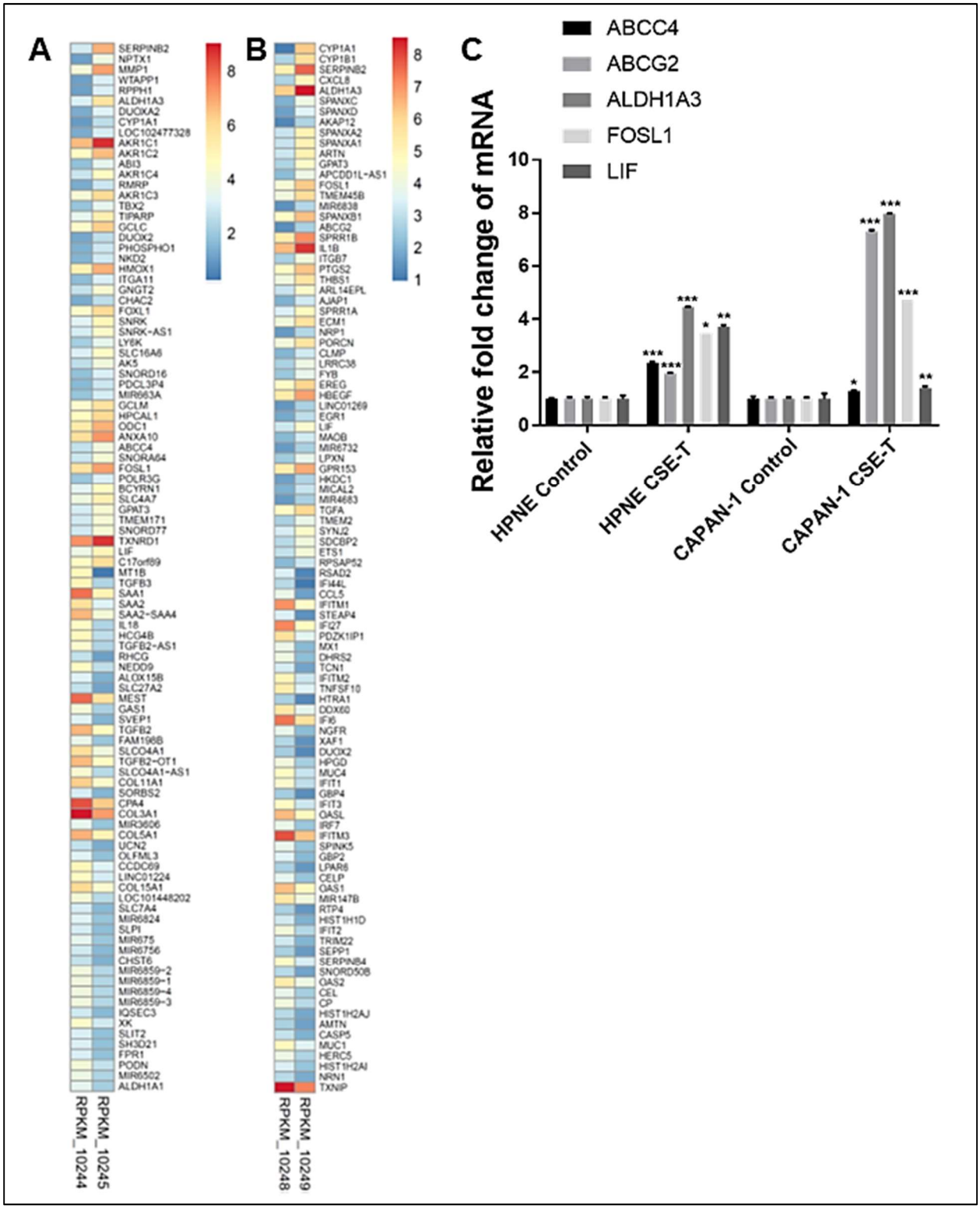

Supplementary Figure 8. Predicted binding sites of phospho-FOSL1 (or AP1) on PAF1 gene promoter. 5' upstream region of PAF1 gene nucleotide sequence was shown. Ten AP1 binding sites (BS1 to BS10) were highlighted in red color. Positions of each binding site in relative to TSS (+1) were shown.

Supplementary Figure 8

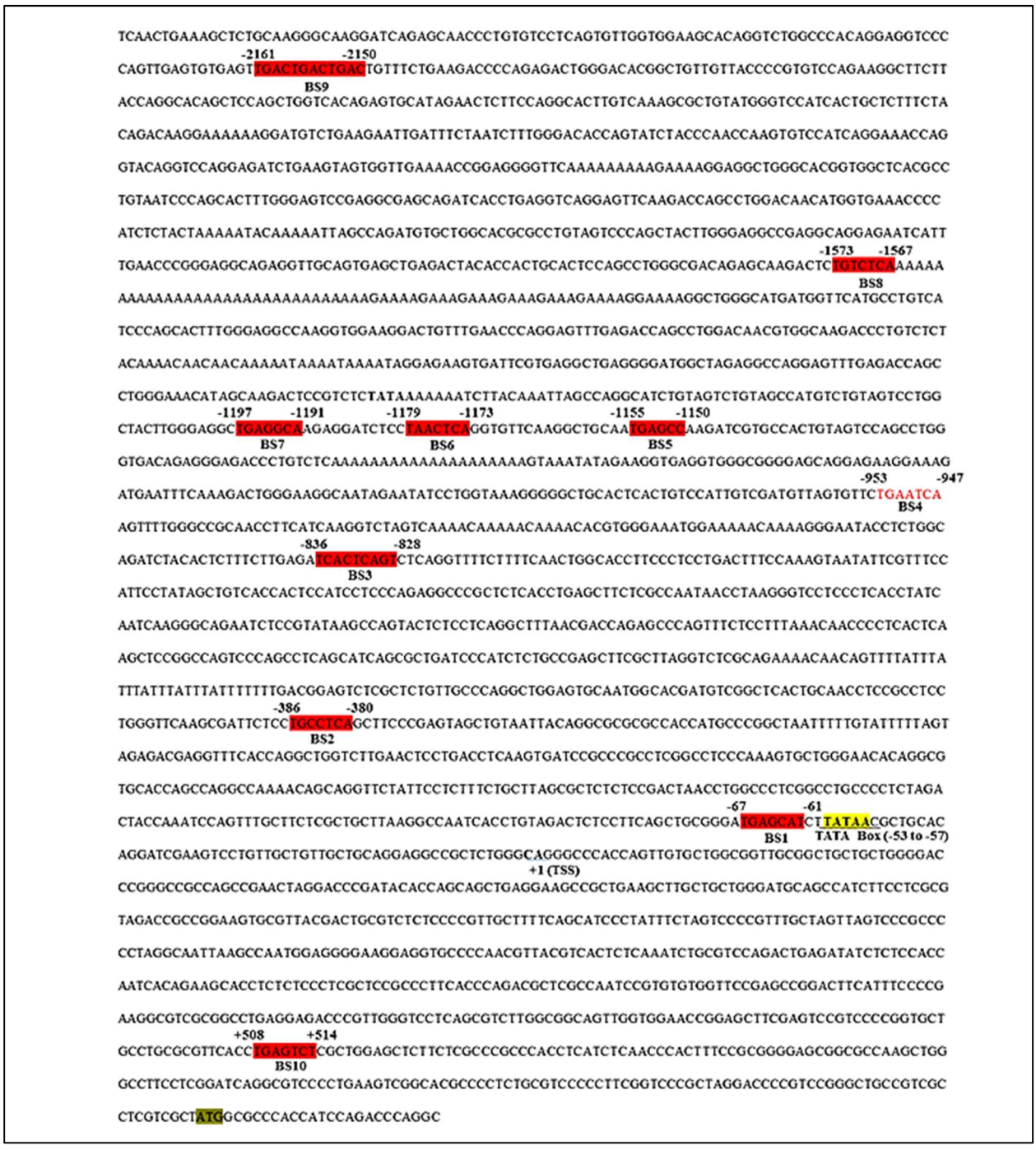

Supplementary Figure 9. FOSL1 binds to its consensus binding site (BS) 3 ($^{-836}$TCACTCAGT^{-827}) or BS 9 ($^{-2162}$TGACTGACTGAC^{-2157}) on PAF1 gene promoter. FOSL1 Chip-enriched DNA was amplified using PCR using primers for BS3 and BS9. Amplified PCR product was run on 2% agarose gel, and DNA bands were excised, purified DNA from gel slices and performed sequencing. Chromatograms obtained from Chip DNA PCR product sequencing and the reference sequence that holds binding sites were shown. Respective binding sites were highlighted in chromatogram.

Supplementary Figure 9

Supplementary Figure 10. Co-relation of CS induced phospho-FOSL1 (p-FOSL1) expression with cancer stemness marker, CD44 *in vivo*. Control and $Kras^{G12D}$ Pdx-Cre mice were exposed to CS for 20 weeks and collected the pancreas tissues. Immunofluorescence staining was performed for p-FOSL1 and CD44 on these CS exposed mice pancreas tissues. Nuclei were stained with DAPI, 4',6-diamidino-2-phenylindole. Scale bar, 50μm.

Supplementary Figure 10

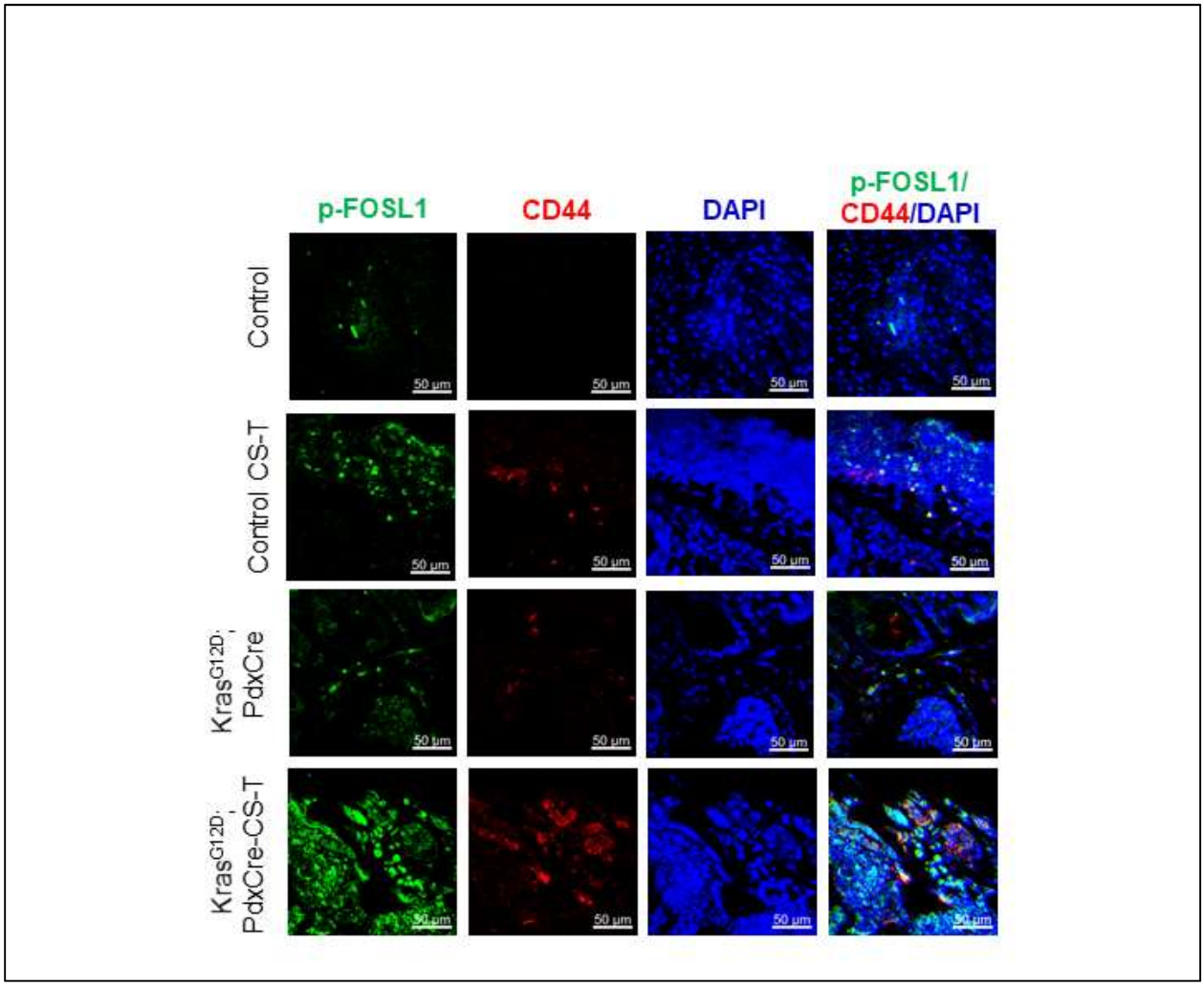

Supplementary Figure 11. (A) Immunoblotting analysis of CS associated receptors, TLR4 and CHRNA1. HPNE and Capan1 cells were left untreated or treated with CSE for 80 days, and analyzed for protein levels of TLR4 and CHRNA1. **(B)** Immunoblotting assay showing that inhibition of CHRNA7 receptor with Macamylamine (MAA) reduces the protein levels of phospho-FOSL1 (p-FOSL1), FOSL1 and PAF1 in chronic CSE exposed HPNE and Capan1 cells. 78 days CSE exposed cells were treated with MAA (200 μM) for 24hr (during 40^{th} passage) followed by 48hr stimulation with CSE. (A-B) β-actin was used as a loading control.

Supplementary Figure 11

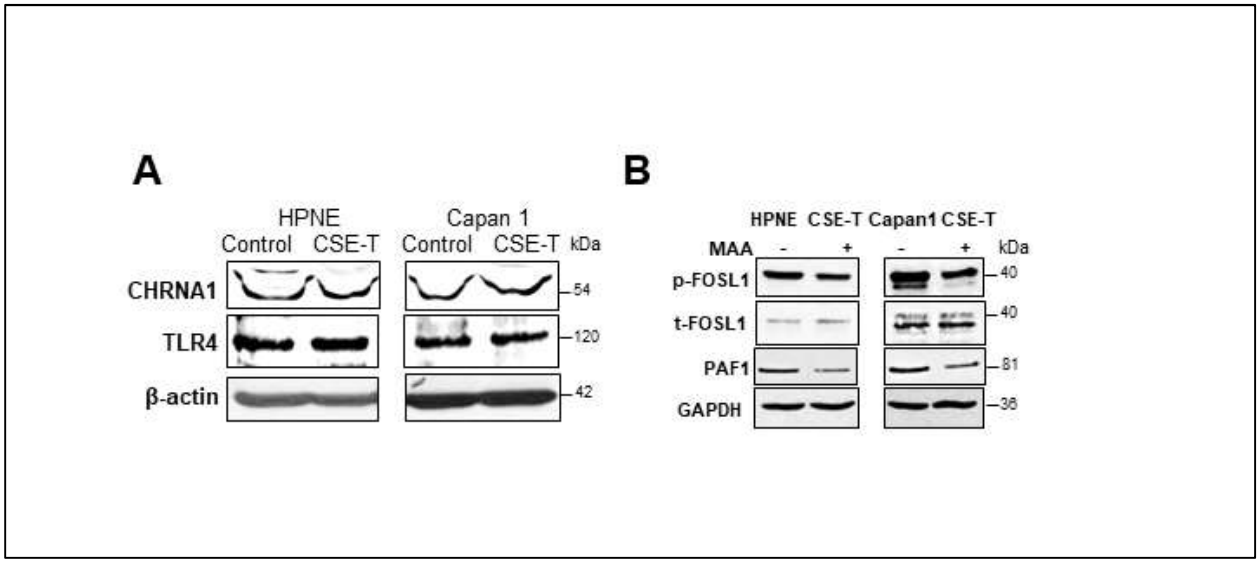

Supplementary Figure 12. (A) Confocal images showing the expression of PAF1 and PHF5A in chronic CSE treated HPNE and Capan1 cells. The co-localization of PAF1 (Green) and PHF5A (Red) was shown. Scale bar, 50μm. Nuclei were stained with DAPI, 4',6-diamidino-2-phenylindole.

Supplementary Figure 12

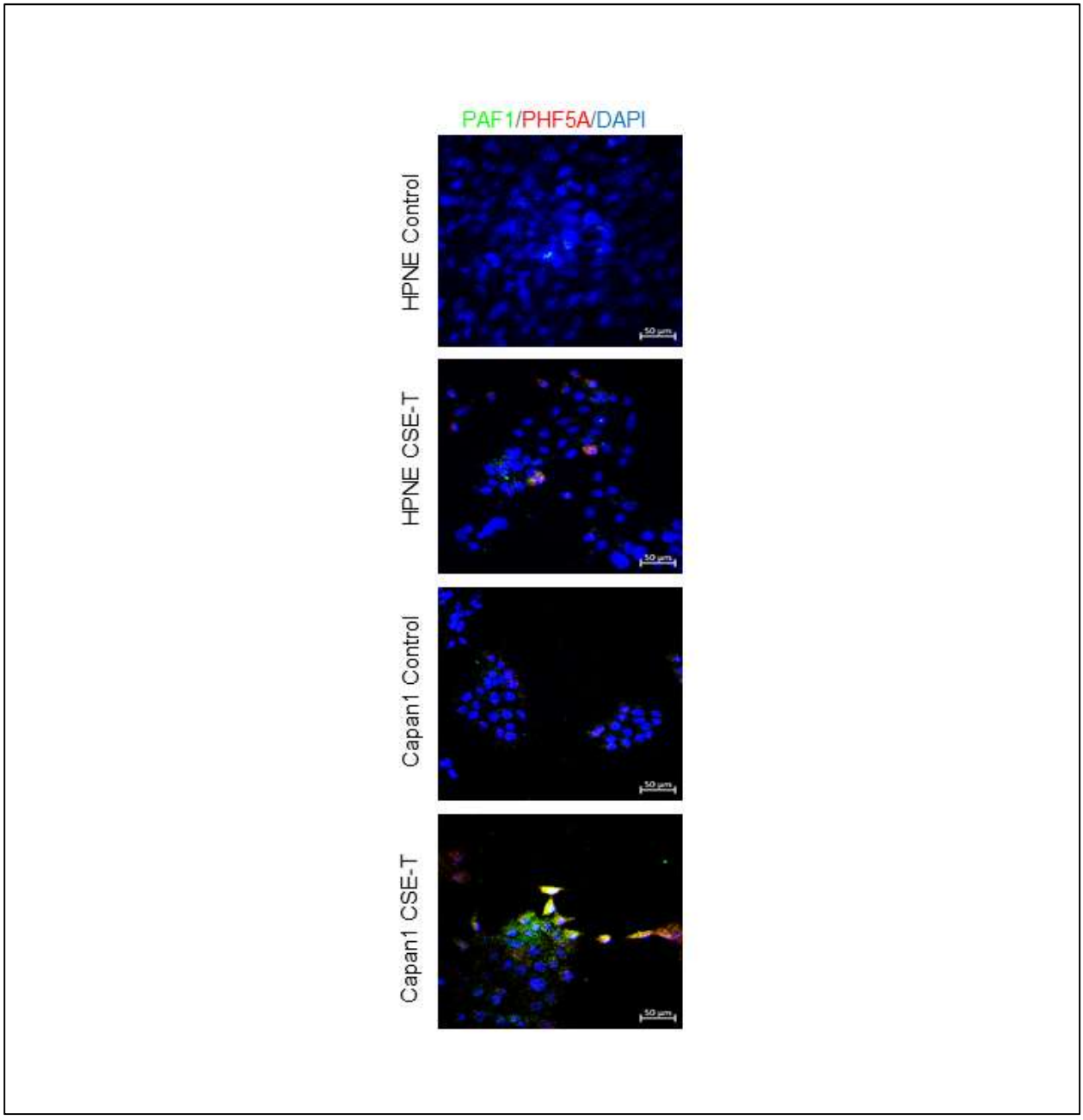

Supplementary Table 1: Chromatographic gradient program used in LC/MS/MS analysis of Nicotine in CSE

Total time (min)	Eluent B (Vol. %)	Flow rate (mL/min)
0.40	10	0.4
1.20	90	0.4
2.20	90	0.4
2.40	10	0.4
3.00 (Column re-equilibration)	10	0.4

Supplementary Table 2: List of antibodies used in western blot

ANTIBODIES	SOURCE	IDENTIFIER/DILUTION
List of primary antibodies used in Western blot		
Non phospho β-CATENIN	Cell Signaling Technology	Cat# CST-19807P (Rb) (1:1000)
ALDH1/2	Santa Cruz	Cat# Sc-50385 (Rb) (1:1000)
CD44	Cell Signaling Technology	Cat# CST-5640S (Ms) (1:1000)
OCT3/4	Santa Cruz	Cat# Sc-5279 (Ms) (1:500)
PAF1	Bethyl	Cat# Bethyl-A300-173A (Rb) (1:5000)
CHRNA7	Santa Cruz	Cat# Sc-5544 (Rb) (1:500)
Phospho ERK	Cell Signaling Technology	Cat# CST-9101S (Rb) (1:1000)
ERK	Cell Signaling Technology	Cat# CST-9102 (Rb) (1:1000)
Phospho c-Jun	Cell Signaling Technology	Cat# CST-9261 (Rb) (1:1000)
c-Jun	Santa Cruz	Cat# Sc-1694 (Rb) (1:1000)
Phospho FOSL1	Cell Signaling Technology	Cat# CST-5841S (Rb) (1:1000)
FOSL1	Cell Signaling Technology	Cat# CST-5281S (Rb) (1:1000)
LEO1	Bethyl	Cat# A300-174A (Rb) (1:1000)
CTR9	Bethyl	Cat# A301-395A-1 (Rb) (1:1000)
CDC73	Bethyl	Cat# A300-170A (Rb) (1:1000)
SKI8	Bethyl	Cat# A305-191A (Rb) (1:1000)
β-Actin	Santa Cruz	Cat# Sc-47778 (Ms) (1:2000)
GAPDH	Santa Cruz	Cat# Sc-47724 (Ms) (1:2000)
TLR4	Abcam	Cat# Ab-47093 (Rb) (1:1000)
PHF5A	Proteintech Group	Cat# 15554-1-AP (Rb) (1:500)
CTD Ser2-Phos RNA PolII	Active Motif	Cat# 61083 (Rat) (1:1000)
SOX2	Santa Cruz	Cat# sc-20088 (Rb) (1:500)
KLF4	Cell Signaling Technology	Cat#12173S (Rb) (1:500)
SOX9	Abcam	Cat#ab182579 (Rb) (1:1000)
CHRNA7	Millipore	Cat# MABN529 (Ms) (1:500)
BMI1	Cell Signaling Technology	Cat#6964S (Rb) (1:1000)
Nanog	Developmental Studies Hybridoma Bank	PCRP-NANOGP1-2D8 (Ms) (1:100)
List of secondary antibodies used in Western blot		
Goat anti-Rb IgG HRP	Invitrogen	Cat# 31460 (1:2000 to 1:5000)
Goat anti-Ms IgG HRP	Invitrogen	Cat#31430 (1:2000 to 1:5000)

Supplementary Table 3: List of antibodies used in this study

ANTIBODIES	SOURCE	IDENTIFIER/DILUTION
List of primary antibodies used in Immunofluorescence		
OCT3/4	Santa Cruz	Cat# Sc-5279 (Ms) (1:100)
ABCG2	Santa Cruz	Cat# Sc-130933 (Rb) (1:200)
SOX9	Abcam	Cat#ab182579 (Rb) (1:300)
PAF1	Bethyl	Cat# Bethyl-A300-173A (Rb) (1:300)
CD44	Cell Signaling Technology	Cat# CST-5640S (Ms) (1:300)
Anti human Fra1 Polyclonal	Invitrogen	Cat#PA5-40361 (Rb) (1:200)
PAF1 mouse mAB	In our lab	N/A (Ms) (1:100)
Phospho FOSL1	Cell Signaling Technology	Cat# CST-5841S (Rb) (1:200)
PHF5A	Proteintech Group	Cat# 15554-1-AP (Rb) (1:200)
Non phospho β-CATENIN	Cell Signaling Technology	Cat# CST-19807P (Rb) (1:300)
ALDH1/2	Santa Cruz	Cat# Sc-50385 (Rb) (1:300)
CD24	Santa Cruz	Cat# Sc-11406 (Rb) (1:300)
List of secondary antibodies used in Immunofluorescence		
Alexa Fluor 568 goat anti-mouse IgG	Life Technologies	Cat#A11004 (1:300)
Alexa Fluor 568 goat anti-rabbit IgG	Life Technologies	Cat#A11011 (1:300)
Alexa Fluor 488 goat anti-mouse IgG	Life Technologies	Cat#A11001 (1:300)
Alexa Fluor 488 goat anti-rabbit IgG	Life Technologies	Cat#A11008 (1:300)
Alexa Fluor 647 goat anti-rabbit IgG	Life Technologies	Cat#A21245 (1:300)
List of antibodies used in Immunohistochemistry		
PAF1 mouse mAB	In our lab	N/A (Ms) (1:100)
SOX9	Abcam	Cat#ab182579 (Rb) (1:200)
FOSL1 (For human tissues)	Invitrogen	Cat#PA5-40361 (Rb) (1:200)
FOSL1 (For mouse tissues)	Cell Signaling Technology	Cat# CST-5281S (Rb) (1:200)
PHF5A	Proteintech Group	Cat# 15554-1-AP (Rb) (1:100)
List of antibodies used in Immunoprecipitation assay		
PAF1	Bethyl	Cat# Bethyl-A300-172A (Rb) (4µg/900µg protein)
PHF5A	Proteintech Group	Cat# 15554-1-AP (Rb) (1:500)
ChromPure IgG	Jackson Immunoresearch Laboratories	Cat# 011-000-003 (Rb) (4µg/900µg protein)
List of antibodies used in Chip assay		
Phospho FOSL1	Cell Signaling Technology	Cat# CST-5841S (Rb)
List of antibodies used in Flow cytometry		
CD338 (ABCG2)-APC, human	Miltenyi Biotech	Cat#130-105-011
CD44 APC Human	Miltenyi Biotech	Cat# 130-098-110
Mouse IgG1 APC	Miltenyi Biotech	Cat#130-113-758
Mouse IgG2b APC	Miltenyi Biotech	Cat#130-098-890

Supplementary Table 4: List of qRT-PCR primers used in this study

Gene Name	(Forward and Reverse primers)	Amplicon Size
FOSL1	F: GGGCCTGTGCTTGAACCTGA	152
	R: TCTCCGCTGCTGCTGCTACTC	
PAF1	F: CTCACAGCATTACAGCAAACC	231
	R: GTCTCTTCTACAGGCAGGAAAT	
SOX9	F: GAGCCGGATCTGAAGAGGGA	151
	R: GCTTGACGTGTGGCTTGTTC	
ABCC4	F: GCGGCTGACGGTTACCCTCTT	189
	R: TCTGATGCCTTATCCCAAAAAGCAGT	
ABCG2	F: GAGCCTACAACTGGCTTAGACTCAA	85
	R: TGATTGTTCGTCCCTGCTTAGAC	
ALDH1A3	F: ATCAACTGCTACAACGCCCT	98
	R: TATTCGGCCAAAGCGTATTC	
LIF	F: CAAGAATCAACTGGCACAGC	244
	R: AGTGGGGTTCAGGACCTTCT	
SOX2	F: CAAAAATGGCCATGCAGGT	63
	R: AGTTGGGATCGAACAAAAGCTAT	
Oct3/4	F: GGAAGGAATTGGGAACACAAAGG	71
	R: AACTTCACCTTCCCTCCAACCA	
β-actin (Human)	F: GGACATCCGCAAAGACCTGTA	143
	R: GCTCAGGAGGAGCAATGATCT	
PAF1 (Mouse)	F: CCAGTTGGAAAACCACGAAC	124
	R: CTCGCTGCCTTCTTTCTCAC	

Supplementary Table 5: List of Chip primers used in this study

Binding site (BS)	(Forward and Reverse)	Amplicon Size
BS 1	F:GCTGCTTAAGGCCAATCACC	84
	R:AGGACTTCGATCCTGTGC	
BS2	F:ATTCTCCTGCCTCAGCTTCC	101
	R:AGCCTGGTGAAACCTCGTC	
BS3	F:GGAAGGCAATAGAATATCCTGGTA	197
	R:AAACCTGAGACTGAGTGAT	
BS4	F:GGAGCAGGAGAAGGAAAGATG	88
	R:CGACAATGGACAGTGAGTGC	
BS 5-8	F: GCTACTTGGGAGGCCGA	562
	R: ACCCAGGCTGGACTACAGTG	
BS9	F: ATCAGAGCAACCCTGTGTCC	163
	R: GCTGTGCCTGGTAAGAAGC	
BS10	F: GACTTCATTTCCCCGAAGG	127
	R: GAGAAGAGCTCCAGCGAGAC	

Supplementary Table 6: Significantly enriched GO terms for genes with higher expression in smoke treated HPNE versus untreated HPNE cells.

Category	Term	Count	PValue	Fold Enrichment	Benjamini	Genes
GOTERM_BP_FAT	GO:0043066~negative regulation of apoptosis	6	0.015305	4.02	0.525075841	GCLC, HMOX1, SERPINB2, ASNS, HSPA1A, GCLM
GOTERM_BP_FAT	GO:0043069~negative regulation of programmed cell death	6	0.016171	3.97	0.525567148	GCLC, HMOX1, SERPINB2, ASNS, HSPA1A, GCLM
GOTERM_BP_FAT	GO:0045787~positive regulation of cell cycle	3	0.023226	12.49	0.530625535	CYP1A1, ASNS, FOSL1
GOTERM_BP_FAT	GO:0008284~positive regulation of cell proliferation	6	0.027921	3.44	0.536533491	LIF, ODC1, TBX2, ITGA2, FOSL1, SERTAD1
GOTERM_BP_FAT	GO:0031668~cellular response to extracellular stimulus	3	0.028805	11.12	0.52622878	HMOX1, ASNS, FOSL1
GOTERM_BP_FAT	GO:0045649~regulation of macrophage differentiation	2	0.04462	43.15	0.629044239	LIF, INHBA
GOTERM_BP_FAT	GO:0045931~positive regulation of mitotic cell cycle	2	0.048579	39.56	0.634462234	CYP1A1, ASNS
GOTERM_BP_FAT	GO:0006916~anti-apoptosis	4	0.053565	4.61	0.646552098	GCLC, HMOX1, SERPINB2, HSPA1A

Supplementary Table 7: Related to Figure 5: Significantly enriched GO terms for genes with higher expression in smoke treated Capan1 versus untreated Capan1 cells.

Category	Term	Count	PValue	Fold Enrichment	Benjamini	Genes
GOTERM_BP_FAT	GO:0042493~response to drug	7	3.44E-04	7.31	0.04004213	PTGS2, CYP1A1, ALDH1A3, IL1B, FOSL1, GCLM, ABCG2
GOTERM_BP_FAT	GO:0045787~positive regulation of cell cycle	6	4.67E-06	23.73	0.00498260	CYP1A1, EREG, TGFA, IL1B, FOSL1, IL1A
GOTERM_BP_FAT	GO:0008284~positive regulation of cell proliferation	10	6.98E-05	5.45	0.02458280	LIF, PTHLH, CSF3, NRP1, PTGS2, EREG, TGFA, IL1B, HBEGF, FOSL1
GOTERM_BP_FAT	GO:0051726~regulation of cell cycle	9	8.83E-05	6.13	0.02331133	LIF, PTGS2, CYP1A1, EREG, ETS1, TGFA, IL1B, FOSL1, IL1A
GOTERM_BP_FAT	GO:0042127~regulation of cell proliferation	13	1.23E-04	3.72	0.02592552	LIF, PTHLH, CSF3, NRP1, EREG, PTGS2, ETS1, TGFA, IL1B, HBEGF, THBS1, FOSL1, IL1A
GOTERM_BP_FAT	GO:0010564~regulation of cell cycle process	6	1.36E-04	11.87	0.02386321	LIF, CYP1A1, EREG, TGFA, IL1B, IL1A
GOTERM_BP_FAT	GO:0045840~positive regulation of mitosis	4	1.69E-04	36.07	0.02552250	EREG, TGFA, IL1B, IL1A
GOTERM_BP_FAT	GO:0051785~positive regulation of nuclear division	4	1.69E-04	36.07	0.02552250	EREG, TGFA, IL1B, IL1A
GOTERM_BP_FAT	GO:0043067~regulation of programmed cell death	12	6.72E-04	3.33	0.05812113	IER3, PTGS2, ETS1, ALDH1A3, SERPINB2, IL1B, THBS1, TNFSF18, FOSL1, GCLM, IL1A, PHLDA1
GOTERM_BP_FAT	GO:0051302~regulation of cell division	4	0.001115	19.19	0.07642029	EREG, TGFA, IL1B, IL1A
GOTERM_BP_FAT	GO:0051783~regulation of nuclear division	4	0.001854	16.10	0.11012361	EREG, TGFA, IL1B, IL1A
GOTERM_BP_FAT	GO:0006916~anti-apoptosis	6	0.002004	6.57	0.11231724	IER3, SERPINB2, IL1B, THBS1, TNFSF18, IL1A
GOTERM_BP_FAT	GO:0010647~positive regulation of cell communication	7	0.003013	4.80	0.13638001	LIF, PTGS2, EREG, TGFA, IL1B, THBS1, ECM1
GOTERM_BP_FAT	GO:0043405~regulation of MAP kinase activity	5	0.003302	8.00	0.14249974	MAP3K9, TGFA, IL1B, THBS1, DUSP6
GOTERM_BP_FAT	GO:0043066~negative regulation of apoptosis	7	0.004314	4.46	0.15733488	IER3, SERPINB2, IL1B, THBS1, TNFSF18, GCLM, IL1A
GOTERM_BP_FAT	GO:0043069~negative regulation of programmed cell death	7	0.004618	4.40	0.15686209	IER3, SERPINB2, IL1B, THBS1, TNFSF18, GCLM, IL1A
GOTERM_BP_FAT	GO:0060548~negative regulation of cell death	7	0.004681	4.38	0.14937605	IER3, SERPINB2, IL1B, THBS1, TNFSF18, GCLM, IL1A
GOTERM_BP_FAT	GO:0000187~activation of MAPK activity	4	0.005467	11.00	0.16733245	MAP3K9, TGFA, IL1B, THBS1
GOTERM_BP_FAT	GO:0000165~MAPKKK cascade	5	0.008424	6.13	0.20697075	MAP3K9, TGFA, IL1B, THBS1, DUSP6

Supplementary Table 8: Details of smoking status and tumor grade of human pancreatic normal and tumor tissue sections.

Block Designator(s)	Smoking Status	Diagnosis
F8	Never Smoker	Benign Pancreas
A12	Former Smoker (QD: 9/29/1961)	Benign Pancreas
A14	Former Smoker (QD: 3/21/1980)	Benign Pancreas
A16-A17	Never Smoker	Benign Pancreas
A1	Never Smoker	Benign Pancreas
C4	Never Smoker	Benign Pancreas
D1-D2	Former Smoker (QD: 8/10/2008)	Benign Pancreas
B3-B4	Never Smoker	Benign Pancreas
C3-C4	Never Smoker	Benign Pancreas
A7-A8	Never Smoker	Benign Pancreas
C8	Never Smoker	Benign Pancreas
A1	Former Smoker (QD: 7/16/1992)	Benign Pancreas
B11-B12	Never Smoker	Benign Pancreas
D5	Never Smoker	Benign Pancreas
B3-B4	Never Smoker	Benign Pancreas
G5	Never Smoker	Ductal Adenocarcinoma, WD
G4	Never Smoker	Ductal Adenocarcinoma, PD
B19	Never Smoker	Ductal Adenocarcinoma, WD
E9-E10	Never Smoker	Ductal Adenocarcinoma, MD
E4-E11, E14	Never Smoker	Ductal Adenocarcinoma, MD
C14-C17	Never Smoker	Ductal Adenocarcinoma, MD
A5-A8	Never Smoker	Ductal Adenocarcinoma, MD
E9, E22-E25	Never Smoker	Ductal Adenocarcinoma, WD
E6-E10	Never Smoker	Ductal Adenocarcinoma, PD
A6-A9, A11-A13	Never Smoker	Ductal Adenocarcinoma, WD
A3-A4, A10-A11, A15-A18	Never Smoker	Ductal Adenocarcinoma, WD
B11-B15	Never Smoker	Ductal Adenocarcinoma, MD
B10-B15	Never Smoker	Ductal Adenocarcinoma, PD
B7-B9	Never Smoker	Ductal Adenocarcinoma, MD
A3, A5-A8	Never Smoker	Ductal Adenocarcinoma, WD-MD
C7-C9, C13, C16-C17	Former Smoker (QD: 2/18/1994)	Ductal Adenocarcinoma, PD
B7-B22	Some Day Smoker (40 pack-years)	Ductal Adenocarcinoma, MD
A8-A9	Former Smoker (QD: 1/1/2013)	Ductal Adenocarcinoma, MD
G9-G13	Former Smoker (QD: 4/27/2014)	Ductal Adenocarcinoma, MD
A5-A6, A8	Former Smoker (QD: 7/2/2014)	Ductal Adenocarcinoma, MD
D3 (Frozen)	Former Smoker (QD: 10/6/1954)	Ductal Adenocarcinoma, MD
D7-D10	Former Smoker (QD: 10/9/1989)	Ductal Adenocarcinoma, MD-PD
B5-B6	Former Smoker (QD: Unknown)	Ductal Adenocarcinoma, MD
E7-E8	Former Smoker (QD: 6/4/2005)	Ductal Adenocarcinoma, WD
F5-F6, F14-F17	Former Smoker (QD: 9/21/2015)	Ductal Adenocarcinoma, MD
C5-C9, C11	Former Smoker (QD: 7/1/2013)	Ductal Adenocarcinoma, WD
B10-B13	Former Smoker (QD: 11/8/2013)	Ductal Adenocarcinoma, MD
G4-G9	Former Smoker (QD: 12/6/1970)	Ductal Adenocarcinoma, MD
C7	Former Smoker (32 pack-years)	Ductal Adenocarcnoma, MD-PD
A7	Every Day Smoker (25 pack-years)	Ductal Adenocarcinoma, MD

Key resources table

REAGENT or RESOURCE	SOURCE	IDENTIFIER
ANTIBODIES (see Supplementary Table 2 and 3) and PRIMERS (see Supplementary Table 4 and 5)	This paper	N/A
Experimental Models: Cell Lines		
hTERT-HPNE cells	Dr. Ouellette (UNMC)	
Capan1	ATCC	ATCC (HTB-79)
Experimental Models: Animals		
Mouse: LSL-$Kras^{G12D}$ and $Kras^{G12D}$; Pdx-1cre	In house developed	N/A
Critical commercial assays		
ALDEFLUOR assay kit	Stem Cell Technologies	Cat #01700
Bio-Rad DC Protein Assay Kit	Bio-Rad	Cat # 500-0114
ECL chemiluminescence kit	Thermo Scientific	Cat#32209
Illumina TruSeq RNA Sample Preparation Kit	Illumina	CAT# RS-122-2001
Double stain IHC kit: M&R on human tissue	Abcam	AB210061
Bloxall blocking solution	Vector Laboratories, Inc.	SP-6000
Chip DNA Clean & Concentrator kit	The Epigenetics Company	CAT# D5205
Software		
TRANSFAC	gene X plain	www.genexplain.com
Sigmaplot	Systat Software, Inc.	www.sigmaplot.co.uk
ImageJ	NIH	https://fiji.sc
BD FACS Diva	BD Biosciences	N/A
Zen Imaging	Zeiss	https://www.zeiss.com/microscopy/us/products/microscope-software/zen-lite.html
PRISM GRAPHPAD	Graphpad	https://www.graphpad.com/scientific-software/prism/
Multiquant	AB Sciex	https://sciex.com/products/software/multiquant-software
Finch TV	Geospiza, Inc.	https://digitalworldbiology.com/FinchTV
Chemicals & Reagents		
3R4F research cigarettes	University of Kentucky	https://ctrp.uky.edu/
PD98059	Sigma	Cat# P215
Mecamylamine	Sigma	Cat# M9020
Hoechst 33342	Ana Spec	Cat#AS-83218
ChromPure Rabbit IgG, whole molecule	Jackson Immunoresearch Laboratories, Inc.	Cat# 011-000-003
Optima™ LC/MS water	Fisher Chemical	W6212
Methanol, Optima™ LC/MS Grade	Fisher Chemical	A456-1
Acetonitrile, Optima™ LC/MS Grade	Fisher Chemical	A955-1
Ammonium bicarbonate	Sigma	09830
Lipofectamine 2000	Invitrogen	Cat# 11668027
Nile Red	Thermofisher Scientific	Cat# N1142
DAPI, FluoroPure™ grade	Thermofisher Scientific	Cat# D21490
N′-Nitrosonornicotine (NNN) solution	Sigma	Cat# N-075
4-(Methylnitrosamino)-1-(3-pyridyl)-1-butanone (NNK) solution	Sigma	Cat#N-076
NICOTINE	Sigma	Cat#N-3876
Commercial Cigarette smoke extract (C-CSE)	Murthy pharmaceuticals.	N/A
Riboflavin	Sigma	R9504
Matrigel	Fisher Scientific (Corning)	08-774-552
Nicotine D4 solution	Sigma	N048
Plasmids/siRNAs		
PAF1 (ID 54623) Trilencer-27 Human siRNA	Origene	SR310177
FOSL1 (ID 8061) Trilencer-27 Human siRNA	Origene	SR322327
CHRNA7 Trilencer-27 Human siRNA	Origene	SR300818

References

1. Kuroczycki-Saniutycz S, Grzeszczuk A, Zwierz ZW, et al. Prevention of pancreatic cancer. Contemp Oncol (Pozn) 2017;21:30-4.

2. Momi N, Ponnusamy MP, Kaur S, et al. Nicotine/cigarette smoke promotes metastasis of pancreatic cancer through alpha7nAChR-mediated MUC4 upregulation. Oncogene 2013;32:1384-95.

3. Xue J, Yang S, Seng S. Mechanisms of Cancer Induction by Tobacco-Specific NNK and NNN. Cancers (Basel) 2014;6:1138-56.

4. Melkamu T, Qian X, Upadhyaya P, et al. Lipopolysaccharide enhances mouse lung tumorigenesis: A model for inflammation-driven lung cancer. Vet Pathol 2013;50:895-902.

5. Pauly JL, Paszkiewicz G. Cigarette Smoke, Bacteria, Mold, Microbial Toxins, and Chronic Lung Inflammation. Journal of Oncology 2011;2011.

6. Yu D, Geng H, Liu Z, et al. Cigarette smoke induced urocystic epithelial mesenchymal transition via MAPK pathways. Oncotarget 2017;8:8791-800.

7. Al-Wadei MH, Banerjee J, Al-Wadei HAN, et al. Nicotine induces self-renewal of pancreatic cancer stem cells via neurotransmitter-driven activation of sonic hedgehog signaling. European journal of cancer (Oxford, England : 1990) 2016;52:188-196.

8. Hermann PC, Sancho P, Canamero M, et al. Nicotine promotes initiation and progression of KRAS-induced pancreatic cancer via Gata6-dependent dedifferentiation of acinar cells in mice. Gastroenterology 2014;147:1119-33.e4.

9. Ponnusamy MP, Batra SK. Insights into the role of nicotine in pancreatic stem cell activation and acinar dedifferentiation. Gastroenterology 2014;147:962-5.

10. Hanson RL, Brown RB, Steele MM, et al. Identification of FRA-1 as a novel player in pancreatic cancer in cooperation with a MUC1: ERK signaling axis. Oncotarget 2016;7:39996-40011.

11. Lau EY, Lo J, Cheng BY, et al. Cancer-Associated Fibroblasts Regulate Tumor-Initiating Cell Plasticity in Hepatocellular Carcinoma through c-Met/FRA1/HEY1 Signaling. Cell Rep 2016;15:1175-89.

12. Milde-Langosch K. The Fos family of transcription factors and their role in tumourigenesis. Eur J Cancer 2005;41:2449-61.

13. Costa PJ, Arndt KM. Synthetic lethal interactions suggest a role for the Saccharomyces cerevisiae Rtf1 protein in transcription elongation. Genetics 2000;156:535-47.

14. Penheiter KL, Washburn TM, Porter SE, et al. A posttranscriptional role for the yeast Paf1-RNA polymerase II complex is revealed by identification of primary targets. Mol Cell 2005;20:213-23.

15. Stolinski LA, Eisenmann DM, Arndt KM. Identification of RTF1, a novel gene important for TATA site selection by TATA box-binding protein in Saccharomyces cerevisiae. Mol Cell Biol 1997;17:4490-500.

16. Chaudhary K, Deb S, Moniaux N, et al. Human RNA polymerase II-associated factor complex: dysregulation in cancer. Oncogene 2007;26:7499-507.

17. Ding L, Paszkowski-Rogacz M, Nitzsche A, et al. A genome-scale RNAi screen for Oct4 modulators defines a role of the Paf1 complex for embryonic stem cell identity. Cell Stem Cell 2009;4:403-15.

18. Ponnusamy MP, Deb S, Dey P, et al. RNA polymerase II associated factor 1/PD2 maintains self-renewal by its interaction with Oct3/4 in mouse embryonic stem cells. Stem Cells 2009;27:3001-11.

19. Strikoudis A, Lazaris C, Trimarchi T, et al. Regulation of transcriptional elongation in pluripotency and cell differentiation by the PHD-finger protein Phf5a. Nat Cell Biol 2016;18:1127-1138.

20. Vaz AP, Deb S, Rachagani S, et al. Overexpression of PD2 leads to increased tumorigenicity and metastasis in pancreatic ductal adenocarcinoma. Oncotarget 2016;7:3317-31.

21. Vaz AP, Ponnusamy MP, Rachagani S, et al. Novel role of pancreatic differentiation 2 in facilitating self-renewal and drug resistance of pancreatic cancer stem cells. Br J Cancer 2014;111:486-96.

22. Kumar S, Torres MP, Kaur S, et al. Smoking accelerates pancreatic cancer progression by promoting differentiation of MDSCs and inducing HB-EGF expression in macrophages. Oncogene 2015;34:2052-60.

23. Liu Y, Luo F, Xu Y, et al. Epithelial-mesenchymal transition and cancer stem cells, mediated by a long non-coding RNA, HOTAIR, are involved in cell malignant transformation induced by cigarette smoke extract. Toxicology and Applied Pharmacology 2015;282:9-19.

24. Miranda-Lorenzo I, Dorado J, Lonardo E, et al. Intracellular autofluorescence: a biomarker for epithelial cancer stem cells. Nat Methods 2014;11:1161-9.

25. Cao D, Kishida S, Huang P, et al. A new tumorsphere culture condition restores potentials of self-renewal and metastasis of primary neuroblastoma in a mouse neuroblastoma model. PLoS One 2014;9:e86813.

26. Wang YJ, Bailey JM, Rovira M, et al. Sphere-forming assays for assessment of benign and malignant pancreatic stem cells. Methods Mol Biol 2013;980:281-90.

27. Marcato P, Dean CA, Pan D, et al. Aldehyde dehydrogenase activity of breast cancer stem cells is primarily due to isoform ALDH1A3 and its expression is predictive of metastasis. Stem Cells 2011;29:32-45.

28. Sainz B, Miranda-Lorenzo I, Heeschen C. The Fuss Over Lipo“fuss”cin: Not All Autofluorescence is the Same. European Journal of Histochemistry : EJH 2015;59:2512.

29. Talotta F, Mega T, Bossis G, et al. Heterodimerization with Fra-1 cooperates with the ERK pathway to stabilize c-Jun in response to the RAS oncoprotein. Oncogene 2010;29:4732-40.

30. Hirata N, Yamada S, Sekino Y, et al. Tobacco nitrosamine NNK increases ALDH-positive cells via ROS-Wnt signaling pathway in A549 human lung cancer cells. The Journal of Toxicological Sciences 2017;42:193-204.

31. Liu L, Xu Y, He M, et al. Transcriptional pause release is a rate-limiting step for somatic cell reprogramming. Cell Stem Cell 2014;15:574-88.

32. Moniaux N, Nemos C, Schmied BM, et al. The human homologue of the RNA polymerase II-associated factor 1 (hPaf1), localized on the 19q13 amplicon, is associated with tumorigenesis. Oncogene 2006;25:3247-57.

33. Mueller CL, Porter SE, Hoffman MG, et al. The Paf1 complex has functions independent of actively transcribing RNA polymerase II. Mol Cell 2004;14:447-56.

34. Huang P, Wang CY, Gou SM, et al. Isolation and biological analysis of tumor stem cells from pancreatic adenocarcinoma. World J Gastroenterol 2008;14:3903-7.

35. Li C, Heidt DG, Dalerba P, et al. Identification of Pancreatic Cancer Stem Cells. Cancer Research 2007;67:1030-1037.

36. An Y, Kiang A, Lopez JP, et al. Cigarette Smoke Promotes Drug Resistance and Expansion of Cancer Stem Cell-Like Side Population. PLOS ONE 2012;7:e47919.

37. Guha P, Bandyopadhyaya G, Polumuri SK, et al. Nicotine Promotes Apoptosis Resistance of Breast Cancer Cells and Enrichment of Side Population Cells with Cancer Stem Cell Like Properties via a Signaling Cascade Involving Galectin-3, α9 Nicotinic Acetylcholine Receptor and STAT3. Breast cancer research and treatment 2014;145:5-22.

38. Shaykhiev R, Wang R, Zwick RK, et al. Airway basal cells of healthy smokers express an embryonic stem cell signature relevant to lung cancer. Stem Cells 2013;31:1992-2002.

39. Little MP, Hendry JH. Mathematical models of tissue stem and transit target cell divisions and the risk of radiation- or smoking-associated cancer. PLoS Computational Biology 2017;13:e1005391.

40. Karmakar S, Seshacharyulu P, Lakshmanan I, et al. hPaf1/PD2 interacts with OCT3/4 to promote self-renewal of ovarian cancer stem cells. Oncotarget 2017.

CHAPTER 5

Metastasis of cancer stem cells in pancreatic cancer and their organ-tropic homing

Synopsis

Pancreatic tumors contain heterogeneous cancer stem cell populations with metastatic abilities. Cellular metabolism governs the stem cell and metastatic features of cancer cells; however, the specific stem cell and metabolic features of heterogeneous cancer stem cell populations and their role in organ-specific homing and colonization remain poorly understood. Here, we identified distinct types of cancer stem cell populations: cells with high aldehyde dehydrogenase (ALDH+) activity and those with high multidrug resistance (MDR1+). Specifically, we demonstrate that ALDH+ cells are oxidative, while MDR1+ cells display increased aerobic glycolysis (Warburg effect). Moreover, the specific metabolic and stem cell features of cancer cells are associated with their metastasis to a specific organ. Spontaneous liver tropic cell line and human liver metastases show multi-drug resistance and aerobic glycolysis, whereas, spontaneous lung tropic cell line and human lung metastases display ALDH activity and oxidative metabolism.

Background and Rationale

Pancreatic cancer is one of the most intractable malignancies, being the seventh leading cause of global cancer-related mortality [1]. Most of the pancreatic cancer patients are diagnosed with an advanced tumor and distant metastasis stages, which are difficult to treat by current treatment strategies.

Cancer stem cells (CSCs) in pancreatic cancer play a central role in tumorigenesis, development of advanced tumors and metastasis [2, 3]. Pancreatic cancer harbors many CSC populations with tumorigenic and metastatic features [2-5]; however, the functional differences between one CSC populations to the other are poorly understood.

Studies in breast and pancreatic cancer indicated that CSC populations differ in their energy metabolism and show metabolic heterogeneity [6, 7]. In breast cancer, CSCs exist in two states: epithelial CSCs and mesenchymal CSCs. Epithelial breast CSCs show aldehyde dehydrogenase activity with oxidative metabolism; however, mesenchymal breast CSCs display CD44+CD24- phenotype with glycolytic metabolism [6]. Moreover, CD133+ pancreatic CSCs rely on oxidative phosphorylation, while a small percentage of metformin resistant pancreatic CSCs show both glycolytic and oxidative (intermediate) metabolism [7]. Gemcitabine is one of the critical chemotherapy drug utilized to treat pancreatic cancer. Clones with acquired gemcitabine resistance show increased glycolytic metabolism and decreased oxidative phosphorylation as compared to gemcitabine sensitive cells [8]. Pancreatic tumors also consist of intrinsic resistant clones that are resistant to gemcitabine [9]. These findings raise the interesting question of whether the gemcitabine-resistant clones have stem cell features and whether these resistant clones are distinct from other CSC sub-clones.

Multiple studies appreciate the role of CSCs in pancreatic cancer metastasis [2, 10]. Based on Stephen Paget's "Seed" and "Soil" theory, cancer cells from primary tumor shed and travel to distant organs, which are welcoming homes in order to form an organ-specific metastasis. This hypothesis implies that the metastasis formation relies on the intrinsic features of distinct cancer cell types in a heterogeneous tumor and the ability of these cancer cells to interact and colonize in the host environment. Recently, several studies provide evidence for the organ-specific metastasis of cancer cells [11, 12], may be due to different genomic and metabolic variation. It is well known that cells within pancreatic tumors are metabolically heterogeneous. Schild et al., have proposed that cancer cells during evolution gain metabolic signature that is compatible with their

colonization and survival in a specific organ [13]. Lehuede et al., have also suggested that only those metabolically flexible cancer cells can survive in distant organs and form metastasis [14]. Based on these studies and owing to the association of CSCs with metastasis, we hypothesize that distinct sub-types of CSC populations with sub-type specific metabolic and stem cell features migrate to a specific organ.

Here we identified distinct subsets of CSC populations in human and mice pancreatic tumors. These populations include aldehyde dehydrogenase (ALDH) and multi-drug resistant (MDR) population. Treatment with the chemotherapeutic drug, gemcitabine further increased MDR population by decreasing the ALDH population. We also demonstrated that the ALDH population relies on oxidative phosphorylation, whereas MDR population display Warburg effect. Moreover, liver tropic cells and human liver metastasis showed MDR stem cell phenotype with intermediate metabolism, whereas lung tropic cells and human lung metastasis showed ALDH stem cell features with oxidative metabolism

Results

A. Aldehyde dehydrogenase and multi-drug resistance identifies distinct sub-types of CSC populations in pancreatic cancer

Previous studies demonstrated ALDH and MDR1 as pancreatic CSC markers. Cells expressing either ALDH or MDR1 shows *in vivo* tumorigenic property involved in tumor progression and metastasis [4, 15, 16]. However, it is not clear whether ALDH and MDR1 CSC markers identify the same or distinct pancreatic CSC populations. For this, we performed immunofluorescence staining using ALDH1A1 and MDR1 antibodies on human pancreatic cancer tissues obtained from PDAC patients treated with or without gemcitabine chemotherapy. Treatment with gemcitabine induces drug resistance leading to the overexpression of MDR1 [17]. As revealed by immunofluorescence staining and confocal imaging, ALDH and MDR1 positive cells were identified mostly as distinct non-overlapping cell populations in pancreatic tumors obtained from patients without gemcitabine treatment (Figure 1A). However, pancreatic tumors with gemcitabine treatment showed the loss of ALDH1A1, but the elevated expression of MDR1 (Figure 1A). Besides, pancreatic tumors of $Kras^{G12D}$; Pdx-1 Cre (KC) mice showed distinct localization of these CSC markers (Figure 1A).

To further explore stem cell features and functional differences between ALDH and MDR1 populations, we developed distinct in vitro CSC models by using sphere culture method, which was described previously [7]. A gemcitabine-resistant cancer cell line was generated by treating Miapaca-2, a non-metastatic pancreatic cancer cell line with an increasing concentration of gemcitabine. Miapaca-2 parental cells and gemcitabine-treated Miapaca-2 cells were grown as spheres and denoted as “Sph” and “Sph+Gem,” respectively. Miapaca-2 cells grown as adherent cultures were considered as non-CSC populations and denoted as “Adh” (Figure 1B). To characterize Sph, Sph+Gem and Adh populations, we performed Hoechst-33342 based side population assay, a gold standard for identifying drug-resistant CSCs [10]. As assessed by flow cytometry, the percentage of side population was significantly elevated in Sph+Gem population as compared to Adh and Sph populations (Figure1C and D). Also, the percentage of autofluorescence (AF), an intracellular marker for CSCs [18, 19] was increased in Sph+Gem cells but lowered in Sph cells (Figure1C and E). Analysis of ALDH population using ALDERED assay showed relatively an increased percentage of ALDH+ population in Sph cells than in Sph+Gem population (Figure1C and F). Gene expression analysis using qRT-PCR also showed overexpression of ALDH1A1 and MDR1 in Sph and Sph+Gem populations, respectively (Figure1G). Interestingly, differential expression of other stem cell markers, KLF4 and CD44v9 were observed in these distinct populations as assessed by qRT-PCR. The expression of KLF4, a pluripotent stem cell marker was higher in Sph-derived cells; however, augmented expression of CD44v9 was identified in Sph+Gem cells (Figure1G). Moreover, flow cytometry analysis showed an increased percentage of CD133+ and MDR1+ population in Sph and Sph+Gem populations, respectively (Figure1H and I). Together, these data elucidate the existence of distinct subtypes of CSC populations in pancreatic tumors with sub-type specific localization and stem cell features.

B. Distinct sub-types of CSC populations in pancreatic cancer show sub-type specific metabolic profiles.

Previous emerging study demonstrates that the metabolic profile of pancreatic CSCs is heterogeneous [7]. Distinct CSC populations in breast tumor display specific metabolic profiles. ALDH+ breast CSCs show oxidative phosphorylation, while CD44+CD24- breast CSCs display glycolysis [6]. In light of these discoveries, we sought to investigate whether the ALDH+ and MDR1+ population display population-specific metabolic features. As shown by immunofluorescence staining on pancreatic tumors from human PDAC patients and KC mice,

MDR1 positive cells were co-expressed with LDH-A, a major enzyme involved in the conversion of pyruvate to lactate (Warburg effect).

On the other hand, the ALDH+ population co-expressed with ATP5B, a subunit of mitochondrial ATP synthase and an essential marker of mitochondria. Interestingly, cells expressing LDH-A did not show co-expression with ALDH1A1 suggesting that ALDH+ population do not display Warburg effect. To further validate this data functionally, we evaluated the extracellular acidification rate (ECAR) and oxygen consumption rate (OCR) using various inhibitors of glycolysis and oxidative phosphorylation. Miapaca-2 Sph+Gem cells displayed increased ECAR, glycolysis and glycolytic capacity relative to non-CSC and Sph populations (Figure 2B-D). In contrast, Sph+Gem cells showed decreased OCR, while Sph population showing elevated maximal respiration, spare respiratory capacity and ATP production (Figure 2F-I). Consistent with this data, lactate release and glucose consumption were also significantly higher in Sph+Gem cells relative to Sph population (Figure 2J and K). We further sought to investigate whether these functional metabolic differences between Sph and Sph+gem populations correlate with their metabolic gene signatures. QRT-PCR analysis showed an elevated expression of genes associated with aerobic glycolysis, PDK1, LDH-A, HIF1α and Myc in Sph+gem cells relative to Sph and non-CSC populations suggesting that drug-resistant CSC population rely on aerobic glycolysis (Warburg effect) for their energy needs (Figure 2L). The gene expression analysis also showed the lower expression of glycolytic genes, GLUT1, HK2 (a rate-limiting glycolytic gene), PGM2 and ENO1, and diminished expression of Warburg effect genes suggesting that Sph cells mostly rely on oxidative phosphorylation (Figure 2L). Further, to evaluate the metabolic profile in these distinct CSC models, we performed targeted liquid-chromatography-tandem mass spectrometry (LC-MS/MS).

Consistent with the results above, our metabolomic studies showed an increase in lactate and other glycolytic metabolites, such as glucose-6-phosphate (Glc-6-P), glyceraldehyde-3-phosphate (GA-3-P), dihydroxyacetone-phosphate (DHAP), 2-phosphoglycerate (2PGA) and phosphoenolpyruvate (PEP) in Sph+Gem cells relative to Sph and non-CSC populations (Figure 2M) suggesting that Sph+Gem cells follow the Warburg effect. Interestingly, increased relative levels of oxidative metabolites, such as citrate, isocitrate, succinate, and malate were also observed in Sph+Gem population (Figure 2N) opposing the Warburg effect, which suggests the complete impairment of mitochondrial function when aerobic glycolysis is active. Later studies challenged this view and identified that the mitochondrial oxidative phosphorylation is still functional in cancer cells undergoing aerobic glycolysis [20, 21]. In agreement with these

identifications, our data also suggest that oxidative phosphorylation is still functional in Sph+Gem cells, in which aerobic glycolysis is active (Figure 2M and N). Decreased lactate levels in Sph cells relative to non-CSCs and Sph+Gem suggest that Sph population is relatively oxidative (Figure 2M). Taken together, distinct sub-types of pancreatic CSC populations display specific metabolic profiles.

C. Organ-tropic metastatic pancreatic cancer cells display specific stem cell features

Our next goal was to investigate whether distinct sub-types of pancreatic CSC populations show organ-specific metastatic potential. To investigate the stem cell features of organ-specific metastatic cells, we selected Miapaca-2 (a non-metastatic cell line), S2-VP10 (a spontaneous lung metastasis pancreatic cancer cell line) and L3.6pL (a spontaneous liver metastatic pancreatic cancer cell line).

As shown by sphere formation assay, lung and liver metastatic cells showed increased sphere formation as compared to non-metastatic cells (Figure 3A). Immunofluorescence staining using ALDH1A1 and MDR1 antibodies followed by confocal imaging showed that lung-specific metastasis cells express ALDH1A1, while liver-specific metastasis cells are MDR1 positive (Figure 3A). As shown by flow cytometry, the percentage of PROM1+ (CD133) population is ~27 fold higher in lung tropic cells as compared to liver tropic and non-metastatic cells (Figure 3B and C). In contrast, the percentage of AF+ and ABCB1+ populations are higher in liver tropic cells as compared to lung tropic and non-metastatic cells. (Figure 3D-F). Further analysis using qRT-PCR showed significant overexpression of ABCB1 and PROM1 in liver tropic and lung tropic cells, respectively (Figure 3H and I). These results conclude that different organ-specific metastatic cells in pancreatic cancer display specific stem cell features.

D. Organ-tropic metastatic pancreatic cancer cells show specific metabolic profiles

Next, we sought to determine the metabolic programs of liver and lung tropic pancreatic cancer metastatic cells. Immunofluorescence staining showed that ATP5B was abundantly expressed and co-expressed with PROM1 in S2-VP10 lung tropic cells, whereas LDH-A is predominantly expressed and co-expressed with ABCB1 in L3.6pL liver tropic cells (Figure 4A). Besides, ECAR, glucose uptake, and lactate release were more in liver tropic cells relative to lung tropic and non-metastatic cells (Figure 4B-D); however, OCR, maximal respiration, spare respiratory capacity, and ATP production were higher in lung-tropic cells (Figure 4E-H). Moreover, liver and lung

metastatic cells showed decreased glutamine uptake (Figure 4I). This is in agreement with recent findings that breast cancer liver-metastasis cells show reduced glutamine metabolism [22], and the pyruvate over glutamine replenish TCA cycle intermediates in lung metastasis [23].

To further confirm the metabolic programs of these organ-tropic cells, we performed LC-MS/MS analysis. The levels of lactate and other glycolytic metabolites, such as Glc-6-P, fructose-6-phosphate (Fru-6-P), fructose-1'6 bisphosphate (Fru-1,6-BP), GA-3-P, DHAP, 2PGA, and PEP were higher in liver tropic cells relative to lung tropic and non-metastatic populations (Figure 4J) suggesting that liver metastatic cells follow the Warburg effect. We also observed increased relative levels of oxidative metabolites (Figure 4K), and this is because mitochondrial respiration is still active in cancer cells undergoing aerobic glycolysis [20, 21]. Diminished levels of lactate in S2-VP10 lung tropic cells relative to non-metastatic and liver tropic L3.6pL cells suggest that lung metastatic cells are relatively oxidative (Figure 4J).

Next, we sought to determine whether phenotypic metabolic changes in distinct organ tropic metastatic cells correlate with their metabolic gene signatures. QRT-PCR analysis showed that the messenger RNAs of major Warburg effect determinants, Myc, PDK1, and UCP2 were highly expressed in liver metastatic cells, whereas the messenger RNAs of these Warburg genes were poorly expressed in lung metastatic cells. Taken together, distinct organ-tropic pancreatic cancer cells display specific metabolic profiles.

E. Human lung and liver metastasis showed specific stem cell and metabolic signatures relative to primary pancreatic tumor

To determine whether lung and liver metastasis show specific stem cell and metabolic profiles, we investigated the expression levels of stem cell and metabolic markers using immunohistochemistry in human primary pancreatic tumor, lung metastasis, and liver metastasis tissues (n=8; Figure 5). Analysis of these tumor sections showed an elevated expression of ALDH1A1 and ATP5B expression in lung metastasis compared to liver metastasis and primary tumor (Figure 5). In contrast, MDR1 and LDHA expression levels were higher in liver metastasis as compared to the primary tumor and lung metastasis (Figure 5A&B).

Discussion

Cancer stem cells (CSCs) are critical players of tumor growth and metastasis in pancreatic cancer [2, 3]. Emerging evidence suggests that CSCs in the pancreatic tumor are heterogeneous with tumorigenic and metastatic properties [2-5, 24]. Studies in breast and pancreatic cancer indicated that CSC populations differ in their energy metabolism and show metabolic heterogeneity [6, 7]. However, the existence of distinct CSC subtype populations with specific stem cell and metabolic signatures and their role in organ-specific metastasis is poorly understood.

Here, we show that distinct subtypes of CSC populations exist in primary pancreatic tumor with subtype-specific stem cell and metabolic profiles. We found ALDH and MDR1 populations as two distinct CSC populations. Gemcitabine treatment has been shown to induce drug resistance and MDR1 expression [17]. In agreement with this, tumors derived from pancreatic cancer patients who underwent gemcitabine therapy showed decreased ALDH population and increased MDR1 expression suggesting that ALDH and MDR1 population are two distinct populations.

Next, we investigated the stemness features of these distinct CSC populations. To further explore the heterogeneity of CSCs, we developed *in vitro* distinct CSC models as shown previously [7]. A previous study showed that pancreatic cancer cells enriched in sphere culture conditions show increased CD133 or ALDH expression [7]. Based on this, we enriched Miapaca-2 cells in sphere culture in order to generate CD133+ or ALDH+ population (Sph). On the other hand, gemcitabine resistant pancreatic cancer cells grown as spheres were considered as drug resistant sub-type of CSCs (Sph+Gem). Pancreatic cancer cells grown as adherent monolayers (Adh) were regarded as the non-CSC population. Cells derived from spheres (Sph) showed CD133 and ALDH phenotype, while cells derived from spheres treated with gemcitabine showed multi drug resistance properties. Besides, Sph and Sph+Gem cells showed specific stem cell features. Sph or CD133+ or ALDH+ cells were positive for KLF4, a pluripotent stem cell marker, whereas CD44v9, a CSC marker was higher in Sph+Gem or multidrug resistant cells. Altogether, these data suggest the existence of distinct subtypes of CSC populations in pancreatic tumors with sub-type specific stem cell signatures.

Recent study showed that the metabolic profile of pancreatic CSCs is heterogeneous [7]. Hence, we investigated whether ALDH and MDR1 distinct CSC populations show population-specific metabolic signatures. Interestingly, we observed that Sph (ALDH+) population shows an increased OCR, while Sph+Gem (MDR1+) population shows elevated ECAR, suggesting that

ALDH+ population is oxidative, whereas, MDR1+ population is glycolytic. Besides, cells derived from Sph+Gem showed elevated glucose uptake and increased lactate release suggesting that Sph+Gem cells are highly glycolytic. Besides, gene expression levels of significant Warburg effect genes are higher in Sph+Gem cells as compared to Sph cells. These results agree with a previous identification that ALDH+ breast CSCs show oxidative phosphorylation, while CD44+CD24- breast CSCs display glycolysis [6]. Also, our results were in agreement with a recent study in which pancreatic cancer cells treated with gemcitabine showed glycolytic metabolism [8]. Overall, distinct CSC populations in pancreatic cancer show population specific metabolic signatures.

Tumor heterogeneity is at least in part due to the presence of distinct CSC population that differentiate and produce heterogeneous tumor bulk [24]. These CSC populations not only initiate and propagate tumor but also involved in metastasis. A study also demonstrated that ALDH+ breast CSCs show increased metastatic ability [25]. Drug-resistant and CD133+CXCR4+ pancreatic CSCs also show elevated metastatic potential [2, 4]. Several recent studies also showed the propensity of different CSCs to metastasize to a specific organ. For instance, CD110+ colorectal CSCs prefer to form liver metastasis, while CDCP1+ colorectal CSCs form lung metastasis [26]. Based on these studies, we hypothesized that distinct sub-types of pancreatic CSC populations show organ-specific metastatic potential. We observed an increased percentage of ALDH+ and CD133+ population in spontaneous lung metastatic cells (S2-VP10), whereas, an elevated percentage of MDR1+ population in spontaneous liver metastatic cells (L3.6pL) relative to non-metastatic cell line, Miapaca-2. These results suggest that lung and liver metastasis show ALDH and multidrug resistance properties, respectively.

Metabolic program of cancer cells in a primary tumor is heterogeneous that dictate their future metastatic destination [22]. Metabolic program in a specific metastasizing cancer cell needs to be compatible with the metabolic environment of its target organ for proper colonization and metastasis formation [13]. The liver environment has increased glycolysis and hypoxia so that the upcoming cancer cell required to be glycolytic to colonize and survive in the liver. In contrast, the lung is with full of oxygen and oxidative stress, and the lung-colonizing cancer cell must be oxidative in order to overcome the oxidative barrier and survive in the lung [13]. In light of these clues from previous studies, we sought to determine the metabolic programs of liver and lung tropic pancreatic cancer metastatic cells. Interestingly, lung tropic cells showed increased oxidative phosphorylation while liver tropic cells showed elevated glycolysis. These results conclude that different organ-specific metastatic cells in pancreatic cancer display specific stem cell and metabolic features.

Moreover, human pancreatic cancer lung metastasis showed elevated expression levels of ALDH1A1 and ATP5B suggesting that the lung metastasis of PDAC rely on oxidative phosphorylation. On the other hand, human pancreatic cancer liver metastasis displayed higher expression levels of MDR1 and LDHA, a Warburg effect enzyme indicating that the liver metastasis depends on the Warburg effect (increased aerobic glycolysis). Altogether, our study showed that human pancreatic tumors consist of distinct sub-types of CSC populations with sub-type specific metabolic signatures and organ-specific metastasis potential. Identifying cell types that metastasize to a specific organ and revealing their stem cell and metabolic features pave the way for the development of anti-metastatic pancreatic cancer therapy.

Figure legends

Figure 1. Distinct sub-types of CSC populations with sub-type specific stem cell features in pancreatic cancer. (**A**) Immunofluorescent staining for ALDH1A1 (green) and MDR1 (red) in mouse $Kras^{G12D}$; Pdx-1 Cre (KC) and human PDAC tissues. The nuclei were stained with DAPI. Scale bar, 100μm. (**B**) Light microscopy images showing Miapaca-2 cells grown in sphere culture conditions with or without gemcitabine (3μM). The Miapaca-2 cells grown in adherent culture were used as non-CSC control. (**C**) Percentage of side population (SP), autofluorescence (AF) and ALDH+ population as analyzed by flow cytometry in Adh, Sph and Sph+Gem cells. (**D-F**) Representative flow cytometry plots of SP assay (D), AF assay (E) and aldered assay (F). (**G**) RT-QPCR analysis of the stem cell markers, ABCB1, ABCG2, PROM1, KLF4 and CD44v9 in cells from adherent culture (Adh), sphere culture (Sph) and sphere culture+gemcitabine (Sph+Gem). (**H&I**) Percentage of ABCB1+ cells (H) and CD133+ cells (I) in Adh, Sph and Sph+Gem cells as analyzed by flow cytometry. For all panels, significance determined with t-test. *p<0.05, **p<0.01, ***p<0.001, ns: non-significant, p>0.05.

Figure 1

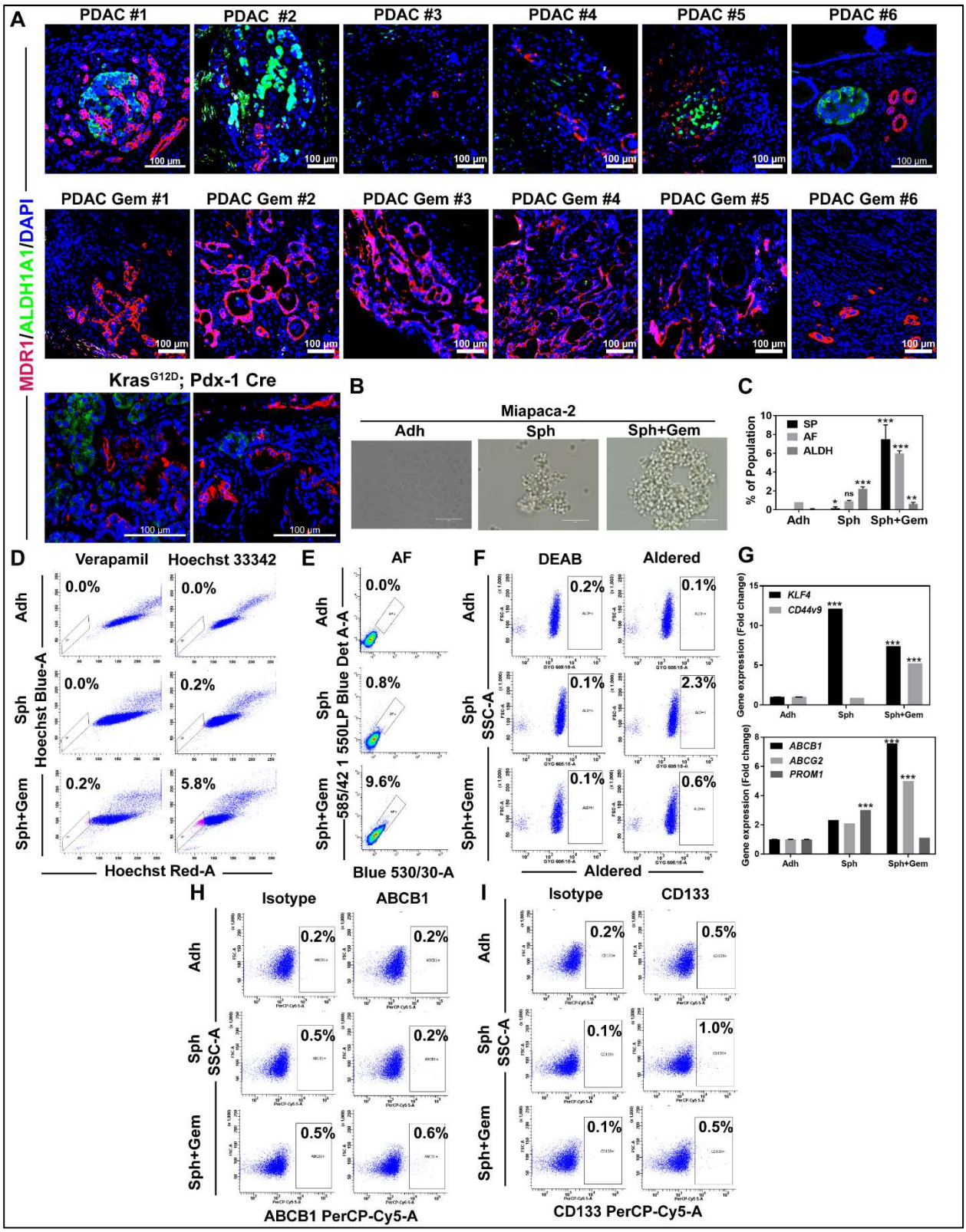
A
PDAC #1
PDAC #2
PDAC #3
PDAC #4
PDAC #5
PDAC #6
PDAC Gem #1
PDAC Gem #2
PDAC Gem #3
PDAC Gem #4
PDAC Gem #5
PDAC Gem #6
MDR1/ALDH1A1/DAPI
100 µm
Kras^{G12D}; Pdx-1 Cre
B
Miapaca-2
Adh
Sph
Sph+Gem
C
SP
AF
ALDH
% of Population
ns
D
Verapamil
Hoechst 33342
Hoechst Blue-A
Hoechst Red-A
0.0%
0.2%
5.8%
E
AF
585/42 1 550LP Blue Det A-A
Blue 530/30-A
0.8%
9.6%
F
DEAB
Aldered
SSC-A
0.1%
2.3%
0.6%
G
KLF4
CD44v9
Gene expression (Fold change)
ABCB1
ABCG2
PROM1
H
Isotype
ABCB1
ABCB1 PerCP-Cy5-A
I
CD133
CD133 PerCP-Cy5-A
0.5%
1.0%

Figure 2. Distinct sub-types of CSC populations show sub-type specific metabolic profiles. (**A**) Immunofluorescent staining for ALDH1A1, MDR1, ATP5B and LDH-A in mouse KC and human PDAC tissues. The nuclei were stained with DAPI. Scale bar, 100μm. (**B**) Extracellular acidification rate (ECAR) measurement in Miapaca-2 Adh, Sph and Sph+Gem cells subjected to sequential injections of glucose (Glc), oligomycin (O), and 2-deoxyglucose (2DG). (C) ECAR simultaneously recorded to Oxygen consumption rate (OCR) as shown in (F). (D) Glycolysis after the addition of glucose. (E) Glycolytic capacity, a change in ECAR after the addition of oligomycin (O), an inhibitor of mitochondrial phosphorylation. (F) OCR in Miapaca-2 Adh, Sph and Sph+Gem cells measured by treating with oligomycin (O), FCCP (F), and antimycin plus rotenone (A+R). Maximal respiration (G), spare respiratory capacity (H), and ATP production (I) were measured from the data acquired from (F). (**J**) Lactate release assay. (**K**) Glucose uptake assay. (**L**) Heat map showing RT-QPCR analysis of energy metabolism (glycolytic and oxidative) genes in Adh, Sph and Sph+Gem cells. (n=3); $P<0.05$. (**M&N**) Relative metabolite abundance in Adh, Sph and Sph+Gem cells. Data are presented as mean total metabolite pools ± s.e.m. (n=3). For all panels, significance determined with t-test. *$p<0.05$, **$p<0.01$, ***$p<0.001$, ns: non-significant, $p>0.05$.

Figure 2

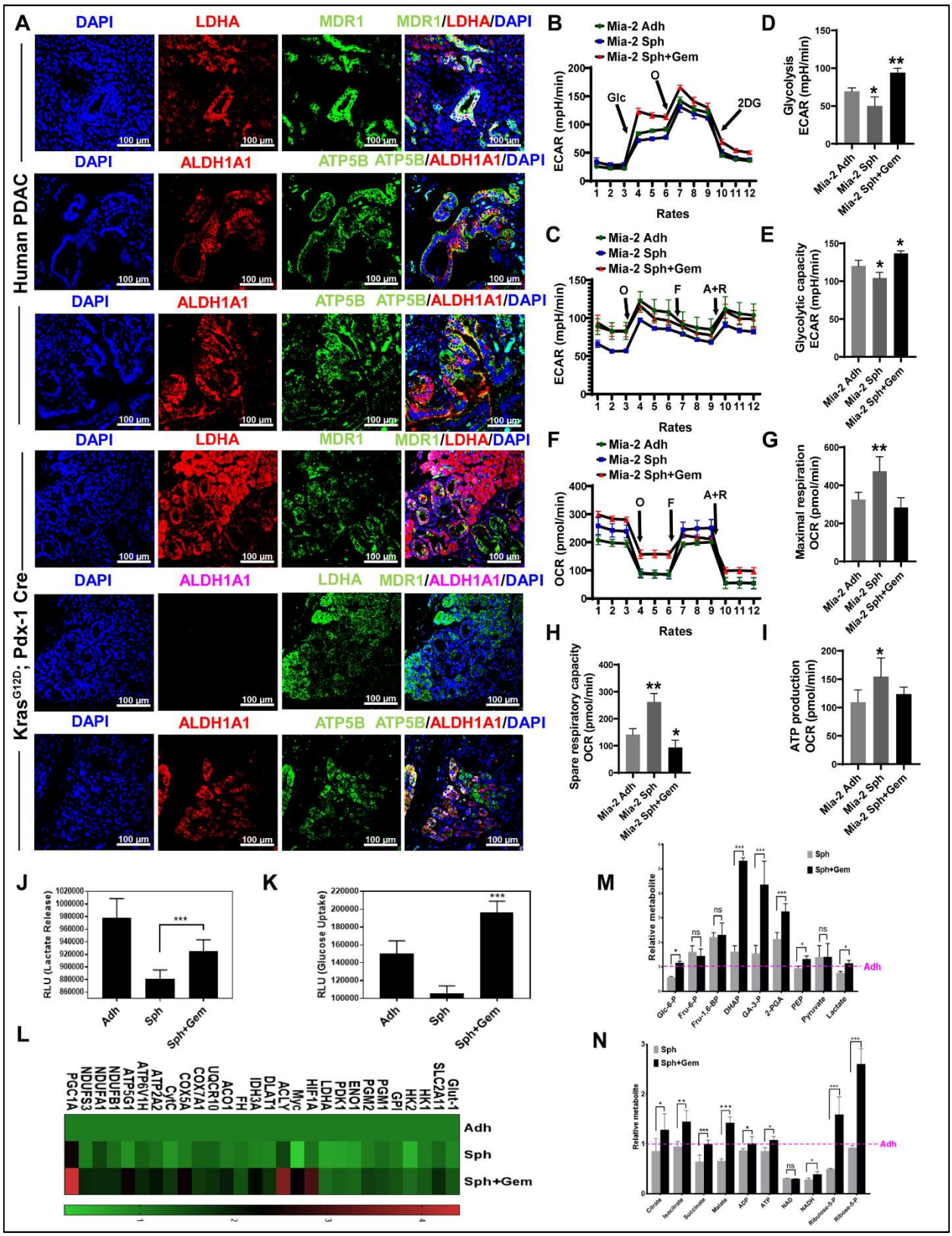
A
DAPI
LDHA
MDR1
MDR1/LDHA/DAPI
ALDH1A1
ATP5B
ATP5B/ALDH1A1/DAPI
MDR1/ALDH1A1/DAPI
Human PDAC
Kras G12D; Pdx-1 Cre
100 μm
B
Mia-2 Adh
Mia-2 Sph
Mia-2 Sph+Gem
Glc
O
2DG
ECAR (mpH/min)
Rates
C
F
A+R
D
Glycolysis ECAR (mpH/min)
E
Glycolytic capacity ECAR (mpH/min)
F
OCR (pmol/min)
G
Maximal respiration OCR (pmol/min)
H
Spare respiratory capacity OCR (pmol/min)
I
ATP production OCR (pmol/min)
J
RLU (Lactate Release)
Adh
Sph
Sph+Gem
K
RLU (Glucose Uptake)
L
PGC1A
NDUFS3
NDUFA1
NDUFB1
ATP5G1
ATP6V1H
ATP2A2
CytC
COX5A
COX7A1
UQCR10
ACO1
FH
IDH3A
DLAT
ACLY
Myc
HIF1A
LDHA
PDK1
ENO1
PGM2
PGM1
GPI
HK2
HK1
SLC2A11
Glut-1
M
Relative metabolite
Glc-6-P
Fru-6-P
Fru-1,6-BP
DHAP
GA-3-P
2-PGA
PEP
Pyruvate
Lactate
N
Citrate
Isocitrate
Succinate
Malate
ADP
ATP
NAD
NADH
Ribulose-5-P
Ribose-5-P

Figure 3. Spontaneous liver and lung tropic metastatic cell lines show organ specific stem cell features. (**A**) Light microscopy images showing sphere formation. Scale bar, 100μm. Immunofluorescent staining for PROM1 (green) and ABCB1. The nuclei were stained with DAPI. Scale bar, 100μm. (**B&C**) Representative flow cytometry plots of CD133+ cell analysis (B). (n=3). Percentage of CD133+ population as analyzed by flow cytometry in Miapaca-2, S2-VP10 and L3.6pL cells (**C**). (**D&F**) Representative flow cytometry plots of AF assay (D). (n=3). Percentage of AF+ population as analyzed by flow cytometry in Miapaca-2, S2-VP10 and L3.6pL cells (**F**). (**E&G**) Representative flow cytometry plots of ABCB1+ cell analysis (**E**). (n=3). Percentage of ABCB1+ population as analyzed by flow cytometry in Miapaca-2, S2-VP10 and L3.6pL cells (G). (**H&I**) RT-QPCR analysis of the stem cell markers, ABCB1 and PROM1 in Miapaca-2 (non-metastatic), S2-VP10 (lung metastatic) and L3.6pL (liver metastatic) cell lines. (n=3). For all panels, significance determined with t-test. *$p<0.05$, **$p<0.01$, ***$p<0.001$, ns: non-significant, $p>0.05$.

Figure 3

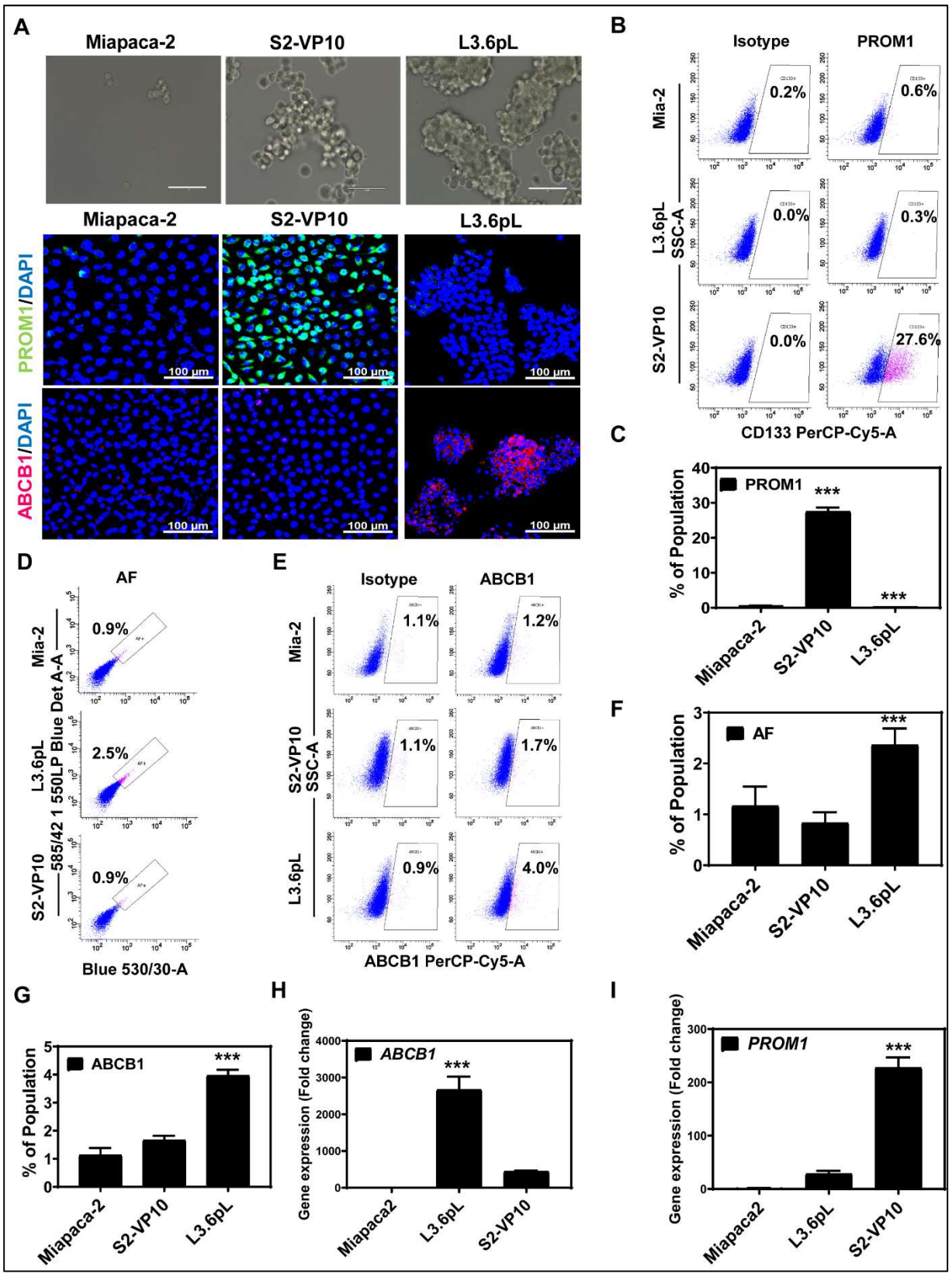
A
Miapaca-2
S2-VP10
L3.6pL
PROM1/DAPI
ABCB1/DAPI
100 µm
B
Isotype
PROM1
Mia-2
L3.6pL
S2-VP10
SSC-A
0.2%
0.6%
0.0%
0.3%
0.0%
27.6%
CD133 PerCP-Cy5-A
C
PROM1
***
% of Population
D
AF
Mia-2
L3.6pL
S2-VP10
585/42 1 550LP Blue Det A-A
0.9%
2.5%
0.9%
Blue 530/30-A
E
Isotype
ABCB1
1.1%
1.2%
1.1%
1.7%
0.9%
4.0%
ABCB1 PerCP-Cy5-A
F
AF
G
ABCB1
H
ABCB1
Gene expression (Fold change)
I
PROM1
Miapaca-2
S2-VP10
L3.6pL
Miapaca2

Figure 4. Spontaneous liver and lung tropic metastatic cell lines show organ specific metabolic features. (**A**) Immunofluorescent staining for PROM1, ABCB1, LDH-A and ATP5B. The nuclei were stained with DAPI. Scale bar, 100μm. (**B**) ECAR measurement in Miapaca-2, S2-VP10 and L3.6pL cells subjected to sequential injections of glucose (Glc), oligomycin (O), and 2-deoxyglucose (2DG). (**C**) Glucose uptake assay. (**D**) Lactate release assay. (**E**) OCR in Miapaca-2, S2-VP10 and L3.6pL cells measured by treating with oligomycin (O), FCCP (F), and antimycin plus rotenone (A+R). Maximal respiration (**F**), spare respiratory capacity (**G**), and ATP production (**H**) were measured from the data acquired from (**E**). (I) Glutamine uptake assay. (**J&K**) Relative metabolite abundance in Miapaca-2, S2-VP10 and L3.6pL cells. Data are presented as mean total metabolite pools ± s.e.m. (n=3). (**L**) Heat map showing RT-QPCR analysis of energy metabolism genes in Miapaca-2, S2-VP10 and L3.6pL. (n=3); $P<0.05$. (**M**) Percentage of $Mito^{High}$ and $Mito^{Low}$ population as analyzed by Mitotracker staining followed by flow cytometry analysis. For all panels, significance determined with t-test. *p<0.05, **p<0.01, ***p<0.001, ns: non-significant, p>0.05.

Figure 4

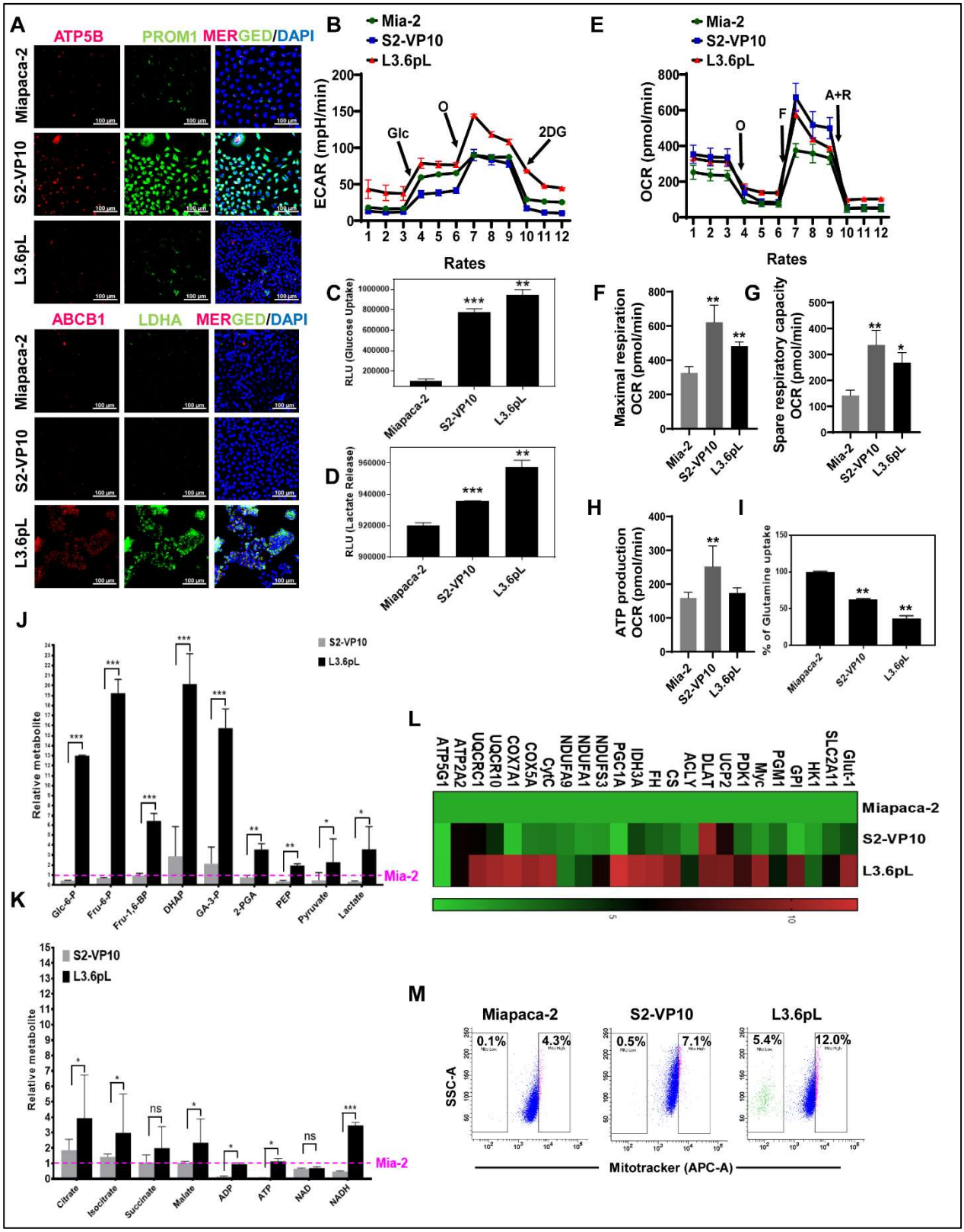
A
ATP5B
PROM1
MERGED/DAPI
Miapaca-2
S2-VP10
L3.6pL
ABCB1
LDHA
MERGED/DAPI
B
Mia-2
S2-VP10
L3.6pL
ECAR (mpH/min)
Glc
O
2DG
Rates
C
RLU (Glucose Uptake)
D
RLU (Lactate Release)
E
OCR (pmol/min)
F
A+R
Maximal respiration OCR (pmol/min)
G
Spare respiratory capacity OCR (pmol/min)
H
ATP production OCR (pmol/min)
I
% of Glutamine uptake
J
Relative metabolite
Glc-6-P
Fru-6-P
Fru-1,6-BP
DHAP
GA-3-P
2-PGA
PEP
Pyruvate
Lactate
K
Citrate
Isocitrate
Succinate
Malate
ADP
ATP
NAD
NADH
L
ATP5G1
ATP2A2
UQCRC1
UQCR10
COX7A1
COX5A
CytC
NDUFA9
NDUFA1
NDUFS3
PGC1A
IDH3A
FH
CS
ACLY
DLAT
UCP2
PDK1
Myc
PGM1
GPI
HK1
SLC2A11
Glut-1
M
SSC-A
0.1%
4.3%
0.5%
7.1%
5.4%
12.0%
Mitotracker (APC-A)

Figure 5. Human lung and liver metastasis show specific stem cell and metabolic profiles relative to primary pancreatic tumors. (A) Representative images of ALDH1A1, ATP5B, MDR1 and LDHA staining in primary pancreatic tumors, lung metastasis, and liver metastasis are shown. (B) Graphs corresponding to the quantification of ALDH1A1, ATP5B, MDR1 and LDHA staining and representing the H-score. Scale bar, 200μm.

Figure 5

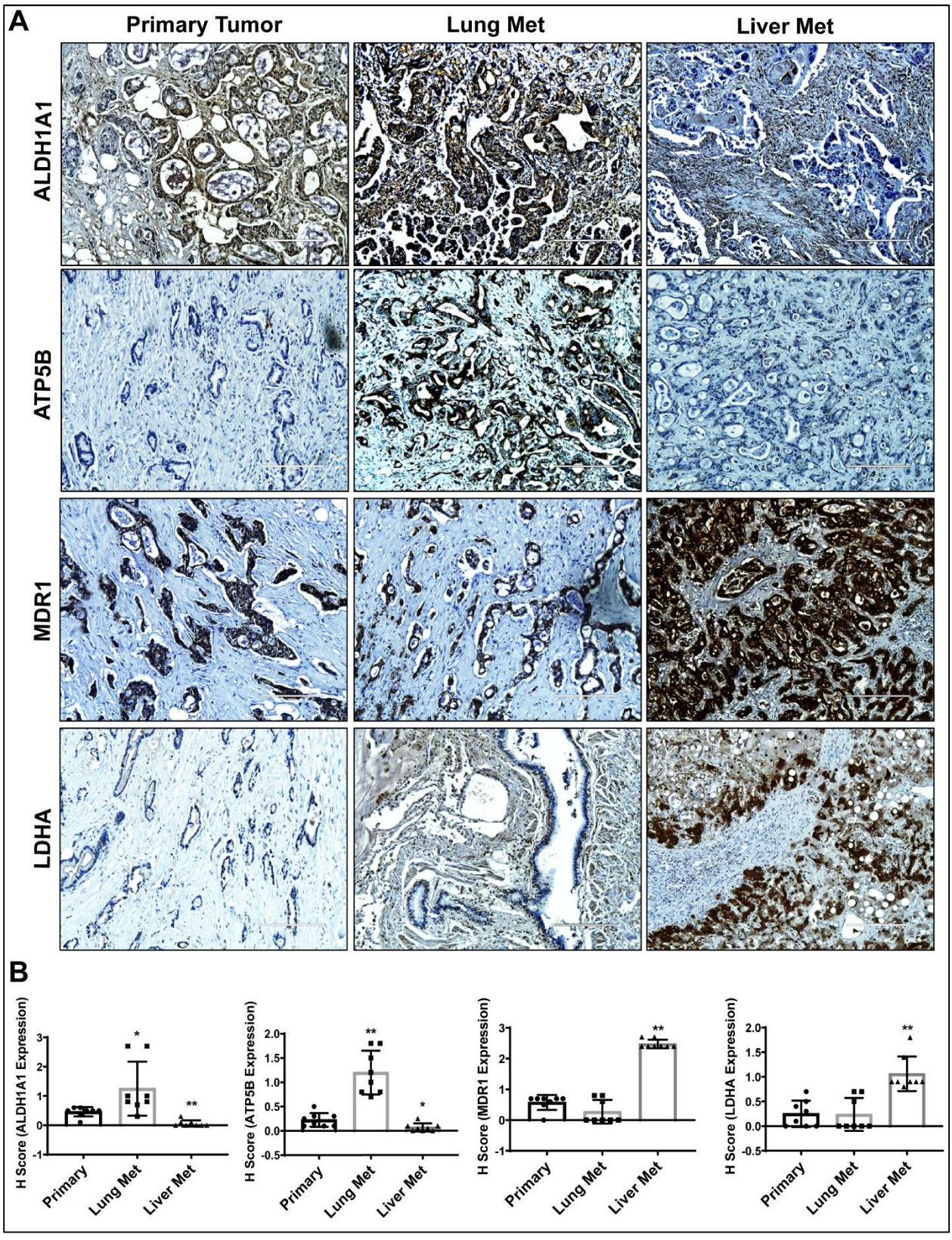
A
Primary Tumor
Lung Met
Liver Met
ALDH1A1
ATP5B
MDR1
LDHA
B
H Score (ALDH1A1 Expression)
H Score (ATP5B Expression)
H Score (MDR1 Expression)
H Score (LDHA Expression)
Primary
Lung Met
Liver Met

Supplementary Table 1: List of antibodies used in this study

ANTIBODIES	SOURCE	IDENTIFIER/DILUTION
List of primary antibodies used in Immunofluorescence		
MDR1	Santa Cruz	Cat# Sc-55510 (Ms) (1:100)
ALDH1A1	Cell Signaling Technology	Cat# 12035S (Rb) (1:200)
LDHA	Cell Signaling Technology	Cat#3582S (Rb) (1:200)
ATP5B	Santa Cruz	Cat# Sc55597 (Rb) (1:100)
Human CD133 VioBright FITC	Miltenyi Biotec	Cat# 130-113-750 (1:100)
List of secondary antibodies used in Immunofluorescence		
Alexa Fluor 568 goat anti-mouse IgG	Life Technologies	Cat#A11004 (1:300)
Alexa Fluor 568 goat anti-rabbit IgG	Life Technologies	Cat#A11011 (1:300)
Alexa Fluor 488 goat anti-mouse IgG	Life Technologies	Cat#A11001 (1:300)
Alexa Fluor 488 goat anti-rabbit IgG	Life Technologies	Cat#A11008 (1:300)
List of antibodies used in Immunohistochemistry		
MDR1	Santa Cruz	Cat# Sc-55510 (Ms) (1:100)
ALDH1A1	Santa Cruz	Cat# Sc374149 (Ms) (1:100)
LDHA	Cell Signaling Technology	Cat#3582S (Rb) (1:100)
ATP5B	Santa Cruz	Cat# Sc55597 (Rb) (1:100)
List of antibodies used in Flow cytometry		
Anti-Human ABCB1 PerCP-eFluor 710	eBioscience	Ref#46-2439-42 (5µL/test)
Anti-Human CD133 PerCP-eFluor 710	eBioscience	Ref# 46-1338-42 (5µL/test)
Mouse/IgG2a, kappa PerCP-eFluor 710	Invitrogen	Cat#46-4724-82 (5µL/test)
Mouse/IgG2a, kappa PerCP-eFluor 710	Invitrogen	Cat#46-1338—42 (5µL/test)

Supplementary Table 2: List of human qRT-PCR primers used in this study

Gene Name	Forward (5'-3') and Reverse (5'-3') primers
KLF4	CCCAATTACCCATCCTTCCT
	ACGATCGTCTTCCCCTCTTT
CD44v9	AGCAGAGTAATTCTCAGAGC
	TGATGTCAGAGTAGAAGTTGTT
ALDH1A1	GTAGCCTTCACAGGATCAAC
	CGGCATCAGCTAACACAA
ABCB1	AGAGGAGCAGCTTATGAAATC
	GATGGGTAACTGAAGTGAACA
ABCG2	GAGCCTACAACTGGCTTAGACTCAA
	TGATTGTTCGTCCCTGCTTAGAC
PROM1	TTGCGGTAAAACTGGCTAAG
	TGGGCTTGTCATAACAGGAT
GLUT1	GATTGGCTCCTTCTCTGTGG
	TCAAAGGACTTGCCCAGTTT
SLC2A11	GTTCCTTCCTGAGACCAAAG
	AGAGTTCTGTTGACTGGATAAC
HK1	GGACTGGACCGTCTGAATGT
	ACAGTTCCTTCACCGTCTGG
HK2	GAGCCACCACTCACCCTACT
	ACCCAAAGCACACACGGAAGT
GPI	CTGAAGCCCTTAAGCCATAC
	TGGTCTCCTGGGTAGTAAAG
PGM1	CCGACTGAAGATCCGTATTG
	TCCAGAGGAACGCAGTTA
PGM2	TTTGTGCCCTTCACAGTATC
	CTGAGCTCCATTATCCCAATAG
ENO1	CTGGTGCCGTTGAGAAGGG
	GGTTGTGGTAAACCTCTGCTC
PDK1	GTGGTTTATGTACCATCCCATCTCT
	TCCATAGTGGCTCTCATTGCAT
LDH-A	TTGACCTACGTGGCTTGGAAG
	GGTAACGGAATCGGGCTGAAT
HIF1A	ACAGCAGCCAGACGATCATGCAG
	GGCTACCACGTACTGCTGGCAA

Myc	CGGAACTCTTGTGCGTAA
	TCAAGACTCAGCCAAGGT
ACLY	CGATTATGCACTGGAAGTAGAG
	GAGTAAAGGACCCACAGTTTC
DLAT1	CAGGACTCATCACACCTATTG
	GCTGTAGTTTACCCTCTCTTG
IDH3A	CTGCTCAGTGCCGTGATG
	TCCTCTGTGAAGTCTGAGCATTT
FH	GAGTCTCTAATGTTGGTGACAG
	GTGAGATAGCCAAGTTCGATAG
ACO1	GGAGCCAAGCAAGGATTT
	CCTAACATCACAGACGGATTAC
UQCRC1	GAGTACCTCAGCACACATTAC
	AGCGGCATGGAGTAAGA
UQCR10	CTTCTGCTGTGTTTGAAGTATG
	GACAAGTGAAGATCAGGTAGAG
COX7A1	CGTTTCCTCACTCTCACATAC
	AAGCGGTACCAGGGAATA
COX5A	GGGAATTGCGTAAAGGGATAA
	TCCTGCTTTGTCCTTAACAACC
CYTC	GGAGGCAAGCATAAGACTGG
	TCCATCAGGGTATCCTCTCC
ATP2A2	GAATGATGCGGAGGAGTTT
	GTGAGGTTGATGGAGAAGTG
ATP6V1H	CCTGAAGAGAAGCAAGAGATG
	CAGCATATCATCCACCATAGTT
ATP5G1	ATCATTGGCTATGCCAGGAA
	ATGGCGAAGAGGATGAGGA
NDUFB1	GTTCTTGTCCCTATGGGATTT
	ACTTCCAGGTAACTTCTTCAC
NDUFA1	CATCCACAGGTTCACTAACG
	CTCCAAACCCTTTGACACATA
NDUFA9	CAGATTGTTCCTCCCATTCC
	GCATCCGCTCCACTTTATC
NDUFS3	GCTGACGCCCATTGAGTCTG
	GGAACTCTTGGGCCAACTCC
PGC1A	AACCGAACTGGTGCTTTAG
	GTTGTTCTCGGAGTCGTTTAG
UCP2	GGTGGTCGGAGATACCAAAG
	CTCGGGCAATGGTCTTGTAG

CS	CACTGTGGACATGATGTATGG
	CTGGCATTCAGGGATACTAAAG
β-actin	F: GGACATCCGCAAAGACCTGTA
	R: GCTCAGGAGGAGCAATGATCT

Key resources table

REAGENT or RESOURCE	SOURCE	IDENTIFIER
ANTIBODIES (see Supplementary Table 2) and PRIMERS (see Supplementary Table 3)	This chapter (Chapter 5)	N/A
Experimental Models: Cell Lines		
Miapaca-2	ATCC	ATCC CRL-1420
L3.6pL	A gift from Dr. Ouellette (UNMC)	
S2-VP10	A kind gift from Dr. Ashok K. Saluja at Miller School of Medicine, University of Miami.	
Experimental Models: Animals		
Mouse: $Kras^{G12D}$; Pdx-1cre	In house developed	N/A
Critical commercial assays		
ALDEFLUOR assay kit	Stem Cell Technologies	Cat #01700
Bio-Rad DC Protein Assay Kit	Bio-Rad	Cat # 500-0114
ECL chemiluminescence kit	Thermo Scientific	Cat#32209
Illumina TruSeq RNA Sample Preparation Kit	Illumina	CAT# RS-122-2001
Bloxall blocking solution	Vector Laboratories, Inc.	SP-6000
Seahorse XF Cell Mito Stress Test Kit	Agilent (Seahorse)	PART NUMBER: 103015-100
Seahorse XF Glycolysis Stress Test Kit	Agilent (Seahorse)	PART NUMBER: 103020-100
Glucose Uptake-Glo Assay	Promega	CAT#J1341
Lactate-Glo Assay	Promega	CAT#J5021
Glutamine/Glutamate-Glo Assay	Promega	CAT#J8021
Software		
BD FACS Diva	BD Biosciences	N/A
Zen Imaging	Zeiss	https://www.zeiss.com/microscopy/us/products/microscope-software/zen-lite.html
PRISM GRAPHPAD	Graphpad	https://www.graphpad.com/scientific-software/prism/
Chemicals & Reagents		
Hoechst 33342	Ana Spec	Cat#AS-83218
Verapamil	Sigma	V4629-1G
DAPI, FluoroPure™ grade	ThermoFisher Scientific	Cat# D21490
Riboflavin	Sigma	R9504
Seahorse XF base medium	Agilent	Part# 103334-100
Seahorse XFe96 FluxPak mini	Agilent	Part#102601-100
Corning® Ultra-low attachment culture dishes	Corning	CLS3262-20EA
B27 supplement	ThermoFisher Scientific	Cat#17504044

References

[1] P. Rawla, T. Sunkara, V. Gaduputi, Epidemiology of Pancreatic Cancer: Global Trends, Etiology and Risk Factors, World journal of oncology, 10 (2019) 10-27.

[2] P.C. Hermann, S.L. Huber, T. Herrler, A. Aicher, J.W. Ellwart, M. Guba, C.J. Bruns, C. Heeschen, Distinct populations of cancer stem cells determine tumor growth and metastatic activity in human pancreatic cancer, Cell stem cell, 1 (2007) 313-323.

[3] C. Li, C.J. Lee, D.M. Simeone, Identification of human pancreatic cancer stem cells, Methods in molecular biology (Clifton, N.J.), 568 (2009) 161-173.

[4] V.J. Bhagwandin, J.M. Bishop, W.E. Wright, J.W. Shay, The Metastatic Potential and Chemoresistance of Human Pancreatic Cancer Stem Cells, PloS one, 11 (2016) e0148807.

[5] H.Q. Duong, K.S. You, S. Oh, S.J. Kwak, Y.S. Seong, Silencing of NRF2 Reduces the Expression of ALDH1A1 and ALDH3A1 and Sensitizes to 5-FU in Pancreatic Cancer Cells, Antioxidants (Basel, Switzerland), 6 (2017).

[6] M. Luo, L. Shang, M.D. Brooks, E. Jiagge, Y. Zhu, J.M. Buschhaus, S. Conley, M.A. Fath, A. Davis, E. Gheordunescu, Y. Wang, R. Harouaka, A. Lozier, D. Triner, S. McDermott, S.D. Merajver, G.D. Luker, D.R. Spitz, M.S. Wicha, Targeting Breast Cancer Stem Cell State Equilibrium through Modulation of Redox Signaling, Cell metabolism, 28 (2018) 69-86.e66.

[7] P. Sancho, E. Burgos-Ramos, A. Tavera, T. Bou Kheir, P. Jagust, M. Schoenhals, D. Barneda, K. Sellers, R. Campos-Olivas, O. Grana, C.R. Viera, M. Yuneva, B. Sainz, Jr., C. Heeschen, MYC/PGC-1alpha Balance Determines the Metabolic Phenotype and Plasticity of Pancreatic Cancer Stem Cells, Cell metabolism, 22 (2015) 590-605.

[8] S.K. Shukla, V. Purohit, K. Mehla, V. Gunda, N.V. Chaika, E. Vernucci, R.J. King, J. Abrego, G.D. Goode, A. Dasgupta, A.L. Illies, T. Gebregiworgis, B. Dai, J.J. Augustine, D. Murthy, K.S. Attri, O. Mashadova, P.M. Grandgenett, R. Powers, Q.P. Ly, A.J. Lazenby, J.L. Grem, F. Yu, J.M. Mates, J.M. Asara, J.W. Kim, J.H. Hankins, C. Weekes, M.A. Hollingsworth, N.J. Serkova, A.R. Sasson, J.B. Fleming, J.M. Oliveto, C.A. Lyssiotis, L.C. Cantley, L. Berim, P.K. Singh, MUC1 and HIF-1alpha Signaling Crosstalk Induces Anabolic Glucose Metabolism to Impart Gemcitabine Resistance to Pancreatic Cancer, Cancer cell, 32 (2017) 71-87.e77.

[9] M. Akada, T. Crnogorac-Jurcevic, S. Lattimore, P. Mahon, R. Lopes, M. Sunamura, S. Matsuno, N.R. Lemoine, Intrinsic chemoresistance to gemcitabine is associated with decreased expression of BNIP3 in pancreatic cancer, Clinical cancer research : an official journal of the American Association for Cancer Research, 11 (2005) 3094-3101.

[10] H. Niess, P. Camaj, A. Renner, I. Ischenko, Y. Zhao, S. Krebs, J. Mysliwietz, C. Jackel, P.J. Nelson, H. Blum, K.W. Jauch, J.W. Ellwart, C.J. Bruns, Side population cells of pancreatic cancer show characteristics of cancer stem cells responsible for resistance and metastasis, Targeted oncology, 10 (2015) 215-227.

[11] A. Hoshino, B. Costa-Silva, T.L. Shen, G. Rodrigues, A. Hashimoto, M. Tesic Mark, H. Molina, S. Kohsaka, A. Di Giannatale, S. Ceder, S. Singh, C. Williams, N. Soplop, K. Uryu, L. Pharmer, T. King, L. Bojmar, A.E. Davies, Y. Ararso, T. Zhang, H. Zhang, J. Hernandez, J.M. Weiss, V.D. Dumont-Cole, K. Kramer, L.H. Wexler, A. Narendran, G.K. Schwartz, J.H. Healey, P. Sandstrom, K.J. Labori, E.H. Kure, P.M. Grandgenett, M.A. Hollingsworth, M. de Sousa, S. Kaur, M. Jain, K. Mallya, S.K. Batra, W.R. Jarnagin, M.S. Brady, O. Fodstad, V. Muller, K. Pantel, A.J. Minn, M.J. Bissell, B.A. Garcia, Y. Kang, V.K. Rajasekhar, C.M. Ghajar, I. Matei, H. Peinado, J. Bromberg, D. Lyden, Tumour exosome integrins determine organotropic metastasis, Nature, 527 (2015) 329-335.

[12] M.A. Rubin, Insights into the mechanism of organ-specific cancer metastasis, Cancer discovery, 4 (2014) 1262-1264.

[13] T. Schild, V. Low, J. Blenis, A.P. Gomes, Unique Metabolic Adaptations Dictate Distal Organ-Specific Metastatic Colonization, Cancer cell, 33 (2018) 347-354.

[14] C. Lehuede, F. Dupuy, R. Rabinovitch, R.G. Jones, P.M. Siegel, Metabolic Plasticity as a Determinant of Tumor Growth and Metastasis, Cancer research, 76 (2016) 5201-5208.

[15] M.P. Kim, J.B. Fleming, H. Wang, J.L. Abbruzzese, W. Choi, S. Kopetz, D.J. McConkey, D.B. Evans, G.E. Gallick, ALDH Activity Selectively Defines an Enhanced Tumor-Initiating Cell Population Relative to CD133 Expression in Human Pancreatic Adenocarcinoma, PloS one, 6 (2011) e20636.

[16] Z.A. Rasheed, J. Yang, Q. Wang, J. Kowalski, I. Freed, C. Murter, S.M. Hong, J.B. Koorstra, N.V. Rajeshkumar, X. He, M. Goggins, C. Iacobuzio-Donahue, D.M. Berman, D. Laheru, A.

Jimeno, M. Hidalgo, A. Maitra, W. Matsui, Prognostic significance of tumorigenic cells with mesenchymal features in pancreatic adenocarcinoma, Journal of the National Cancer Institute, 102 (2010) 340-351.

[17] S.P. Hong, J. Wen, S. Bang, S. Park, S.Y. Song, CD44-positive cells are responsible for gemcitabine resistance in pancreatic cancer cells, International journal of cancer, 125 (2009) 2323-2331.

[18] I. Miranda-Lorenzo, J. Dorado, E. Lonardo, S. Alcala, A.G. Serrano, J. Clausell-Tormos, M. Cioffi, D. Megias, S. Zagorac, A. Balic, M. Hidalgo, M. Erkan, J. Kleeff, A. Scarpa, B. Sainz, Jr., C. Heeschen, Intracellular autofluorescence: a biomarker for epithelial cancer stem cells, Nature methods, 11 (2014) 1161-1169.

[19] R.K. Nimmakayala, P. Seshacharyulu, I. Lakshmanan, S. Rachagani, S. Chugh, S. Karmakar, S. Rauth, R. Vengoji, P. Atri, G.A. Talmon, S.M. Lele, L.M. Smith, I. Thapa, D. Bastola, M.M. Ouellette, S.K. Batra, M.P. Ponnusamy, Cigarette Smoke Induces Stem Cell Features of Pancreatic Cancer Cells via PAF1, Gastroenterology, 155 (2018) 892-908.e896.

[20] C.E. Griguer, C.R. Oliva, G.Y. Gillespie, Glucose metabolism heterogeneity in human and mouse malignant glioma cell lines, Journal of neuro-oncology, 74 (2005) 123-133.

[21] D.A. Scott, A.D. Richardson, F.V. Filipp, C.A. Knutzen, G.G. Chiang, Z.A. Ronai, A.L. Osterman, J.W. Smith, Comparative metabolic flux profiling of melanoma cell lines: beyond the Warburg effect, The Journal of biological chemistry, 286 (2011) 42626-42634.

[22] F. Dupuy, S. Tabaries, S. Andrzejewski, Z. Dong, J. Blagih, M.G. Annis, A. Omeroglu, D. Gao, S. Leung, E. Amir, M. Clemons, A. Aguilar-Mahecha, M. Basik, E.E. Vincent, J. St-Pierre, R.G. Jones, P.M. Siegel, PDK1-Dependent Metabolic Reprogramming Dictates Metastatic Potential in Breast Cancer, Cell metabolism, 22 (2015) 577-589.

[23] K. Sellers, M.P. Fox, M. Bousamra, 2nd, S.P. Slone, R.M. Higashi, D.M. Miller, Y. Wang, J. Yan, M.O. Yuneva, R. Deshpande, A.N. Lane, T.W. Fan, Pyruvate carboxylase is critical for non-small-cell lung cancer proliferation, The Journal of clinical investigation, 125 (2015) 687-698.

[24] R.K. Nimmakayala, S.K. Batra, M.P. Ponnusamy, Unraveling the journey of cancer stem cells from origin to metastasis, Biochimica et Biophysica Acta (BBA) - Reviews on Cancer, 1871 (2019) 50-63.

[25] E. Charafe-Jauffret, C. Ginestier, F. Iovino, J. Wicinski, N. Cervera, P. Finetti, M.H. Hur, M.E. Diebel, F. Monville, J. Dutcher, M. Brown, P. Viens, L. Xerri, F. Bertucci, G. Stassi, G. Dontu, D. Birnbaum, M.S. Wicha, Breast cancer cell lines contain functional cancer stem cells with metastatic capacity and a distinct molecular signature, Cancer research, 69 (2009) 1302-1313.

[26] W. Gao, L. Chen, Z. Ma, Z. Du, Z. Zhao, Z. Hu, Q. Li, Isolation and Phenotypic Characterization of Colorectal Cancer Stem Cells With Organ-Specific Metastatic Potential, Gastroenterology, 145 (2013) 636-646.e635.

CHAPTER 6

Summary and Future Directions

Summary

Pancreatic tumors consist of cancer cells with stem cell features known as “cancer stem cells (CSCs)”. Pancreatic CSCs are highly tumorigenic and metastatic [1, 2]. However, it is not clear how CSCs are induced, and how these cells are involved in the metastasis process. An external factor, cigarette smoking has been shown to induce CSCs in lung and breast cancers [3, 4]. Also, 30% of pancreatic cancer cases are associated with cigarette smoking. Based on these studies, **our first goal** is to investigate whether and how cigarette smoke induces CSCs in pancreatic cancer.

My second goal primarily explores the metastatic function of CSCs in pancreatic cancer. Emerging evidence suggests the existence of distinct types of CSC populations in a heterogeneous tumor with type-specific genotypic, phenotypic and functional characteristics [5]. For instance, breast tumors consist of two distinct CSC populations such as ALDH+ and CD44+CD24-. The study also demonstrated that ALDH+ cells rely on oxidative phosphorylation for their energy needs, whereas CD44+CD24- population rely on glycolysis [6]. Recent studies also proposed the propensity of a specific cancer cell with specific metabolic profile metastasizes to a specific organ. For instance, the liver has a high glycolytic environment, and a metastatic cell required to be highly glycolytic to overcome the glycolytic barrier in the liver [7]. Based on these studies, **our second goal** is to investigate whether distinct types of CSC populations with type-specific stemness and metabolic profiles metastasize to a specific organ.

First, we observed that cigarette smoke induces cancer cells with stem cell features by activating CHRNA7 mediated FOSL1 signaling. **Second**, I identified distinct sub-types of CSC populations with sub-type specific stem cell and metabolic features in pancreatic cancer. I also observed that these distinct sub-types of CSC populations with type-specific metabolic profiles involved in organ-specific metastasis.

The summary of all the two projects is described below:

A. Mechanistic role of cigarette smoking on the induction of pancreatic CSCs

Smoking induces or aggravates diseases in almost all organ systems. Long term smoking is the most established risk factor for many cancers, including pancreatic cancer [8]. In our previous studies, we have demonstrated that smoking induces metastasis of pancreatic cancer [9, 10]. Also, we also observed that smoke exposure induces the progression of pancreatic cancer from pre-neoplastic condition (Pancreatic Intraepithelial lesions-PanINs) [9]; however, these studies have not discussed the role and importance of cancer stem cells which is an essential factor for progression of the disease. Recently, several studies have demonstrated the significant

involvement of CSCs in promoting growth and progression of several lethal malignancies including pancreatic cancer [2, 11-13]. We have recently demonstrated that PAF1 is a novel molecule for the maintenance of self-renewal and drug-resistance of pancreatic CSCs [13]. More recently, it has been shown that smoke induces the enrichment of CSC populations in different cancers such as lung, esophageal and breast cancer [14-17]. However, it is not known whether and how cigarette smoke induces pancreatic CSCs. Based on the previous studies, we hypothesized that cigarette smoking induces CSCs in pancreatic cancer by activating key stem cell pathways.

First, we examined the impact of chronic exposure to cigarette smoke on the induction of stemness or CSCs. We found that chronic cigarette smoke exposure induces pancreatic stemness or CSCs *in vitro* and *in vivo*. Next, we sought to identify the mechanism involved in this process. Interestingly, we found that chronic exposure of cigarette smoke induces pancreatic CSCs inducing PAF1, a significant stem cell marker via CHRNA7 mediated AP1 signaling. We also identified NNN and NNK as an essential cigarette smoke ingredient that induces CSCs through this mechanism. This study demonstrates for the first time a novel mechanism of cigarette smoke-induced expansion of the pancreatic CSC population. In the future, our findings may contribute to the development of targeted therapy for patients with pancreatic cancer who have a smoking history.

B. Cancer stem cell heterogeneity in pancreatic cancer and their role in organ-specific metastasis

Emerging evidence suggests the existence of CSC heterogeneity in pancreatic tumors [5]. Identification of distinct subtypes of breast CSCs such as ALDH+ and CD44+CD24- with subtype-specific metabolic profiles and stem cell features is important evidence for the heterogeneity of CSCs [6]. Several recent clues also suggest that CSCs have metastatic abilities [1, 18]. Recent studies also proposed the propensity of a specific cancer cell with specific metabolic profile metastasizes to a specific organ. For instance, the liver has a high glycolytic environment, and a metastatic cell required to be highly glycolytic to overcome the glycolytic barrier in the liver. Similarly, the lung has an oxidative environment, and an upcoming metastatic cell must be oxyolytic to survive in the lung environment [7]. Based on these previous studies, we hypothesized that distinct sub-types of CSC populations with type-specific stem cell and metabolic signatures metastasize to specific organs.

First, we sought to investigate whether distinct subtypes of pancreatic CSC populations exist in pancreatic cancer with subtype-specific stem cell features. We found that pancreatic cancer consists of distinct CSC populations: ALDH+ CSCs and MDR1+ CSCs. Interestingly, ALDH+ population showed oxidative phosphorylation, whereas, MDR1+ population showed elevated aerobic glycolysis (Warburg effect). Next, we wanted to see whether distinct subtypes of CSC populations are associated with organ-specific metastasis. To our interest, a spontaneous lung metastatic (tropic) cells and human lung metastasis showed ALDH phenotype and oxidative phosphorylation. In contrast, spontaneous liver tropic cells and human liver metastasis showed multidrug resistance phenotype with increased glycolysis (Warburg effect).

This study demonstrates for the first time the existence of distinct sub-types of pancreatic CSCs in pancreatic tumors with sub-type specific metabolic and organ-specific metastasis features. Identifying a specific CSC sub-type population that metastasizes to a specific organ and understanding their metabolic preferences will be instrumental in developing anti-metastatic PDAC therapies based on metabolic and stemness features of CSCs.

Future Directions

A. Mechanistic role of cigarette smoking on the induction of pancreatic CSCs

(i) Does cigarette smoke induce the oncogenic transformation of normal pancreatic stem/progenitor cells into cancer stem cells?

Several studies in the past have demonstrated the propensity of normal adult stem/progenitor cells to transform into CSCs. This has been shown in intestinal adenomas using lineage tracing experiments. This has also been demonstrated in mammary stem/progenitor cells, where ectopic expression of mutated oncogenes resulted in their transformation to malignant phenotype [19]. However, the molecular mechanism underlying the malignant transformation of normal stem cells to CSCs remains unclear [20, 21]. Interestingly, in our preliminary data, we also found enrichment of stem cell population in smoke treated normal epithelial cells (HPNE cells) and PAF1 elevation in smoke-exposed normal animal pancreas (**Figure 1-3 in Chapter 4**). Collectively, these studies suggest that CSCs may arise from a normal proliferative progenitor cell via mutations caused by several causative agents including smoking. Based on these previous pieces of evidence and our preliminary results, we will try to understand the effect of smoking on the malignant transformation of normal pancreatic stem/progenitor cells.

(ii) Does cigarette smoke induce the metabolic reprogramming of pancreatic normal/cancer cells into stem cells/cancer stem cells?

In our most recent study, we demonstrated that chronic exposure to cigarette smoking induces stem cell features in pancreatic cells and PC cells by the upregulation of PAF1 through CHRNA7 mediated AP1 signaling [22]. Emerging evidence suggests that perturbed metabolism and consequent metabolic reprogramming are the underlying causes of various cancers including pancreatic cancer and its metastasis [23-25]. Evidence from a previous study suggests that metabolic reprogramming drives the conversion of normal somatic cells into induced pluripotent stem (iPC) cells through a metabolic shift [26]. Folmes et al. have also shown that alteration in metabolism occurs before pluripotent marker upregulation during the reprogramming of the somatic cell into iPS cells [27]. In our preliminary data, we also observed an altered energy metabolism in human normal pancreatic cells (**Figure 1**). Based on these studies, we will investigate whether cigarette smoking-induced metabolic reprogramming and deregulated metabolic pathways contribute to the emergence of pancreatic CSCs and induce metastasis.

B. Cancer stem cell heterogeneity in pancreatic cancer and their role in organ-specific metastasis:

(i) Does targeting aerobic glycolysis and oxidative phosphorylation in MDR1+ and ALDH+ population, respectively attenuate their organ-specific metastasis?

Our results have shown that pancreatic tumors harbor distinct subtypes of pancreatic CSC populations. The results also demonstrated that a specific subtype of the CSC population holds specific stem cell and metabolic signature. For instance, ALDH+ population showed increased oxidative phosphorylation, whereas, MDR1+ population showed glycolysis. Besides, metastasis in specific organ showed specific stem cell and metabolic signatures. For instance, lung and liver metastasis showed ALDH+ Oxidative^{high} population and MDR1+ Glycolysis^{high} population, respectively. In the future, we will target the metabolic pathway in a specific CSC subtype population using specific inhibitors, such as metformin and see if it can inhibit organ-specific metastasis.

(ii) Do exosomes mediate and determine organ-specific metastasis of distinct CSC populations?

Hoshino et al., have shown that exosomes secreted by primary tumor cells expressing unique integrins determine organotrophic metastasis by preparing pre-metastatic niche (PMN) in target organ [28]. Since distinct subtypes of CSC populations metastasize to a specific organ, it may be possible that the exosomes released by a specific CSC subtype population travel to a specific organ, where it forms a premetastatic niche for the survival and growth of future up-coming CSCs.

In the future, we will investigate to see whether exosomes secreted by ALDH+ or MDR1+ population travel to specific organ to form PMN for the survival of the upcoming CSC population.

Figure Legends

Figure 1. Chronic exposure to cigarette smoke increases oxidative phosphorylation in normal pancreatic cells. Heat map showing the differential expression of metabolism genes in smoke treated HPNE cells as compared to untreated control cells. HPNE cells were exposed to cigarette smoke extract (CSE) for 80 days followed by whole transcriptomic analysis using RNA sequencing.

Figure 1

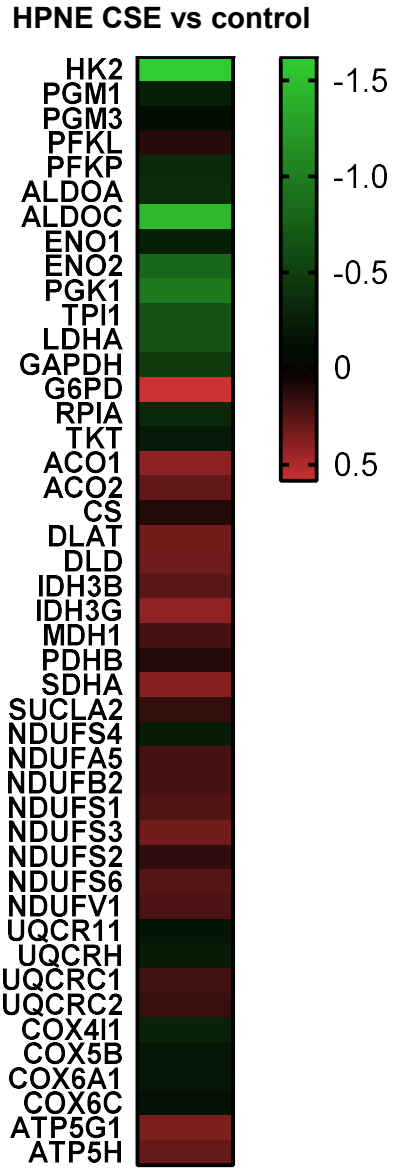
HPNE CSE vs control
HK2
PGM1
PGM3
PFKL
PFKP
ALDOA
ALDOC
ENO1
ENO2
PGK1
TPI1
LDHA
GAPDH
G6PD
RPIA
TKT
ACO1
ACO2
CS
DLAT
DLD
IDH3B
IDH3G
MDH1
PDHB
SDHA
SUCLA2
NDUFS4
NDUFA5
NDUFB2
NDUFS1
NDUFS3
NDUFS2
NDUFS6
NDUFV1
UQCR11
UQCRH
UQCRC1
UQCRC2
COX4I1
COX5B
COX6A1
COX6C
ATP5G1
ATP5H
-1.5
-1.0
-0.5
0
0.5

References

[1] P.C. Hermann, S.L. Huber, T. Herrler, A. Aicher, J.W. Ellwart, M. Guba, C.J. Bruns, C. Heeschen, Distinct populations of cancer stem cells determine tumor growth and metastatic activity in human pancreatic cancer, Cell Stem Cell, 1 (2007) 313-323.

[2] C. Li, D.G. Heidt, P. Dalerba, C.F. Burant, L. Zhang, V. Adsay, M. Wicha, M.F. Clarke, D.M. Simeone, Identification of Pancreatic Cancer Stem Cells, Cancer research, 67 (2007) 1030-1037.

[3] P. Guha, G. Bandyopadhyaya, S.K. Polumuri, S. Chumsri, P. Gade, D.V. Kalvakolanu, H. Ahmed, Nicotine Promotes Apoptosis Resistance of Breast Cancer Cells and Enrichment of Side Population Cells with Cancer Stem Cell Like Properties via a Signaling Cascade Involving Galectin-3, α9 Nicotinic Acetylcholine Receptor and STAT3, Breast cancer research and treatment, 145 (2014) 5-22.

[4] C.M. Schaal, N. Bora-Singhal, D.M. Kumar, S.P. Chellappan, Regulation of Sox2 and stemness by nicotine and electronic-cigarettes in non-small cell lung cancer, Molecular cancer, 17 (2018) 149.

[5] R.K. Nimmakayala, S.K. Batra, M.P. Ponnusamy, Unraveling the journey of cancer stem cells from origin to metastasis, Biochimica et Biophysica Acta (BBA) - Reviews on Cancer, 1871 (2019) 50-63.

[6] M. Luo, L. Shang, M.D. Brooks, E. Jiagge, Y. Zhu, J.M. Buschhaus, S. Conley, M.A. Fath, A. Davis, E. Gheordunescu, Y. Wang, R. Harouaka, A. Lozier, D. Triner, S. McDermott, S.D. Merajver, G.D. Luker, D.R. Spitz, M.S. Wicha, Targeting Breast Cancer Stem Cell State Equilibrium through Modulation of Redox Signaling, Cell metabolism, 28 (2018) 69-86.e66.

[7] T. Schild, V. Low, J. Blenis, A.P. Gomes, Unique Metabolic Adaptations Dictate Distal Organ-Specific Metastatic Colonization, Cancer cell, 33 (2018) 347-354.

[8] N. Momi, S. Kaur, M.P. Ponnusamy, S. Kumar, U.A. Wittel, S.K. Batra, Interplay between Smoking-induced Genotoxicity and Altered Signaling in Pancreatic Carcinogenesis, Carcinogenesis, 33 (2012) 1617-1628.

[9] S. Kumar, M.P. Torres, S. Kaur, S. Rachagani, S. Joshi, S.L. Johansson, N. Momi, M.J. Baine, C.E. Gilling, L.M. Smith, T.A. Wyatt, M. Jain, S.S. Joshi, S.K. Batra, Smoking accelerates pancreatic cancer progression by promoting differentiation of MDSCs and inducing HB-EGF expression in macrophages, Oncogene, 34 (2015) 2052-2060.

[10] N. Momi, M.P. Ponnusamy, S. Kaur, S. Rachagani, S.S. Kunigal, S. Chellappan, M.M. Ouellette, S.K. Batra, Nicotine/cigarette smoke promotes metastasis of pancreatic cancer through alpha7nAChR-mediated MUC4 upregulation, Oncogene, 32 (2013) 1384-1395.

[11] C. Li, C.J. Lee, D.M. Simeone, Identification of human pancreatic cancer stem cells, Methods in molecular biology (Clifton, N.J.), 568 (2009) 161-173.

[12] A.P. Vaz, M.P. Ponnusamy, S.K. Batra, Cancer stem cells and therapeutic targets: an emerging field for cancer treatment, Drug Deliv Transl Res, 3 (2013) 113-120.

[13] A.P. Vaz, M.P. Ponnusamy, S. Rachagani, P. Dey, A.K. Ganti, S.K. Batra, Novel role of pancreatic differentiation 2 in facilitating self-renewal and drug resistance of pancreatic cancer stem cells, Br J Cancer, 111 (2014) 486-496.

[14] Y. An, A. Kiang, J.P. Lopez, S.Z. Kuo, M.A. Yu, E.L. Abhold, J.S. Chen, J. Wang-Rodriguez, W.M. Ongkeko, Cigarette Smoke Promotes Drug Resistance and Expansion of Cancer Stem Cell-Like Side Population, PLOS ONE, 7 (2012) e47919.

[15] F. Di Cello, V.L. Flowers, H. Li, B. Vecchio-Pagan, B. Gordon, K. Harbom, J. Shin, R. Beaty, W. Wang, C. Brayton, S.B. Baylin, C.A. Zahnow, Cigarette smoke induces epithelial to mesenchymal transition and increases the metastatic ability of breast cancer cells, Molecular cancer, 12 (2013) 90.

[16] N. Hirata, Y. Sekino, Y. Kanda, Nicotine increases cancer stem cell population in MCF-7 cells, Biochemical and biophysical research communications, 403 (2010) 138-143.

[17] A.T. Ooi, V. Mah, D.W. Nickerson, J.L. Gilbert, V.L. Ha, A.E. Hegab, S. Horvath, M. Alavi, E.L. Maresh, D. Chia, A.C. Gower, M.E. Lenburg, A. Spira, L.M. Solis, Wistuba, II, T.C. Walser, W.D. Wallace, S.M. Dubinett, L. Goodglick, B.N. Gomperts, Presence of a putative tumor-initiating progenitor cell population predicts poor prognosis in smokers with non-small cell lung cancer, Cancer research, 70 (2010) 6639-6648.

[18] H. Niess, P. Camaj, A. Renner, I. Ischenko, Y. Zhao, S. Krebs, J. Mysliwietz, C. Jackel, P.J. Nelson, H. Blum, K.W. Jauch, J.W. Ellwart, C.J. Bruns, Side population cells of pancreatic cancer show characteristics of cancer stem cells responsible for resistance and metastasis, Targeted oncology, 10 (2015) 215-227.

[19] C.Y. Zhong, Y.M. Zhou, G.C. Douglas, H. Witschi, K.E. Pinkerton, MAPK/AP-1 signal pathway in tobacco smoke-induced cell proliferation and squamous metaplasia in the lungs of rats, Carcinogenesis, 26 (2005) 2187-2195.

[20] S.J. Buczacki, H.I. Zecchini, A.M. Nicholson, R. Russell, L. Vermeulen, R. Kemp, D.J. Winton, Intestinal label-retaining cells are secretory precursors expressing Lgr5, Nature, 495 (2013) 65-69.

[21] A.G. Schepers, H.J. Snippert, D.E. Stange, M. van den Born, J.H. van Es, M. van de Wetering, H. Clevers, Lineage tracing reveals Lgr5+ stem cell activity in mouse intestinal adenomas, Science (New York, N.Y.), 337 (2012) 730-735.

[22] R.K. Nimmakayala, P. Seshacharyulu, I. Lakshmanan, S. Rachagani, S. Chugh, S. Karmakar, S. Rauth, R. Vengoji, P. Atri, G.A. Talmon, S.M. Lele, L.M. Smith, I. Thapa, D. Bastola, M.M. Ouellette, S.K. Batra, M.P. Ponnusamy, Cigarette Smoke Induces Stem Cell Features of Pancreatic Cancer Cells via PAF1, Gastroenterology, 155 (2018) 892-908.e896.

[23] F. Dupuy, S. Tabaries, S. Andrzejewski, Z. Dong, J. Blagih, M.G. Annis, A. Omeroglu, D. Gao, S. Leung, E. Amir, M. Clemons, A. Aguilar-Mahecha, M. Basik, E.E. Vincent, J. St-Pierre, R.G. Jones, P.M. Siegel, PDK1-Dependent Metabolic Reprogramming Dictates Metastatic Potential in Breast Cancer, Cell metabolism, 22 (2015) 577-589.

[24] Natalya N. Pavlova, Craig B. Thompson, The Emerging Hallmarks of Cancer Metabolism, Cell metabolism, 23 (2016) 27-47.

[25] C.M. Sousa, A.C. Kimmelman, The complex landscape of pancreatic cancer metabolism, Carcinogenesis, 35 (2014) 1441-1450.

[26] P. Sancho, D. Barneda, C. Heeschen, Hallmarks of cancer stem cell metabolism, Br J Cancer, 114 (2016) 1305-1312.

[27] C.D.L. Folmes, T.J. Nelson, A. Terzic, Energy metabolism in nuclear reprogramming, Biomarkers in medicine, 5 (2011) 715-729.

[28] A. Hoshino, B. Costa-Silva, T.L. Shen, G. Rodrigues, A. Hashimoto, M. Tesic Mark, H. Molina, S. Kohsaka, A. Di Giannatale, S. Ceder, S. Singh, C. Williams, N. Soplop, K. Uryu, L. Pharmer, T. King, L. Bojmar, A.E. Davies, Y. Ararso, T. Zhang, H. Zhang, J. Hernandez, J.M. Weiss, V.D. Dumont-Cole, K. Kramer, L.H. Wexler, A. Narendran, G.K. Schwartz, J.H. Healey, P. Sandstrom, K.J. Labori, E.H. Kure, P.M. Grandgenett, M.A. Hollingsworth, M. de Sousa, S. Kaur, M. Jain, K. Mallya, S.K. Batra, W.R. Jarnagin, M.S. Brady, O. Fodstad, V. Muller, K. Pantel, A.J. Minn, M.J. Bissell, B.A. Garcia, Y. Kang, V.K. Rajasekhar, C.M. Ghajar, I. Matei, H. Peinado, J. Bromberg, D. Lyden, Tumour exosome integrins determine organotropic metastasis, Nature, 527 (2015) 329-335.

Bibliography of Rama Krishna Nimmakayala

1. **Nimmakayala RK**, Seshacharyulu P, Lakshmanan I, Rachagani S, Chugh S, Karmakar S, Rauth S, Vengoji R, Atri P, Talmon GA, Lele SM, Smith LM, Thapa I, Bastola D, Ouellette MM, Batra SK, Ponnusamy MP, Cigarette Smoke Induces Stem Cell Features of Pancreatic Cancer Cells via PAF1, **Gastroenterology 2018**; 155 (3): 892-908.e6.

2. **Nimmakayala RK**, Batra S.K, Ponnusamy M.P., Unraveling the journey of cancer stem cells from origin to metastasis. **Biochim Biophys Acta Rev Cancer. 2019**; 1871(1):50-63.

3. Chugh S, Barkeer S, Rachagani S, **Nimmakayala RK**, Perumal NK, Pothuraju R, Atri P, Mahapatra S, Thapa I, Talmon GA, Smith LM, Yu X, Neelamegham S, Fu J, Xia L, Ponnusamy MP and Batra SK. Disruption of C1galt1 Gene Promotes Development and Metastasis of Pancreatic Adenocarcinomas in Mice, **Gastroenterology 2018**; 155(5): 1608-1624.

4. Lakshmanan I., Rachagani S., Hauke R., Krishn S.R., Paknikar S., Seshacharyulu P., Karmakar S., **Nimmakayala R.K**., Kaushik G., Johansson S.L., Carey G.B., Ponnusamy M.P., Kaur S., Batra S.K., Ganti A.K. MUC5AC interactions with integrin beta4 enhances the migration of lung cancer cells through FAK signaling. **Oncogene 2016**; 35 (31):4112-21. 8.5

5. Lakshmanan I, Salfity S, Seshacharyulu P, Rachagani S, Thomas A, Das S, Majhi P, **Nimmakayala RK**, Vengoji R, Lele SM, Ponnusamy MP, Batra SK and Ganti AK. MUC16 regulates TSPYL5 for lung cancer cell growth and chemoresistance by suppressing p53. **Clinical Cancer Research 2017**; 23(14): 3906-3917. 9.6

6. Karmakar S., Kaushik G., **Nimmakayala R.K.,** Ponnusamy M.P., Batra S.K. MicroRNA regulation of Ras and opportunities for therapeutic intervention. **Seminars in Cancer Biology 2017**; 54:63-71.